

Sunday Afternoon, October 28, 2012

Biomaterials Plenary Session

Room: 23 - Session BP+AS-SuA

Biomaterials Plenary - Bioimaging: In Vacuo, In Vitro, In Vivo

Moderator: M.R. Alexander, University of Nottingham, UK

4:00pm **BP+AS-SuA1 NanoBio Imaging for New Biomedical Applications**, *D.W. Moon*, Korea Research Institute of Standards and Science **INVITED**

Surface and interface analysis techniques have been mainly developed to meet the demands on atomic scale characterization from semiconductor industries. KRIS has been trying to meet the surface and interface analysis challenges from semiconductor industries and furthermore to extend the application scope to biomedical areas. In this presentation, I'd like to report our recent activities of nanobio imaging for new biomedical applications such as 1) Coherent Anti-Stokes Raman Scattering (CARS) for atherosclerotic plaque imaging 2) Time-of-flight secondary ion mass spectrometry (TOF-SIMS) for mass imaging of collagen fibrils, atherosclerotic plaques, and cancer tissues and 3) Surface Plasmon Resonance Imaging Ellipsometry for cell adhesion, migration, and infiltration dynamics for HUVEC, CASMC, and T cells 4) TOF-medium energy ion scattering spectroscopy (TOF-MEIS) for nanothin films and nanoparticles such as CdSe/ZnS quantum dots and calcium hydroxyapatite nano-size biominerals. Future challenges of nanobio imaging for biomedical applications will be discussed.

4:40pm **BP+AS-SuA3 3-D View into Cells by X-ray Nano-Tomography**, *G. Schneider, P. Guttman, S. Werner, K. Henzler, S. Rehbein*, Helmholtz-Zentrum Berlin für Materialien und Energie GmbH, Germany **INVITED**

X-ray imaging offers a new 3-D view into cells. With its ability to penetrate whole hydrated cells it is ideally suited for pairing fluorescence light microscopy and nanoscale X-ray tomography. The HZB TXM at the undulator U41 provides a spectral resolution of 10.000 and a spatial resolution of 11 nm. For high resolution tomography, we adopted a tilt stage originally developed for electron tomography. The stage is able to tilt samples up to $\pm 80^\circ$. Such a large tilt of flat sample holders is impossible with TXM at bending magnet sources because they require a monochromator pinhole to be positioned close to the specimen. In our TXM, the holder geometry is no longer restricted to glass tubes. Conventional fluorescence images are diffraction-limited to ~ 200 nm, whereas current TXM achieve a ten-fold improvement in resolution. Since fluorescence and X-ray microscopy permit analysis of whole cells, it is possible to investigate the same cell in both microscopes by correlative microscopy. These correlative studies are ideally suited to X-ray microscopy because of its ability to image cells in 3D. In the talk, we present the cryo TXM and selected applications. In particular, we will show the internal structures of mammalian cells, i.e. plasma membrane, nuclear membrane, nuclear pores, nucleoli, endoplasmic reticulum, vesicles, lysosomes and mitochondria. It is now also possible to resolve internal organellar structures, such as mitochondrial cristae, the double nuclear membrane and lysosomal inclusions. In addition, we discuss ways towards 10 nm 3D imaging of cells. Keywords: X-ray microscopy, tomography, cell organelles, correlative microscopy

References

1. S. Rehbein, S. Heim, P. Guttman, S. Werner, G. Schneider, Phys. Rev. Lett. 103, (2009) 110801
2. G. Schneider, P. Guttman, S. Heim, S. Rehbein, F. Mueller, K. Nagashima, J.B. Heymann, W.G. Müller, J.G. McNally, Nature Methods 7 (2010), 985-987
3. P. Guttman, C. Bittencourt, S. Rehbein, P. Umek, X. Ke, G. Van Tendeloo, C. P. Ewels and G. Schneider, Nature Photonics 6 (2012), 25-29
4. G. Schneider, P. Guttman, S. Rehbein, S. Werner, R. Follath, J. Struct. Biol. 177 (2012), 212-223

5:20pm **BP+AS-SuA5 Nanoscopy with Focused Light**, *S.W. Hell*, Max-Planck-Institut für Biophysikalische Chemie, Germany **INVITED**

In STED microscopy¹, fluorescent features are switched off by the STED beam, which confines the fluorophores to the ground state everywhere in the focal region except at a subdiffraction area of extent. In RESOLFT microscopy,^{2,3} the principles of STED have been expanded to fluorescence

on-off-switching at low intensities I , by resorting to molecular switching mechanisms that entail low switching thresholds I_s . An I_s lower by many orders of magnitude is provided by reversibly switching the fluorophore to a long-lived dark (triplet) state² or between a long-lived 'fluorescence activated' and 'deactivated' state.^{2,5} These alternative switching mechanisms entail an I_s that is several orders of magnitude lower than in STED. In imaging applications, STED/RESOLFT enables fast recordings and the application to living cells, tissues, and even living animals.^{6,7}

Starting from the basic principles of nanoscopy we will discuss recent developments^{8,9} with particular attention to RESOLFT and the recent nanoscale imaging of the brain of living mice⁷ by STED.

1 Hell, S. W. & Wichmann, J. Breaking the diffraction resolution limit by stimulated-emission - stimulated-emission-depletion fluorescence microscopy, 780-782, doi:10.1364/OL.19.000780 (1994).

2 Hell, S. W. Toward fluorescence nanoscopy, 1347-1355 (2003).

3 Hell, S. W., Jakobs, S. & Kastrup, L. Imaging and writing at the nanoscale with focused visible light through saturable optical transitions, 859-860 (2003).

4 Hell, S. W. Far-Field Optical Nanoscopy, 1153-1158 (2007).

5 Hofmann, M., Eggeling, C., Jakobs, S. & Hell, S. W. Breaking the diffraction barrier in fluorescence microscopy at low light intensities by using reversibly photoswitchable proteins, 17565-17569 (2005).

6 Rankin, B. R. Nanoscopy in a Living Multicellular Organism Expressing GFP, L63 - L65 (2011).

7 Berning, S., Willig, K. I., Steffens, H., Dibaj, P. & Hell, S. W. Nanoscopy in a Living Mouse Brain, 551 (2012).

8 Grotjohann, T. Diffraction-unlimited all-optical imaging and writing with a photochromic GFP, 204-208 (2011).

9 Brakemann, T. A reversibly photoswitchable GFP-like protein with fluorescence excitation decoupled from switching, 942-947 (2011).

Monday Morning, October 29, 2012

Applied Surface Science
Room: 20 - Session AS-MoM

Quantitative Surface Chemical Analysis, Technique Development, and Data Interpretation - Part 1

Moderator: J.A. Ohlhausen, Sandia National Laboratories, S. Suzer, Bilkent University, Turkey

8:20am AS-MoM1 2012 AVS Albert Nerken Award Lecture: Characterization of Thin-Film Nano-Structures by XPS, S. Tougaard*, University of Southern Denmark **INVITED**

This is a brief summary of the work that was involved in the development of the technique for quantitative XPS from analysis of the background of inelastically scattered electrons. About 30 years ago it became evident that these electrons must carry valuable information about the depth where the XPS electrons are excited. Theoretical modeling started and algorithms were developed. It was necessary to have an accurate description of the electron energy loss processes which at that time was not available. Theoretical calculations of inelastic cross sections based on a dielectric response description were done and a new experimental method to determine this from analysis of reflected electron energy loss spectra (REELS) was also developed.

To make these procedures for quantitative XPS analysis work in practice it is however not possible to use calculations valid only for specific sample compositions. Therefore an effort was made early on to find cross sections which can be used as an approximation for wide classes of materials and compositions. This resulted in the Universal cross sections which are now widely used and without which practical use of the formalism would have been very limited. The resulting XPS analysis technique was summarized in [1].

In the following years, much effort was then centered on applications to increasingly finer details of the morphology of nanostructures. This requires a careful data analysis since otherwise the uncertainty on the determined morphology may be large. Sometimes the detailed morphology is however not the most important issue for technological applications. Things like speed of analysis, robustness, and automation is often more important in industrial environments. It was therefore decided to develop a simpler algorithm which does not give as detailed information but which is very robust and therefore faster to use and less dependent on a meticulous analysis procedure. The resulting algorithm [2] has been shown to be very robust and therefore suitable for automation. It proved also effective in generating 3D images of nano-structures where automation is mandatory since thousands of spectra (one per pixel) must be analyzed.

Throughout, efforts were always exerted to test the validity of each step in the development of algorithms and procedures by designing and performing critical experiments. This is of utmost importance to ensure progress which does not lead to dead ends.

In this talk I will give an overview of the development of the technique and discuss some technological applications.

1. S. Tougaard, J. Vac. Sci. Technol. A14, 1415 (1996)
2. S. Tougaard, J. Vac. Sci. Technol. A23, 741 (2005)

9:00am AS-MoM3 Simulation of Electron Spectra for Surface Analysis (SESSA): (Hard) X-ray Photoelectron Spectra of Nanostructured Surfaces, W.S.M. Werner, W. Smekal, Vienna University of Technology, Austria, C.J. Powell, National Institute of Standards and Technology

The National Institute of Standards and Technology (NIST) Database for the Simulation of Electron Spectra for Surface Analysis (SESSA) [1,2] has been modified to allow a user to simulate XPS spectra of nanostructured surfaces, such as surfaces covered with rectangular islands, pyramids, spheres, layered spheres, etc. The effect of the nanomorphology of the surface on the emitted angular and energy distribution of photoelectrons is investigated. Comparison with simple models in the literature, which neglect several aspects of the physics of signal generation, such as elastic electron scattering, the dependence of the inelastic mean free path of the position of the electron in the specimen, the anisotropy of the photoelectric cross section, etc. gives good agreement when the same model assumptions are made in the simulations, but show significant deviations for more physically realistic simulations. The extent to which information on the

nanomorphology can be extracted from the photoelectron angular/energy distribution is investigated, in particular the question is addressed whether the average size of nanostructures on a surface is accessible by means of analysis of angular/energy photoelectron spectra. This is done for standard AlK α and Mg K α laboratory sources, but the possibility to gain additional information by increasing the photon energy to the hard x-ray regime is also examined.

1. <http://www.nist.gov/srd/nist100.cfm>.
2. W. Smekal, W. S. M. Werner, and C. J. Powell, Surf. Interface Anal. 37, 1059 (2005).

9:20am AS-MoM4 XPS Characterisation of InP Features Etched in Cl₂-Ar and Cl₂-H₂ Inductively Coupled Plasmas, C. Cardinaud, CNRS, France, R. Chanson, CNRS-IMN, France, S. Bouchoule, CNRS-LPN, France, A. Rhallabi, M.-C. Fernandez, Université de Nantes, France

High-aspect-ratio etching of InP-based heterostructures is a critical building block for photonic device fabrication. This study is focused on the chemical characterisation of the bottom and sidewall surfaces of InP ridge patterns etched with Cl₂-Ar and Cl₂-H₂ plasmas using a SiN_x mask. Each sample contains five arrays combining various ridge widths (1.5 to 4 μ m) and space widths (5 to 16 μ m) plus four InP and mask open areas. Experiments are carried out in a Kratos-Axis-Ultra. The direction of analysis is vertical, i.e. normal to the sample surface, while the x-rays strike the surface with an angle of incidence $\alpha = 60^\circ$. The sample can be rotated in azimuth to align precisely the arrays, either parallel to or perpendicular to the plane defined by the x-source and the analyser. The first arrangement enables the analysis of the bottom (as well as the top of the ridge), whereas the second arrangement allows the analysis of the sidewall after tilting the sample. In this latter case two configurations are used. Taking advantage of the absorption of the x-rays by the InP ridges (1.8 μ m of InP absorbs 99% of AlK α under 60° of angle of incidence), the first configuration consists in tilting the sample opposite to the x-ray source until the bottom is totally screened. Simultaneously this brings the sidewall that is irradiated in the analyser line of sight. Tilting the sample towards the x-ray source to an angle $\theta = \text{atan}(\text{space width} / \text{ridge height})$ allows to shadow the bottom and observe photoelectrons coming from the sidewall (and the top of the ridges), in this case θ needs to be larger than α to obtain full irradiation of the sidewall that comes in the analyser line of sight.

For each array, the intensity of the In, P, N and Si core levels, normalised with respect to that measured on the mask and InP open spaces, are compared to the corresponding ratio calculated from the geometry of the array and the analysis arrangement or configuration. Modelling takes into account the contribution of the various surfaces (mask, InP) in the line of sight of the analyser, and the rate of irradiation according to the geometry of the array and the nature of the materials (InP ridge, mask) the x-rays pass through. This comparison points out the relation between the intensity emitted from the bottom and the aspect ratio of the array. A good agreement is obtained when including the analyser acceptance angle to the model. Concerning the sidewall the discrepancy between experiment and simulation corroborates the presence of a passivation layer. The presentation will discuss in detail the influence of the plasma chemistry on the quantitative composition of the sidewall and the bottom.

9:40am AS-MoM5 Simplified Extrinsic Background for XPS Data Fitting, A. Herrera-Gomez, UAM-Azacapotzalco and CINVESTAV-Queretaro, Mexico

In this presentation it is described a simplified form of the background for extrinsic scattering in the near-peak regime for X-Ray Photoelectron Spectroscopy (XPS) data peak-fitting. It directly accounts for the change on the slope of the background between the two sides of the core-level peak. With an approach similar to the employed for the Shirley background, it is proposed that the change on the background slope at energy E is proportional to the integrated signal above E . This functional form can be reproduced by assuming that the inelastic cross section is proportional to the energy loss. As for the Shirley background, and in contrast to the currently employed extrinsic background models, the background here introduced only employs one parameter. It has some extra advantages for XPS data peak fitting, such that its functional form is the same regardless of the core level, it account for the finiteness of the peak width in the generation of the background signal, it can be employed simultaneously with the intrinsic Shirley background, and last, but not least, it provides for good fits. Some implementations of the method are discussed.

* Albert Nerken Award Winner

10:00am **AS-MoM6 Effective Attenuation Lengths for Photoelectrons in Thin Films of Silicon Oxynitride and Hafnium Oxynitride on Silicon**, *C.J. Powell*, National Institute of Standards and Technology, *W.S.M. Werner, W. Smekal, G. Tasneem*, Vienna University of Technology, Austria
 We have used the National Institute of Standards and Technology (NIST) Database for the Simulation of Electron Spectra for Surface Analysis (SESSA) [1,2] to simulate photoelectron intensities for thin films of $\text{SiO}_{1.6}\text{N}_{0.4}$ and $\text{HfO}_{1.9}\text{N}_{0.1}$ on silicon with excitation by Al K α X-rays. We considered Si 2p_{3/2} photoelectrons from $\text{SiO}_{1.6}\text{N}_{0.4}$ and the substrate and Hf 4f_{7/2} photoelectrons from $\text{HfO}_{1.9}\text{N}_{0.1}$. The simulations were performed for ranges of film thicknesses and photoelectron emission angles and for two common configurations for X-ray photoelectron spectroscopy (XPS), the sample-tilting configuration and the Theta Probe configuration. We determined photoelectron effective attenuation lengths (EALs) by two methods, one by analyzing photoelectron intensities as a function of film thickness for each emission angle (Method 1) and the other by analyzing photoelectron intensities as a function of emission angle for each film thickness (Method 2). Our analyses were made with simple expressions that had been derived with the assumption that elastic-scattering effects were negligible. We found that EALs from both methods were systematically larger for the Theta Probe configuration, by amounts varying between 1 % and 5 %, than those for the sample-tilting configuration. These differences were attributed to anisotropy effects in the photoionization cross section that are expected to occur in the former configuration. Generally similar EALs were found by each method for each film material although larger EALs were found from Method 2 for film thicknesses less than 1.5 nm. SESSA is a useful tool for showing how elastic scattering of photoelectrons modifies EALs for particular materials, film thicknesses, and XPS configurations.

[1] <http://www.nist.gov/srd/nist100.cfm>.

[2] W. Smekal, W. S. M. Werner, and C. J. Powell, Surf. Interface Anal. 37, 1059 (2005).

10:40am **AS-MoM8 Valence Band XPS: A Valuable, but Underexploited, Tool for the Identification of Subtle Differences in Surface Chemistry**, *P.M.A. Sherwood*, Oklahoma State University
INVITED

Valence band X-ray photoelectron spectroscopy (XPS)¹ gives spectral features (peak positions and peak intensities) that arise from different physical principles than the core spectral region. This difference leads to the valence band region providing complimentary information to that of the core region. In many cases the valence band region can be used to detect subtle chemical differences that cannot be determined in core XPS studies. The value of using valence band XPS interpreted by calculation models will be demonstrated for various systems, and the use of core and valence band XPS for the study of buried interfaces will be discussed. Examples discussed will include the formation and study of thin (less than 100Å) oxide-free phosphate films, polymer films, composite surfaces, and the identification of different oxide films (including aluminum oxides) with similar chemical composition. Studies of shallow buried interfaces will be discussed. Recent work involving the preparation of hydroxyapatite films formed on metals which were coated with a thin oxide free film of metal etidronate will be reported. The metals studied were stainless steel and titanium. The key to adhesion of the hydroxyapatite films is the initial formation of a thin, oxide free, etidronate film on the metal. It was not found possible to prepare the hydroxyapatite films directly on the metal surfaces. Since hydroxyapatite is a key component of bone and teeth, it is likely that the coated metals will have desirable biocompatible properties, and that these treated metals may find applications in the production of medical implants.

¹P.M.A. Sherwood, "XPS Valence Bands", chapter in "Surface Analysis by Auger and X-ray Photoelectron

Spectroscopy" edited by D Briggs and J T Grant, SurfaceSpectra Ltd and IM Publications, Chapter 19, 531-555,

2003.

11:20am **AS-MoM10 Multitechnique Electron Spectroscopic Characterisation of Optoelectronic Devices**, *A.E. Wright, P. Mack, R.G. White, A. Bushell*, Thermo Fisher Scientific, UK

Optoelectronic devices, used for inter-conversion of light and electricity (e.g. photovoltaics and displays), depend upon careful optimisation of chemical, electronic and structural properties for efficient operation and useful operating lifetime.

Characterisation of such a device will typically identify the chemical bonding states, valence band positions, band gap and work function for each component. Lateral and depth resolution may be required to evaluate cell/pixel and multilayer structures.

Electron spectroscopic surface analysis techniques are ideal for the detailed analysis of the electronic structures of optoelectronic devices. Such techniques allow full quantitative characterisation of materials with chemical state and structural information. Surface specificity of spectroscopic information ensures that thin films can be analysed without interference from deeper parts of the sample. Multilayer structures may be studied with depth profiling techniques, and imaging functionality may be used to study cell or pixel structures.

The Thermo Scientific Escalab250Xi offers several such spectroscopic techniques, which have been employed in this study. X-ray Photoelectron Spectroscopy (XPS) offers surface-sensitive, quantified chemical state analysis and imaging capabilities. Ultraviolet Photoelectron Spectroscopy (UPS) allows measurement of valence band positions. Reflected Electron Energy Loss Spectroscopy (REELS) yields information on the electronic band gap and hydrogen content of a material. These techniques are combined for a thorough characterisation of the electronic structure of optoelectronic devices.

11:40am **AS-MoM11 Chemically Resolved Electrical Characterisation of Working Devices by XPS**, *S. Suzer*, Bilkent University, Turkey

A noncontact chemical and electrical measurement technique of XPS is performed to investigate a CdS based Photoresistor and a Si-Diode during their operation. The main aim of the technique is to trace chemical and location specified surface potential variations as shifts of the XPS peak positions under operating conditions. For the Photoresistor Cd3d and for the Diode (p-n junction) Si2p peaks positions have been recorded, respectively. The variations in the Cd3d peak without and under photoillumination with 4 different lasers is extracted to yield the location dependent resistance values, which are represented; (i) two dimensionally for line scans, and (ii) three dimensionally for area measurements. In both cases one of the dimensions is the binding energy. For the Si p-n junction the variations in the Si2p peak position under normal and reverse bias are recorded to differentiate and identify the nature of the doping (p- or n-). The main advantage of the technique is its ability to assess element-specific surface electrical potentials of devices under operation based on the energy deviation of core level peaks in surface domains/structures. Detection of the variations in electrical potentials and especially their responses to the energy of the illuminating source *in operando*, is also shown to be capable of detecting, locating, and identifying the chemical nature of structural and other types of defects.

MEMS and NEMS

Room: 10 - Session MN+AS-MoM

Characterization of Surfaces and Interfaces in MEMS and NEMS

Moderator: A.V. Sumant, Argonne National Laboratory

8:20am **MN+AS-MoM1 Probing Dynamical Surface and Interfacial Effects in High-Speed Nanoelectromechanical Systems (NEMS)**, *X.-L. Feng*, Case Western Reserve University
INVITED

Nanoelectromechanical systems (NEMS), especially vibrating or resonant-mode NEMS based upon advanced materials and new nanostructures, are emerging as attractive candidates for many nanoscale sensing and signal transduction technologies. Understanding and controlling various surface and interfacial effects in NEMS are important for engineering NEMS toward such goals. In this talk, we focus on using high-speed NEMS themselves as highly sensitive transducers for probing dynamical surface effects and interfacial behavior in these devices.

First, the behavior of physisorbed thin layers on solid surfaces is both interesting for fundamental studies and important for technological applications. For many solid-state devices, ranging from conventional commodity transducers to emerging miniaturized sensors, surface contaminants and adsorbates can be critical for the device performance. Recent advances in NEMS, particularly their excellent sensitivities, make it possible and to probe surface adsorbates and their behavior in the new regime – where a small number of adatoms can cause a detectable frequency shift for a NEMS resonator with a high quality factor (Q); and random fluctuations in the sub-monolayer adsorbates may result in variations of the NEMS resonance. We experimentally measure the frequency noise induced by fluctuations of adsorbed xenon (Xe) atoms on the surface of a very high frequency (VHF, ~200MHz), high- Q , SiC NEMS resonator. The measured adsorption spectrum and phase noise suggest interesting kinetics of Xe atoms on the surface. We further examine contributions from both surface diffusion and adsorption-desorption. The combined measurements and analyses not only demonstrate that surface

diffusion dominates the measured noise in the experimental regime, but also reveal new power laws of noise processes that may be important in various low-dimensional nanosystems.

Second, in NEMS devices with contacts and contact-mode operations, a lot of studies have to date yielded good intuitive understanding and empirical laws. For many new devices with genuinely nanoscale contacts, it has been highly desired but very challenging to understand these nanocontacts with greater details and with quantitative information. By combining experimental measurements and modeling, we explore the detailed electronic and nanomechanical characteristics in contact-mode NEMS with high-speed operations, with a focus on NEMS based on SiC nanowires and nanocantilevers.

9:00am MN+AS-MoM3 Fabrication of Nanomechanical Switch Based on Ultrananocrystalline Diamond Nanowire, A.V. Sumant, Argonne National Laboratory, K.J. Pérez Quintero, University of Puerto Rico, D.A. Czaplewski, Argonne National Laboratory

Fabrication of nanomechanical switches using various materials is being actively pursued over conventional solid state switch technology because of advantages of zero leakage current, ultra low power consumption and reasonable switching speeds reaching to 100 ns. Diamond is an ideal candidate material for nanomechanical switches due to high Young's modulus, moderate electrical conductivity when doped with boron or incorporated with nitrogen, high thermal conductivity and chemically inert nature. Recently, fabrication of nanomechanical switches in single crystal diamond has been demonstrated. However, batch fabrication of nanomechanical switches and their integration with complementary metal oxide semiconductor (CMOS) technology in bulk diamond is not feasible.

Ultrananocrystalline diamond (UNCD), originally developed at Argonne National Laboratory is an excellent candidate material for nanomechanical switches due to its high Young's modulus (comparable to single crystal diamond), semi-metallic conductivity when doped with boron or incorporated with nitrogen and because it is the only diamond film that can be deposited at temperatures as low as 400 °C, at wafer scale, with demonstrated integration with CMOS electronics [1]. We have previously fabricated horizontally aligned N-incorporated UNCD nanowires by a top down approach using Electron Beam Lithography (EBL) patterning and Reactive Ion Etching (RIE) processes [2] with nanowire lengths of 50-100 um and widths as small as 30 nm.

We demonstrate a fabrication of UNCD nanowire based switch with a movable source anchored at both ends. An immobile drain electrode is separated from the center of the source beam by a narrow gap. Two electrically connected gate electrodes are separated from the source by the gate gap, which is larger than the drain gap [3]. A UNCD layer was deposited on top of a sacrificial SiO₂ layer and covered with a SiO₂ layer that served as a hard mask for the RIE process. The UNCD layer represents the mechanical layer of the switch, the switch contacts and the gate electrodes. We aim to fabricate a reliable switch with fast switching times and low actuation voltages.

References:

- [1] Sumant *et al.* MRS Bulletin, 35, 281 (2010)
- [2] Wang *et al.* Nanotechnology, 23, 075301 (2012)
- [3] Czaplewski *et al.* Electronics Letters 45(11): 550 (2009)

9:20am MN+AS-MoM4 Carbon Nanotube Templated MEMS: Three Dimensional Microstructures in Semiconductors, Ceramics, and Metals, R.C. Davis, L. Barrett, R. Hansen, A. Konneker, D.D. Allred, B.D. Jensen, R. VanFleet, Brigham Young University

We discuss a materials breakthrough for MEMS. In contrast with conventional electromechanical devices, whose constituents are chosen from a vast range materials and alloys to optimize fabrication, performance and cost, MEMS have largely been made using the same materials and methods as those used in the silicon-based microelectronics industry. In order to make MEMS out of a much richer suite of materials, including metals, semiconductors, and ceramics, we have developed a process termed carbon nanotube templated microfabrication (CNT-M). In CNT-M we employ patterned, vertically aligned carbon nanotube forests as a three-dimensional microfabrication scaffold to create precise high-aspect-ratio (up to 200:1) microstructures. The "as grown" CNT forests are very low density (at 0.009 g/cc the forest is ~1% carbon and 99% air) and not useful as mechanical materials because they are extremely fragile, due to their low density and weak intratube bonding. However, when we replace the air spaces between tubes in the forest with a filler material by atomistic deposition, the infiltrated CNT framework becomes a robust microstructure consisting mostly of the filler material. Thus, by patterning the CNT microstructure and limiting the deposition of the filler material, CNT-M gives us control over structural features on both the nano and microscales (nanoscale porosity and microscale structure). We have used chemical

vapor deposition to infiltrate the CNT framework with semiconductors (Si) and ceramics (SiO₂, SiN_x, and nanocrystalline carbon) for applications in microactuation, sensing, and chemical separations. But many potential MEMS applications would benefit from structures fabricated from functional metals. We now report on the fabrication of metal microstructures using the CNT-M process. We demonstrate the versatility of this fabrication approach by demonstrating both chemical vapor infiltration (making tungsten and molybdenum structures) and electrodeposition (making nickel structures) based metal CNT-M processes. These metals provide several desirable materials properties to high aspect ratio MEMS applications including high electrical and thermal conductivity, high melting temperatures, resistance to corrosion, low thermal expansion, high Young's modulus, hardness and yield strength. Electrical, mechanical, and structural characterization of the microfabricated metal structures will also be presented.

9:40am MN+AS-MoM5 Filling through Silicon vias with a Carbon Nanotube/Copper Matrix, M.B. Jordan, M. Rao, The University of Alabama, A.V. Sumant, R.S. Divan, Argonne National Laboratory, S.L. Burkett, The University of Alabama

The performance of through silicon vias (TSVs) depends on the material used to fill them. Copper and tungsten are two conventional metals used to fill TSVs. Recently carbon nanotubes (CNTs) have been considered as a filling material due to their superior material properties. CNT bundles can allow ballistic transport of electrons resulting in low resistivity and enabling them to carry a larger current density. CNT bundles also have a high Young's modulus, low coefficient of thermal expansion, and a high thermal conductivity. These properties make CNTs appealing for use as power delivery systems and as heat sinks. Protecting the CNTs after growth and making electrical contact to them remains a challenge. We have investigated a hybrid CNT/Cu TSV structure as a possible solution to these problems. Blind vias were formed using a cryogenic inductively coupled plasma (ICP) etch process. A copper seed layer was sputtered on the via base and along the sidewalls. The vias were filled using a periodic reverse pulse electroplating technique to reduce voids in the high-aspect ratio structures. The center region of the copper filled vias were then etched by ion milling. The growth of CNT bundles in the center of the copper filled vias was done by thermal chemical vapor deposition (CVD). Electron-beam evaporated Fe serves as a catalyst for CNT growth.

Use of the Center for Nanoscale Materials at Argonne National Lab was supported by the U. S. Department of Energy, Office of Science, Office of Basic Energy Sciences, under Contract No. DE-AC02-06CH11357.

10:00am MN+AS-MoM6 Optimization of STiGer Process used to Etch High Aspect Ratio Silicon Microstructures, T. Tillocher, P. Lefaucheur, GREMI CNRS/Université d'Orléans, France, J. Ladroue, M. Boufnichel, ST Microelectronics, Tours, France, P. Ranson, R. Dussart, GREMI CNRS/Université d'Orléans, France

The STiGer process, which can be used in MEMS fabrication, is a time-multiplexed cryogenic process designed to etch deep anisotropic features in silicon: passivation and etching plasmas are cycled to get vertical structures. The passivation layer is a SiO_xF_y film which requires cryogenic substrate temperature conditions to grow. It desorbs and disappears when the substrate is heated back to room temperature. This is an advantage since no extra cleaning steps are required. Additionally, with the benefit of the periodic passivation cycles, this process is less sensitive to temperature or flow rate variations than standard cryoetching. This enhanced passivation helps to reduce undercut as well. Nevertheless, like in Bosch etching, the alternations induce a scalloping on the sidewalls.

We have already shown that trenches having critical aperture of about 0.8 μm can be etched with high aspect ratios (> 40). We have highlighted a defect called "extended scalloping", which is composed of anisotropic cavities developed on the feature sidewalls, just below the mask. It originates from ions scattered at the feature entrance that hit the top profile and remove locally the passivation layer. This defect is observed for aspect ratios higher than 10. Consequently, large structures, with openings larger than 100 μm, etched to a few hundred of μm show no extended scalloping.

We have proposed two methods that can help to reduce this defect. The first consists in adding a low oxygen flow in the etch cycle, favouring a low additional passivation. The second technique consists in gradually increasing the SF₆ flow, in the etching steps, during the first minutes of the recipe. Consequently, the process starts with a low etch rate and a more efficient passivation, which helps to limit the extended scalloping. These two techniques efficiently reduce the defects but the profiles tend to be always positive. It seems impossible to get at the same time vertical sidewalls and low defects.

We will present other ways to fix this problem. For example, we are currently investigating processes running at -50°C instead of usual

cryogenic temperatures (-100°C). This aims to have a more conformal passivation layer, which may prevent the initiation of the extended scalloping. Additionally, this range of substrate temperatures is of interest since it can be reached with chillers and thus, liquid nitrogen is no longer required.

Finally, we will present our results on downscaled structures. We have designed a mask with e-beam lithography comprising 200 nm to 800 nm wide trenches. It is used to evaluate the performances of the STiGer process on submicron structures.

11:00am MN+AS-MoM9 The Effect of Back-action Force for the Electron Tunneling Transduction in MEMS Measurement, M.R. Kan, University of Alberta, Canada, **Z. Diao,** National Institute for Nanotechnology, NRC Canada, **V.T.K. Sauer, M.R. Freeman,** University of Alberta, Canada, **W.K. Hiebert,** National Institute for Nanotechnology, NRC Canada

Nano-electromechanical systems (NEMS) have exciting potential for fields ranging from quantum measurement science to ultrasensitive mass detection. For many of these applications, a key challenge is implementing a fast, reliable, low-noise technique for translating small mechanical motion to electronic signals. Electron tunneling transduction based on quantum tunneling is a promising technique to measure small displacements, because the tunneling current is so sensitive to the change in distance between the probing tip and the sample surface (one angstrom distance change causes 7 times tunneling current change). With frequency downmixing, the bandwidth limitation associated with the large RC time constant in the circuits can be overcome; very high frequencies may become accessible, fundamentally limited only by the tunneling rate I_T/e in the GHz range.

Using electron tunneling to sense nanomechanical motion comes with an inherent risk of back-action of the sensing probe (STM tip) on the mechanical device. The local tip-sample energy gradients introduce spring forces that can produce sizable shifts in resonance frequencies and may also affect sample quality factors. Understanding these effects is important for reliable use of downmixed tunneling transduction. Controlling them will allow for novel methods of MEMS and NEMS tuning of both frequency and quality factor.

In this presentation, we will report our observation of back-action forces on MEMS devices during downmixed electron tunneling transduction. We explore differences in the magnitude of the back-action force for different flexural and torsional vibrational modes (with varying degrees of inherent stiffness). We also discuss the perturbation to device quality factors. Finally, the vibration of the back-action force as a function of tip-sample distance is investigated.

11:20am MN+AS-MoM10 Electric-Stimulus-Responsive Pluronic Hydrogels as Actuators, L. Engel, I. Sokolov, O. Berkh, Tel Aviv University, Israel, **K. Adesanya, E. Vanderleyden, P. Dubruel,** Ghent University, Belgium, **J. Shklovsky, I. Harari, Y. Shacham-Diamand, S. Krylov,** Tel Aviv University, Israel

Due to their unique mechanical and chemical characteristics, stimuli responsive hydrogels have garnered much interest in the field of biomedics. They perform dramatic volume transitions in response to external environmental stimuli such as pH and ionic strength of the solvent, temperature, and electrical field. Their soft elastomeric nature, serves to minimize mechanical and frictional irritation to the tissue bed, suggesting applications in artificial muscles and biomimetics, and their swelling capacity results in high permeabilities for certain drug molecules and metabolites making them ideal materials for drug delivery. Because the swelling rate of a hydrogel is inversely related to its size, MEMS offers a unique opportunity to exploit the capabilities of responsive hydrogels by minimizing actuator response time. While it is known that hydrogels with fixed charge groups deform when subjected to an externally applied electric field inside an electrolyte bath, the exact mechanism responsible for the deformation continues to be debated.

In this work, we have investigated the volume transformation of Pluronic based electroactive hydrogels immersed in a Krebs bathing solution under an applied electric field. The swelling characteristics of the crosslinked hydrogels were investigated and a model based on finite element analysis is proposed. Bias was applied via parallel Pt electrodes and the distance between the electrodes was varied as was the ionic concentration and pH of the solution inside the testing tank. The feasibility of using an array of interdigitated electrodes fabricated on a printed circuit board as a means of actuation hydrogel was demonstrated with the goal of downsizing the hydrogel electrical-stimulation system for the creation of MEMS electro-responsive hydrogel actuators.

11:40am MN+AS-MoM11 CMOS MEMS Metal-based Tactile Sensors Development, Y.C. Lin, C.J. Hsieh, L.B. Wang, J.C. Liou, W.-C. Tian, National Taiwan University, Taiwan, Republic of China

A CMOS MEMS tactile sensor using a pure metal-based structure by a special etchant (Silox Vapox III) to remove oxide sacrificial layers was developed. The tactile sensor was fabricated through a commercial 0.35mm 2 polysilicon and 4 metal CMOS technology followed by the self-developed post processes. In order to increase the effective gap between two electrodes, the tactile sensor used oxide as the sacrificial layer to replace the conventional metal sacrificial layer. Moreover, the CMOS MEMS-based tactile sensors provides the advantages such as lower cost, small size, compatible with the integrated circuits, and mass-production compared to other types of tactile sensors.

Two different capacitive-based tactile sensor designs, parallel-plate type and vertical-comb-drive type, were proposed in this work. A boss-structure was implemented to provide the uniformity of the membrane displacement during the device operation. The dynamic range of the sensor detection was targeted from 0 to 200 mmHg according to the human vessel pressure. The capacitance variation was measured and analyzed via an integrated circuit board, the arduino board, and an A/D IC, AD7746. The readout circuit module reduced the noise and improved the sensor accuracy to 4fF and the resolution down to 4 aF. The sensitivity of the parallel-plate type is measured to be 1.39 fF/mmHg which is suitable for the blood flow monitoring. More characterizations on the vertical-comb-drive type sensors will be presented.

Nanomanufacturing Science and Technology Focus Topic

Room: 16 - Session NM+AS+MS-MoM

Metrology and Environmental Issues in Nanomanufacturing

Moderator: N.A. Burnham, Worcester Polytechnic Institute, **L.J. Gamble,** University of Washington

8:20am NM+AS+MS-MoM1 Nanomanufacturing – Beyond Silicon, J.A. Liddle, National Institute of Standards and Technology **INVITED**

The fabrication of integrated circuits in silicon is the preeminent nanomanufacturing technology, and it occupies a very special niche in terms of functionality and value provided per unit area. As a consequence, it is economically viable to use very expensive fabrication processes to generate the required nanostructures. In addition, the degree of control over the manufacturing process that is required necessitates the use of complex and expensive metrology systems. In contrast the vast majority of other nanotechnology products cannot support the cost of comparably sophisticated manufacturing methods or the associated metrology schemes. In this talk I will give examples of how the complexity of the final product and its value dictate what type of nanomanufacturing approach is viable. In particular, I will describe the need for new metrology techniques that can provide nanoscale information, but do so at rates consistent with the high-volume manufacturing of low-cost products.

9:00am NM+AS+MS-MoM3 Use of Mueller Matrix – Spectroscopic Ellipsometry for Scatterometry based Measurement of Critical Dimensions during Semiconductor Manufacturing, G.R. Muthini, A.C. Diebold, University at Albany-SUNY, **B. Peterson,** Nanometrics Inc.

Scatterometry is one of the most useful metrology methods for the characterization and control of critical dimensions (CD) during nanoelectronic manufacturing. Most Scatterometry is based on Spectroscopic Ellipsometry (SE) and Normal Incidence Reflectometry (NI) measurement and the simulation of the measured spectra through the Rigorous Coupled Wave Approximation. Evolution of better optical hardware and faster computing capabilities led to the development of Mueller Matrix (MM) based Scatterometry (MMS). Typically, spectroscopic ellipsometry based Scatterometry uses Y the D measured at each wavelength. In this presentation we discuss dimensional metrology using full Mueller Matrix (16 element) Scatterometry in the wavelength range of 245nm-1000nm measured using a dual rotating compensator spectroscopic ellipsometer. Unlike SE and NI, MM data provides complete information about the optical reflection and transmission of polarized light through a sample. The advantage of MMSE over traditional SE Scatterometry is its ability to measure samples that have anisotropic optical properties and depolarize light. We demonstrate this using a series of structures fabricated by e-beam lithography.

9:20am **NM+AS+MS-MoM4 Atomic Layer Deposition Monitored and Characterized by Joint *In Situ* Real-Time Spectroscopic Ellipsometry and Direct Surface Analysis**, M. Junige, M. Geidel, M. Knaut, M. Albert, J.W. Bartha, Technische Universität Dresden, Germany

Atomic layer deposition (ALD) is a special kind of chemical vapor deposition, which pulses at least two chemical reactants into a vacuum reactor alternately and separated by purging steps. ALD has emerged as a powerful technique for the conformal and uniform coating of complex three-dimensional structures, even on large-sized substrates. Accordingly, ALD has a high potential for application throughout the entire field of nanotechnology.[1]

Since ALD alters the physical and chemical properties of a surface during a material's deposition, these changes are observable by direct surface analysis techniques like photoelectron spectroscopy (PES) or scanning probe microscopy (SPM) and also by spectroscopic ellipsometry (SE). As previously described in the References [2] - [4], we acquired ellipsometric spectra *in situ* and in real-time and thus monitored the ALD processes at exactly the place and the time of a sample's modification. In addition, we conducted PES as well as SPM measurements without breaking a high vacuum after the ALD. This revealed, among others, the chemical composition as well as the roughness of a coated surface without alteration in air and so enabled the generation of appropriate optical models, which translate the ellipsometric spectra into rather descriptive quantities like a film thickness or a surface roughness.

In the present work, we will demonstrate the capability of joint *in-situ* real-time SE and direct surface analysis based on the ALD of two exemplary materials: tantalum nitride and ruthenium. In the linear homogeneous film growth regime of both the ALD processes, the film thickness increment per cycle (also growth per cycle, GPC) was quantified and studied for varying process parameter sets. The initial ALD growth of TaN showed all the three possible growth modes according to Puurunen [5] depending on the starting substrate material. In the case of Ru, the ALD growth initiation indicated a substrate-inhibited island growth mode irrespective of the starting substrate.

[1] G. N. Parsons, S. M. George, and M. Knez, in *MRS Bulletin* **36**, 865 (2011).

[2] M. Junige, M. Geidel, M. Knaut, M. Albert, J. W. Bartha, in *IEEE 2011 Semiconductor Conference Dresden* (Dresden, 2011). – DOI: 10.1109/SCD.2011.6068739

[3] M. Knaut, M. Junige, M. Albert, J. W. Bartha, *J. Vac. Sci. Technol. A* **30**, 01A151 (2012).

[4] M. Geidel, M. Junige, M. Albert, J. W. Bartha: In-situ analysis on the initial growth of ultra-tin ruthenium films with atomic layer deposition, *Microelectron. Eng.* (manuscript submitted).

[5] R. L. Puurunen, *J. Appl. Phys.* **97**, 121301 (2005).

10:40am **NM+AS+MS-MoM8 Transformation of Engineered Nanomaterials in the Environment: Effects of Size, Shape and Morphology on Nanomaterial Toxicity**, S. Obare, Western Michigan University

INVITED

Engineered nanomaterials (ENMs) are known to possess unique size and shape dependent chemical and physical properties. As a result of their properties, ENMs have been effective in several important applications including catalysis, sensor design, photonics, electronics, medicine, and the environmental remediation of toxic pollutants. Such properties and applications have led to an increase in the manufacture of ENMs and a rise in their presence in consumer products. The increase of ENMs in consumer products presents several opportunities and challenges, and necessitates a proactive study of their health and safety. An important and essential criterion toward a systematic study of the environmental safety of ENMs is the need to control their size, shape and morphology, and to produce them in high quantities. Synthetic procedures that produce gram-scale, well defined and monodisperse metallic nanoparticles with controlled size and shape, is not trivial and requires careful control of reaction conditions. This presentation will demonstrate our ability to develop new organic ligands that when used as stabilizers for metal nanoparticles, provide the ability to gain control of the particle size in one-step synthetic procedures. Monodisperse metallic nanoparticles were synthesized and characterized using spectroscopic, microscopic and x-ray techniques. The chemical composition, surface reactivity, solubility, and aggregation tendency of ENMs were studied under various environmental conditions. We will also discuss how ENMs interact with various components in the environment with an emphasis of their interaction with Gram-negative and Gram-positive bacteria. The results provide insights on the need for green manufacturing strategies of ENMs, their use and safe disposal practices.

11:20am **NM+AS+MS-MoM10 An Integrated Approach Toward Understanding the Environmental Fate, Transport, Toxicity and Occupational Health Hazards of Nanomaterials**, V. Grassian, University of Iowa

INVITED

Nanoparticles, the primary building blocks of many nanomaterials, may become suspended in air or get into water systems, e.g. drinking water systems, ground water systems, estuaries and lakes etc. Therefore, manufactured nanoparticles can become a component of the air we breathe or the water we drink. One important issue in understanding the environmental fate, transport, toxicity and occupational health hazards of nanoparticles is in characterizing the nature and state of nanoparticles in air, water or *in vivo*. For the nanoparticles of interest in these studies, metals and metal oxides, it can be asked: (i) will metal oxide and metal nanoparticles be present in air or water as isolated particles or in the form of aggregates? (ii) will metal oxide and metal nanoparticles dissolve in aqueous solution or *in vivo*? and (iii) under what conditions will metal oxide and metal nanoparticles aggregate or dissolve? As the size regime will be very different depending on the state of the nanoparticles, as dissolved ions, isolated nanoparticles or nanoparticle aggregates, these questions are important to address as it impacts the size regime that needs to be considered or modeled in for example environmental transport or lung deposition models. Furthermore, the effect on biological systems including nanoparticle-biological interactions and toxicity will depend on the state of nanoparticles. In the studies discussed here, macroscopic and molecular-based probes that includes quantitative solution phase adsorption measurements, molecular based probes, light scattering and zeta-potential measurements to investigate the behavior of nanoparticles in aqueous suspensions. We have focused on several different metal and metal oxide nanoparticles including Fe, Ag, Zn, Cu, Ce and Ti. Some of our newest results which focus on aggregation and dissolution, including detailed size-dependent studies, in the presence and absence of organic acids will be discussed. This research is beneficial as it significantly contributes to the growing database as to the potential environmental and health implications of nanoscience and nanotechnology and how nanomaterials will behave in the environment and impact human health.

Monday Afternoon, October 29, 2012

Applied Surface Science
Room: 20 - Session AS-MoA

Quantitative Surface Chemical Analysis, Technique Development, and Data Interpretation - Part 2

Moderator: J.A. Ohlhausen, Sandia National Laboratories, S. Suzer, Bilkent University, Turkey

2:00pm **AS-MoA1 Polyatomic and Gas Cluster Ion Beam Depth-Profiling: A Model Indicating the Most Appropriate Source for an Arbitrary, Known Polymer Matrix and Estimates of Polymer Sputter Rates**, *P.J. Cumpson, N. Sano*, NEXUS XPS Facility, Newcastle University, UK

There has been excellent progress in the SIMS community in recent years[1,2] to identify the optimum conditions and primary ions for SIMS depth-profiling of polymers. A key step forward was the identification of Type I and Type II behaviour[3], in which polymer damage is dominated by cross-linking and polymer backbone bond-scission respectively. In many cases it is difficult, especially for a non-expert, to judge which of these two types a given polymer matrix is likely to be. For example, PAA, PMAA, PMA and PMMA are of types I, II, I and II respectively, even though their structures are very similar.

We examine this system in detail, largely in the context of XPS where polyatomic and cluster ion sources are set to become much more popular. We develop equations based on a 3D Ising "resistor removal" model. Some of the difficult parameters in this model can be estimated from literature values for rates of cross-linking and bond scission of polymers seen in radiation treatment at much higher energies. This model leads to some reasonably simple equations allowing analysts to make objective estimates of (a) which primary ion source is most appropriate for a particular polymer matrix, and (b) an estimate of the sputter-rate, for any arbitrary polymer matrix whose repeat unit is known.

The reliability of the model is tested using measured sputter rates for samples of 20 polymers using polyatomic (coronene) and GCIB (argon cluster) sources. White-light interferometry combined with a novel kinematic mount for semi-automatic measurement of sputter crater volume have accelerated and improved the accuracy of these measurements.

Finally, based on the new model, we tabulate and plot estimated values for 103 polymers of technological significance.

[1] N. Winograd, *Anal Chem* 77 (2005) 143A

[2] J. S. Fletcher, X. A. Conlan, E. A. Jones, G. Biddulph, N. P. Lockyer, J. C. Vickerman, *Anal Chem* 78 (2006) 1827

[3] C. M. Mahoney, *Mass Spectrometry Reviews*, 29 (2010) 247

2:20pm **AS-MoA2 XPS Profiling of Biosensor Materials with Argon Cluster Ions**, *P. Mack, R.G. White, T.S. Nunnery*, Thermo Fisher Scientific, UK, *J.J. Pireaux, P. Louette, N. Wehbe, L. Houssiau*, FUNDP, Namur, Belgium

Sensors for biological compounds are becoming increasingly important in a wide variety of applications. These devices are typically composed of complex stacks of thin/ultrathin layers of biochemical compounds. The overall behaviour of the sensor is strongly influenced by the elemental and chemical properties of the individual layers, but the interactions at layer interfaces may also have an effect.

There is an increasing requirement for compositional profiling of these devices, combining the chemical selectivity and surface specificity of XPS with some kind of ion beam sputtering. Traditional methods such as argon monomer ion profiling can result in a high degree of chemical modification during the acquisition of depth profiles for organic materials. Over the last few years, there have been numerous studies and investigations into the use of argon cluster beams for depth profiling with the goal of preserving chemical information during analysis of organic materials.

This talk will present data from cluster profiling studies of amino acid based biosensors. The chemical variation between amino acid layers is very subtle, but it will be demonstrated that the combination of rapid acquisition XPS and argon cluster profiling is able to characterise the changes in chemistry throughout the layer stack.

2:40pm **AS-MoA3 ToF-SIMS and NanoSIMS Imaging of Uranium Distributions in the Sediment of Hanford Site**, *Z. Zhu, Z. Wang*, Pacific Northwest National Laboratory

Nuclear materials processing over the past seventy years has left approximately 55 million gallons of nuclear wastes stored in underground tanks at Hanford site. Some of these wastes are leaking into the ground and the DOE has been working on developing remediation technologies. As a part of these activities, sediment samples have been extensively studied to understand chemical speciation and aqueous mineral chemistry. Although concentrations and distributions of radioactive elements, such as uranium (U), plutonium (Pu), and technetium (Tc) are of great interest, U is the most important one because its concentration in the wastes is significantly higher compared to other radioactive elements. Previous studies show that the sediment samples contain low concentration of U (<10 ppm). However, non-uniform distribution of U is found, and the U appears to be mainly in micron- or sub-micron-size particles. Although an understanding of the chemistry and speciation of these particles is important, it is extremely difficult to obtain the composition of these particles using conventional analytical capabilities such as AES, XPS, and SEM/EDX because of the low concentration of U in the samples. Secondary ion mass spectrometry (SIMS) can be effectively used to discover the chemical components of these U-containing particles with excellent sensitivity and decent spatial resolution. We used ToF-SIMS and Nano-SIMS to image some of these U-containing particles in the sediment samples. Preliminary results indicated that U was present across the sample at lower concentrations, while spots of sub-micron particles with much higher U concentrations were irregularly distributed. The major elements in these "hot" spots appeared to be uranium, sodium, phosphorus, and oxygen.

3:00pm **AS-MoA4 ToF-SIMS MCs_x^+ Dual Beam Depth Profiling with Improved Dynamic Range**, *S. Kayser*, ION-TOF GmbH, Germany, *N. Havercroft*, ION-TOF USA, Inc., *F. Kollmer, R. Moellers, E. Niehuis*, ION-TOF GmbH, Germany

In recent years MCs_x^+ depth profiling has become increasingly popular for the analysis of thin films using Time-of-Flight SIMS (ToF-SIMS). The MCs_x^+ mode offers quantitative or semi-quantitative SIMS data and allows for the measurement of electropositive and electronegative elements simultaneously by detecting MCs_x^+ and MCs_x^+ , respectively. In addition, the use of heavy cluster ions like Bi_3^+ or C_{60}^+ allows for a significant increase of the MCs_x^+ yields by a factor of up to 1000 with respect to Ga as primary ion projectile and leads to a remarkable improvement of the achievable detection limits [1].

However, one disadvantage of current TOF-SIMS instruments for the quantification in MCs_x^+ mode is the limited dynamic range, which restricts the possibility of achieving high sensitivity on the MCs_x^+ clusters and of using the Cs_x^+ intensity for normalization. The normalization is especially important for the analysis of layer systems where sputter rates or the cesium surface concentration might change from layer to layer. This requires a registration system which is able to detect more than 100 secondary ions of a specific element per primary ion gun pulse with high linearity.

We have developed a new registration system for TOF-SIMS, which increases the useable dynamic range by a factor of 100 i. e. 1E7 counts/sec with an excellent linearity. In addition, the maximum pulsed primary ion current of the bismuth liquid metal ion gun was increased in order to further improve the detection limits for low concentration elements. In this paper we will discuss the characteristics of this new experimental setup and the benefits for the quantitative depth profiling in the MCs_x^+ mode.

[1] E. Niehuis, T. Grehl, F. Kollmer, R. Moellers, D. Rading, SIMS Europe, Muenster, 2006

3:40pm **AS-MoA6 Surface Diffusion of Carbon on Metals and Complications for Auger Spectroscopy of Carburized Steels**, *W.D. Jennings*, Case Western Reserve University **INVITED**

The development of low temperature colossal super saturation of stainless steels produces carburized case hardened materials with superior corrosion resistance and mechanical properties. Auger characterization of these materials requires line scan analysis of steel cases that contain substantial carbon concentration. Long acquisition times and surface migration of contaminating carbon complicate the measurement process, and lead to the need for continuous ion sputtering during acquisition of Auger spectra. This process in turn leads to the further complication of differential sputtering effects which alter the apparent composition of the material. This study details the corrections to the Auger relative sensitivity factors needed to achieve accurate characterization of these materials. Fundamental measurements of carbon surface diffusion are also presented.

4:20pm AS-MoA8 Charge Referencing Complex Organic Materials in XPS using Hexatriacontane, L. Lohstreter, Medtronic, Inc.

Excess charge build up on insulators can obscure interesting chemical shifts during XPS analysis. The common practice to correct for this is to charge reference the C1s peak of organic materials to 285 eV, the C-C, C-H bond that is ubiquitous due to atmospheric hydrocarbon contamination. However, for samples with complex organic chemistry, it is often the very information within the C1s envelope that is in question. Moreover, the peak can be convoluted with no distinct shoulders. This makes shifting the maximum of the peak to 285 eV a dubious process with little assurance that it will correlate to the true chemistry of an unknown sample. This work will show that even unknown, complex C1s envelopes can be accurately charge referenced with a combination of an application of hexatriacontane to the surface and spectral subtraction. Applications in model material characterization and plasma treated surfaces will be discussed.

4:40pm AS-MoA9 PADI: Ambient Surface Analysis of Polymers and Molecules – Metrology Development for Reliable Analysis, T.L. Salter, I.S. Gilmore, National Physical Laboratory, UK

Reliable and repeatable measurements are essential for the strong uptake of any analytical technique. Ambient surface mass spectrometry has demonstrated exciting and revolutionary measurement capability but for wider acceptance in industry they need a secure metrology foundation. Plasma sources are increasingly being used since the development of DART (direct analysis in real time) in 2005¹ and subsequent imaging methods such as PADI (plasma assisted desorption ionisation)² and LTP (low temperature plasma)³. Here, we commence establishing the essential metrology for PADI, which has already been shown to be successful at analysing pharmaceuticals² and personal care products⁴. A detailed study of the instrumental contributions to the spectral repeatability is conducted. Firstly, we identify and separate out the contributions to the repeatability (relative standard deviation) of the peak intensities. We show that the Thermo LTQ-Orbitrap mass spectrometer used in the study has a noise distribution approximately as expected for random noise. However, the standard deviation of the peak intensity is proportional to the peak intensity which is clearly not random but related to systematic effects in the source operation. Optimisation of the plasma source is essential for ensuring robustness and reliability. We show how the signal varies with geometry, helium flow rate and plasma power. Thermal imaging of the sample surface shows that the temperature rises approximately linearly with plasma power and at 19 W is 70°C. To reduce the effects of damage for surface sampling, we recommend keeping the surface temperature below 40 °C by operating at less than 15 W. General guidance is given for practical analysis. Importantly, PADI can analyse a wide variety of polymers. Analysis of polymers gives mass spectra with repeating series containing different fragments and adducts. Preliminary studies of sample surfaces after PADI analysis show that the chemical damage, quantified by XPS, is less than 10%. With the recommended operating parameters, the plasma erodes the polymer sample at a rate of 0.87 nm s⁻¹ (for PMMA). This shows the potential for polymer depth profiling.

References

1. RB Cody, JA Laramée, HD Durst, *Analytical Chemistry* **2005**, *77*, 2297.
2. LV Ratcliffe, FJM Rutten, DA Barrett, T Whitmore, D Seymour, C Greenwood, Y Aranda-Gonzalvo, S Robinson, M McCoustra, M. *Analytical Chemistry* **2007**, *79*, 6094.
3. JD Harper, NA Charipar, CC Mulligan, XR Zhang, RG Cooks, Z Ouyang, *Analytical Chemistry* **2008**, *80*, 9097.
4. TL Salter, FM Green, N Faruqi, IS Gilmore, *Analyst*, 2011, *136*, 3274.

5:00pm AS-MoA10 Ion Beam Analysis of Surfaces and Thin Films, L.S. Wielunski, R.A. Bartynski, Rutgers University

Rutherford Backscattering (RBS) of ~2MeV He ions is well known technique used in surface and thin film analysis. This technique is very sensitive to heavy elements (Au, Pt, Hf, In, Ru) present on surface or in thin film on lower mass substrate (Si, Ti, Cr, Fe, Ge), but have very limited sensitivity for low mass elements on heavy mass substrates. Numbers of examples will be shown for both cases.

Nuclear reaction analysis (NRA) is very good alternative for detection of low mass elements in a heavy elements substrates. This technique uses similar experimental set-up as RBS but is using a different ion beam and it detects different particle. Examples will be shown for Li detection on steel and in LiFePO₄ crystal.

Detection of Hydrogen is not possible using RBS in a typical RBS geometry, and NRA can detect Hydrogen, but it require special high energy ¹⁵N beam (7MeV), but He Forward Scattering (FS) or Elastic Recoil Detection (ERD) can be used for Hydrogen detection and profiling. Examples of ERD will be shown and discussed.

Each of these techniques has its own limitations and advantages. Depth resolution and sensitivity will be discussed in details.

**Spectroscopic Ellipsometry Focus Topic
Room: 19 - Session EL+TF+BI+AS+EM+SS-MoA**

Spectroscopic Ellipsometry: From Organic and Biological Systems to Inorganic Thin Films

Moderator: M.S. Wagner, The Procter & Gamble Company

2:00pm EL+TF+BI+AS+EM+SS-MoA1 Biochemical Optical Sensors Based on Highly-Ordered Slanted Columnar Thin Films, D. Schmidt, K.B. Rodenhausen, University of Nebraska-Lincoln, J. VanDerslice, T.E. Tiwald, J.A. Woollam Co., Inc., E. Schubert, M. Schubert, University of Nebraska-Lincoln

Highly-ordered three-dimensional nanostructure thin films offer substantially increased surface area for attachment of organic layers, and in addition, new detection principles due to the physical properties of the nanostructures. For example, upon material attachment the optical birefringence of the nanostructures changes due to screening of polarization charges. Because of these advantages, highly-ordered three-dimensional nanostructure thin films lend themselves as suitable candidates for studying of organic attachments as well as for low-cost humidity sensing, for example.

We utilize glancing angle electron-beam deposition for fabrication of highly spatially coherent metal slanted columnar thin films. Subsequently, the nanostructures may be further functionalized with thin conformal coatings by means of atomic layer deposition. The ellipsometry model analysis and resulting anisotropic optical properties of hybrid metal slanted columnar thin films determined by generalized spectroscopic ellipsometry in the visible and near-infrared spectral region will be discussed. We will be reviewing research in this area and report in particular on in-situ monitoring of organic attachments using ellipsometry combined with quartz crystal microbalance with dissipation. Exemplarily, we discuss studies of fibronectin protein adsorption, octanethiol chemisorption (self-assembled monolayer growth) on platinum coated titanium slanted columnar thin films as well as relative humidity sensing.

2:20pm EL+TF+BI+AS+EM+SS-MoA2 Studies of Optical Properties of Hybrid J-aggregates and Nanocrystal Quantum Dots Layers for Photonic Applications, K. Roodenko, H.M. Nguyen, L. Caillard, A. Radja, O. Seitz, Yu.N. Gartstein, A.V. Malko, Y.J. Chabal, The University of Texas at Dallas

The integration of organic materials and inorganic nanocrystal quantum dots (NQDs) on the nanoscale offers the possibility of developing new photonic devices that utilize the concept of resonant energy transfer between an organic material and NQDs. Electromagnetic coupling that takes place between excitons—bound electron-hole pairs—at the interfaces of the hybrid composite can be utilized for light-emitting, photovoltaic and sensor applications.

As the key ingredients for the nanocomposite material system reported in this work are the J-aggregates (JA, dye self-assembled molecules) that have exceptional optical absorption due to their strong oscillator strength. NQDs on the other hand combine a variety of important properties, such as high quantum yields, excellent photo- and chemical stability, and size dependent, tunable absorption and emission. Excitation energy transfer in NQDs / J-aggregate hybrids is characterized by their strong excitonic transitions at room temperature with spectrally well-defined absorption and emission.

In order to understand the energy transfer mechanisms in such complex systems, optical properties of JA and NQDs/JA hybrid systems were characterized by means of spectroscopic ellipsometry and polarized IR spectroscopy.

Spectroscopic ellipsometry in 0.6-5 eV spectral range was employed to study optical properties of J-aggregates drop-casted on silicon surfaces. Thin JA films were found to exhibit strong optical anisotropy due to the specific molecular orientation of thin layers on Si substrates. Variation of optical properties due to the deposition of nanocrystal quantum dots (NQDs) was systematically studied for applications in new photonic devices that utilize excitonic energy transfer from NQDs to JA layer. Ellipsometric results were cross-referenced with atomic force microscopy (AFM) data to derive a quantitative understanding of the distribution of NQDs upon deposition on JA layer. Integration of hybrid colloidal NQD/JA structures could be potentially attractive for a range of optoelectronic applications.

2:40pm **EL+TF+BI+AS+EM+SS-MoA3 Love and Death, the Story of Most Proteins and Most Surfaces as Told by Spectroscopic Ellipsometry.** *T. Benavidez, K. Chumbuni-Torres, J.L. Felhofer, C.D. Garcia*, The University of Texas at San Antonio

INVITED

Biosensors are analytical platforms that integrate a biological recognition element with a signal transducer. Because they have the potential to provide rapid, real-time, and accurate results, biosensors have become powerful tools in clinical and biochemical settings. Our group is particularly interested in the development of electrochemical biosensors based on enzymes adsorbed to nanomaterials. When integrated to microfluidic devices, these sensors offer sensitivity, portability, low cost, and the possibility of analyzing turbid samples. Adsorption was selected to immobilize the biorecognition element because it is one of the simplest and most benign methods, avoiding cross-linking reactions or additional components (such as entrapping polymers). Most importantly, as adsorption is a required (and sometimes limiting) step for any immobilization mechanism, the identification of key variables influencing this process can be applied to a variety of strategies. Although several techniques have been used to study the adsorption of proteins to nanomaterials,¹ only a few of them provide information about the kinetics of the process in real time. This is a critical aspect, as most of the post-adsorption conformational changes occur within a few minutes after the interaction.² Among those, reflectometry was used by our group to perform the first kinetic study related to the interaction of proteins with carbon nanotubes.³ These kinetic studies have been recently extended to the interaction of enzymes (D-amino acid oxidase,⁴ catalase,⁵ and glucose oxidase⁶) by variable angle spectroscopic ellipsometry, which enabled a more thorough analysis of the interaction process with a much more versatile experimental design.^{7,8} The use of VASE demonstrated that a number of variables, (being the amount of enzyme only one of them) can influence the biological activity of proteins adsorbed to the substrate. Furthermore, our results indicate that the activity of enzymes adsorbed to nanomaterials can be directly related to the kinetics of the adsorption process (dG/dt).⁵

Please see supplemental document for figures and footnotes.

3:40pm **EL+TF+BI+AS+EM+SS-MoA6 Detailed Photoresist and Photoresist Processing Studies using Spectroscopic Ellipsometry.** *C. Henderson*, Georgia Institute of Technology

INVITED

Spectroscopic ellipsometry has become an invaluable tool for the study of a wide variety of thin film systems. In particular, it has become extremely valuable in the development and study of advanced photoresists and of lithographic processes used in the production of integrated circuits and other related semiconductor devices. In our work, we have used spectroscopic ellipsometry to study a variety of problems related to photoresists including swelling phenomena, exposure induced refractive index changes, and ultra-fast dissolution phenomena. We have combined spectroscopic ellipsometry with quartz crystal microbalance techniques to simultaneously study thin film optical properties, thickness, film mass, and film modulus. Such techniques have been particularly useful in understanding the dissolution properties of polymeric photoresists developed for 193 nm lithography. This talk will review some of the applications for spectroscopic ellipsometry in this field and in particular will highlight some of the results of our work made possible using spectroscopic ellipsometry.

4:20pm **EL+TF+BI+AS+EM+SS-MoA8 Ellipsometric Characterization of a Thin Titaniumoxide Nanosheets Layer.** *H. Wormeester, G. Maidecchi, S. Kumar, A. Kumar, A. ten Elshof, H.J.W. Zandvliet*, MESA+ Institute for Nanotechnology, University of Twente, The Netherlands

The photochemical properties of titaniumoxide make this a widely studied material. Of special interest is a thin nanostructured layer of such a material. A variety of a nanostructured material is the single sheet titaniumoxide that can be obtained by delaminating a layered titanate, with stoichiometry $Ti_{1-x}O_{2-4x}$ ($x=0.0875$). The slight titanium deficiency leads to a negatively charged nanosheet that can be used as a building block in a layer by layer assembled composite film [1]. In this work we used Langmuir Blodgett to deposit successive thin layers of nanosheets. The electronic properties of these layers were investigated with ellipsometry and Scanning Tunneling Microscopy (STM). The optical spectra show the well known absorption peak at 4.6 eV for titaniumoxide nanosheets. The optical spectra can be well modeled with a Cody-Lorentz dielectric function profile providing a bandgap of ... eV, a value also found from STM IV spectroscopy. The Cody-Lorentz profile also indicates a slight below band gap light absorption by the nanosheet material.

[1] T. Sasaki, Y. Ebina, T. Tanaka, M. Harada, M. Watanabe and G. Decher, Chem. Mater. 2001, 13, 4661

4:40pm **EL+TF+BI+AS+EM+SS-MoA9 Preparation of Abrupt LaAlO₃ Surfaces Monitored by Spectroscopic Ellipsometry.** *C.M. Nelson, M. Spies, L.S. Abdallah, S. Zollner, Y. Xu, H. Luo*, New Mexico State University

LaAlO₃ is a polar perovskite oxide, used as a single-crystal substrate in oxide epitaxy. It has created much interest for novel electronic applications, because a two-dimensional electron gas is formed at LaAlO₃/SrTiO₃ heterostructures. The purpose of our work is twofold: First, we are interested in an accurate determination of the complex refractive index of LaAlO₃ at room temperature. Second, we studied the impact of various cleaning methods on the abruptness of the LaAlO₃ surface.

We obtained a commercial single-side polished LaAlO₃ substrate with 2-inch diameter and a (100) pseudo-cubic surface orientation. The surface was polished with an rms roughness below 0.8 nm. We determined the ellipsometric angles ψ and Δ for LaAlO₃ at 300 K from 0.7 to 6.5 eV. For a bulk insulator with a clean smooth surface, the phase change Δ should be zero or π below the band gap. In practice, this never happens, because surfaces are covered with overlayers (adsorbed organic or water vapors). Surface roughness has a similar effect on the ellipsometric spectra as a surface overlayer. Even for an abrupt bulk/air interface, there is a thin (~0.5nm) transition region where the electron wave functions leak from the crystal into the ambient. For the as-received sample, the data were described with a Tauc-Lorentz model for LaAlO₃, plus 2.1 nm of surface layer thickness (described as an effective medium with 50% density of the bulk). After ultrasonic cleaning in acetone, the overlayer thickness decreased to 1.8nm. Next, we mounted the wafer in a UHV cryostat, pumped down to below 10⁻⁸Torr, and acquired an ellipsometric spectrum at 70°. The surface layer thickness was reduced to 1.2 nm, presumably because a part of the adsorbed surface layer (especially water) desorbed under vacuum.

So far, everything worked as expected, but here it gets interesting: We heated the sample to 700 K for about an hour to desorb the remaining surface overlayer. After cooling down to 300 K, we measured the ellipsometric angles again at 70° angle of incidence from 0.7 to 6.5 eV. The ellipsometric angle Δ at 2 eV was reduced to below 0.2°, consistent with a surface layer thickness of less than 1 Å, much less than the surface roughness specified by the supplier (8 Å).

In conclusion, a macroscopically smooth and clean LaAlO₃ surface was prepared by ultrasonic cleaning of the wafer in acetone, followed by heating in UHV to 700 K. The resulting surface layer thickness was below 1 Å, as measured by spectroscopic ellipsometry. We will report Tauc Lorentz parameters. We will also describe the temperature dependence of the LaAlO₃ dielectric function from 77 to 700 K. This work was supported by NSF (DMR-11104934).

5:00pm **EL+TF+BI+AS+EM+SS-MoA10 Determination of the Refractive Index of a Gold-Oxide Thin Film Using X-Ray Photoelectron Spectroscopy and Spectroscopic Ellipsometry.** *K. Cook, G.S. Ferguson*, Lehigh University

A two-step procedure will be presented for measuring the complex refractive index of an electrochemically produced oxide film on a gold surface. In the first step, the composition and the thickness of the oxide film were determined using angle-resolved X-ray photoelectron spectroscopy. The experimental composition defined the system, thereby avoiding assumptions about the film stoichiometry that would otherwise be required. The value of thickness derived from these measurements was then used to calculate n and k from ellipsometric data collected across the visible spectrum (350 - 800 nm).

Tuesday Morning, October 30, 2012

Applied Surface Science

Room: 20 - Session AS+BI-TuM

Practical Surface Analysis

Moderator: A. Belu, Medtronic, Inc., D.L. Pugmire, Los Alamos National Laboratory

8:00am **AS+BI-TuM1 Clinical Application of Surface Analysis Technologies – Needs, Requirements and Challenges, J. Schnekenburger**, Muenster University, Germany **INVITED**

Surface analysis technologies offer tremendous applications in clinical fields. The interface of cells and materials is a crucial determinant for implant integration, artificial organ regeneration and stem cell differentiation. Cells are highly sensitive not only to chemical but also to structural determinants of their environment. Material softness, roughness and distance of adhesion points are known factors for adhesion, differentiation and the maintenance of cell function. The characterization of cell environments and surfaces for advanced cell culture by surface analysis technologies is a key element of the successful generation of bioimplantable materials and tissue regeneration.

Dental implants and liver regeneration are high impact examples for surface analysis needs. Dental implants should have a structure and chemical composition which facilitates osteoblast adhesion and bone development but impairs microbial growth and adhesion. Different implants were characterized and cell adhesion presented. The regeneration of functional liver cells from mesenchymal stem cells would allow the replacement of donor organs by cell implants. Stem cell differentiation not only requires genetic reprogramming and soluble factors but also a three dimensional environment with key elements of mature hepatocyte surrounding. These surface structures need to be identified and transferred in tissue culture dishes.

The analysis of cells and tissues as materials is challenging. The clinical environment requires technology application processes different from material science. Clinical routine analysis is cost driven and performed by technicians or MDs without deeper technical training. Expert personnel are available only in high throughput clinical centers. Also research is based on understanding the molecular determinants like DNA and proteins rather than material aspects. Furthermore cells and tissues need preparation since biological material can not be measured in high vacuum. The preparation like chemical fixation limits the analysis to specific time points of biological processes and may alter the samples compared to the original state. The combination of technologies like mass spectrometry or scanning electron microscopy with atomic force microscopy or digital holography allows the analysis of preparation artifacts and the generation of reliable data.

Overcoming the current restrictions surface analysis technologies have the potential to replace the biomedical gold standard light microscopy and fluorescence microscopy in the high resolution and three dimensional structural and chemical analysis of biological samples.

8:40am **AS+BI-TuM3 The Application of XPS to the Study of Protein Lyophilizates, S.J. Coultas, J.D.P. Counsell, A.J. Roberts, S.J. Hutton, C.J. Blomfield**, Kratos Analytical Ltd, UK, R. Geidobler, G. Winter, Ludwig-Maximilians-University, Germany

Long term storage of proteins is most often achieved by freeze drying (lyophilization). For this to be successful it is essential that the process retains the stability and biological activity of the protein. Despite its widespread use there are still problems associated with the process, not least the aggregation of the protein at the ice/liquid interface which develops during the freezing stage. To overcome this problem excipients are commonly used to ease the stresses at this interface and stabilise the protein. Polysorbates are commonly used for this purpose but there has been recent interest in using other excipients.

X-ray photoelectron spectroscopy (XPS) is ideally suited to the study of these materials due to its surface sensitivity (1-10 nm) and the quantitative nature of the data.

In this study we use XPS to investigate the protein stabilisation mechanism in lyophilizates produced using different excipients. We show there to be clear differences in the surface chemistry of the resultant lyophilizates. We also investigate the effect of temperature on the protein surface chemistry and stability.

9:00am **AS+BI-TuM4 Characterization of Real-World Surfaces and Interfaces of Devices in the Biomedical Industry, W. Theilacker, A. Belu, L. Lohstreter, L. LaGoo**, Corporate Technology and Innovation, Medtronic, Inc.

This presentation will highlight the use of surface analysis methods for the characterization of medical devices. Examples will be presented to demonstrate a range of practical applications in solving industrial problems. A multi-technique approach is used to better understand issues of cleanliness, adhesion, and intentional surface modification with regards to pacemakers, leads, and other cardiovascular devices. Oftentimes the samples provided are non-ideal for surface sensitive techniques, e.g. they are large, non-flat, and have been handled, or have been in contact with other materials. This presentation will also address approaches for characterization of real-world, non-ideal samples. The surface is an important zone as it is the interface between a material of interest and its environment. Knowledge of interface chemistry is critical for understanding how a biomaterial or drug delivery system will interact with the biological environment of the body. For other materials, particularly those that are employed in the manufacture of medical devices, evaluation of the surface is important to further understand issues with welding, adhesion, contamination, discoloration, etc. Many techniques may be utilized in order to gain a comprehensive understanding of surface morphology and chemistry, including traditional techniques such as SEM-EDS (scanning electron microscopy energy dispersive spectroscopy), IR (infrared) spectroscopy, along with other techniques such as confocal Raman microscopy, interferometry, ellipsometry, XPS (x-ray photoelectron spectroscopy), and TOF-SIMS (time-of-flight secondary ion mass spectrometry). A comparison of the techniques will be made to help elucidate which method or methods are best for specific problems. Further, the power of and the problems with data acquisition and interpretation will be highlighted with regards to each technique.

9:20am **AS+BI-TuM5 Ageing Processes Occurring on Nanoscaled Aminated Surfaces as Observed by ToF-SIMS/PCA, NEXAFS Spectroscopy and XPS, W.E.S. Unger**, BAM Federal Inst. for Materials Res. and Testing, Germany, H. Min, BAM Federal Inst. for Materials Res. and Testing and KAIST Korea, S. Swaraj, BAM Federal Inst. for Materials Res. and Testing and Soleil Synchrotron France, P.-L. Girard-Lauriault, BAM Federal Inst. for Materials Res. and Testing and McGill Univ. Toronto, A. Lippitz, BAM Federal Inst. for Materials Res. and Testing, Germany

Ultrathin organic surfaces covered by amines as coupling sites are often used in recent technologies as biosensing, adhesion in composite materials and layer-by-layer deposition of nano structures on self-assembled monolayer platforms. Ageing processes occurring with those aminated surfaces have to be regularly controlled in order to guarantee their functionality in applications.

We used a combined XPS, NEXAFS spectroscopy and ToF-SIMS/PCA approach to follow ageing of different kinds of amino-terminated surfaces stored on ambient air up to ~1 year. Test samples have been prepared as (1) aliphatic and aromatic aminosilanes on glass slides, (2) aminothiols prepared as self assembled monolayers and (3) by different plasma polymerization technologies (low pressure and atmospheric pressure DBD plasma polymerization).

The observation common to all investigated films is that the ageing process ends with a formation of amides which has been clearly proven by NEXAFS N K-edge spectra and PCA of ToF-SIMS data. However the kinetics of the ageing processes, the decay of amines, has been found to be rather different for the different kinds of samples investigated. The susceptibility of plasma deposited films is much higher due to the radicals inherently produced by the deposition technique. Furthermore storage conditions have been found at which the decay of amines in course of ageing can be suppressed to some extent.

9:40am **AS+BI-TuM6 Signature Discovery in Explosives and Bioagents using Imaging Mass Spectrometry, C.M. Mahoney**, Pacific Northwest National Laboratory

Recent terrorist attacks, both in the US and abroad, have indicated that significant improvements in intelligence operations are required for adequate prevention and prosecution of terrorist acts. This includes the ability to accurately and rapidly attribute pre-detonated and post-detonated explosive devices and/or other weapons-based material to a particular source, and/or region of the world. Surface mass spectrometry methods have the potential to greatly advance the field of forensics science, allowing for simultaneous elemental, isotopic and molecular imaging on a sub-micron to nano-scale range, with superior chemical specificity and

sensitivity. With recent advancements in the field of surface mass spectrometry, the versatility of these methods has increased dramatically, allowing for the direct analysis of samples at atmospheric pressure (e.g. Desorption ElectroSpray Ionization or DESI). The potential for 3-D molecular analysis in soft samples with depth resolutions on the order of 5 nm has also been realized with advent of the gas cluster ion beam (GCIB) source. Finally substantial improvements in the mass resolving power (by at least a factor of 10) has been observed when employing FT-MS mass spectrometers, allowing for even greater improvements in the chemical specificity. Here we describe our efforts to develop a suite of advanced mass spectral analysis and imaging techniques for the characterization and attribution of plastic explosives and other complex explosive mixtures from around the world. We will also provide initial feasibility studies for the characterization and differentiation of biological agents based on their unique molecular fingerprints. With the development of these very powerful “chemical signature microscopes” it is expected that significant advancements will be made in the field of forensics, both on the home front, and abroad.

10:40am **AS+BI-TuM9 Topography and Field Effects in the Inner Side of Micro via Hole using ToF-SIMS**, *J.C. Lee, Y.K. Kyoung, I.Y. Song*, Samsung Advanced Institute of Technology, Republic of Korea, *S. Iida*, Ulvac Phi, Japan

Surface topography is often important role in the functionality and activity of electronic devices including MEMS, composite materials, catalysts, sensors, biomedical, and packaging of semiconductor devices. Especially, trench structure such as via hole or etched pattern is one of the important processes in the through silicon via or ball grid array. If there is contaminated on the wall or bottom of via hole, it may cause contact failure between integrated circuits and printed circuit board (PCB) because of increasing contact resistance. For the recent decade, many research activities are focused on the quantitative analyses of topographic samples using TOF-SIMS. However, the most of results were focused on the nanowire, nano particle, and etched surface, it is relatively rarely dealt with the trench shape sample. It is not easy to characterize the contaminant level of ~ppm or less on the bottom of trench shape sample such as via hole. It is well known that a ToF-SIMS is one of powerful tools to analyze organic contaminants. However there are some limitations to apply it to the trench shape sample because of high sample bias voltage and short focal length of emersion lens of ToF-SIMS analyzer. If we want to characterize contaminants on the bottom of via hole using a ToF-SIMS, the side wall of via hole should be removed by mechanical treatments. In this study, we aim to establish an optimized method that is able to characterize the bottom and wall of via hole of BGA using ToF-SIMS without any mechanical or chemical treatments. This is performed by combining ToF-SIMS experiments using via hole systems with computer modeling using SIMION.

For this study, trench structure samples with the diameter of 90 μ m and width of 90 μ m were used for TOF-SIMS imaging. Via holes were fabricated by laser drilling method. Samples were mounted on the sample holders which were specially designed with tilted angles of 15, 28, and 40 degrees surfaces for this experiment. Secondary ion trajectory and potential contour were calculated using SIMION for 0, 15, 28, 40 degree tilted samples for understanding the angle dependence of field effects.

According to the simulation results, secondary ions ejected from near corner between wall and bottom of via hole are aimed to diagonal direction due to Coulomb repulsive force between secondary ions and wall of via hole. When specially designed 40 degree tilted angle sample holder which is based on simulation result is used, the bottom and wall of via hole of BGA can be fully characterized using ToF-SIMS without any mechanical treatment.

11:00am **AS+BI-TuM10 Using XPS to Probe the Surface Chemistry of Ionic Liquids**, *J.D.P. Counsell, S.J. Coultas, A.J. Roberts, S.J. Hutton, C.J. Blomfield*, Kratos Analytical Ltd., UK

Ionic liquids have attracted much attention due to their possible “green chemistry” applications. Due to the recent use of ionic liquids as corrosion resistant thin-films, it has become important to fully understand the complex nature of their surface environments.

A series of commercially available ionic liquids (e.g. [BMIM][PF₆]) were studied and characterised using x-ray photoelectron spectroscopy. Angle-resolved experiments indicate an increased concentration of the organic cation in the liquid’s surface. The surface composition becomes enriched with contributions from the linear alkyl substituent of the cation which is significantly greater than that expected from the nominal stoichiometry. A maximum entropy method algorithm was used to build an accurate structure of the surface and near-surface region

We also explore the possibilities of using ionic liquids as potential new reference standards. They present the opportunity to offer a clean reference

surface without the need for ion sputtering and present a number of core level peaks for spectrometer energy scale and transmission function calibration and validation.

11:20am **AS+BI-TuM11 XPS Profiling and Work Function Mapping of a Damaged Solar Cell**, *B. Strohmaier*, Thermo Fisher Scientific, *P. Mack, T.S. Nunnery, J. Wolstenholme*, Thermo Fisher Scientific, UK

In many areas of materials technology, it is important to control both the chemical composition and the electrical properties of the material. One example of this need is in the manufacturing of solar cells. In this case, the solar cell is based on a thin film of CIGS (Cu (In, Ga) Se₂). The full structure of the device includes an upper electrode containing indium tin oxide (ITO), zinc oxide, and cadmium sulfide. The whole structure is separated from a steel substrate using layers of molybdenum and chromium.

It has been demonstrated previously that X-ray Photoelectron Spectroscopy (XPS) is the ideal technique for characterizing the compositional depth profiles of CIGS solar cells, similar to the one described above. Using XPS it is possible to measure elemental composition gradients in the CIGS layers (allowing engineers to tune the band gap of the device) and also to investigate chemistry at interfacial layers. XPS can also be used to measure another very important parameter of solar cells, i.e. the work function. This measurement relies upon the spectrometer being accurately calibrated and the photon energy being accurately known. On a modern XPS instrument, internal standard samples (copper, silver, and gold) may be used to automatically calibrate the XPS binding energy scale. The photon energy can be checked by measuring the position of an X-ray induced Auger peak on the binding energy scale and adding it to the known kinetic energy for that peak in the Auger spectrum.

This work demonstrates the use of XPS to characterize a damaged solar cell, using depth profiling to identify the delamination zone in the solar cell stack. The surface of the delaminated cell has also been mapped for elemental and work function information.

11:40am **AS+BI-TuM12 Application of XPS Imaging Analysis in Understanding of Interfacial Delamination and Related Problems**, *H. Piao*, General Electric Global Research Center, *N. Fairley*, Casa Software Ltd, UK, *J. Walton*, The University of Manchester, UK

The recent development of X-ray Photoelectron Spectroscopy (XPS) instrumentation with near-micron spatial resolution has advanced the capability of elemental and chemical state imaging. This work extends the application of imaging XPS to the analysis of real world samples. The presentation also focuses on description of radiation damage of polymers encountered in XPS imaging analysis. The imaging analysis can cause extensive damage to polymers since the acquisition time for creating datasets can be excessive. Understanding of radiation damage in polymers is necessary for successful and validated application of XPS spectromicroscopy.

Keywords: XPS, chemical states, imaging, delamination.

Biomaterial Interfaces

Room: 23 - Session BI+SS+AS-TuM

Biomolecules at Interfaces

Moderator: P. Kingshott, Swinburne University of Technology, Australia

8:20am **BI+SS+AS-TuM2 Computer Simulation of Water-Mediated Adhesion between Organic Surfaces**, *A.J. Pertsin, M.H. Grunze*, University of Heidelberg, Germany

The adhesive forces operating between various surfaces in aqueous media are of interest in many areas ranging from biology to electronics. This refers, in particular, to surfaces formed by self-assembled monolayers (SAMs) on solid substrates to modify the surface-sensitive properties of the latter. Another important example is provided by supported lipid bilayers, where the water-mediated bilayer-substrate adhesion determines the stability of the system. The present study is concerned with surfaces formed by a hydrophobic methyl-terminated SAM (C-SAM), a hydrophilic carboxyl-terminated SAM (hereafter, O-SAM), and a phosphatidylethanolamine (PE) bilayer. The surface-water-surface system was treated as an open one using the grand canonical Monte Carlo technique. The free energies of adhesion were evaluated by integration of simulated pressure-distance relations. For SAMs, both symmetric and asymmetric confinements were considered, as formed by like and unlike SAMs, respectively. As the confinement was increased, water confined by the C-SAMs experienced capillary evaporation. As a consequence, the adhesion energy was mainly determined by the direct interaction between

bare C-SAMs. In the asymmetric SAM system, an incomplete capillary evaporation was observed, with the number of water molecules dropped by more than an order of magnitude. The remaining water molecules were all adsorbed on the O-SAM, while the C-SAM was separated from the rest of the system by a thin vapor layer. The calculated free energies of adhesion were in acceptable agreement with available experimental data. Unlike the SAM systems involving the hydrophobic C-SAM, the PE/water/C-SAM system did not experience capillary evaporation up to the highest confinements tried. A likely reason is a high molecular-level "roughness" of the PE/water interface due to a deep penetration of water in the PE bilayer. The pressure-distance dependence showed a slightly repulsive region with a depth comparable with the statistical uncertainty in pressure. By contrast, the pressure-distance curve of the PE/water/O-SAM system showed a well-defined minimum with a depth of about 0.7 kbar. The integration of this curve resulted in an adhesion free energy of 19 ± 3 mJ/m², close to the value obtained for the O-SAM/water/O-SAM and O-SAM/water/C-SAM systems (~ 25 mJ/m²).

8:40am **BI+SS+AS-TuM3 Adsorption from Saliva - Properties of Adsorbed Layers and Comparison with Other Systems**, *T. Arnebrant, L. Lindh, J. Sotres*, Malmö University, Sweden **INVITED**

Adsorbed salivary protein layers will cover soft and hard surfaces in the oral cavity, where they fulfill a protective function influencing adhesion and wear, and also surfaces of devices exposed to saliva. Properties of salivary films will depend on the characteristics of the surface on which they are formed as well as solution conditions (salt, pH) and will affect surface properties such as wettability and charge. Moreover, normal and lateral forces between surfaces bearing salivary films will be distinctly different than for bare surfaces. Such changes in surface properties and interactions may be relevant not only for events at oral interfaces but also for the operation of monitoring or sampling devices immersed in or exposed to saliva. Here, we show how a combined characterisation of these systems through different surface techniques provides important information on the role of this body fluid which is not available through more common chemical or biochemical approaches. The presentation will describe adsorption characteristics of salivary proteins from the total secretion as well as for purified fractions including single protein preparations. Influence by surface properties and ambient (solution) conditions will be outlined. Data on structure of salivary films as obtained by *in situ* ellipsometry, QCM-D and neutron reflectivity will be reported. Furthermore, SFA and AFM measurements of DLVO, steric, adhesive and frictional forces between surfaces bearing salivary films will be discussed. A new method for estimating the strength of salivary films based on simultaneous recording of roughness and friction data from AFM will also be described.

References: Protein Adsorption in the Oral Environment, Arnebrant T, In Biopolymers at Interfaces 2nd ed. (M. Malmsten Ed.) Marcel Dekker, 2003, pp 811-856

Friction force spectroscopy as a Tool to Study the Strength and Structure of Salivary Films. Sotres J., Liselott L., Arnebrant T. 2011. *Langmuir*, 27 (2011), 13692-13700.

9:20am **BI+SS+AS-TuM5 An Atomic Force Microscopy Based Method for the Determination of Protein Stability**, *O. Croad*, University of Nottingham, UK, *S. Rigby-Singleton*, Molecular Profiles Ltd., UK, *C.J. Roberts, D.J. Scott, P.M. Williams, S. Allen*, University of Nottingham, UK

A method for the early detection of instability and aggregation propensity of proteins and other biological macromolecules would be valuable for the rapid development of novel biopharmaceutical formulations. The aim of this study was to investigate the potential of atomic force microscopy (AFM) based adhesion force measurements to meet this need. We report the first key step in demonstrating this approach; a clear relationship between how frequently an AFM probe adheres to a protein coated surface and the fraction of unfolded proteins on that surface. Instability and subsequently protein denaturation are commonly linked with protein aggregation, and hence formulation failure. It was found that for the protein bovine serum albumin (BSA), the adhesion between AFM tips and protein-coated samples occurred much more frequently as either the concentration of a denaturant or temperature was gradually increased. We compared this behaviour with fluorescence based studies of the BSA unfolding in solution. Both methods provided us with almost identical ΔG values of stability and 50% unfolding ($[D]^{50\%}$) values. The data demonstrates for the first time, an AFM based method for protein stability determination. Interestingly, the method also appears to be a good reporter of the protein solution behaviour. With further development this approach could be utilized to screen for instability and aggregation propensity of a given protein therapeutic, in a range of conditions. The ultimate aim is to create a robust technique that can be performed rapidly and routinely.

9:40am **BI+SS+AS-TuM6 Von Willebrand Factor A1 Domain Structure and Function Changes on Surfaces**, *E. Tronic, W. Thomas, D.G. Castner*, University of Washington

The clotting protein von Willebrand Factor (VWF) binds to platelet receptor glycoprotein 1ba (GP1ba) when VWF is activated, such as when VWF is exposed to a surface or is under high shear. However, the mechanism of surface activation is not known. This study characterizes function and adsorption behavior of the VWF A1 domain, which contains the GP1ba binding site. Surfaces tested are glass, polystyrene, and tissue culture polystyrene. Highest VWF A1- GP1ba binding is observed when A1 is adsorbed onto polystyrene, as measured by platelet rolling velocity in a parallel plate flow chamber assay. X-ray photoelectron spectroscopy (XPS) showed comparable A1 amounts are present on each surface, suggesting functional differences were not explained by differences in surface coverage. A1 surface structure was investigated using ELISA, time-of-flight secondary ion mass spectrometry (ToF-SIMS) and near-edge x-ray absorption fine structure (NEXAFS). Using monoclonal antibodies binding to a nonlinear epitope within A1, ELISA showed lower antibody binding for A1 adsorbed to polystyrene than to glass or tissue culture polystyrene. ToF-SIMS was used to identify differences in amino acid exposure, and NEXAFS showed different amide backbone ordering on the three surfaces. These studies demonstrate that the surface dependence of A1 function is likely due to differences in adsorbed surface orientation and/or conformation. This is an important consideration in *in vitro* models, where A1 is typically immobilized onto synthetic surfaces, and is also of interest for blood-contacting biomaterials. Additional studies have been done on A1 and two A1 mutants adsorbed on collagen coated tissue culture polystyrene. One mutant exhibits similar ELISA and ToF-SIMS results to the wild type A1, while the other mutant exhibits differences. This indicates that mutations in A1 can affect the conformation/orientation changes that result from A1 adsorption onto collagen.

10:40am **BI+SS+AS-TuM9 Combining Catalysis and Self-Assembly: Towards Evolvable Soft Matter**, *R. Ulijn*, University of Strathclyde, UK **INVITED**

Molecular networks are key to the adaptiveness of biological systems and it would be very useful if this concept could be introduced into simple man-made functional materials, which could adapt to changing environments. In biology, adaptiveness (as a consequence of evolution) is achieved through a combination of catalysis, self-assembly, molecular recognition and compartmentalisation. These individual molecular processes are closely linked, a situation which may be achieved in laboratory based systems by sharing of building blocks between these individual processes, thereby giving rise to networked systems that are highly responsive and adaptive to changing external conditions. We have made the first steps towards developing evolvable materials, and will present progress in (i) structure/function relationships in peptide self-assembly, (ii) development of catalytic peptides, (iii) self-selecting peptide libraries achieved by combining fully reversible amino acid exchange in self-assembling peptide systems. The overall aim of this area is to produce laboratory made molecular materials that incorporate the above features and are able to adapt and change their properties in response to external environmental changes. Potential applications in biomaterials science will be discussed.

11:20am **BI+SS+AS-TuM11 Bio/Nano Interfaces of De Novo Design: Small Proteins with Large Potential**, *M.G. Ryadnov*, National Physical Laboratory, UK

Our ability to manipulate function at interfaces in native and near-native environments is critical for the fabrication of nanostructured materials and devices. Biomolecular self-assembly lends itself to robust bio-nano systems. However, exact construction strategies to enable desired applications stumble upon the lack of control over self-assembly processes. De novo peptide design provides a saving solution to this.[1] Small proteins can be designed to deliver functions that are otherwise accessible only to macromolecular subcellular complexes. Examples include gene delivery systems,[2] fibrillar microscopic structures for tissue repair[3] and responsive antimicrobial agents[4]. A key factor in all such designs is their structural and functional relevance to native self-assembling structures, be these viruses, extracellular matrices or host defence systems. Thus, this is our ability to construct such materials at will that advances the development of efficient bio/nano-interface technologies.[5] **References** 1. Ryadnov, M. G. (2012) Prescriptive peptide design. In *Amino acids, peptide and proteins*. (Farkas, E. & Ryadnov, M. G., eds.) SPR, RSC Publishing (2012), v.37. 2. Lamarre, B., Ravi, J. & Ryadnov, M. G. (2011) GeT peptides: a single-domain approach to gene delivery. *Chem. Commun.*, 47, 9045-9047. 3. Bella, A., Ray, S., Shaw, M. & Ryadnov, M. G. (2012) Arbitrary self-assembly of peptide extracellular microscopic matrices. *Angew. Chem. Int. Ed.*, 51, 428-431. 4. Ryadnov, M. G., Mukamolova, G. V., Hawrani, A. S., Spencer, J. & Platt, R. (2009) RE-coil: an antimicrobial peptide regulator.

11:40am **BI+SS+AS-TuM12 Application of CD and SRCD Techniques to the Study of Protein/Nanoparticle Complexes**, *G. Ceccone, S. Laera, L. Calzolari, D. Gilliland, EC-JRC-IHCP, Italy, R. Hussein, G. Siligardi, Diamond Light Source, UK, F. Rossi, EC-JRC-IHCP, Italy*

Nanotechnology is having a large impact in very different scientific fields and the use of nanotechnology-based materials is not just limited to research laboratories, but has already been applied in several industrial sectors and into real products as disparate as medical diagnostic tools, drug delivery systems, cosmetics, and consumer products.

In particular, engineered nanoparticles (ENPs) are used in different applications such as cosmetics, food and medicine and currently more than 600 products containing nanomaterials are already on the market[1,2,3]. At the same time there is a growing public concern about the safety of ENPs since it has been demonstrated that those intended for industrial and medical applications could cause adverse effects in mammals or aquatic organisms by specific mechanisms depending on their physical chemical properties[4]. However, the interaction of nanomaterials with complex matrices is far to be understood. In fact, although it is now increasingly accepted that the surface of nanoparticles in a biological environment is modified by the so called "protein corona"[5,6], the importance of the detailed structure of the adsorbed protein-solution interfaces is still not much addressed in the nanotoxicology literature[7].

In this work, we report the use of Circular Dichroism (CD) and Synchrotron Radiation Circular Dichroism (SRCD) to detect changes in the secondary structure and stability of different classes of proteins interacting with nanoparticles. In particular, we show that by using the SRCD we can detect structural changes of proteins in the nanomolar concentration range when they form protein-nanoparticle complexes[8]. Furthermore, the adsorption of protein on NP modifies their melting point in a composition and size dependent manner, indicating once more that the protein corona formation is strongly depending on the nanoparticles physico-chemical properties. For instance, while the presence of Au NPs do not influence the thermal unfolding process of human serum albumin (HSA), a significant decrease of the HSA melting temperature (about 6°C) is observed in presence of Ag NPs.

-
- [1] R.A. Petros, J. M. DeSimone, *Nature Rev.*, **9**, (2010), 616.
 - [2] G.J. Noynek et al., *Crit. Rev. Toxicol.*, **37**, (2007), 251.
 - [3] N. Sozer, J.L. Kokini, *Trends in Biotechnol.*, **27(2)**, (2009), 82.
 - [4] G. Obersdortner et al., *Env. Health Persp.* **113**, (2005), 823
 - [5] I. Lynch, K. A. Dawson, *Nanotoday*, **3(1-2)**, (2008), 40
 - [6] M.P. Monopoli et al., *J. Am. Chem Soc.*, **133**, (2011), 2525
 - [7] P. Sabatino et al., *J. Coll Interface Sci.*, **314**, (2007), 389
 - [8] S. Laera et al., *Nano Lett.* **11**, (2011), 4480.

Graphene and Related Materials Focus Topic

Room: 13 - Session GR+AS+EM+MI+MN-TuM

Optical, Magnetic, Mechanical and Thermal Properties

Moderator: K.I. Bolotin, Vanderbilt University

8:00am **GR+AS+EM+MI+MN-TuM1 Characterization of Magnetically Tunable Iron Nanorod Coated Graphene Nanoplatelets**, *S.D. Johnson, M.H. Gowda, S.-F. Cheng, N.Y. Garces, B. Feigelson, F.J. Kub, C.R. Eddy, Jr., U.S. Naval Research Laboratory*

Composites made from iron coated graphene nanoplatelets (GNPs) show promise for applications such as, magnetic switches, electromagnetic interference shielding, and electromagnetic waveguides due to the large conductivity of GNPs combined with the magnetism of iron. Additionally, this composite can be easily formed into millimeter thick sheets making it a promising composite for other applications.

We report a novel method to synthesize iron oxide compound onto GNP using microwave hydrothermal synthesis at 60° C and reaction times between 10 and 120 minutes. Scanning electron microscopy imaging reveals iron oxide nanorods approximately 100 nm long adhered to the GNPs for reaction times as short as 10 minutes. X-ray photoemission spectroscopy reveals that the iron/carbon ratio remains constant across these reaction times. The resistivity of the composite increases with reaction time from 0.2 to 0.6 ohm-cm. Saturation magnetization and coercive field values follow a decreasing trend with increasing reaction time. From 10 to 120

minutes saturation magnetization decreases by 70% from 170 emu/g and coercive field decreases by 40% from 52 Oe. Remnant magnetization of around 0.7 memu/g remains constant throughout. We also report the temperature-dependent magnetic response of the compound across the Morin transition, which for submicron particles of α -Fe₂O₃ is near 250 K.

Preliminary results suggest that while the nanorod size and quantity remains constant with reaction time, the resistive and magnetic properties change. This may suggest that we are tuning the magnetism of the system by changing the iron structure between the ferromagnetic γ -Fe₂O₃ and the antiferromagnetic α -Fe₂O₃.

8:20am **GR+AS+EM+MI+MN-TuM2 Dynamical Origin of Blue Photoluminescence from Graphene Oxide**, *A.L. Exarhos, M.E. Turk, P.M. Vora, J.M. Kikkawa, University of Pennsylvania*

The tunable broadband emission from graphene oxide (GO) has sparked significant interest in research regarding its potential for band gap engineering. Here, we use polarization sensitive time-resolved optical spectroscopy to study the spectral diffusion and sub-picosecond dynamics of the excited carriers in GO and photo-exposed GO, where photo-exposure has been demonstrated to constitute a reducing condition. In steady state measurements, a significant blueshifting of the photoluminescence (PL) is observed with photo-exposure. This blueshift correlates with a marked difference in the temporal behavior of the PL from GO and photo-exposed GO. The PL spectra are very similar at short delay times, but an increased non-radiative recombination rate in the exposed GO leads to a decreased lifetime in the material. Utilizing in-plane polarization memory measurements, we examine the electron-hole polarization in these systems which can probe excitonic effects and help to provide a better understanding of the role of the sp² graphene lattice in GO and exposed GO. We further discuss the relevance of our data to the origins of PL in these systems.

A.L.E. gratefully acknowledges the support of NSF DMR-0907226. M.E.T., P.M.V., and the construction of a Kerr gate system are supported by the Department of Energy Office of Basic Energy Sciences Award DE-SC0002158.

8:40am **GR+AS+EM+MI+MN-TuM3 Spin-Transport and Magnetism in Graphene**, *R. Kawakami, University of California, Riverside INVITED*

Graphene is an attractive material for spintronics due to its high mobility and the low intrinsic spin-orbit and hyperfine coupling, which should lead to excellent spin transport properties. In 2007, graphene became the first material to exhibit gate tunable spin transport and spin precession at room temperature. However, the spin injection efficiency was low and the spin lifetime was much shorter than predicted theoretically. In this talk, I will report on our progress in this area. The low spin injection efficiency into graphene is due to the conductivity mismatch between the ferromagnetic metal (Co) spin injector and the single layer graphene (SLG). To alleviate this problem and enhance the spin injection efficiency, we developed atomically smooth MgO tunnel barriers by utilizing a TiO₂ seed layer. With tunneling contacts, the non-local spin signal is found to be as high as 130 ohms at room temperature, with a spin injection efficiency of 30%. In addition to improving the spin injection efficiency, the tunneling contacts were found to improve the spin lifetime as well. This indicates that the short spin lifetimes reported before are due to the contact-induced spin relaxation from the ferromagnetic electrodes. Using tunneling contacts, we investigate spin relaxation in single layer graphene (SLG) and bilayer graphene (BLG). At low temperatures, contrasting behaviors of gate voltage dependence of the spin lifetime are observed between SLG and BLG, which suggest different mechanisms for spin relaxation in SLG and BLG. A final topic of interest is magnetism and the formation of magnetic moments in graphene. While there is substantial theoretical work on magnetic moments generated by hydrogen adatoms and lattice vacancies, the experimental situation is less clear. We have developed a new method for detecting magnetic moment formation based on scattering of pure spin currents in graphene spin valves. We will report the progress on our efforts to identify magnetism with this approach.

10:40am **GR+AS+EM+MI+MN-TuM9 A "How To" for Magnetic Carbon**, *H. Ohldag, SLAC National Accelerator Laboratory, E. Arenholz, T. Tylliszczak, Lawrence Berkeley National Laboratory, D. Spemann, R. Hoehne, P. Esquinazi, M. Ungureanu, T. Butz, University of Leipzig, Germany*

While conventional wisdom says that magnetic materials have to contain some metallic atoms, the confirmation of intrinsic magnetic order in pure metal free carbon represents an ultimate and general scientific breakthrough because of the fundamental importance of carbon as an elemental building block of organic as well as inorganic matter. The common controversy raised across all disciplines is whether the magnetism of carbon is intrinsic or induced by other elements. We address this controversy by providing clear experimental evidence that metal free carbon can be ferromagnetic at

room temperature using dichroism x-ray absorption spectro-microscopy. For this purpose we acquired soft x-ray microscopy images of magnetic structures on a thin carbon film that have been produced by irradiation with a focused 2.25MeV proton beam. Our element specific magnetic probe shows no indication of magnetically ordered Fe, Co or Ni impurities in these samples. In a second step we investigate the particular electronic states that are involved in carbon magnetism and find that the carbon p-states as well as C-H bonds show a magnetic moment, indicating that hydrogenation plays a crucial role in developing the ferromagnetic order. Our surface sensitive approach reveals that the magnetism at the surface of the irradiated graphite samples is much larger than in the bulk of the sample. We observe a surface magnetic moment similar to what is typically present in classical ferromagnetic 3d transition metals.

REFERENCES

P.Esquinazi et al., *Magnetic order in graphite: Experimental evidence, intrinsic and extrinsic difficulties*, Journal of Magnetism and Magnetic Materials, Vol 322, 1156 (2010).

H. Ohldag et al., *p-Electron ferromagnetism in metal free carbon probed by soft x-ray dichroism*, Phys. Rev. Lett. 98, 187204 (2007) H. Ohldag et al., *The role of hydrogen in room temperature ferromagnetism at graphite surfaces*, New J. Phys. 12 123012 (2010)

11:00am **GR+AS+EM+MI+MN-TuM10 From Graphene to Amorphous Carbon by Sublimation and Condensation**, B. Steele, R. Perriot, V. Zhakhovskiy, I.I. Oleynik, University of South Florida

The mechanisms of the non-equilibrium melting process of graphene and the structure of the liquid phase of carbon was studied by molecular dynamics (MD). Graphene undergoes a non-equilibrium melting process at high temperature and low pressure as the carbon chains are formed out of the graphene sheet, thus making up a transient liquid phase of carbon. As the chains expand the material sublimates to a low dense gas of carbon chains. Under higher pressure the gas phase will condense to an intermediate porous phase of carbon with a significant sp^2 fraction of atoms, followed by the liquid phase, and finally an amorphous phase. Mechanisms of melting of graphene, including formation of topological and Stone Wales (SW) defects in two and three dimensions will be discussed.

In Situ Microscopy and Spectroscopy Focus Topic

Room: 7 - Session IS+AS+SS+EN-TuM

In Situ Spectroscopic Studies of Catalysis and Gas-Solid Reactions

Moderator: B. Roldan Cuenya, University of Central Florida

8:00am **IS+AS+SS+EN-TuM1 Ambient Pressure XPS for Alternative Energy Research and Environmental Science**, H. Bluhm, Lawrence Berkeley National Laboratory

INVITED

Solid/vapor and liquid/vapor interfaces play a major role in many processes in the environment and technology. Examples include heterogeneous catalysis, fuel cell technology, aerosol chemistry, and weathering of minerals and rocks. The measurement of these interfaces under realistic conditions of gas pressure and temperature has gained increasing importance over the last decades. Ambient pressure photoelectron spectroscopy (APXPS) is a promising technique for the investigation of liquid and solid surfaces in the presence of gases at pressures in the Torr range. The heart of an APXPS instrument is a differentially pumped electrostatic lens system that separates the sample, which is in a gas atmosphere at pressures of up to 5 Torr, from the electron spectrometer, which is kept in vacuum. This talk will discuss the history and basics of APXPS and show examples of the application of APXPS to the study of aqueous solution, metal oxides, soot, and fuel cell electrodes under reaction conditions.

8:40am **IS+AS+SS+EN-TuM3 In Situ Soft X-ray Photon-in/Photon-out Spectroscopy of Photo-electrochemical Reactions of Hematite in Water Splitting**, J.H. Guo, Lawrence Berkeley National Laboratory, A. Braun, Empa, Swiss Federal Laboratories for Materials Science and Technology, K. Sivula, Ecole Polytechnique Fédérale de Lausanne (EPFL), Switzerland, D. Bora, Lawrence Berkeley National Laboratory, J.F. Zhu, L. Zhang, University of Science and Technology of China, M. Grätzel, Ecole Polytechnique Fédérale de Lausanne (EPFL), Switzerland, E.C. Constable, University of Basel, Switzerland

Hydrogen fuel generation by solar water splitting in photoelectrochemical cells (PEC) is one of the first steps in artificial photosynthesis and an

essential part of the holy grail of solar energy conversion. Iron oxide, literally "rust", is an interesting PEC photoanode material because of its affordability, good stability, good spectral match of the solar spectrum, and yet controversial because of its poor electronic structure. At present, iron oxide is taking center stage as prospective PEC anode material.

PEC electrodes are typically semiconducting metal oxides to form electron-hole pairs when struck by light. In the photoanodes such as hematite, the generated holes must diffuse to the iron oxide surface where they can oxidize water to oxygen. However, the electronic structure of iron oxide is such that the photogenerated holes tend to recombine and annihilate with the electrons before reaching the surface and performing the required chemical work on water splitting. Currently, researchers worldwide try to understand the peculiarities of iron oxide so as to invent strategies to improve this material.

The Advanced Light Source produces soft X-rays which are optimally suited to study the electronic structure of electrode materials and which can detect electron holes. But the holes needed for solar water splitting by iron oxide require an anodic electric bias plus the illumination. Moreover, the holes are transitional and quite elusive. Also, soft X-rays cannot easily peek into a PEC cell. The unique design of the in-situ cell at the ALS has overcome the burden [1-3]. Recently the experiment has been performed for studying, under in-situ and operando conditions, the hole generation in a specifically designed photoelectrochemical cell. The oxygen valence band signature was recorded while tuning the PEC relevant parameters, two different types of holes in the valence band near the Fermi energy are discovered [4].

References:

[1] "X-ray Emission Spectroscopy of Hydrogen Bonding and Electronic Structure of Liquid Water", J.-H. Guo et al., Phys. Rev. Lett. **89**, 137402 (2002).

[2] "Electronic Structure of Cobalt Nanocrystals Suspended in Liquid", H. Liu et al., Nano Lett. **7**, 1919 (2007).

[3] "In situ soft X-ray absorption spectroscopy investigation of electrochemical corrosion of copper in aqueous NaHCO_3 solution", P. Jiang et al., Electrochem. Comm. **12**, 820 (2010).

[4] "Direct Observation of Two Electron Holes in a Hematite Photoanode during Photoelectrochemical Water Splitting", A. Braun et al., J. Phys. Chem. C **116**, 16870 (2012).

9:00am **IS+AS+SS+EN-TuM4 XANES and Ambient Pressure XPS (APXPS) Study: Investigations of the Local Structure and Final-State Effect in Partially Reduced SnO_x Nanoislands on Pt(111)**, S. Axnanda, Z. Liu, B. Mao, Lawrence Berkeley National Laboratory

Heterogeneous catalysts consisting of small particles having a high concentration of structural defects and under-coordinated sites make up the majority of the catalytic processes in industrial chemistry. One important recent example of interest shows that the interface-confined coordinatively unsaturated ferrous (CUF) sites together with the metal supports ($\text{FeO}_{1-x}/\text{Pt}(111)$) are active for dioxygen activation which causes the ensemble to be highly efficient for CO oxidation at low temperature under typical operating conditions of a proton-exchange membrane fuel cell.[1-2] In this work, we report another spectroscopic evidence to further confirm an enhanced reactivity at the edges of small catalyst particles. The system of interest is partially oxidized SnO_x (Sn^{2+}) nanoislands supported on Pt(111) for ethanol oxidation reaction (EOR), an electrode material in a direct alcohol fuel cell (DAFC). Our findings suggested that $\text{SnO}_x/\text{Pt}(111)$ inverse catalysts have improved activity for EOR in acidic media as compared to a bare Pt(111) surface.[3] We also found that the most active surface had a small coverage of SnO_x (0.3- 0.4 ML). Water activation at low potentials is currently attributed to be the promoting effect of SnO_x nanoparticles, since this enhances the oxidation of chemisorbed CO formed on Pt sites during the EOR.[4] To better understand this increased activity, we performed study with the goal to indicate the actual state of Sn in SnO_x nanoislands before and after the $\text{SnO}_x/\text{Pt}(111)$ is used in EOR showing the increased activity: purely oxide Sn or mixed Sn alloy and Sn oxide, using a combination of APXPS and XANES techniques. BE shift in the XPS core-line spectra of Sn and O, soft X-ray XANES spectra (Sn M4,5-edge, O K-edge) will be collected and compared to the corresponding XPS spectra (Sn 3d, O 1s) to explain the actual state of Sn before and after the $\text{SnO}_x/\text{Pt}(111)$ is used in the EOR.

1. Fu, Q., et al., Interface-Confined Ferrous Centers for Catalytic Oxidation. Science, 2010. 328: p. 1141.

2. Deng, X., et al., Reactivity Differences of Nanocrystals and Continuous Films of $\alpha\text{-Fe}_2\text{O}_3$ on Au(111) Studied with In Situ X-ray Photoelectron Spectroscopy. J. Phys. Chem. C, 2010. 114: p. 22619.

3. Zhou, W.P., et al., Enhancement in Ethanol Electro-Oxidation by SnOx Nanoislands Grown on Pt(111): Effect of Metal Oxide-Metal Interface Sites. *Journal of Physical Chemistry C*, 2011, 115: p. 16247.

4. Axnanda, S., W.P. Zhou, and M.G. White, CO Oxidation on Nanostructured SnOx/Pt(111) surfaces: Unique Properties of Reduced SnOx. *Phys. Chem. Chem. Phys.*, 2012. Submitted.

9:20am **IS+AS+SS+EN-TuM5 Epitaxial Strontium Substituted Lanthanum Cobalt Oxides Investigated using *In Situ* Ambient Pressure X-ray Photoelectron Spectroscopy Near Operating Conditions Under Applied Potentials.** E. Crumlin, E. Mutoro, Massachusetts Institute of Tech., Z. Liu, Lawrence Berkeley National Lab, M.D. Biegalski, Oak Ridge National Lab, W.T. Hong, Massachusetts Institute of Tech., H.M. Christen, Oak Ridge National Lab, H. Bluhm, Lawrence Berkeley National Lab, Y. Shao-Horn, Massachusetts Institute of Tech.

Operating conditions for solid oxide fuel cell (SOFC) are typically at high temperatures (~500 – 1000 °C) and ambient pressures (~1 atm). We have to understand how the physical and chemical properties of SOFC materials, particularly the cathode which is responsible for a majority of the fuel cells area specific resistance, change under operating conditions. Such data can provide insights into the mechanism of the oxygen reduction reaction (ORR) which may lead to material development strategies to improve the cathode performance. However, these operating conditions are far away from conventional characterization techniques that are often applied at room temperature or even in ultrahigh vacuum (UHV). Our recent work using *in situ* ambient pressure X-ray photoelectron spectroscopy (APXPS) has shown that (001) oriented epitaxial films of $\text{La}_{0.8}\text{Sr}_{0.2}\text{CoO}_{3-\delta}$ (LSC₁₁₃) can exhibit Sr enrichment in the near-surface perovskite lattice structure ("lattice") as temperatures were raised from 220 °C to 520 °C in a $p(\text{O}_2)$ of 1×10^{-3} atm. In contrast under the same conditions, a bulk pellet of LSC demonstrated no changes in Sr content within the "lattice" region. The Sr enrichment is believed to play a key role in the observed one order of magnitude enhancement in ORR activity (as measured by the surface exchange coefficient, k^0) of the (001) epitaxial films relative to bulk LSC₁₁₃. In this work, we continue the previous investigations of the chemical properties of (001) epitaxial LSC₁₁₃ as a function of temperature cycling between 220 °C and 520 °C at a $p(\text{O}_2)$ of 1×10^{-3} atm. Additionally, the comparison of LSC₁₁₃, $(\text{La}_{0.5}\text{Sr}_{0.5})_2\text{CoO}_{4+\delta}$ (LSC₂₁₄), and LSC₂₁₄-decorated LSC₁₁₃ (LSC_{113/214}) at $p(\text{O}_2)$ of 1×10^{-3} atm as a function of temperature and under applied cathodic potentials will be presented in order to provide insights into the physical origin responsible for the observed ~3 orders of magnitude ORR activity enhancement of LSC_{113/214} relative to (001) epitaxial LSC₁₁₃.

9:40am **IS+AS+SS+EN-TuM6 Probing Nitrogen and Metal Speciation in Non-Platinum Electrocatalysts by Ambient Pressure X-ray Photoelectron Spectroscopies and DFT Calculations.** K. Artyushkova, B. Halevi, A. Serov, The University of New Mexico, B. Kiefer, New Mexico State University, P. Atanassov, The University of New Mexico

X-ray Photoelectron Spectroscopy (XPS) has been the main surface analysis method for determining the chemical environment and coordination of nitrogen and transition metal (TM) in the non-precious group metal oxygen reduction reaction (ORR) electrocatalysts. Even though there is an agreement that Me-N_x serve as one of the possible active sites in ORR, the distribution of Me-N₂ vs Me-N₄ centers and their specific role still remains unresolved. XPS which heavily relies on use of reference spectra in accurate identification of species cannot address this issue directly as no reference compounds with Me-N₂ moieties are available. The assignment of peaks and nitrogen coordination is not straightforward due to overlapping peaks that appear within a narrow energy window of 2.5-eV and the full width half maximum (fwhm) for individual species is on the order of 1.2-1.5-eV. Being able to calculate binding energy shifts based on molecular structure can be very important tool for assisting in this task. We will report on BE shifts that have been calculated at the DFT level and their comparison to experimentally obtained values for metal-less and metal-containing porphyrins. Information obtained from the DFT calculations will be used as input into curve-fitting XPS spectra for various model N-Me containing compounds as well as from electrocatalyst. We will compare chemical information derived from conventional XPS as well as *in-situ* ambient-pressure XPS using variable energy synchrotron source.

10:40am **IS+AS+SS+EN-TuM9 Resolving Growth of Palladium Nanocatalysts Using *In Situ* FT-IR, XAS and PDF under Practical Atomic Layer Deposition Conditions.** Y. Lei, J. Lu, B. Liu, H. Zhao, J. Greeley, P. Chupas, J. Miller, J.W. Elam, Argonne National Laboratory

Nanostructured Pd catalysts prepared by ALD have been demonstrated highly active for alkene hydrogenation, methanol decomposition reaction, and alcohol oxidation for fuel cells. Development of supported Pd nanoparticles with Controlled size/structure relies on the fundamental

understanding of the two half reactions with high precision during Pd ALD. However, evolution of Pd surface species, as well as the subsequent nucleation and growth of palladium nanoparticles during Pd ALD is still not clear.

Mechanism of assembly of highly dispersed Pd nanoparticles on TiO₂ surfaces from palladium hexafluoroacetylacetonate (Pd(hfac)₂) were investigated by means of *in situ* Infrared (IR) spectroscopy, X-ray absorption spectroscopy (XAS) and pair distribution function (PDF) under practical atomic layer deposition condition simultaneously. Density function theory simulation was applied to understanding the reaction mechanism. On chlorine-containing TiO₂ surface, Pd(hfac)₂ primarily adsorbed on TiO₂ surface as Pd(hfac)Cl₂* species, confirmed by both XAS and DFT calculations. *In-situ* FT-IR results reveal that deligation of Pd(hfac)Cl₂* species began at as low as 100 °C with the present of formalin. Further on, *in-situ* XAS results indicated that cleavage of Pd-O bond occurred first, followed by cleavage of Pd-Cl bond. Sequentially, Pd atoms started to gain mobility and agglomerate to small nanoparticles. The hfac ligands spilled to TiO₂ surface as site blockers for ALD. The surface poisons were eventually removed at 225 °C. Nano-size palladium-carbon phase was also found after long exposure of formalin. Atomic resolution aberration-corrected STEM image showed one nanometer size crystalline Pd particles were synthesized using ALD. The catalytic performance of these Pd nanocatalysts was further demonstrated in several applications.

In summary, dynamic growth of Pd nanocatalysts was obtained utilizing a combination of *in-situ* techniques.

11:00am **IS+AS+SS+EN-TuM10 Catalyst Characterization using *In Situ* XAS and XPS: From Nanoparticles Synthesis to Evolution of Structural/Electronic Properties under Reaction Conditions.** A.M. Karim, Pacific Northwest National Laboratory **INVITED**

Catalysts are used to facilitate the important industrial chemical processes, leading to products valued in the trillions of dollars annually just in the U.S and most catalysts used in large-scale processes are solids. To maximize the number of sites available for reaction, catalysts are typically comprised of metallic/metal oxide nanoparticles dispersed on high surface area supports. The activity and selectivity of metallic nanoparticles strongly depend on their size, shape and composition [1-8]. In order to design more active and selective catalysts, it is essential to identify the catalytically active sites and understanding their geometric and electronic properties which requires: (1) synthesis of well-defined catalyst structures and (2) the ability to correlate individual reaction pathway(s) with the type of active site(s) available on the catalyst surface under reaction conditions.

This talk is going to cover our work on *in situ* characterization of nanoparticles from the synthesis stage to the evolution of their structural/electronic properties under reaction conditions using X-ray photoelectron and X-ray absorption spectroscopies. The catalyst systems that will be covered include:

Pd nanoparticles synthesis in solution: Understanding the nucleation and growth mechanisms.

Supported Pt, PtRe and PtNi nanoparticles under aqueous phase reaction condition: Correlating the structural and electronic properties with the catalytic activity and selectivity.

References:

- [1] Boudart, M. *Adv. Catal.* 1969, 20, 153.
- [2] Boudart, M. *Journal of Molecular Catalysis* 1985, 30, 27.
- [3] Ichikawa, S.; Poppa, H.; Boudart, M. *Journal of Catalysis* 1985, 91, 1.
- [4] Somorjai, G. A.; Carrazza, J. *Industrial & Engineering Chemistry Fundamentals* 1986, 25, 63 [5] Liu, Z.; Hu, J. E.; Wang, Q.; Gaskell, K.; Frenkel, A. I.; Jackson, G. S.; Eichhorn, B. *Journal of the American Chemical Society* 2009, 131, 6924.
- [6] Alayoglu, S.; Nilekar, A. U.; Mavrikakis, M.; Eichhorn, B. *Nature Materials* 2008, 7, 333.
- [7] Sinfelt, J. H. *Journal of Catalysis* 1973, 29, 308.
- [8] Sinfelt, J. H. *Accounts of Chemical Research* 1977, 10, 15.

11:40am **IS+AS+SS+EN-TuM12 *In Situ* Study of the Oxidation of CO over Ir(111).** J. Knudsen, Lund University, Sweden, Y. Monya, Keio University, Japan, J. Schnadt, M.A. Arman, E. Grånäs, Lund University, Sweden, H. Kondoh, Keio University, Japan, J.N. Andersen, Lund University, Sweden

The platinum group metals are known to be excellent catalysts for the oxidation of carbon monoxide, and the reaction mechanisms over the surfaces of these metals have been studied for a long time. Nevertheless, only during recent years a new picture has emerged which suggests that the catalytically active phase often is formed first under reaction conditions –

which implies realistic pressures rather than ultrahigh vacuum (UHV) – and that it is different from the adsorption structures known from UHV experiments. In the case of the Pt(111) surface a very oxygen-rich chemisorbed phase has been suggested as the catalytically active phase [1], whereas a surface oxide has been suggested for the Ru(0001) surface [2]. Thus, for each different surface different phases and mechanisms might be at play, and, moreover, the phase might depend quite strongly on the conditions (pressure and temperature) used.

With this in mind we have studied the CO oxidation reaction over the Ir(111) surface and the related adsorption systems of CO and oxygen on Ir(111) using a combination of *in situ* Ambient pressure x-ray photoelectron spectroscopy (APXPS) – carried out at the new APXPS instrument at the Swedish synchrotron radiation facility MAX IV Laboratory – and *ex situ* Scanning tunnelling microscopy (STM) and x-ray photoelectron spectroscopy (XPS) measurements performed in UHV.

A recent surface x-ray diffraction study reports different oxygen phases for the Ir(111) surface at oxygen pressures from 10^{-6} to 100 mbar – chemisorbed oxygen, a trilayer, a multilayer oxide, and a bulklike oxide [3]. Concentrating on pressures at around 1 mbar, we find a variety of oxygen-rich structures. The corresponding CO adsorption phase formed at 1 mbar CO pressure is an assembly of separated CO_{16} clusters with the CO molecules sitting in on-top sites [4].

The reactivity at 1 mbar total pressure ($\text{O}_2:\text{CO}$ ratio 9:1) and at different temperatures was studied by APXPS and simultaneous monitoring of the gas composition. We find that the phase with the highest activity for the oxidation of CO is a surface phase which contains both CO and oxygen. By comparing with the measured adsorption structures of oxygen we find that the oxygen structure is quite similar to the $p(2\times 1)\text{-O}$ structure formed on Ir(111) under UHV conditions. This contrasts with what is found for other platinum group metals such as the Pt(111) surface [2], for which CO oxidation is favoured over oxygen rich phases.

[1] A. L. Gerrard, J. F. Weaver, J. Chem. Phys. **123** (2005) 224703.

[2] H. Over et al., Science **287** (2000) 1474.

[3] Y. B. He et al., J. Phys. Chem. **112** (2008) 11946.

[4] L.-M. Yang, S.-L. Yau, J. Phys. Chem. B. **104** (2000) 1769.

Tuesday Afternoon, October 30, 2012

Applied Surface Science

Room: 20 - Session AS+BI-TuA

Surface Analysis of Materials Using Vibrational Techniques (2:00-3:20 pm)/ Multi-Technique Analysis (4:00-6:00 pm)

Moderator: D. Roy, National Physical Laboratory, UK, C. Szakal, National Institute of Standards and Technology

2:00pm AS+BI-TuA1 Vibrational Spectrum and Stability of the Long-Debated Models for the $(\sqrt{7}\times\sqrt{7})R19^\circ$ Phase of S/Cu(111). *M. Alcantara Ortigoza, M. Aminpour, T.S. Rahman*, University of Central Florida

Recently, the structure of the copper sulfide overlayer formed on Cu(111) upon sulfur exposure has attracted attention because it serves as a substrate to form MoS₂ monolayers and MoS_x nanostructures in a controlled manner, which may have numerous technological applications. In the past, at least eight experimental techniques have been used to characterize the $(\sqrt{7}\times\sqrt{7})R19^\circ$ Cu-S overlayer on Cu(111) and to support or refute a large number of possible models but, as yet, at least three models are still in dispute. In this study, we provide firmer arguments to resolve the structure of CuS/Cu(111) at the atomic scale. Specifically, we perform density-functional-theory calculations of the total energy and the vibrational spectrum of the proposed structures to (1) attest their dynamical stability; (2) compare their thermodynamic stability as obtained from the total free energy; and (3) provide the vibrational frequencies that uniquely fingerprint these structures and which may serve for further experimental confirmation or refutation.

This work was supported in part by DOE grant DE-FG02-07ER15842

[1] Kim et al., Langmuir 27, 11650 (2011)

[2] Alfonso J. Phys. Chem. C 115, 17077 (2011)

2:40pm AS+BI-TuA3 First-principle Investigation of the Stability and Vibrational Spectrum of MoS_x Nanostructures Grown on Cu(111). *M. Aminpour, M. Alcantara Ortigoza, T.S. Rahman*, University of Central Florida

Recent experiments have successfully synthesized MoS_x nanostructures in a controlled manner by evaporating Mo adatoms on the copper sulfide monolayer that forms on Cu(111) upon sulfur preloading[1,2]. Based on STM observations and total-energy calculations based on density functional theory, including *ab initio* van-der-Waals interactions, several structures for MoS_x/Cu(111) have been proposed. In this study, we investigate the plausibility of those structures and provide elements for further experimental substantiation or refutation. Namely, we perform density-functional-theory calculations (also including *ab initio* van-der-Waals interactions) of the total energy and the vibrational spectrum of the proposed structure to (1) attest their dynamical stability; (2) compare their thermodynamic stability as obtained from the total free energy; and (3) provide the vibrational frequencies that uniquely fingerprint the proposed structures.

[1] Kim et al., Langmuir 27, 11650 (2011)

[2] Le et al., PRB 85, 075429 (2012)

This work was supported in part by DOE grant DE-FG02-07ER15842

4:40pm AS+BI-TuA9 New Desorption Mass Spectrometry Approaches for Inorganic Particle Analysis. *C. Szakal, A.R. Konicek, M. Ugelow, D.S. Simons, A. Herzing, R.D. Holbrook*, National Institute of Standards and Technology

Chemical characterization of inorganic particles becomes more difficult as the particle sizes decrease. For application areas ranging from semiconductor failure analysis to nanotoxicology, the distinct chemical signatures of both the surface and bulk of particles can provide insight into system mechanisms and behavior. New methods that aim to explore the surface chemistry of inorganic nanoparticles for both their elemental and organic overlayer signatures will be presented. Specifically, the “static” nature of time-of-flight-secondary ion mass spectrometry is used to provide mass spectral characterization at the very surfaces and sub-surfaces of well-prepared (via drop-on-demand inkjet printing) and well-characterized (via scanning transmission electron microscopy and ultraviolet-visible spectroscopy) nanoparticle aggregates. This information can potentially be combined with full aggregate analysis using more elementally sensitive dynamic SIMS instrumentation once target species are identified with ToF-SIMS. Both sets of SIMS data can be used to obtain a chemical distribution

of signals throughout the particle depths. Additionally, the question of whether the centers of inorganic nanoparticle aggregates are chemically similar to the overall aggregate surfaces will be explored.

5:00pm AS+BI-TuA10 TOF SIMS Analyses of Ga Concentration as a Function of Distance from FIB Milled Features. *C. Santeufemio*, University of Massachusetts, *B.P. Gorman*, Colorado School of Mines, *C. Zhou, F.A. Stevie*, North Carolina State University, *L.A. Giannuzzi*, L.A. Giannuzzi & Associates LLC

Focused ion beams are routinely used for site-specific specimen preparation, nanopatterning, and analysis. It is important to know whether the primary ion beam is present outside the region targeted for ion beam modification. A previous report showed that $> 1E12$ atoms/cm² of Ga was detected up to several millimeters away from a focused ion beam (FIB) milled feature [1]. In this work, we reproduce this earlier report using a blind study of 2 different state-of-the-art Ga-FIB columns. Each column was used to FIB mill a 100 μm x 100 μm square into a (100) Si wafer at 30 keV with a nominal beam current of 20 nA at constant dose. Time of flight secondary ion mass spectrometry (TOF SIMS) was used to measure Ga depth profiles and Ga surface concentration at a distance up to 6.5 mm from the FIB milled square. In column “A,” $> 1E12$ atoms/cm² of Ga was detected up to ~ 5 mm from the FIB milled square. Column “B” showed considerably less Ga with $> 1E12$ atoms/cm² detected within ~ 250 μm from the FIB milled square. The depth profiles show that the Ga concentration was fairly uniform to a depth of ~ 2 nm from the surface for column “A” and ~ 1 nm into the surface for column “B”. Using SRIM [2] simulations we determine that these implantation depths correspond to an ion energy < 500 eV. The consequences of the presence of Ga at long distances from desired FIB milled features will be discussed.

[1] U. Muehle, R. Gaertner, J. Steinhoff, W. Zahn, “Characterisation of Ga-distribution on a silicon wafer

after inline FIB-preparation using inline ToFSIMS,” M. Luysberg, K. Tillmann, T. Weirich (Eds.): EMC 2008, Vol. 1: Instrumentation and Methods, pp. 749–750, DOI: 10.1007/978-3-540-85156-1_375, © Springer-Verlag Berlin Heidelberg 2008

[2] www.srim.org

5:20pm AS+BI-TuA11 The Surface Characterization of Oligo(Ethylene Glycol) Functionalized Gold Nanoparticles. *A. Rafati, D.G. Castner*, University of Washington

Extensive surface analysis of available gold nanoparticles (AuNPs) is crucial to understand how their production and functionalization affects their final properties. This information is needed to improve the performance of engineered nanoparticles in research and commercial applications. Ethylene glycol functionality is desirable owing to the benefits such as the reduction of protein adhesion which if not properly controlled can lead to activation of an immune response and/or clearance.

In this work AuNPs ~14nm and ~40nm in diameter are synthesized and functionalized with 1-undecanethiol (HS-CH₂)₁₁ terminated with either (OEG)₄OH or (OEG)₄CH₃. The AuNPs were characterized with transmission electron microscopy (TEM), time of flight secondary ion mass spectrometry (ToF-SIMS), X-ray photoelectron spectroscopy (XPS), attenuated total reflectance Fourier transform infrared spectroscopy (ATR-FTIR) and low energy ion scattering (LEIS). These studies provided both qualitative and quantitative information about the functionalization of the AuNPs with an OEG containing monolayer.

TEM showed the 14nm AuNPs had a narrower size distribution and more spherical shape than the 40nm AuNPs. ToF-SIMS clearly differentiates the two SAMs based on the C₃H₇O⁺ peak attributed to the CH₃ terminated SAM. Angle-resolved XPS high-resolution C1s spectra from flat gold samples at photoelectron take-off angles of 0°, 55° and 75° from the surface normal shows an increase in the ether component and reduction in CH with an increase in take-off angle. The changes in these values are comparable for both SAMs. This illustrates the increased presence of ethylene glycol monomers in the outer surface region and shows little difference between the two types of terminal functional groups. The 40 nm AuNPs show a slightly greater surface OEG concentration than 14 nm AuNPs, possibly indicating a more vertically oriented SAM on the 40 nm AuNPs. FTIR indicates similar crystalline CH₂ backbones for all samples, however it appears the structure of OEG head groups are less crystalline on the 14nm AuNPs. This likely results in thicker and/or higher density SAMs on the 40 nm AuNPs compared to the 14nm AuNPs. This is consistent with the nearly identical XPS determined surface elemental compositions determined for OEG SAMs on the two different sized AuNPs. This is contrary to previously XPS results observed for AuNPs functionalized with COOH SAMs [1].

1. Techane, S.D., L.J. Gamble, and D.G. Castner, *Multi-technique Characterization of Self-assembled Carboxylic Acid Terminated Alkanethiol Monolayers on Nanoparticle and Flat Gold Surfaces*. J Phys Chem C Nanomater Interfaces, 2011. **115**(19): p. 9432-9441.

5:40pm **AS+BI-TuA12 Characterization Challenges of Ceria Nanoparticles: When is a Nanoparticle Not a Nanoparticle?**, **D.R. Baer**, **P. Munusamy**, **A.S. Karakoti**, EMSL, Pacific Northwest National Laboratory, **S.V.N.T. Kuchibhatla**, Battelle Science and Technology India, **S.S. Seal**, University of Central Florida, **S. Thevuthasan**, **C.F. Windisch, Jr.**, EMSL, Pacific Northwest National Laboratory

Cerium oxide (ceria) nanoparticles are widely studied for their current and potential use in catalytic, energy, environmental protection and bio-medical applications. The performance of ceria in many of these applications depends on the ability of cerium to switch between +3 and +4 oxidation states. Unfortunately the physical and chemical properties of ceria nanoparticles reported in the literature are often in consistent and at times contradictory. Our research involves examination of the properties of ceria nanoparticles as they apply to materials science research and impact biological systems. We have found that it is possible to obtain what appears to be a self-consistent understanding of these particles by integrating dynamic light scattering, surface potential and UV-Vis adsorption measurements made in solution with *ex situ* x-ray photoelectron spectroscopy (XPS), x-ray diffraction (XRD) and transmission electron microscopy (TEM) observations. These measurements have demonstrated that a simple understanding of the chemical state of ceria nanoparticles as dependent on size is not adequate and has led to some of the inconsistent results in the literature. However, Raman and microXRD of wet ceria nanoparticles (pseudo *in situ*) show that the nature of the particles in solution is even more complex than indicated the above measurements. Raman and microXRD measurements indicate that both the chemical state and structure of the smallest nanoparticles can change depending on the nature of the solution. In solutions with low oxygen activity these particles have a ceria structure with cerium in +3 oxidation state while in highly oxidizing conditions the chemical state switches to +4 but the structure can be highly defected (XRD) and appears to be some type of cerium oxyhydroxide (Raman). The extent of the transformation depends on the size of the particles and appears complete for the smallest particles and partial or possibly not present for larger particles. These measurements demonstrate that the environment, size and time can impact the nature of these particles and that a variety of analysis methods – *in situ* as well as *ex situ* – are required for comprehensive understanding of ceria nanoparticle behaviors. Acknowledgement - Aspects of the work have been supported by the National Institute of Environmental Health Sciences under grant NIH U19 ES019544. Portions of this work were conducted in the Environmental Molecular Sciences Laboratory, a DOE user facility operated by Pacific Northwest National Laboratory for the Office of Biological and Environmental Research of the DOE.

Biomaterial Interfaces

Room: 23 - Session BI+AS-TuA

Characterization of Biointerfaces

Moderator: L. Meagher, CSIRO Materials Science and Engineering, Australia

2:00pm **BI+AS-TuA1 Surface Characterization Meets Cells and Proteins**, **B.D. Ratner**, University of Washington **INVITED**

Surfaces such as Ni(100) and Si(100) have been extensively studied and each has been found to be more complicated than simple geometric models would suggest. In this context, consider more mobile surfaces than these precisely defined crystal surfaces that are comprised of 20 amino acids integrated into hundreds of different proteins. Also, these surfaces may contain lipids and complex saccharide structures. It should be apparent that these surfaces can be staggeringly complex, and yet, as with surfaces in general, they efficiently catalyze complex reactions. But they do this at room temperature and atmospheric pressure in a way that makes life possible. For these reasons, the ability to characterize such surfaces will certainly lead to advances in surface design and surface functionality. Tools taken from the “surface science tool chest” can be applied in special ways to complement the tools developed by biologists for molecularly characterizing such surfaces. This talk, primarily focused on electron spectroscopy for chemical analysis (ESCA) and secondary ion mass spectrometry (SIMS), will start with analysis of amino acids and peptides, move to adsorbed protein films and finally consider complex surfaces such as decellularized extracellular matrices and cell monolayers.

2:40pm **BI+AS-TuA3 Using Binary Solvent Mixtures Produces High Graft Density Poly (Ethylene Glycol) Layers**, **A.R. Arcot**, Aalto University, Finland, **S. Zhang**, **R.L. Meyer**, **R. Ogaki**, Aarhus University, Denmark, **P. Kingshott**, Swinburne University of Technology, Australia

The success of PEG based non fouling surfaces depends on several factors such as graft density [1] and nature of head group-substrate interaction. [2] The ‘grafting-to’ technique though simple, often results in low pinning density when compared to ‘grafting-from’ technique. [3] This limitation of ‘grafting-to’ technique can be overcome by grafting under reduced solubility conditions. [4] We demonstrate a simple and versatile way to coat surfaces with PEG at high graft density using binary solvent mixtures, where a poor and a good PEG solvent are mixed with the PEG. The addition of poor solvent decreases the hydrodynamic radius of PEG molecules and hence results in thicker films due to diminished steric repulsion (Supplementary Fig 1a and 1b). The ‘good’ and ‘poor’ solvent pair was chosen based on solubility parameter distance calculated from Hansen solubility parameters. [5]

The PEG thiol films on gold formed from acetone-ethanol mixtures were analyzed using x-ray photoelectron spectroscopy (XPS), ellipsometry and atomic force microscopy. The PEG film gets thicker with more ethanol, which is a poorer solvent for PEG (Supplementary table 1). The high resolution sulfur 2p spectra confirmed the absence of precipitate particles. Grafting under high ionic strength conditions used by Kingshott et al. was used as reference for comparison. [4] The PEG thiol films were exposed to fetal bovine serum (FBS) and it was observed that thicker films could resist protein adsorption better than thin films that were formed from high solubility conditions. This method of using binary solvent mixtures can be extended to any polymer-substrate system by choosing appropriate ‘good-poor’ solvent pair. To demonstrate this point we also studied 5 kDa PEG silane films grafted using acetone-diethyl ether solvent mixture.

References:

1. L. D. Unsworth, H. Sheardown and J. L. Brash, *Biomaterials* (30), 5927-5933 (2005).
2. P. Kingshott, J. Wei, D. Bagge-Ravn, N. Gadegaard and L. Gram, *Langmuir* (17), 6912-6921 (2003).
3. N. Luo, J. B. Hutchison, K. S. Anseth and C. N. Bowman, *Macromolecules* (7), 2487-2493 (2002).
4. P. Kingshott, H. Thissen and H. J. Griesser, *Biomaterials* (9), 2043-2056 (2002).
5. B. A. Miller-Chou and J. L. Koenig, *Progress in Polymer Science* (8), 1223-1270 (2003).

3:00pm **BI+AS-TuA4 Adsorption Behavior of Serum Albumin on Nanocrystalline Apatites**, **K. Fears**, **D. Burden**, **C. Love**, U.S. Naval Research Laboratory, **D. Day**, Missouri University of Science and Technology, **T. Clark**, U.S. Naval Research Laboratory

The adsorption behavior of bovine serum albumin (BSA) on nanocrystalline hydroxyapatite (HA) and strontium apatite (SrHA) microspheres, derived from borate glasses, was assessed using circular-dichroism spectroscopy (ECD). Numerous reports have shown that surfaces which present nano-sized features can exhibit better cellular response than surfaces with features in the micron regime. The microspheres were incubated in BSA solutions (40 mg/mL; ~64% helix; ~1% sheet) to determine if BSA adsorbed in a fundamentally different manner than on bioinert yttria-alumina-silicate (YAS) spheres that induced minimal conformational changes (~56% helix; ~4% sheet). On the apatite spheres, BSA loss a substantial amount of its helical structure and strained disulfide bonds were detected. However, the protein density on the SrHA spheres was 50% lower than on the HA spheres, indicating that BSA has a higher affinity for irreversible adsorption on HA. 5,5'-Dithio-bis-(2-nitrobenzoic acid), was used to selectively modify free thiols post-adsorption, indicating that solvent-accessible free cysteines were present on the apatite spheres, despite the absence of a reducing agent. Subsequent BSA molecules, or other proteins *in vivo*, could potentially form intermolecular disulfide bonds leading to increased adhesion of proteins or support the formation of macroscopic protein structures.

4:00pm **BI+AS-TuA7 Quantitative Characterization of Cells in Biofilms and on Surfaces**, **A.C. Areias**, **C. Sousa**, **G.P. Mendes**, University of Minho, Portugal, **P. Mack**, Thermo Fisher Scientific, UK, **S. Lanceros-Méndez**, University of Minho, Portugal, **D.Y. Petrovykh**, International Iberian Nanotechnology Laboratory, Portugal

Films of cells on solid substrates are encountered in a variety of biological and biomedical environments, including cells in biofilms that spontaneously colonize medical devices and multilayers of cells filtered from suspensions for analysis. Understanding the chemical properties of cells in such films is important for providing clues about the behavior of the cells or about the effects of treatments that had been applied to the cells. Similarly to other

types of surface-based systems, the characterization of cells on solid substrates poses several analytical challenges. In particular, the small number of cells on each sample, the interference from surface interactions, and the absorbance of the substrate material prevent the characterization of cells on surfaces by the standard optical methods that are used in solution. We show that protocols similar to those used for preparing samples for electron microscopy can be adapted to prepare biofilm samples for characterization by X-ray photoelectron spectroscopy (XPS). Modern XPS instruments also provide the functionality required for characterization of these complex samples, for example, sample charging on insulating substrates can be efficiently and consistently compensated. Finally, the Ar cluster ion beam technology that recently became available on XPS instruments provides additional capabilities for a more detailed characterization of cells in biofilms, which typically have thicknesses larger than the sampling depth of XPS. We characterized several types of fixed and dried cell samples, including biofilms and cells filtered from suspensions, to compare different preparation protocols and to identify qualitative and quantitative parameters that can be reliably obtained from XPS analysis of such films of cells. We will present the results of our comparative analysis and possible applications of our methodology for characterization of cells in biological and biomedical experiments.

4:20pm BI+AS-TuA8 Antimicrobial Multilayers and Their Analysis by Laser Desorption Postionization Mass Spectrometry, M. Blaze, C. Bhardwaj, A. Akhmetov, L. Hanley, University of Illinois at Chicago

Bacterial biofilms are structured communities of microbes encapsulated within a self-developed polymeric matrix which adhere to surfaces and display genetic expression distinct from freely floating bacteria. Biofilms are frequently found to populate medical devices, leading to significant problems of infection in the first few days after implantation. Polyelectrolyte multilayers are developed for the delayed delivery of antibiotics to inhibit biofilm growth on biomedical devices [1]. Ten layers each of chitosan and alginate are prepared on a gold substrate, then infused with a novel antibiotic compound. This antibiotic-infused multilayer is found to inhibit the growth of *Enterococcus faecalis* bacterial biofilms on membranes over an 18 hour exposure. Laser desorption postionization mass spectrometry (LDPI-MS) is used to characterize the antibiotic after synthesis [2]. LDPI-MS analysis shows that the antibiotic survives sterilization of the multilayer surface, but <1% of the antibiotic remains after exposure to the biofilm.

[1] M. Blaze M.T., L.K. Takahashi, J. Zhou, M. Ahmed, G.L. Gasper, F.D. Pleticha, and L. Hanley, *Anal. Chem.* 83(2011) 4962.

[2] A. Akhmetov, J.F. Moore, G.L. Gasper, P.J. Koin, L. Hanley, *J. Mass Spectrom.* 45 (2010) 137.

4:40pm BI+AS-TuA9 Combining Colloidal Probe Atomic Force and Reflection Interference Contrast Microscopy to Study the Mechanics of Biopolymer Films, R.P. Richter, CIC biomaGUNE, Spain; Joseph Fourier University, France; Max Planck Institute for Intelligent Systems, Germany, S. Attili, CIC biomaGUNE, Spain; Max Planck Institute for Intelligent Systems, Germany, V. Borisov, Institut Pluridisciplinaire de Recherche sur l'Environnement et les Matériaux, France

Highly solvated polymer films have naturally evolved as multifunctional interfaces in biological systems, e.g. as mucosal films, cellular coats or bacterial biofilms. Surface-confined polymer films are also becoming increasingly popular as biomaterials and in various (bio)technological applications. The mechanical response of such polymer films is not only important for functional performance, but it can also provide valuable information about the film's internal organization, interactions and dynamics.

Here, we present a method that combines colloidal probe atomic force microscopy (AFM) and reflection interference contrast microscopy (RICM) to measure the mechanical properties of thin and solvated polymer films. When analyzing such films, a fundamental problem in colloidal probe AFM experiments is to determine the distance at closest approach between the probe and the substrate on which the film is deposited. By combining AFM and RICM *in situ*, forces and absolute distances can be measured simultaneously, and experimental drifts that otherwise would pass unnoticed can be corrected (1).

We used the combined setup to quantify the compressive mechanics of films of end-grafted hyaluronan (HA brushes) (2). Hyaluronan is a polysaccharide that plays a vital role in the organization and function of pericellular coats and extracellular matrices in vertebrates, and that is also attractive for biomedical applications. We show that HA brushes can swell dramatically as a function of ionic strength or upon binding of the cartilage proteoglycan aggrecan. Detailed comparison of the experimental data with polymer theory reveals that hyaluronan is a prototype of a strongly charged, semiflexible polyelectrolyte with intrinsic excluded volume (3).

The novel combined AFM/RICM setup should be broadly applicable to quantify the mechanical properties of soft hydrated polymer films with precise control of probe-sample separation. The generated data on HA brushes represent a valuable reference for future quantitative studies of more complex HA-rich films and to refine theories of polyelectrolyte brushes of strongly charged and intrinsically stiff polyelectrolytes.

References:

- (1) Attili and Richter *Langmuir* **2012**, 28:3206;
- (2) Richter et al. *J. Am. Chem. Soc.* **2007**, 129:5306;
- (3) Attili et al. *Biomacromolecules* **2012**, in press.

5:00pm BI+AS-TuA10 Surface Modification of Silicone Hydrogels through Adsorption of Diblock Copolymers, Y.J. Huo, S.S. Perry, University of Florida

The interaction between an ethylene oxide-*block*-butylene oxide (EOBO) copolymer surfactant and the surfaces of four silicone hydrogel (SH) contact lenses—PureVision® (PV), O₂OPTIX® (O₂), ACUVUE® Oasys® (AO), and Biofinity® (BF)—was investigated using angle-resolved X-ray photoelectron spectroscopy (AR-XPS) following treatment in test solutions containing various concentrations of EOBO. The nature of this interaction was further understood by quantifying the amount of eluted EOBO from each lens following the same treatment using ultra performance liquid chromatography (UPLC). The elution study revealed a large disparity in the amount of EOBO uptake by the different samples following each solution treatment. The XPS results, however, suggested that the amount of EOBO retained on the surface of the lenses demonstrated a largely different trend. For example, AO and BF displayed little evidence of signal at binding energies characteristic of the EO blocks, whereas O₂ and PV exhibited a clear EO signature. The correlation between the elution and XPS results highlights the difference in the interaction mechanism of the EOBO copolymer with different lenses. For lenses such as O₂OPTIX®, this interaction is predominantly bound to the surface; for ACUVUE® OASYS®, however, EOBO was uniformly distributed through the lens structure.

5:20pm BI+AS-TuA11 Microfluidic Devices for High-Throughput Quantitation in Biology: From Biophysics to Diagnostics, S. Maerkl, Ecole Polytechnique Fédérale de Lausanne (EPFL), Switzerland INVITED

Microfluidic devices promise to have a significant impact on human health, particularly in diagnostics and drug development. We have developed a suite of microfluidic devices for high-throughput protein biochemistry and applied them to a wide range of applications spanning from protein biophysics to diagnostics, drug development, and vaccine development. Here I will discuss a novel approach to obtaining hundreds of kinetic rate measurements of bimolecular interactions on a single microfluidic device. In a second example I will present a generic microfluidic platform capable of quantitating biomarkers from a wide variety of samples in high-throughput and ultra-low cost, which could ultimately supersede the classical ELISA assay. We applied this platform to vaccine development by quantitating the activation of dendritic cells in response to a large panel of binary adjuvant combinations.

**Graphene and Related Materials Focus Topic
Room: 13 - Session GR+AS+NS+SP+SS-TuA**

Graphene Characterization Including Microscopy and Spectroscopy

Moderator: J.C. Hone, Columbia University

2:00pm GR+AS+NS+SP+SS-TuA1 High Resolution Real and Reciprocal Space Photoelectron Emission Microscopy on Heterogeneous Graphene/SiC(000-1), K. Winkler, B. Kroemker, 10micron NanoTechnology, Germany, N. Barrett, IRAMIS, Saclay, France, E. Conrad, GeorgiaTech

We present energy filtered electron emission spectromicroscopy with high spatial and wave-vector resolution on few-layer epitaxial graphene on SiC(000-1) grown by furnace annealing.

Conventional electron spectroscopy methods are limited in providing simultaneous real and reciprocal or k-space information from small areas under laboratory conditions. Therefore, the characterization of materials with only micron scale sample homogeneity such as epitaxially grown graphene requires new instrumentation. Recent improvements in aberration compensated energy-filtered photoelectron emission microscopy (PEEM) can overcome the known limitations in both synchrotron and laboratory environments. Here we report 2D maps of the k-parallel π - π * band

dispersion in micron-scale regions and correlate them with spatially resolved chemical information on the same regions. Only the combination of high lateral, high energy, high k-resolution and controlled switching between real space and k-space allows detailed understanding of micron size sample sites with 1–3 layers graphene. The experiments underline the importance of simultaneous lateral, wave vector and spectroscopic resolution on the scale of future electronic devices in order to precisely characterize the transport properties and band alignments.

2:20pm GR+AS+NS+SP+SS-TuA2 Evidence of Nanocrystalline Semiconducting Graphene Monoxide during Thermal Reduction of Graphene Oxide in Vacuum, C. Hirschmugl, E. Mattson, H. Pu, S. Cui, M. Schofield, S. Rhim, G. Lu, M. Nasse, University of Wisconsin Milwaukee, R.S. Ruoff, University of Texas at Austin, M. Weinert, M. Gajardziska-Josifovska, J. Chen, University of Wisconsin Milwaukee

As silicon-based electronics are reaching the nanosize limits of the semiconductor roadmap, carbon-based nanoelectronics has become a rapidly growing field, with great interest in tuning the properties of carbon-based materials. Chemical functionalization is a proposed route, but syntheses of graphene oxide (G-O) produce disordered, nonstoichiometric materials with poor electronic properties. We report synthesis of an ordered, stoichiometric, solid-state carbon oxide that has never been observed in nature and coexists with graphene. Formation of this material, graphene monoxide (GMO)[1], is achieved by annealing multilayered G-O. A combination of transmission electron microscopy and infrared microscopy have provided critical experimental evidence to identify the novel structure. These results indicate that the resulting thermally reduced G-O (TRG-O) consists of a two-dimensional nanocrystalline phase segregation: unoxidized graphitic regions are separated from highly oxidized regions of GMO. GMO has a quasi-hexagonal unit cell, an unusually high 1:1 O:C ratio, and a calculated direct band gap of approximately 0.9 eV.

This work was supported by the NSF (CMMI-0856753 and CMMI-0900509). This work is based upon experiments performed at the Synchrotron Radiation Center. The SRC is funded by the University of Wisconsin-Madison and the University of Wisconsin-Milwaukee. Work performed at the SRC IRENI beamline been done with support from an NSF Major Research Instrumentation grant (DMR-0619759). The authors thank Bruker Technologies for the Grazing Angle Objective used for this work.

[1] Mattson, E.C. et al., ACSNano (2011) 5 (2011) 9710-9717.

2:40pm GR+AS+NS+SP+SS-TuA3 Scanning Tunneling Spectroscopy of Epitaxial Graphene: Local Band Mapping and Wavefunction Engineering, P.N. First, Georgia Tech

Because the crystalline orientation is determined prior to growth, epitaxial graphene (EG) on silicon carbide is an excellent material to consider for 2D wavefunction engineering, where device properties are designed through wavefunction confinement and material strain. In pursuit of this goal, we use scanning tunneling microscopy (STM) and spectroscopy (STS) to characterize the local structural and electronic properties of EG and a simple EG nanostructure. With some care, STS can be used to measure the full energy-momentum dispersion of both filled and empty states, on length scales determined by the coherence of the graphene wavefunctions. Applying a magnetic field introduces a field-tunable comb of discrete Landau level energies that we use to obtain high momentum resolution, to characterize the tip-induced surface potential, and to detect subtle interlayer interactions in a multilayer graphene stack. * Work performed in collaboration with NIST Center for Nanoscale Science and Technology ** Funded in part by NSF and by NRI-INDEX.

4:00pm GR+AS+NS+SP+SS-TuA7 Intercalation of O₂ and CO Controlled by the Mesoscopic Structure of Graphene, E. Grånäs, J. Knudsen, Lund University, Sweden, U. Schröder, T. Gerber, C. Busse, Universität zu Köln, Germany, M.A. Arman, K. Schulte, J.N. Andersen, Lund University, Sweden, T.W. Michely, Universität zu Köln, Germany

Intercalation of gases between epitaxial graphene and its substrate has become a topic of interest for studies due to, for example, the unique opportunities to modify the graphene-substrate interaction and the possibilities to perform chemistry under the graphene layer. Further, a profound knowledge about graphenes stability in gases at elevated temperatures and pressures is essential for, among other things, the correct interpretation of gas adsorption studies on graphene supported metal cluster arrays.

We have studied intercalation and etching of Ir(111) supported graphene upon gas exposure to common gasses such as O₂ and CO in the entire pressure interval from 10⁻⁸ to 0.1 mbar. Comparing perfect graphene layers without holes with graphene films, that only covers a fraction of the Ir(111)

surface, we reveal that the holes - or more specific the graphene edges - are essential for intercalation.

For oxygen exposed graphene we develop a coherent picture of temperature dependent oxygen etching and intercalation. Using X-ray photoemission spectroscopy (XPS) and scanning tunnelling microscopy (STM) we show that a perfect graphene layer is stable against etching and intercalation up to 700 K, whereas at higher temperatures etching, but no intercalation, takes place. In contrast, a partial graphene coverage on Ir(111) enables dissociative oxygen adsorption on the bare Ir and subsequent intercalation underneath graphene flakes at 355 K and above. Intercalated oxygen remains stable up to a temperature of 600 K, above this temperature it desorbs in the form of CO or CO₂. We have determined XPS and STM fingerprints for the intercalated oxygen structure and we unambiguously assign it to a p(2x1)-O structure similar to the one observed on clean Ir(111). The decoupling of the intercalated graphene film from the metal substrate is directly visualized through the inability to form well-ordered Pt cluster arrays on the O-intercalated areas of graphene on Ir(111). Further, we have identified the rate limiting step for oxygen intercalation to be unlocking of the graphene edge and propose that this takes place through bond breaking between graphene edge bonds and the Ir substrate.

Using a combination of high pressure X-ray photoemission spectroscopy (HP-XPS) and STM we also show that CO intercalation takes place at room temperature and pressures in the 1 mbar range. The adsorption structure of intercalated CO is determined to be (3√3 × 3√3)R30°, identical to the structure observed on clean Ir(111) upon high pressure CO exposure.

4:20pm GR+AS+NS+SP+SS-TuA8 Long-range Atomic Ordering and Variable Interlayer Interactions in Two Overlapping Graphene Lattices with Stacking Misorientations, T. Ohta, T.E. Beechem, Sandia National Laboratories, J.T. Robinson, Naval Research Laboratory, G.L. Kellogg, Sandia National Laboratories

We report a method to examine the effect of stacking misorientation in bilayer graphene by transferring chemical vapor deposited (CVD) graphene onto monolithic graphene epitaxially grown on silicon carbide (SiC) (0001). The resulting hybrid bilayer graphene displays long-range Moiré diffraction patterns having various misorientations even as it exhibits electron reflectivity spectra nearly identical to epitaxial bilayer graphene grown directly on SiC. These varying twist angles affect the 2D (G')-band shape of the Raman spectrum indicating regions of both a monolayer-like single π state and Bernal-like split π states brought about by the differing interlayer interactions. This hybrid bilayer graphene fabricated via a transfer process therefore offers a means to systematically study the electronic properties of bilayer graphene films as a function of stacking misorientation angle.

The work at Sandia National Laboratories was supported by LDRD and by the US DOE Office of Basic Energy Sciences, Division of Materials Science and Engineering. Sandia National Laboratories is a multi-program laboratory managed and operated by Sandia Corporation, a wholly owned subsidiary of Lockheed Martin Corporation, for the U.S. Department of Energy's National Nuclear Security Administration under contract DE-AC04-94AL85000. The work at NRL was funded by the Office of Naval Research.

4:40pm GR+AS+NS+SP+SS-TuA9 Chemically-resolved Interface Structure of Epitaxial Graphene on SiC(0001), J.D. Emery, Northwestern Univ., B. Detslefs, European Synchrotron Radiation Fac., France, H.J. Karmel, Northwestern Univ., V.D. Wheeler, U.S. Naval Research Lab, J.M.P. Alaboson, Northwestern Univ., L.O. Nyakiti, R.L. Myers-Ward, C.R. Eddy, Jr., D.K. Gaskill, U.S. Naval Research Lab, M.C. Hersam, Northwestern Univ., J. Zegenhagen, European Synchrotron Radiation Fac., France, M.J. Bedzyk, Northwestern Univ.

The implementation of graphene into next-generation electronics will require production high-quality graphene at the wafer scale. One promising route for the production of wafer-scale graphene is to grow epitaxial graphene (EG) via thermal decomposition of Si-terminated SiC (SiC(0001)). This method produces high-quality EG, but is accompanied by the formation of the so-called "buffer layer" at the interface, which is known to affect the electronic properties of the graphene. Despite numerous efforts to determine the nature of the buffer layer, debate persists concerning its atomic and chemical structure. Here, we use the X-ray Standing Wave (XSW) technique to create a precise chemically-sensitive description of the distributions of Si and C at the interface. This technique, which combines X-ray scattering and X-ray Photoelectron Spectroscopy (XPS), is capable of locating coherent distributions of chemically distinct species above a single crystal surface. This allows for a more detailed description of the interface than those afforded by scattering or XPS alone. Our analysis shows that the buffer layer, which is present in both UHV and furnace-grown EG/SiC(0001), contains no substantial non-bulk or oxide silicon component, and is thus purely carbon. We identify two chemically distinct carbon species within the interface layer, each with a distinct

location above the Si-terminated surface, and report their positions and distributions with sub-angstrom precision. These results help to clarify long-standing uncertainties about the interfacial structure of graphene/SiC(0001). Further, we also highlight the potential for XSW with XPS as a valuable tool in the structural determination of complex interfaces, such as functionalized, doped, or intercalated epitaxial graphene.

5:00pm GR+AS+NS+SP+SS-TuA10 Formation of Graphene on SiC(000-1) in Disilane and Neon Environments, G. He, N. Srivastava, R. Feenstra, Carnegie Mellon University

We have prepared graphene on the SiC(000-1) surface (the so-called C-face of the {0001} surfaces), by heating the SiC in a Si-rich environment produced either by using disilane ($\approx 10^{-4}$ Torr) or cryogenically-purified neon (1 atm). With the Si-rich environments, we obtain considerably better uniformity in the thickness for thin, \approx ML-thick graphene on the C-face compared to that observed in samples prepared in vacuum or in an argon environment. We also find that different interface structures occur in these environments. In particular, we find a graphene-like buffer layer forming at the interface, analogous to the well known behavior of the SiC(0001) surface (the Si-face).

Studies are performed using atomic force microscopy (AFM), low-energy electron diffraction (LEED), and low-energy electron microscopy (LEEM). For graphene prepared in vacuum, LEED patterns show a characteristic 3×3 pattern together with graphene streaks. In contrast, for the graphene produced in either the disilane environment ($\approx 10^{-4}$ Torr) or 1 atm of neon, LEED patterns reveals a complex $\sqrt{43} \times \sqrt{43}$ - $R \pm 7.6^\circ$ arrangement along with graphene spots. This structure is somewhat similar to the well known $\sqrt{3} \times \sqrt{3}$ - $R30^\circ$ "buffer layer" of the Si-face, with satellite spots surrounding the primary Si spots, and is interpreted as arising from a C-rich buffer layer on the SiC. Selected area diffraction on those surface areas reveals a wavevector magnitude precisely equal to that of graphene, thus proving that the buffer layer does indeed have structure very close to that of graphene (the pattern is interpreted as a distortion of the buffer-layer graphene due to bonding to the underlying SiC). Using LEEM, measurements from the buffer layer of the reflected intensity of the electrons as a function of their energy reveal a new characteristic reflectivity curve, not seen for vacuum-prepared graphene.

After oxidation of the samples, the $\sqrt{43} \times \sqrt{43}$ - $R \pm 7.6^\circ$ spots disappear and $\sqrt{3} \times \sqrt{3}$ - $R30^\circ$ spots appear on the surface. This latter behavior is interpreted as oxidation of the SiC surface beneath the buffer layer. Selected area diffraction on portions of the surface that were previously identified as buffer layer still reveal a wavevector magnitude precisely equal to that of graphene. However, LEEM reflectivity curves on those areas reveal a completely new spectrum, indicative of a "decoupling" of the buffer from the SiC. This decoupling is consistent with our interpretation of this new interface structure as being a graphene buffer layer on C-face SiC.

This work is supported by NSF.

5:20pm GR+AS+NS+SP+SS-TuA11 Characterization of Few Layer Graphene Films Grown on Cu-Ni and SiC Substrates, P. Tyagi, J.D. McNeilan, J. Abel, F.J. Nelson, Z.R. Robinson, R. Moore, A.C. Diebold, V.P. LaBella, C.A. Ventrice, Jr., University at Albany - SUNY, A.A. Sandin, D.B. Dougherty, J.E. Rowe, North Carolina State Univ., C. Dimitrakopoulos, A. Grill, C.Y. Sung, IBM T.J. Watson Res. Center, S. Chen, A. Munson, Y. Hao, C.W. Magnuson, R.S. Ruoff, Univ. of Texas at Austin

The electronic structure of graphene depends on the number of graphene layers and the stacking sequence between the layers. Therefore, it is important to have a non-destructive technique for analyzing the overlayer coverage of graphene directly on the growth substrate. We have developed a technique using angle-resolved XPS to determine the average graphene thickness directly on metal foil substrates and SiC substrates. Since monolayer graphene films can be grown on Cu substrates, these samples are used as a standard reference for a monolayer of graphene. HOPG is used as a standard reference for bulk graphite. The electron mean free path of the C-1s photoelectron is determined by analyzing the areas under the C-1s peaks of monolayer graphene/Cu and bulk graphite and results in a value of 12.3 ± 0.8 Å. With this electron mean free path, the graphene coverage of a film of arbitrary thickness can be determined from the areas under the C-1s peaks of the sample of interest, the monolayer graphene/Cu, and HOPG samples. Analysis of graphene coverages for graphene films grown on Cu-Ni substrates shows that a uniform monolayer is first formed before the growth of a second layer. The thickness of both the graphene overlayer and intermediate buffer layer has been determined on 6H-SiC substrates. Raman spectroscopy data have also been taken on these samples and compared to the overlayer coverages determined with XPS. This research was supported in part by the National Science Foundation (grant no. 1006350/1006411).

5:40pm GR+AS+NS+SP+SS-TuA12 Thickness-related Electronic Properties of Single-layer and Few-layer Graphene Revealed by Single-pass Kelvin Force Microscopy and dC/dZ Measurements, J. Yu, S. Wu, Agilent Technologies, Inc.

Graphene has attracted much attention recently due to their exotic electronic properties. Potential applications of graphene sheets as ultrathin transistors, sensors and other nanoelectronic devices require them supported on an insulating substrate. Therefore, a quantitative understanding of charge exchange at the interface and spatial distribution of the charge carriers is critical for the device design. Here, we demonstrate that atomic force microscopy (AFM)-based technique Kelvin force microscopy (KFM) can be applied as an experimental means to quantitatively investigate the local electrical properties of both single-layer and few-layer graphene films on silicon dioxide. Our measurements indicate that the surface potential of single-layer graphene is 60 mV higher than that of the silica interfacial layer. The effect of film thickness on the surface potential of few-layer graphene is observed. For example, a 66 mV increase in the surface potential is detected for an eleven-layered film with respect to a nine-layer film. Furthermore, with the introduction of multiple lock-in amplifiers (LIAs) in the electronics for scanning probe microscopes, single-pass kelvin force microscopy and probing of the other electric property such as local dielectric permittivity via the capacitance gradient dC/dZ measurements are allowed by the simultaneous use of the probe flexural resonance frequency ω_{mech} in the first LIA targeting the mechanical tip-sample interactions for surface profiling, and a much lower frequency ω_{elec} (both in the second LIA and its second harmonic in the third LIA) for sample surface potential and dC/dZ measurements, respectively. In contrast to surface potentials, the dC/dZ measurements show that local dielectric permittivity of few-layer graphene films maintain at the same level regardless of the film thickness. Such simultaneous monitoring of multiple electronic properties that exhibit different behaviors in response to the graphene layers provides us a way to achieve both a comprehensive characterization and a better understanding of graphene materials.

**In Situ Microscopy and Spectroscopy Focus Topic
Room: 7 - Session IS+AS+BI+ET+GR+NS-TuA**

In Situ Studies of Organic and Soft Materials and In Situ Microscopy

Moderator: K. Artyushkova, The University of New Mexico, J.A. Eastman, Argonne National Laboratory

2:00pm IS+AS+BI+ET+GR+NS-TuA1 Micronutrient Detection and Quantification from Data Obtained from Plasma Pencil Atmospheric Mass Spectrometry, M.J. Stein, E. Lo, C. Waterton, D.G. Castner, B.D. Ratner, University of Washington

The analysis of micronutrient quantities is one component in the strategy to reduce the global burden of malnutrition-related disease. Accessibility of the proper equipment and equipment complexity impede nutrient testing in the areas that might benefit most from these studies. In this work, we present an analysis of micronutrients in a physiological range from blood plasma using plasma pencil atmospheric mass spectrometry (PPAMS), a method for sampling a sample's surface at ambient temperature and pressure conditions. The effectiveness of our PPAMS system is demonstrated using characteristic and tandem mass spectra on raw nutrient controls. Key micronutrient peaks and fragmentation patterns are observed. Next, we analyze a sample matrix of micronutrients in porcine plasma in which the nutrient concentrations are varied. Principal component analysis (PCA) is then employed on the spectra. The resulting PCA scores showed that these nutrients are separable at different nutrient concentrations to 95% confidence. The loadings peaks are shown to contain several of the key peaks observed in the raw nutrient powders as principal separators. The PPAMS technique is compared to several traditional techniques such as time-of-flight secondary ion mass spectrometry (ToF-SIMS) and electrospray ionization mass spectrometry (ESI-MS). Separation of the nutrients at concentrations relevant for human blood-based nutrient detection is possible in both ESI-MS and PPAMS. However, ToF-SIMS is found to require 5x to 1000x higher concentrations than PPAMS for folate, vitamin A, and iodine in order to achieve similar separation of the micronutrients. In addition to the qualitative information obtained from the PCA results, quantitative predictive values are obtained by the application of a Bayesian wavelet-based functional mixed model. Since the mass spectra are modeled as functions in this model, peak detection methods are not required and the final results utilized the full spectral response. The final predicted values are compared to the known concentration values and the mean standard error of prediction (MSEP) is calculated. The accuracy of the predictive model was found to be dependent on the ionization potential of

the individual nutrients. Metallic-nutrients were hypothesized to be more sensitive to outside cationization effects than their larger organic counterparts. In addition to quantitation, the physical properties of the ionization process were explored. Using XPS and ellipsometry in conjunction with carefully timed exposures and concurrent fragment PCA, it is determined that the PPAMS ionization is a softer form of ionization than most vacuum-based techniques.

2:20pm IS+AS+BI+ET+GR+NS-TuA2 *In Situ* Real Time Examination of the Thin Film Growth of Pentacene on Polymeric Dielectrics Using X-Ray Synchrotron Radiation: Unexpected Changes in the Evolution of Surface Morphology with Substrate, T.V. Desai, A.R. Woll, J.R. Engstrom, Cornell University

We have examined the thin film growth of pentacene on SiO₂ and on three different polymeric dielectrics using *in situ* synchrotron x-ray scattering and *ex situ* atomic force microscopy (AFM). The polymeric dielectrics investigated spanned the range from a low surface energy hydrophobic surface (polystyrene, PS), to a medium surface energy hydrophobic surface (polymethylmethacrylate, PMMA), to a high surface energy hydrophilic surface [poly(ethylene imine), PEI]. We have also compared these results to pentacene growth on clean SiO₂. On all surfaces, pentacene forms a polycrystalline thin film, whose structure is that of the previously identified "thin film" phase. From *in situ* real-time x-ray scattering, we find that pentacene exhibits layer-by-layer (LbL) growth on all surfaces investigated, but the extent of LbL growth is a strong function of the underlying substrate. This result is unexpected as the transition to more 3D-like growth occurs for thicknesses where the underlying substrate is effectively almost entirely covered by the growing pentacene thin film. Layer-by-layer growth is significantly more prolonged on PEI (up to ~6 MLs), followed by SiO₂ and PMMA (up to ~4 MLs) and finally PS (up to ~3 MLs). This trend is also seen in the variation of both the roughness and the in-plane feature sizes of ~10 ML thick films, where the films are the smoothest, and the feature sizes are the largest for growth on PEI, whereas on PS, the films are roughest, and the feature sizes are the smallest. Concerning possible reasons for this behavior, we can exclude the effects of the structure of the crystalline thin film (they were the same in all cases), and the roughness of the polymeric dielectric (rms roughness differed by < 0.1 nm) as major contributing factors. Surface energy of the polymeric thin films, however, provided the best explanation for the observed behavior, suggesting that thermodynamic driving forces play an important role in the evolution of thin film structure. In terms of molecular scale phenomena, interlayer transport and step-edge crossing events may be influenced by the mobility of the near-surface polymeric layers in the underlying substrate, which can be quite different for the ultrathin PEI layers vs. the much thicker PMMA and PS thin films.

2:40pm IS+AS+BI+ET+GR+NS-TuA3 *In Situ*, Real-Time Diagnostics of Colon Cancer and Inflammatory Bowel Diseases by Direct Combination of Endoscopy and Rapid Evaporative Ionization Mass Spectrometry, Z. Takats, Imperial College, UK, L.A. Sasi-Szabo, University of Debrecen, Hungary, J. Kinross, Imperial College, UK, J. Balog, Medimass Ltd., L. Muirhead, K.C. Schafer, C. Guallar-Hoyas, Imperial College, UK

INVITED

Rapid identification of biological tissues is a long-standing problem on various fields of interventional medicine, with special regard to cancer diagnostics and cancer surgery. While histological techniques provide the ultimate solution for the cellular-level identification of cancer cells, the approach is extremely complex and time consuming. Nevertheless, accelerated version of histopathology (so-called 'frozen section' method) is widely used for the intraoperative characterization of tissue samples removed from the surgical area. Since frozen section histology is less reliable than the traditional approaches, and the accelerated procedure still takes approx. 30 minutes for a single sample, there has been ongoing research for the development of more accurate and faster methods.

Molecular spectroscopy techniques including IR, Raman, solid state NMR and mass spectrometry have been used for the characterization of intact biological tissues and showed enormous potential for the differentiation of tissues with various histologies, including multiple different types of cancer.

Rapid Evaporative Ionization Mass Spectrometry is based on the observation that electrosurgical dissection of vital tissues involves the ionization of various tissue constituents, with special emphasis on membrane lipids. Electrosurgical methods employ electric current for the rapid heating and evaporation of tissue material and they are widely used both for dissection and coagulation on practically all fields of surgery. Hence, the direct combination of electrosurgery with mass spectrometry provides a tissue identification methodology, where the tissue manipulation part is already widely used by surgeons and fully approved from regulatory point of view. Electrosurgical methods are also employed on the field of endoscopy, both for coagulation and dissection. Combination of endoscopy with *in-situ* mass spectrometric tissue identification resulted in a diagnostic

device which can potentially identify lesions in body cavities *in-situ*, in real-time.

Electrosurgical electrode assembly and ion transfer device were embedded into working channel of commercially available colonoscope. The device was coupled with a linear ion trap mass spectrometer, and the system was utilized during diagnostic colonoscopic interventions. Adenomae, adenocarcinomae and mucosal areas affected by inflammatory bowel diseases were successfully identified, in complete agreement with histopathological examination.

4:00pm IS+AS+BI+ET+GR+NS-TuA7 Nanocrystal Phase Transformations in ZBLAN Glass Ceramics, J.A. Johnson, University of Tennessee Space Institute, C. Alvarez, Northwestern University, Y. Lui, Argonne National Laboratory, C.E. Johnson, University of Tennessee Space Institute, A. Peiford-Long, Argonne National Laboratory

In-situ and *ex-situ* TEM investigations of fluorochlorozirconate (FCZ) glass have led to the discovery of previously unreported BaF₂ in the face-centered-cubic (FCC) and orthorhombic phases. These FCZ glasses are a class of material based on ZBLAN glasses, which are being developed for uses in advance mammography systems. The FCZs of interest have been doped with Eu (II) for use as either a scintillator or a storage phosphor material but need to be partially crystalline to show good optical properties. The photo-stimulated luminescence of this material, for use as storage phosphor, is attributed to the characteristic 5d-4f emission of Eu²⁺ present in the BaCl₂ nanocrystals. The crystals formed are known from XRD experiments to be hexagonal and orthorhombic BaCl₂ depending on the annealing temperature, 265 and 295°C respectively. *In-situ* and *ex-situ* TEM heating experiments were used to study the nucleation and growth process of the nanocrystals at the EMC. The nanocrystals nucleate and grow through-out the glass matrix when annealing FCZ glasses, therein producing a nanocomposite glass-ceramic system. The traditional BaCl₂ orthogonal phase in addition to the unreported FCC and orthogonal BaF₂ phase have been found in multiple ZBLAN compositions in which the content of Cl and F has been varied. This indicates that annealing FCZ glasses produces polymorphic crystals of both BaCl₂ and BaF₂, which vary in size from 10 nm to 100 nm.

Mössbauer Spectroscopy has also given indisputable evidence that the divalent Europium enters the nanocrystals.

4:20pm IS+AS+BI+ET+GR+NS-TuA8 *In Situ* Microscopy of Organic Film Growth: Zn-Phthalocyanine on Ag(100), A. Al-Mahboob, J.T. Sadowski, Brookhaven National Laboratory

Metal phthalocyanines are attracting significant attention, owing to their potential for applications in chemical sensors, solar cells and organic magnets. As the electronic properties of molecular films are related to their crystallinity and molecular packing, the optimization of film quality is important for improving the performance of organic devices.

In this work, we studied the dynamics of nucleation and structural evolution of zinc-phthalocyanine (ZnPc) films on Ag(100) surface, employing real-time low-energy electron microscope (LEEM) complemented by DFT calculations. We have observed two different modes of ZnPc nucleation, depending on the growth temperature. At lower temperatures ZnPc nucleates in a double domain structure, with bulk-like square lattice similar to one reported by Dou et al. [2]. LEED patterns recorded in LEEM experiment show that ZnPc monolayer (ML) grows epitaxially, having a square lattice with $(4/3)\sqrt{13} \times (4/3)\sqrt{13} R33.69^\circ$ unit cell (denoted R33.69) with respect to the substrate lattice. At temperatures of 170°C or above, nucleation of less dense epitaxial ZnPc, having single domain orientation, was observed, with square lattice parameters exactly 5 times larger (5x5) than the Ag(100) substrate.

Utilizing LEEM to observe the ZnPc nucleation at varying substrate temperatures – from room temperature (RT) to 225°C – we have observed that the nominal ZnPc coverage required for the onset of nucleation has strong temperature dependence. The nucleation commences at about 0.2 ML at RT, while 0.7 ML is required at 190°C. At the same time the completion of 1st layer occurs at constant nominal coverage of ZnPc, independent of substrate temperature. Based on that observation, the delay in onset of nucleation could be understood as a result of increased equilibrium concentration of diffusing ZnPc molecules at higher temperatures. This is in contrast to a delay in nucleation and giant island growth observed during vacuum deposition of anisotropic molecules like pentacene (Pn), in which case the energy barrier for the reorientation of the molecule from diffusing state into its crystalline orientation plays a critical role [3]. Real-time tracking of the evolution of ZnPc island area at varying deposition conditions combined with DFT analysis revealed that the 5x5 structure has both, a detachment barrier with respect to attachment, and a pre-factor (or attempt frequency), lower than those for bulk-like structures, allowing for controlling of the resulting ZnPc structure.

[1] E. Bauer, Rep. Prog. Phys. **57**, 895 (1994).

- [2] W. Dou et. al, *J. Chem. Phys.* **133**, 144704 (2010).
 [3] Al-Mahboob et al, *Phys. Rev. B* **82**, 235421 (2010).

4:40pm **IS+AS+BI+ET+GR+NS-TuA9 *In Situ* Sub-Micrometer Scale Chemical Imaging with Scanning Transmission X-ray Microscopy**, *S.T. Kelly, P. Nigge*, Lawrence Berkeley National Laboratory, *A. Laskin, B. Wang*, Pacific Northwest National Laboratory, *A. Tivanski, S. Ghorai*, University of Iowa, *T. Tyliczszak, M.K. Gilles*, Lawrence Berkeley National Laboratory

Spatially resolved chemical information on length scales shorter than 50 nm has become crucial in many areas of science and engineering -- from analyzing the chemistry of geological and environmental samples to quantifying the detailed chemical structure of novel materials engineered on the nanoscale. Scanning transmission x-ray microscopy (STXM) allows collection of specific chemical speciation data on these length scales through the acquisition and analysis of near-edge x-ray absorption fine structure (NEXAFS) spectra at each image pixel. However, the full usefulness of the STXM instrument may ultimately be realized in the *in situ* analysis of chemical transformations by controlling the local sample environment.

In situ STXM/NEXAFS measurements have been made in several ways thus far, ranging from simple to very complex. Introducing gases directly into the microscope chamber is effective, yet the presence of the gas along the entire optical path of the x-rays reduces signal at the detector. Furthermore, gas choice with this configuration is limited to those compatible with the microscope components. Separate *in situ* reactor cells circumvent these limitations by confining the gaseous environment to a small region immediately around the sample. Several groups have used reactor cells to this end, with reactors ranging widely in complexity -- from simple cells with limited capability to complex systems which require substantial instrument reconfiguration.

Ideally, an *in situ* reactor for STXM should be capable, flexible, easy to install and configure, and easily fabricated. We have developed a gas phase STXM reactor cell to meet many of these requirements. The reactor mounts directly to the standard STXM sample mount (making installation relatively simple) and contains an integrated sensor to actively measure relative humidity inside the cell for experiments using water vapor. We present here recent results using the reactor cell to examine two different systems. In the first system, we observed the hygroscopic properties of mixed organic/inorganic aerosol particles at increasing levels of relative humidity. In the second system, we monitored carbon dioxide sorption in metal organic framework materials. The advantages afforded by this reactor (and future improvements to it) will enable new scientific discoveries across a wide range of fields.

5:40pm **IS+AS+BI+ET+GR+NS-TuA12 *In Situ* SEM and ToF-SIMS Imaging of Liquids for Biological Applications**, *L. Yang, X.-Y. Yu, Z. Zhu, S. Thevuthasan*, Pacific Northwest National Laboratory, *J. Cowin*, Cowin In-Situ Science, L. L. C.

A vacuum compatible microfluidic interface was developed to enable surface analysis of liquids. The unique feature of the liquid flow cell is that the detection window is open to the vacuum allowing direct probing of the liquid surface. The flow cell is composed of a silicon nitride membrane and polydimethylsiloxane; and it is fully compatible with vacuum operations for surface analysis. The aperture can be drilled through the 100 nm silicon nitride membrane by using the focused ion beam/scanning electron microscope (FIB/SEM). Alternatively the primary Bi⁺ ions in ToF-SIMS can be used to fabricate the aperture window in real-time. New results using this vacuum interface and recent development will be presented in this paper. Several aqueous solutions containing conjugated IgG gold nanoparticles and representative biological solutions were studied *in situ* using scanning electron microscope (SEM) and time-of-flight secondary ion mass spectrometry (ToF-SIMS). Characteristic signals of the conjugated gold nanoparticles were successfully observed through the aperture by both energy-dispersive X-ray spectroscopy (EDX) in SEM and ToF-SIMS. Comparisons were also made among wet and dry samples and liquid sample in the flow cell using SEM/EDX. Stronger gold signal can be observed in our novel portable device by SEM/EDX compared with the wet or dry samples, respectively. Our results indicate that analyses of the nanoparticle conjugated antibodies are better made in their native liquid environment. Our unique microfluidic flow cell permits *in situ* liquid observations. In addition, a variety of aqueous solutions relevant to biological systems were analyzed. Our results indicate that chemical imaging by SEM and ToF-SIMS is applicable in analyzing more complicated aqueous solutions when coupled with our novel portable microfluidic platform.

Scanning Probe Microscopy Focus Topic Room: 16 - Session SP+AS+BI+ET+MI+NS-TuA

Advances in Scanning Probe Imaging

Moderator: S. Allen, The University of Nottingham, UK, Z. Gai, Oak Ridge National Laboratory

2:00pm **SP+AS+BI+ET+MI+NS-TuA1 Molecules Investigated with Atomic Resolution using Scanning Probe Microscopy with Functionalized Tips**, *L. Gross, F. Mohn, N. Moll, G. Meyer*, IBM Research - Zurich, Switzerland

Single organic molecules were investigated using scanning tunnelling microscopy (STM), noncontact atomic force microscopy (NC-AFM), and Kelvin probe force microscopy (KPFM). With all of these techniques submolecular resolution was obtained due to tip functionalization by atomic manipulation. The techniques yield complementary information regarding the molecular structural and electronic properties.

Using NC-AFM with CO terminated tips, atomic resolution on molecules has been demonstrated and the contrast mechanism was assigned to the Pauli repulsion [1]. On the other hand, by using STM the molecular frontier orbitals, i.e., the highest occupied and the lowest unoccupied molecular orbitals (HOMO and LUMO), were mapped [2]. Using a CO terminated tip for orbital imaging with the STM, the resolution can be increased and the images correspond to the gradient of the molecular orbitals due to the *p*-wave character of the tip states [3]. Finally, KPFM reveals information about the distribution of charges within molecules by measuring the *z*-component of the electrostatic field above the molecule, as demonstrated on the hydrogen tautomerization switch naphthalocyanine [4].

References :

- [1] L. Gross *et al. Science* **325**, 1110 (2009).
 [2] J. Repp *et al. Phys. Rev. Lett.* **94**, 026803 (2005).
 [3] L. Gross *et al. Phys. Rev. Lett.* **107**, 086101 (2011).
 [4] F. Mohn *et al. Nature Nanotechnol.* **7**, 227 (2012).

2:40pm **SP+AS+BI+ET+MI+NS-TuA3 Functional Imaging of Jahn-Teller Dynamics at the Single-molecule Scale**, *J. Lee, S.M. Perdue, A. Rodriguez Perez, P.Z. El-Khoury, V.A. Apkarian*, University of California, Irvine

Taking advantage of both elastic and inelastic tunneling processes of a molecule isolated at the double-barrier tunneling junction of a scanning tunneling microscope, both static and dynamic parts of the Hamiltonian can be visualized with submolecular resolution. This is illustrated by imaging Jahn-Teller (JT) driven vibronic dynamics within Zn-etiochlorophyllin (ZnEtio), in its various reduced forms, in what may be regarded as nature's choice of a molecule as a controllable current switch. Unique interpretations are afforded through simultaneously recorded functional images, such as maps of: a) energy resolved differential current, b) spectrally resolved electroluminescence, c) conduction bistability, d) reduction/oxidation potentials (maps of charging and discharging). We focus on the radical anion, ZnEtio⁻, which is reduced by injecting an electron to a single ZnEtio molecule adsorbed on a thin aluminum oxide film grown on NiAl(110). In contrast with the neutral, the saddle-shaped radical anion lies flat on the surface of the oxide. The discharge map directly shows that the excess electron is localized in the ²p_x orbital of the entire porphyrin macrocycle, as a result of the JT active rectangular (B_{1g}) distortion of the molecule. The static JT potential leads to conduction bistability, with reversed switching polarity depending on whether tunneling electrons are injected in the occupied ²p_x orbital or the diamond (B_{2g}) coordinate which serves as a transition state that connects the p_x and p_y orbitals at the two B_{1g} minima. In addition to the JT switching, the dynamic JT states are directly imaged through electroluminescence spectra, induced by injection of a second electron in the anion. The spectra consist of a continuum due to radiative ionization of the dianion, and sharp Fano resonances of the vibronic progression of the JT active modes. A detailed analysis of the spectra yields the vibronic couplings and the wavefunctions. Vibronic structure is inherent in STM topographic images, and has hitherto not been fully recognized.

3:00pm **SP+AS+BI+ET+MI+NS-TuA4 Atomic and Chemical Resolution of Heterogeneous 1-D Metallic Chains on Si(100) by Means of nc-AFM and DFT**, *M. Setvin, M. Ondracek, P. Mutombo, Z. Majzik, P. Jelinek*, Institute of Physics of ASCR, Czech Republic

Scanning Probe techniques are widely used to image atomic and electronic structure of surfaces and nanostructures. However atomic and chemical resolution of complex nanostructures (e.g. molecules, nanoparticles or nanowires) is still the large challenge. Several methods (see e.g. [1-3]) have been already proposed to achieve the single-atom chemical resolution. In

the work [3] it was showed that the single-atom chemical identification can be achieved via force-site spectroscopy measurements using Frequency Modulation Atomic Force Microscopy (FM-AFM). The validity of the method was demonstrated on semiconductor surface alloy composed of isovalent species (Si, Sn and Pb). In this particular case, the valence electrons of surface atoms possess very similar electronic structure close to sp^3 hybridization with characteristic dangling bond state. Hence the maximum short-range force is mainly driven by the position of the dangling bond state with respect to the Fermi level.

In this work, we investigated atomic and chemical structure of heterogeneous 1-D chains made of III and IV group metals grown on Si(100) surface [4] by means of room-temperature (RT) FM-AFM measurements combined with DFT simulations. Here 1D chains consist of heterogeneous buckled-dimer structures with unknown chemical ordering. What more, the presence of buckled dimers composed by chemical species of different valence makes this system very challenging for true atomic and chemical resolution by means of SPM.

In this contribution, we will show first that FM-AFM technique even at RT is able to achieve atomic resolution of individual atoms forming dimers, much superior to the contrast obtained by the traditional STM technique. Secondly, we will demonstrate that the single-atom chemical identification is still possible combining the force-site spectroscopy at RT with DFT simulations even in such complex systems as the heterogeneous 1D metallic chains.

[1] M. Schmid, H. Stadler, P. Varga *Phys. Rev. Lett.*, 70, p. 1441 (1993)

[2] L. Gross et al, *Science* 325, 5944 (2009).

[3] A. Foster et al *Phys. Rev. Lett.* 102, 256103 (2009).

[4] Y. Sugimoto, P. Pou, M. Abe, P. Jelinek, R. Perez, S. Morita, O. Custance, *Nature* 446, 64 (2007)

[5] L. Magaud, A. Pasturel, and J.-Y. Veuillen, *Phys. Rev. B* 65, 245306 (2002).

4:00pm **SP+AS+BI+ET+MI+NS-TuA7 Simple Routes to High Speed and Super Resolution AFM**, *J.K. Hobbs*, University of Sheffield, UK **INVITED**

Over the past two decades atomic force microscopy has developed to become the workhorse of molecular nanotechnology. However, despite this success, it has failed to deliver consistently in two areas where it arguably has most potential, namely sub-molecular resolution imaging and the following of processes in real time. Here our work to tackle these challenges will be discussed.

We have developed a new approach to reaching high resolution within a conventional AFM, based on torsionally driven T-shaped cantilevers, dubbed "torsional tapping AFM". The use of torsional oscillations gives improved dynamics (high Q-factor, high frequency), without excessively increasing the spring constant. The small offset of the tip from the axis of rotation gives improved lever sensitivity. Combined, these result in an approximately 12 fold improvement in sensitivity when compared to the same AFM with a conventional tapping cantilever. This improved sensitivity allows ultra-sharp whisker tips to be used in a routine manner, giving true molecular resolution even on soft materials presenting surfaces with tens of nanometres of topography. For example, individual polyethylene chains both in the crystalline phase, and at the interface with the amorphous phase, can be clearly imaged in a conventionally processed sample of plastic, with polymer chain-to-chain resolution down to 0.37 nm [1]. Data from semi-crystalline polymers to naturally occurring protein crystals will be presented.

High speed AFM requires methods for scanning rapidly, for maintaining tip-sample contact ("feedback"), and for constructing the topography image. We have shown that resonant scanners [2] give a robust method for rapid scanning. In a conventional AFM the feedback and the topographic image are inextricably linked. However, this places a limit on scan speed as it demands that the tip has reached equilibrium at each point on the image if the height is going to be accurately obtained. We have adopted a different approach, in which the height of the tip is directly measured using an interferometric approach, freeing the feedback loop to minimising tip-sample forces. This allows topographic images with height traceable to the wavelength of the interferometric laser to be obtained at imaging rates greater than one frame a second. Coupled with resonant scanners, giving scan areas up to $40 \times 40 \mu\text{m}^2$ an AFM platform capable of in-line industrial applications is obtained.

1. Mullin, N.; Hobbs, J. K., *Phys Rev Lett* **2011**,107

2. Humphris, A. D. L.; Miles, M. J.; Hobbs, J. K *Appl Phys Lett* **2005**,86 (3)

4:40pm **SP+AS+BI+ET+MI+NS-TuA9 A Scanning Probe Microscopy Study of Trimesic Acid Self-Assembly on Highly Oriented Pyrolytic Graphite**, *V. Korolkov, S. Allen, C.J. Roberts, S.J.B. Tendler*, The University of Nottingham, UK

We have investigated trimesic acid (1,3,5-benzenetricarboxylic acid, TMA) adsorption on highly oriented pyrolytic graphite (HOPG) surfaces from aqueous medium at room temperature. Both atomic force (Peak Force Tapping mode) and scanning tunnelling microscopy were utilized to follow the adsorption dynamics and molecular arrangements. A chicken-wire arrangement for adsorbed molecules with an average pore size of $11 \pm 1 \text{ \AA}$ was established and observed using both scanning techniques. We found that this structure forms a monolayer within ~ 100 seconds of exposure of the HOPG surface to $50 \mu\text{M}$ TMA solution in H_2O . The monolayer structure was found to be stable for at least 48h under ambient conditions. STM was observed to lead to some desorption of TMA from a dynamically formed TMA film, and was only able to image the monolayer of TMA molecules in intimate contact with the HOPG. AFM revealed that TMA films formed using higher concentrations or longer adsorption times formed multilayers with similar molecular spacings and displayed an island growth morphology.

We have achieved an excellent resolution on an ambient running AFM. We have demonstrated that the combination of STM and AFM is essential, if not a must, to look at ultimate monolayers in the ambient conditions. Overall a facile green chemistry method for TMA monolayer fabrication from aqueous media on a HOPG surface has been established.

5:00pm **SP+AS+BI+ET+MI+NS-TuA10 Understanding the Role of the Probe in SPM Imaging of Metal Oxides: New Opportunities for In-Depth Surface Analysis**, *H. Mönig*, Univ. of Münster, Germany, *M. Todorovic*, Univ. Autónoma de Madrid, Spain, *M.Z. Baykara*, Yale Univ., *T.C. Schwendemann*, Southern Connecticut State Univ., *J. Götzten*, *Ö. Ünverdi*, *E.I. Altman*, Yale Univ., *R. Perez*, Univ. Autonoma de Madrid, Spain, *U.D. Schwarz*, Yale Univ.

Metal oxide surfaces play an indispensable role in a number of catalytic processes of technological and scientific importance. A fundamental understanding of the role that metal oxide surfaces play in such applications requires an experimental technique that allows analyzing chemical and electronic surface properties down to the atomic scale. The powerful method of three-dimensional atomic force microscopy (3D-AFM) in combination with scanning tunneling microscopy (STM) can be used towards this goal with great success. However the interpretation of results is not straightforward, particularly because the structure and chemistry of the probe tip employed in the experiments influences the measured data.

In this talk, using a combination of experimental STM data and density functional theory (DFT) calculations, we will study the effect of changing the tip structure and chemistry, as well as imaging parameters such as tip-sample distance and bias voltage on STM images obtained on the model surface of Cu(100)-O, a surface oxide layer consisting of nearly co-planar copper (Cu) and oxygen (O) atoms. We observe that STM image contrasts and atomic species with highest tunneling probability vary greatly with changing tip properties and imaging parameters. Reasonable matches between calculated and experimentally recorded STM images are observed, allowing the determination of particular tip models used in the experiments. Additionally, the effect of rotating the model tip structures with respect to the sample surface results in asymmetric features in simulated STM images, reproducing certain peculiar patterns observed experimentally. To sum up, the results presented here underline the significant role that the tip plays in SPM measurements and describe potential routes to optimize the gathered information through deliberate manipulation of tip properties as well as imaging parameters.

5:20pm **SP+AS+BI+ET+MI+NS-TuA11 Characterizing the Best Tips for NC-AFM Imaging on Metal Oxides with Force Spectroscopy and Theoretical Simulations**, *D. Fernandez-Torre*, Universidad Autónoma de Madrid, Spain, *A. Yurtsever*, Osaka University, Japan, *P. Pou*, Universidad Autónoma de Madrid, Spain, *Y. Sugimoto*, *M. Abe*, *S. Morita*, Osaka University, Japan, *R. Perez*, Universidad Autónoma de Madrid, Spain

Metal oxides play a key role in a wide range of technological applications. To optimize their performance, it is essential to understand their surface properties and chemistry in detail. Noncontact atomic force microscopy (nc-AFM) provides a natural tool for atomic-scale imaging of these insulating materials. Some of these materials, including ceria (CeO_2), and particularly titania (TiO_2), have been extensively studied with nc-AFM in the last few years. Experiments on the rutile $\text{TiO}_2(110)$ surface show, at variance with STM, that a variety of different contrasts can be obtained, and frequent changes among different imaging modes are observed during scanning. The two most common contrasts are the "protrusion" and the "hole" mode imaging modes, that correspond, to imaging bright the positive or the negative surface ions respectively, but other contrasts like the "neutral"

mode and the “all-inclusive” mode—where all the different chemical species and defects are imaged simultaneously—have been also identified.

Understanding the image contrast mechanisms and characterizing the associated tip structures is crucial to extract quantitative information from nc-AFM measurements and to identify the nature of the observed defects. While in many cases the same nc-AFM image can be explained by different models, and even different underlying tip-sample interactions, we show here that the combination of force spectroscopy (FS) measurements and first-principles simulations can provide an unambiguous identification of the tip structure and the image contrast mechanism. In particular, we show that the best tips to explain the protrusion and hole mode forces are TiO_x-based clusters differing in just one H atom at the tip apex, discarding previously proposed Ti-terminated tips that would lead to forces much larger than the ones observed in the experiments. The less frequent neutral and all-inclusive images are associated to Si tips where contamination is limited to just an O atom or OH group at the apex. These models provide a natural explanation for the observed contrast reversals by means of H transfer to/from the tip, an event that we indeed observe in our simulations. As tip contamination by surface material is common while imaging oxides, we expect these tips and imaging mechanisms to be valid for other oxides. Our results for the imaging of CeO₂ surfaces and of metal atoms (K, Pt) adsorbed on TiO₂ support this conclusion.

5:40pm **SP+AS+BI+ET+MI+NS-TuA12 Direct Probe of Interplay between Local Structure and Superconductivity in FeTe_{0.55}Se_{0.45}.** *M.H. Pan, W.Z. Lin, Q. Li, B.C. Sales, S. Jesse, A.S. Sefat, S.V. Kalinin*, Oak Ridge National Laboratory

A key challenge in high-temperature superconductivity is to determine the role of local crystallographic structure and chemical effects on the superconducting critical temperature, T_c . Iron chalcogenide superconductors (‘11’) are ideal model systems for deciphering the role of local effects on the superconductivity, primarily because they cleave leaving non-polar surfaces unlike other families of iron arsenide superconductors (‘1111’ or ‘122’) and cuprates. **Here, we explore the interplay between local crystallographic structure, composition and local electronic and superconductive properties. Direct structural analysis of scanning tunneling microscopy (STM) data allows local lattice distortions and structural defects across a FeTe_{0.55}Se_{0.45} surface to be explored on a single unit-cell level. Concurrent superconducting gap (SG) mapping reveals suppression of the SG at well-defined structural defects, identified as a local structural distortion (Guinier-Preston zone). The strong structural distortion is related to the vanishing of the superconducting state. This study provides insight into the origins of superconductivity in iron chalcogenides by providing an example of atomic-level studies of the structure-property relationship.**

Thin Film

Room: 10 - Session TF+AS-TuA

Modeling and Analysis of Thin Films

Moderator: D. Irving, North Carolina State University

2:00pm **TF+AS-TuA1 Nanoconfined Fluids: Fundamentals and Application to Ionic-Liquid-Based Supercapacitors.** *G. Feng, S. Li, P.T. Cummings*, Vanderbilt University **INVITED**

Phase transitions in nanoconfined fluids have been contentious for two decades. In the 1980s and early 1990s a large number of surface force apparatus (SFA) experiments on a variety of ultrathin nonpolar liquid films (e.g., such as dodecane, cyclohexane and octamethylcyclotetrasiloxane (OMCTS)), reached a common conclusion: When their confinement between molecularly smooth mica sheets reached the order of several molecular diameters (approximately 3 or less, depending on the fluid being studied) they exhibited behavior typical of the stick-slip response of a crystalline solid structure.

In contrast to the solid-like behavior under extreme nanoconfinement, when the mica surface separation is sufficiently large, the confined fluid exhibits bulk-like liquid behavior. Thus, a phase transition as a function of separation must exist. In this talk, we review the two-decade-old debate on the nature of this phase transition (first order vs continuous), and its effective resolution using very high fidelity molecular dynamics simulations. In particular, the origin of the phase transition from fluid to solid-like behavior is, unexpectedly, driven by electrostatic interactions between ions in mica and partial charges on the atoms in the nonpolar organic molecules.

More recently, our interest in nanoconfined fluids has focused on novel energy storage devices: electrical double layer (EDL) capacitors, also called

supercapacitors. Supercapacitors have attracted considerable attention, owing to their desirable properties, such as high power density, high capacitance, and excellent durability. As emerging electrolytes for these supercapacitors, room-temperature ionic liquids (RTILs) have attracted considerable attention due to their wide electrochemical windows, excellent thermal stability, non-volatility, relatively inert nature, and high ionic conductivity. With high specific surface area and electrical conductivity, nanoporous carbon-based materials are the most widely used electrodes for supercapacitors, including activated carbons, templated and carbide-derived carbons (CDC). Using molecular simulations, model porous carbon electrodes (e.g., CDC), supercapacitors composed of slit-shaped micropores ranging in size from 0.67 nm to 1.8 nm in an IL were studied to investigate the dependence of capacitance on pore size. The capacitance was found to show an oscillatory behavior with pore size. In good agreement with experiment, we find that, as the pore shrinks from 1.0 nm to 0.7 nm, the capacitance of the micropore increases anomalously. The persistence of oscillations in capacitance beyond 1.0 nm is a new theoretical prediction currently being probed experimentally.

2:40pm **TF+AS-TuA3 XPS Analysis of Monomolecular Films Prepared by Self-Assembly and Langmuir-Blodgett Techniques.** *G.G. Jernigan, F.K. Perkins, M.G. Ancona, A.W. Snow*, Naval Research Laboratory

Characterization of self-assembled monolayers (SAMs) using x-ray photoelectron spectroscopy (XPS) measurements of the gold (4f) attenuation from increasing molecular length alkane thiols were pioneered by Bain and Whitesides[1]. Since then, the gold attenuation has been used by many others as a method for determining the length/thickness of molecular films formed as SAMs on gold. We have done similarly with carboxylic acid (COOH) terminated alkane thiols SAMs deposited on gold with the aid of additives[2], and we obtained similar results. We discovered, however, that the attenuation of the sulfur (2p) signal did not correspond with the gold attenuation. Additionally, neither the gold or sulfur attenuation could correctly account for the observed carbon (1s) signal in the XPS measurements. This fact was originally noted, but not addressed, by Bain and Whitesides.

In conjunction with experiments, we will present our successful solution to the modeling of XPS measurements of molecular films prepared by self-assembly and by the Langmuir-Blodgett (LB) technique. In a classic alkanethiol SAM, one third of the surface gold atoms, typically, are bound to a thiol-terminated molecule, due to the steric effect of a radial shell created by the molecule. Thus, the gold signal is only partially attenuated by the molecule. Use of the attenuation of the sulfur signal associated with the S-Au bond (obtained by fitting the XPS signal), we find that we are able to correctly determine the electron escape depth (λ) for sulfur and carbon through the molecular film. Using a poly(thiomethyl methacrylate) thin film as a carbon and sulfur XPS standard combined with the correct λ , we developed a model for the packing density and molecular orientation of COOH terminated alkane thiols that is consistent with gold, sulfur, and carbon XPS measurements as a function of molecule length. We have expanded our model to include SAMs formed of sterically crowded tertiary thiols, where fewer molecules per gold atom can attach to the surface, and to LB films formed from carboxylic acid terminated alkanes on gold surfaces, where no sulfur linkage is made. The consistent interpretation provided by our model will be presented at the talk.

[1] C.D. Bain and G.M. Whitesides, *J. Phys. Chem.* **93**, 1670 (1989).

[2] A.W. Snow, G.G. Jernigan, and M.G. Ancona, *Analyst* **136**, 4935 (2011).

3:00pm **TF+AS-TuA4 The Dynamics of Atomic-Scale Transport on the Anisotropic Compound Surface TiN(001).** *D.G. Sangiovanni, V. Chirita, L. Hultman*, Linköping University, Sweden, *I. Petrov, J.E. Greene*, University of Illinois at Urbana Champaign

We use classical molecular dynamics (MD) and the modified embedded atom method (MEAM) formalism to investigate the dynamics of atomic-scale transport on a low index anisotropic model compound, TiN(001). Our simulations, totaling 0.25 ms for each case study, follow the pathways and migration kinetics of Ti and N adatoms, as well as TiN_x complexes with x = 1, 2 and 3, all of which are known to contribute to the growth of TiN thin films by reactive deposition from Ti, N₂, and N precursors. The simulations are carried out at 1000 K, a reasonable temperature for TiN(001) epitaxial growth. We find Ti adatoms to be the highest mobility species on TiN(001), with the primary migration path involving jumps of one nearest-neighbor distance d_{NN} between four-fold hollow sites along in-plane <100> channels.

Long jumps, $2d_{NN}$, are also observed, but at much lower frequency. N adatoms exhibit much lower migration rates than Ti, diffuse only along in-plane $\langle 110 \rangle$ directions, and are unstable to associative formation of N_2 molecules which desorb at kinetic rates. As expected, TiN and TiN_3 complexes migrate at even lower rates with complex diffusion pathways involving rotations, translations, and roto-translations. TiN_2 trimers, however, are shown to have surprisingly high diffusion rates, comparable to that of Ti adatoms, due to, as revealed in our density functional theory (DFT) investigations, the significantly more symmetric charge transfer between trimer and terrace atoms, as compared with the charge distributions observed for dimers and tetramers.

4:00pm **TF+AS-TuA7 Multi-Method Calculations of the Thermodynamics of Film Deposition on Fuel Rods in Light Water Reactors**, *D.W. Brenner, A.D. Dongare, C.J. O'Brien*, North Carolina State University **INVITED**

Corrosion products in light water reactors are driven to deposit on the fuel rods, which reduces their efficiency and lifetime. The thermodynamics and kinetics that lead to this deposition are notoriously difficult to characterize *in situ* experimentally due to the extreme conditions of temperature and radiation within the reactor, and the relationship of deposits studied *ex situ* to processes under reactor conditions is unclear. It is thought that deposition is related to bubbles that form at the surface of the fuel rods due to sub-cooled boiling, but further details are lacking. We have been using first principles methods combined with molecular modeling to understand the thermodynamic driving force for this deposition, including how pH, pressure, temperature, and aqueous versus semi-aqueous “bubble” environments affects this driving force. The results of these calculations, which include studies of solvated ions, clusters and solid surfaces containing Ni, Fe, O, B, C and H will be presented along with ideas for suppressing deposition based on these results. The broader implications of our calculations for understanding and controlling film deposition in various types of aqueous environments will also be discussed.

This research is supported by the Department of Energy

4:40pm **TF+AS-TuA9 Toughness Enhancement in Transition Metal Nitride Thin Films by Alloying and Valence Electron Concentration Tuning**, *D.G. Sangiovanni, V. Chirita, L. Hultman*, Linköping University, Sweden

Enhanced toughness in hard and superhard thin films is a primary requirement for present day ceramic hard coatings, known to be prone to brittle failure during *in-use* conditions, in modern applications. Based on the successful approach and results obtained for TiN- and VN-based ternary thin films [1,2], we expand our Density Functional Theory (DFT) investigations to TiAlN-based quaternary thin films. $(TiAl)_{1-x}MxN$ thin films in the B1 structure, with $0.06 \leq x \leq 0.75$, are obtained by alloying with $M = V, Nb, Ta, Mo$ and W , and results show significant ductility enhancements, hence increased toughness, in these compounds [3]. Importantly, these thin films are also predicted to be hard/superhard, with hardness values comparable to TiAlN. For $(TiAl)_{1-x}WxN$ these results have been experimentally confirmed [4]. The general, electronic mechanism responsible for the ductility increase is rooted in the enhanced occupancy of d-t_{2g} metallic states, induced by the valence electrons of substitutional elements (V, Nb, Ta, Mo, W). This effect is more pronounced with increasing valence electron concentration (VEC), and, upon shearing, leads to the formation of a layered electronic structure, consisting of alternating layers of high and low charge density in the metallic sublattice. This unique electronic structure allows a selective response to tetragonal and trigonal deformation: if compressive/tensile stresses are applied, the structure responds in a “hard” manner by resisting deformation, while upon the application of shear stresses, the layered electronic arrangement is formed, bonding is changed accordingly, and the structure responds in a “ductile/tough” manner, as dislocation glide along the $\{110\}\langle -1-10 \rangle$ slip system becomes energetically favored [2]. The findings presented herein open new avenues for the synthesis of hard, yet tough, ceramic coatings, by tuning the VEC of alloying elements to optimize the hardness/toughness ratio in relevant applications.

[1] D. G. Sangiovanni et. al. Phys. Rev. B **81** (2010) 104107.

[2] D. G. Sangiovanni et. al. Acta Mater. **59** (2011) 2121.

[3] D.G Sangiovanni et. al. Thin Solid Films **520** (2012) 4080.

[4] T. Reeswinkel et. al. Surf. Coat. Technol. **205** (2011) 4821.

5:00pm **TF+AS-TuA10 Non-Destructive Element Specific Density Depth Profiling by Resonant Soft X-ray Reflectometry**, *S. Macke*, Max Planck - UBC Centre for Quantum Materials, Canada, *A. Radi*, University of British Columbia, Canada, *R. Sutarto*, Canadian Light Source, Canada, *G. Christiani*, *G. Logvenov*, Max-Planck-Institute for Solid State Research, Germany, *G. Sawatzky*, University of British Columbia, Canada, *B. Keimer*, Max-Planck-Institute for Solid State Research, Germany, *V. Hinkov*, Max Planck - UBC Centre for Quantum Materials, Canada

X-ray resonant reflectometry (XRR) is the ideal tool to study the depth resolved and element-specific electronic structure of multilayer films. Besides the structural parameters of thin films like thicknesses and roughnesses one is sensitive to the dielectric tensor of the film which allows to retrieve depth profiles of the magnetic, orbital[1] and valence configuration.

Due to the complex physics of reflectometry this measurement method needs sophisticated tools to analyze the results quantitatively [2]. The issues arising with this method are addressed and discussed.

By changing angle, energy and polarization of the incoming beam complete reflectivity maps can be measured leading in principle to an accurate picture of the depth resolved electronic states of thin films. The standard model used in reflectometry is based on compound layers with a defined thickness, roughness and dielectric tensor. But such a simple model is usually not capable to reproduce a full measured reflectivity map. The main reasons are especially contaminations, additional oxide layers and interdiffusion between layers.

However, introducing a layer system based on the element specific atomic density and scattering factors instead of dielectrics tensors allows more degrees of freedom for the system and allows to reproduce the reflectivity maps. Thereby the advanced model is capable to retrieve the element specific density profiles of thin films.

The method is introduced by analyzing a simple film of PrNiO₃ grown on an LSAT substrate. The reflectivity map is measured from 500eV to 1100eV.

[1] E. Benckiser et. al., Nature Materials **10**, 189 (2011)

[2] ReMagX, www.simulationcorner.net/ReMagX/

5:20pm **TF+AS-TuA11 Monte Carlo Radiation Model for Heat Transfer of Lamp for Advanced Thermal Annealing Process**, *K. Bera, J. Ranish, U. Kelkar*, Applied Materials, Inc.

Advanced thermal annealing process of semiconductor wafer uses lamp heating, specially for rapid thermal oxidation, silicidation, ion-implant anneal and spike anneal. As the technology node shrinks and the wafer size increases, wafer temperature uniformity becomes significant. The thermal modeling challenge includes complexity of the lamp filament and chamber configuration, and complex optical properties of semitransparent media. In order to analyze lamp heating, two-dimensional Monte-Carlo based radiation, and thermal conduction model for a single lamp is built using CFD-ACE+. The Tungsten lamp filament is immersed in Nitrogen. The single lamp is enclosed by a reflector, and protected at the top by a quartz plate. For the single lamp thermal model, effective surface area and volume of the coil are considered. The irradiance profile of the lamp at a distance of a few cm from the quartz plate compared well with the experimental data. The single lamp model is simplified using a cylindrical filament structure that matches the irradiance profile. The cylindrical filament structure is used in 3D chamber model that considers thermal convection in addition to radiation and conduction. In both single lamp and chamber models, for semi-transparent non-gray media, wavelength dependent real and imaginary parts of refractive indices are used in optical database to calculate thermal absorption. For gray material, surface emissivity of the material is defined. For reflective material, the degree of specularly on the surface is defined as well. For gas conduction, temperature dependent thermal properties are used. The single lamp power is varied by several hundreds of Watts. The irradiance profile shows a peak at the center that decays substantially as we move radially outwards. The effect of quartz plate thickness on irradiance profile is evaluated. The chamber model is used to determine wafer temperature distribution and transient thermal response for a range of lamp assembly power.

5:40pm **TF+AS-TuA12 First Principles Studies of Oxygen Transfer at Buried Metal/Metal Oxide Interfaces**, *C. Goldstein, E. Mily, J.-P. Maria, D.W. Brenner, D. Irving*, North Carolina State University

Heterogeneous material interfaces between metals and metal-oxides provide a unique opportunity to create active functional materials. The functionality of these heterostructures can hinge either on limiting or enabling oxygen transfer across the interface. For example, there has been recent research on how to use thin film metal/metal-oxide super-structures to control the power output generated by the exothermic exchange of oxygen across the as-deposited interface. In all of these heterogeneous systems, it is imperative to

fundamentally understand the mechanisms that facilitate oxygen exchange, as the dynamics are not currently well understood. In the work presented here, chemically accurate Density Functional Theory calculations have been used to predictively determine likely reaction pathways for oxygen transport in energetic nanocomposite materials and to characterize the stability of novel heterogeneous material interfaces. Our ultimate goal is to tune power output through an understanding of the mechanisms of oxygen transport across heterogeneous interfaces and within the super-structure. Several systems have been investigated, including more traditional thermite materials such as Al and Ti paired with Cu_2O . In these systems, the energy release is large, but there is also a high degree of strain when ideal systems are modeled. Other model systems were chosen based on structural similarity, minimal lattice mismatch, and the degree of exothermicity associated with oxygen transfer. Results on these systems will also be presented. Preliminary calculations simulate systems at various early stages to isolate factors that could influence the reaction, such as strain or initial barrier height. The results presented here show qualitative agreement between calculations and experimental observations. This project has been supported by the Army Research Office through grant # W911NF-10-1-0069 and the NSF Graduate Research Fellowship Grant # DGE0750733.

Tuesday Afternoon Poster Sessions

Applied Surface Science

Room: Central Hall - Session AS-TuP

Applied Surface Science Poster Session

AS-TuP1 Sub-Micrometer Imaging of Lipids and Trace Elements in Various Cells with ToF-SIMS and Laser-SNMS, H.F. Arlinghaus, F. Draude, S. Galla, A. Pelster, M. Körsgen, University of Muenster, Germany, J. Tentschert, H. Jungnickel, A. Haase, A. Luch, German Federal Institute of Risk Assessment, Germany, T. Schwerdtle, J. Muthing, University of Muenster, Germany

In recent years, molecular imaging with submicron lateral resolution has become of more and more interest for characterizing specialized compounds in biological samples. As an example, nanoparticles (NPs) gain great commercial interest in the medical field due to their high mobility in human tissue. Despite broad applications close to the human body, so far, there is only little knowledge of possible toxicity. In this context, the distribution of NPs within cells is of particular interest. Moreover, not only the distribution of NPs but also elemental and molecular cellular distributions such as metabolites and lipids are interesting for medical research.

In this study, we used time-of-flight secondary ion mass spectrometry (ToF-SIMS) and laser-secondary neutral mass spectrometry (Laser-SNMS) to investigate different cells both unexposed and exposed in vitro to silver NPs (AgNPs) and arsenic species. To optimize the analysis, a special silicon wafer sandwich preparation technique was employed; this entails freeze-fracturing and washing of cell cultures that were grown on silicon wafers. The data showed that during freeze-fracturing, the cell membrane is often stripped from the cell, enabling direct analysis of the interior of the cells on one sandwich wafer and the remaining lipid membrane as a mirror image on the opposite wafer. During analysis, the signal from the nutrient materials was observed to diminish the contrast of the molecular signals in the images. By optimizing the preparation and washing procedures, both the contrast and the imaging resolution could be significantly increased due to higher molecular yields and lower background. With these optimization procedures it was possible to detect lipid ions in a higher mass range, especially from those membranes that were stripped from the cells.

Under these optimized conditions, several studies were performed to detect the distributions of trace elements in cells. One study dealt with AgNPs. In this context the uptake of AgNPs of human macrophages was measured with nanometer-scale resolution. 2D and 3D Laser-SNMS images clearly showed that AgNPs are incorporated by macrophages and in part agglomerate to silver aggregates with a diameter of ~3-7 μm . In a similar approach, the distribution of arsenic in cells was measured to obtain more information on the reasons why inorganic arsenic proves carcinogenic in humans. A comparison with ToF-SIMS data showed that especially the high elemental sensitivity of Laser-SNMS makes it possible to detect these trace elements in cells.

AS-TuP2 Comparative Study on the Methods to Determine the Interface Locations in SIMS Depth Profiling Analysis of Multilayer Films, H.H. Hwang, University of Science and Technology (UST), Republic of Korea, J.S. Jang, H.J. Kang, Chungbuk National University (CBNU), Republic of Korea, K.J. Kim, University of Science and Technology (UST), Republic of Korea

In-depth analysis by secondary ion mass spectrometry (SIMS) is very important for the development of electronic devices using multilayered structures, because the quantity and depth distribution of some elements are critical for the electronic properties. Correct determination of the interface locations is critical for the calibration of the depth scale in SIMS depth profiling analysis of multilayer films. However, the interface locations are distorted from real ones by the several effects due to sputtering with energetic ions.

In this study, we compared the three definitions for the determination of interface locations in SIMS depth profiling of multilayer films. Especially, we investigated the feasibility of 50 atomic % definition for Si/Ge and Si/Ti multilayer films by various SIMS analysis parameters. In 50 atomic % definition, the original SIMS depth profiles are converted into compositional depth profiles by the relative sensitivity factors (RSF) derived from the alloy reference films with well-known compositions determined by Rutherford backscattering spectroscopy (RBS).

The application of the 50% definition determined from the ion intensities was found to be very limited to specific systems showing clear interfaces. The definition of the interface by the dimer ions between the atoms in the two different layers was also difficult to apply due to the small intensity and the unclear variation at the interfaces.

AS-TuP3 Estimation of Useful Yield of Electrospray Droplet Impact/Secondary Ion Mass Spectrometry, R. Takaiishi, K. Hiraoka, University of Yamanashi, Japan

The electrospray droplet impact secondary ion mass spectrometry (EDI/SIMS) has been developed as cluster SIMS[1]. EDI utilizes charged water droplets generated by ambient electrospray. The typical droplet is represented as $[(\text{H}_2\text{O})_{90,000} + 100\text{H}]^+$ with mass of $\sim 10^6$ u. The kinetic energy of droplets is about 10^6 eV with the velocity of 12 km/s. EDI/SIMS has the atomic/molecular level etching abilities[1][2]. EDI/SIMS was found to be applicable to many kinds of inorganic and organic material [1][3]. In spite of the shallow surface etching, relatively high secondary ion yields can be obtained by EDI.

The high ionization efficiency may be due to the occurrence of supersonic collision taking place between the droplet and the sample surface. In order to estimate the useful yield (i.e., total ions generated divided by the total molecules desorbed), mass spectra were measured for binary mixtures of C_{60} /Rhodamine B (1:1) and C_{60} /Aerosol OT (1:1). The equimolar samples were crushed and mixed in mortar and deposited on a stainless steel target as thin films using a spatula. This method was adopted from solvent-free MALDI. By assuming that (1) the desorption efficiency is the same for C_{60} , Rhodamine B and Aerosol OT, and (2) the desorbed ionic compounds directly give secondary ion signals, the useful yield was crudely estimated to be ~ 0.1 . This high value explains the high ionization efficiency of EDI/SIMS.

Reference

- [1] K. Hiraoka, D. Asakawa, S. Fujimaki, A. Takamizawa, K. Mori, Eur. Phys. J. D38, 225 (2006)
- [2] D. Asakawa, K. Mori, K. Hiraoka, Appl. Surf. Sci. 255 (2008) 1217
- [3] K. Hiraoka, K. Mori, D. Asakawa, J. Mass. Spectrom. 41 (2006) 894

AS-TuP4 Multivariate Analysis Models to Predict Surface Chemistry or Performance using ToF-SIMS Mass Spectra Datasets, N. Sano, M.-L. Abel, J.F. Watts, University of Surrey, UK

Latent (that is unintentional) adhesion between organics and inorganic surfaces is a well known phenomenon in many areas of materials science, e.g. the moulding of polymeric components and the storage of coated metal products where a polymeric surface is in intimate contact with the back of another sheet. A complete understanding of the adhesion and adhesion processes that occur at this interface may provide a key to obtaining optimum performance for a particular application.

In this work, we are considered with the effects of migration of organics to the surface of the polymeric host and their role at the polymer/inorganic interface. We have focused on three characteristic organics widely used as additives in a wide range of polymer formulations. In the samples we have studied, characteristic peaks from these additives dominate the ToF-SIMS analysis of the inorganic surface. In addition, surface chemistry of the inorganic surface induces different mechanical performances of the products. The storage period has the potential to play a significant role in the migration of minor components towards the interface under investigation, and data will be presented at two different periods (early and late stages).

In this study we show models using multivariate analysis describing how ToF-SIMS analysis can be applied to understand the surface chemistry of industrial materials. The behaviour of migration from the polymer to the inorganic side of the polymeric assembly induces three characteristic surface chemistries which influence mechanical performance. Our models show good predictions for a validation sample of materials.

AS-TuP5 Method for Cross-sectional Analysis Using FIB, ToF-SIMS and Multivariate Analysis, J.A. Ohlhausen, M.J. Rye, P.G. Kotula, J.R. Michael, T.J. Garino, Sandia National Laboratories

We have developed a method to create a cross-section of small samples for Time-of-Flight Secondary Ion Mass Spectrometry (ToF-SIMS) utilizing a Focused Ion Beam (FIB) approach. Using this method, a nearly ideal surface for elemental and molecular analysis of the cross-sectional surface is produced, thus providing complimentary information to other microanalytical techniques like scanning electron microscopy (SEM) and scanning transmission electron microscopy (STEM).

FIB is commonly used to create cross sections for SEM and STEM imaging and analysis. Benefits of this technique include controlled extraction area and high spatial resolution. Unfortunately, elemental analyses in the SEM and STEM are not sensitive to low-Z elements and have detection limits that may prevent the detection of some species of interest. Although ToF-SIMS produces lower spatial resolution ($\sim 200\text{nm}$), it has excellent low-Z

sensitivity and has detection limits in the ppm to ppb range. Traditional FIB lift-out sections have been used as cross sections for ToF-SIMS analysis, but they are typically fragile and difficult to handle, thus complicating ToF-SIMS analysis. We have developed a method to create cross sections of particles and small fragments of material that can be analyzed in the "as cut / as mounted" condition. Samples are placed on a traditional SEM mount, and then coated with a conductive layer of AuPd. With the use of special mounts, a cross section that is parallel to the sample surface is milled in the FIB. The resulting samples are sturdy, allowing the removal of the Ga implants by O₂ sputtering. The cross sectioned sample can now be analyzed with ToF-SIMS. Using data from ZnO multi-grain particles, we will show that ToF-SIMS analysis of the cross section yields elemental and molecular information with low detection limits. Additionally, we will demonstrate that multivariate analysis of ToF-SIMS data acquired by this technique is complimentary to a FIB-STEM analysis.

§Sandia National Laboratories is a multi-program laboratory managed and operated by Sandia Corporation, a wholly owned subsidiary of Lockheed Martin Corporation, for the U.S. Department of Energy's National Nuclear Security Administration under contract DE-AC04-94AL85000.

AS-TuP6 XPS Depth Analysis of Metal/Polymer Multilayer by Electro Spray Droplet Impact, Y. Sakai, R. Takaishi, S. Ninomiya, K. Hiraoka, University of Yamanashi, Japan

The electro spray droplet impact (EDI) has been developed for cluster SIMS [1]. EDI utilizes the charged water droplets as projectiles for reducing the sample surface degradations often encountered in atomic-ion SIMS. EDI projectiles are extremely large water cluster ions generated by an ambient electro spray (masses of several 10⁶ u). EDI is capable of atomic- and molecular-level etching with little damage after the irradiation. The EDI gun has been installed in X-ray Photoelectron Spectroscopy (XPS) instrument to analyze the dynamic etching processes during the EDI irradiation. This system has been applied to various organic and inorganic materials. A comparative study of Ar⁺ and EDI etching was performed. While selective etching was observed for almost all of the samples examined by Ar⁺, no chemical modification was recognized by EDI [2,3]. The multilayer metal/polymer samples are used for many practical applications such as transducer, optical device and packaging, etc. For example, the metal layers in integrated circuits are used as the electrical connection and barrier. The interface analysis of metal/ polymer multilayer is of significant importance to clarify the diffusion phenomena taking place between metal and polymer interface. Thus, the ion gun for the interface analysis that is capable of molecular-level etching with no chemical modification is highly demanded. Our preliminary experimental data showed that the EDI gun is very useful for metal/polymer interface analysis. In this report, the depth analysis of Cu/Polymer/Si by EDI etching will be presented. Reference[1] K. Hiraoka, D. Asakawa, S. Fujimaki, A. Takamizawa, K. Mori, Eur. Phys. J. D 38, 225 (2006)[2] Y. Sakai, Y. Iijima, D. Asakawa and K. Hiraoka, Surf. Interface Anal. 42, 658 (2010)[3] Y. Sakai, S. Ninomiya and K. Hiraoka, Surf. Interface Anal. 43,1605 (2011)

AS-TuP7 A Combined HAXPES and Electrical Characterisation Study of Si and III-V based MOS Structures, L.A. Walsh, G.J. Hughes, Dublin City University, Ireland, P.K. Hurley, J.H. Lin, Tyndall National Laboratory, Ireland, J.C. Woicik, National Institute of Standards and Technology

The aim of this study was to use synchrotron radiation based HAXPES measurements to study the intrinsic electronic properties of both Si and III-V based MOS structures. High quality thermally grown SiO₂ layers, with a thickness of 8 nm, were grown on both n (5x10¹⁵ cm⁻³) and p (5x10¹⁵ cm⁻³) doped silicon. While Al₂O₃ layers 8nm thick were deposited on both n (Si - 5x10¹⁷ cm⁻³) and p (Zn - 5x10¹⁷ cm⁻³) doped GaAs, and n and p (~4x10¹⁷cm⁻³ for both) doped InGaAs substrates. All substrates were treated by a wet chemical ammonium sulphide based passivation treatment. The samples for HAXPES analysis were capped with 5 nm Ni or Al blanket films by electron beam evaporation. For electrical characterisation, Ni/Au (70 nm/90 nm) and Al (160 nm) gate electrodes were patterned by electron beam evaporation and a lift off lithography process. HAXPES measurements using a photon energy of 4150 eV were used to probe the MOS structures in order to investigate the differences in substrate core level binding energies caused by changes in doping type, and metal work function. The sampling depth for these high energy photons was sufficient to detect core level peaks originating from the substrate, the 8 nm thick dielectric layer, and the top metal contact. The binding energy of core levels in photo emission are referenced with respect to the Fermi level, therefore changes in the binding energy of a particular core level reflect differences in the position of the Fermi level in the semiconductor band gap. For the MOS structures fabricated using SiO₂/Si, changes in the Fermi level positions and differences in the potential drops across the dielectric layers have been directly correlated with the metal workfunction differences observed in the

CV and GV measurements. A binding energy difference of 0.6 eV was measured between the GaAs core levels of the n and p doped substrates, independent of metal work function indicating the strong Fermi level pinning present at the Al₂O₃/GaAs interface. Binding energy measurements for the core levels of native oxide covered n-type doped InGaAs substrates with no metal cap were found to be consistently (~0.3 eV) higher than p-type samples reflecting the fact that the Fermi level is in a different position in the band gap. A binding energy difference of 0.25eV for the core levels of the n and p samples just with the Al₂O₃ dielectric layer present, indicating different Fermi level positions in the band gap. Deposition of the different workfunction metals resulted in limited change in the InGaAs core level binding energies, indicating the partially pinned nature of the Al₂O₃/InGaAs interface.

AS-TuP9 The Development of Charged Particle Lenses for High Spatial Resolution XPS Studies, R. Walker, Shimadzu Research Laboratory (Europe) LTD, UK

The development of selected area and imaging XPS made significant advances with the adoption of Magnetic Snorkel lenses. This lens type of an unconventional design, projects from its main bulk an axial magnetic field that enables focusing of charged particles with low optical aberrations. Simulation techniques, calculate typical lens aberration coefficients of spherical, Cs=3mm and chromatic, Cc=8mm. In the XPS application original theoretical expressions used to characterize this lens type, have been re-modeled, to use present day data and predict some future improvements with this and other lens types. The spatial resolution of present commercial instruments (3µm) is limited by signal to noise. With the large collection angles involved, it is shown that astigmatism is a major contribution that limits the spatial resolution. Furthermore the spatial resolution of the detected signals is insufficient to resolve the stigmatic foci of the astigmatism present in the XPS image. Snorkel lenses are positioned under the specimen and to enable sufficient working distance between the lens and the specimen surface, the lens is highly excited. Typical working distances measure 15mm. By refining the lens coil and iron circuit design, the lens excitation is increased to a maximum and a lens working distance of 19mm is achieved. Consequently with the Snorkel lens positioned in this manner, the thickness of sample will remain limited. A Snorkel lens may also be positioned above the specimen surface so that previous spatial constraints imposed on the specimen form no longer apply. The lens is conical in shape with a bore to focus the photoelectrons through. It will be shown that a Snorkel lens with a 45° access to the specimen surface and at a 2mm working distance has been experimentally proved with very low lens aberration coefficients (Cs, Cc) of 1mm. Calculations show that with only small increases to existing laboratory x-ray powers, it is possible to use this lens to image XPS spatial resolutions of 1µm with present day count rates. Snorkel lenses can have limitations with specimens that magnetize, particularly specimens with topography. Substitution of an Electrostatic accelerating lens for a Magnetic Snorkel lens may result in only a small deterioration of the detected photo electron photoelectron spatial resolution. The ultimate spatial resolution of an image exhibiting the same signal to noise is calculated to be 7µm (Electrostatic) as opposed to 3µm (present day Magnetic). Details of an accelerating electrostatic lens are shown, that is proved to operate reliably with no electrical breakdown.

AS-TuP10 Image Depth Profiling for Three-Dimensional Characterisation of Microelectronic Structures, B. Sgammato, A.E. Wright, A. Bushell, Thermo Fisher Scientific, UK

Microelectronic devices typically consist of elaborate three-dimensional structures, and careful control of chemical and structural properties is required for effective operation. Structures such as pads and bond pads must be carefully assessed for correct size, composition, layering and contamination levels. Supporting structures and substrates must also have the correct composition, integrity and electronic properties.

X-ray photoelectron spectroscopy (XPS) is a surface-sensitive material characterisation technique that offers sensitive chemical state information, and is already established as a method of choice for the analysis of microelectronic devices. Parallel XPS imaging offers high spatial resolution for observing the lateral distribution of chemical states at the surface of a material, and recent advances in spectroscopic imaging allow the generation of quantitative chemical state images for maximal information content.

Depth profiling, typically with ion beams, allows the gradual removal of material from a sample surface, so that XPS can be used to probe further than its characteristic nanometre-scale analysis depth.

The combination of spectroscopic parallel imaging and depth profiling, using the Thermo Scientific Escalab250Xi, permits unmatched spatial resolution combined with layering information, and permits the clear identification of subsurface structures and chemical states. The powerful, intuitive Avantage software datasystem makes data processing

straightforward, so that profile information from small parts of the sample are simple to generate.

AS-TuP11 Developing a Methodology for XPS Profiling of Biofilms and Biological Materials, R.G. White, Thermo Fisher Scientific, UK, *D.Y. Petrovykh,* International Iberian Nanotechnology Laboratory, Portugal, *A.C. Areias, C. Sousa, G.P. Mendes,* University of Minho, Portugal

Films of cells on solid substrates are encountered in a variety of biological and biomedical environments, including cells in biofilms that spontaneously colonize medical devices and multilayers of cells filtered from suspensions for analysis. Understanding the chemical properties of cells in such films is important for providing clues about the behavior of the cells or about the effects of treatments that had been applied to the cells.

X-ray Photoelectron Spectroscopy (XPS), with its combination of chemical selectivity and surface specificity, is an ideal technique for analysing these biofilms and multilayers, but it needs to be combined with profiling to more fully characterise the samples. It is well known that profiling with traditionally used argon monomers results in a high degree of chemical modification for most organic materials. Recent studies have shown, however, that argon cluster beams may be used for depth profiling of organic materials while preserving the chemical information.

This poster will present data from cluster profiling studies of biofilms and biomaterials. The methodology required for optimum profiling of these samples will be discussed, including an evaluation of XPS data acquisition protocols, as well as sputtering conditions.

AS-TuP12 XPS and Auger Analysis of Single and Multi-Layer Graphene Films: What is Graphene and What is Not?, H.M. Meyer III, *I. Vlassiuk,* Oak Ridge National Laboratory, *A.V. Sumant,* Argonne National Laboratory

Graphene has received unprecedented attention since 2010 when the Nobel Prize was awarded to Geim and Novoselov for “groundbreaking experiments regarding the two-dimensional material graphene.” Many graphene-related publications use the C 1s spectrum to demonstrate the existence or formation of graphene, but unique photoemission spectral signatures are difficult due to the inherent thinness of single or even multi-layer graphene. The difficulty is due to the surface sensitivity of XPS and Auger spectra and the analysis of spectra that include graphene, substrate-related carbon and possible adsorbed carbonaceous material on the graphene. This poster explores various XPS and Auger spectral features from studies of graphene grown by the CVD method on Cu (near-single layer) and Ni (multi-layer). In one study, graphene grown on Cu was heated in air to determine if the graphene provided any protection to the underlying Cu substrate. The results indicated not only oxidation (i.e. corrosion) protection, but that there was a time and heat dependence of the protection. To aid in the understanding of graphene vs. substrate contributions to the C 1s XPS spectrum, additional studies were performed on CVD-grown diamond substrates. Diamond substrates (very low oxygen and pure sp³-type carbon) offer an interesting contrast to most substrates that have inherent O and C contributions to the O 1s and C 1s spectra. Unique XPS and Auger related features of graphene will be highlighted in this poster.

AS-TuP13 XPS Sputter Depth Profiling of Organic Thin Films Using an Ar Cluster Ion Source, A.J. Roberts, S.J. Hutton, C.J. Blomfield, *W. Boxford,* Kratos Analytical Ltd., UK

A new 20 keV Ar cluster ion source has been used to successfully sputter profile through a range of organic thin films and multilayers. Samples were analysed using XPS between sputter cycles to allow the chemical composition of the sample to be probed as a function of depth into the material. Use of massive Ar cluster ions (1000 to 2000 Ar atoms per ion) promote the retention of sample chemistry throughout the depth profile. In this study we report the performance of the Ar cluster ion source on a range of organic thin films, from fields as diverse as organic PV materials, OLED's, cross-linked plasma polymers and multilayers. Analysis conditions were optimised to maximise retention of chemical functionalities and minimise ion induced interlayer broadening.

AS-TuP14 Quantitative XPS Depth Profiling of Mobile Ions in Soda-Lime-Silica Glasses using a Polyatomic Ion Source, C.J. Blomfield, S.J. Hutton, W. Boxford, Kratos Analytical Ltd., UK

Soda-lime-silica glass is widely used not only for architectural and automotive applications but increasingly in electrical devices as display panels and in photovoltaic applications. The role of mobile ions such as alkali or alkaline-earth ions in these glasses can affect the quality in architectural glass but can have a large impact on electrical device performance. It is important to know the concentration of these mobile ions in the glass surface region and deeper into the glass substrate to understand the leaching process.

Alkali migration has been a noted artefact of sputtering with monatomic Ar ion beams and the use of polyatomic ion beams more commonly applied to organic materials has been shown to yield some benefits in reduced migration without incorporation of C into the glass matrix.

In this investigation we compare the results with monatomic Ar ion sputtering and polyatomic (Coronene) for a number of soda-lime-silica glass samples.

AS-TuP15 XPS Assessment of the Thickness of Fe Oxide Layers using Standard and Active Shirley Background, M. Bravo-Sanchez, CINVESTAV-Unidad Queretaro, Mexico, *F. Espinosa-Magaña,* CIMAV Unidad-Chihuahua, Mexico, *A. Herrera-Gomez,* UAM-Azcapotzalco and CINVESTAV-Queretaro, Mexico

The thickness of metal oxide nanolayers can be assessed through X-Ray Photoelectron Spectroscopy (XPS) measurements. This is done by comparing the signal from oxide and metallic XPS peaks. The correct assessment of the oxide layer thickness depends on how accurate the peak areas are quantified through peak fitting. Since the oxide and metallic peaks overlaps in XPS spectra, the calculation of their areas could be tricky. This is specially the case for iron since the Fe 2p peak, which is the iron peak most employed in XPS experiments, is largely asymmetric. In this work, we show that the assessment of the peak areas can carry errors as large as 120% if the traditional Shirley background is employed. The problem is solved by the use of the “active” background removal method, in which the background intensity is optimized during the peak-fitting process. This method is described in detail, as well as its software implementation. The results are supported with High Resolution Transmission Electron Microscopy micrographs.

AS-TuP16 Active Fitting for Optimized Shirley Background Determination, J. Muñoz-Flores, UAM-Xochimilco, Mexico, *A. Herrera-Gomez,* UAM-Azcapotzalco and CINVESTAV-Queretaro, Mexico

To subtract the Shirley background to X-Ray Photoelectron Spectroscopy data it is necessary to choose two points, one at each side of the main features of the spectrum. It is common that these points are set close to the peaks to avoid other features present in the spectrum or simply because the data was not acquired with a wide enough energy range. The latter is a common error since it is difficult to discriminate by eye where the contribution of the peaks becomes negligible and the signal is completely due to the background. This is particularly true for peaks with large kurtosis (i.e., large Lorentzian widths) and even more for asymmetric peaks. In the traditional Shirley method, the background is forced to pass through the set points, not allowing any contribution of the peaks to the total signal at those points. As a consequence, the area of the peaks is usually underestimated. In this work we describe the error in the quantification of the peak areas as a function of the energy range and peak width when the traditional Shirley method is applied. This type of error can be avoided if the intensity of the Shirley background is optimized during the peak-fitting procedure, without the restriction of the background passing through the set points. This “active” method is described in detail, as well as its software implementation. By the use of simulated data, it is shown that the active method assesses the peak areas very precisely even when the data is obtained with a too-short energy range.

AS-TuP18 Atom Probe Tomography Analysis of Grain Boundaries in CdTe, V.S. Smentkowski, General Electric Global Research Center, *D.J. Larson, D.A. Reinhard, T.J. Prosa,* CAMECA Instruments Inc., *D. Olson,* Cambridge University, UK, *D. Lawrence, P.H. Clifton, R.M. Ulfig, T.F. Kelly,* CAMECA Instruments Inc.

Photovoltaic materials convert photons to electrical energy (e.g., solar cells) or convert electrical energy into light (e.g. light emitting diodes). Films based on the II-VI compound CdTe are currently regarded as one of the leading type II materials for development of cost-effective solar cells as the CdTe band gap is near ideal for photovoltaic conversion efficiency [1]. While theoretical efficiency values approach 30% [2], commercial and laboratory tests of CdS/CdTe heterojunctions range from ~10% to ~17%, respectively [3,4]. The presence of grain boundaries in these structures likely plays an important role in the observed efficiency. In the current work we investigate, for the first time, the applicability of atom probe tomography (APT) to characterize grain boundaries within the CdTe layer of a solar device. APT data were collected on a CAMECA LEAPTM 4000X HR operated at a base temperature of 40K with a laser energy of 3pJ, a repetition rate of 100kHz and an ion detection rate of 1%. Specimens for APT were prepared by standard focused-ion-beam milling methods [5] from a CdTe layer within a solar cell. Laser-pulsed APT spectra from CdTe-based alloys are quite complex [6,7]. There are two reasons for this: 1) Cd and Te each have eight isotopes and 2) Cd and Te field evaporate in a multitude of complex molecular ions species. The following ions were detected in mass spectra: Cd⁺, Te⁺, CdTe⁺, Cd₂⁺⁺, and Te₂⁺⁺, Cd₂Te⁺⁺ and

CdTe₂⁺⁺, Cd₂⁺, CdTe⁺ and Te₂⁺. In spite of the complex nature of these spectra, all of the peaks are identifiable as some combination of Cd and/or Te. This poster will show both the measured spectra and CdTe composition estimate, as well as 3D images revealing enhancement of S and Cl at a grain boundary.

References

- [1]. Z. Fang et al., *International Journal of Photoenergy* 2011 (2011) 297350.
- [2]. A. Bosio et al., *Progress in Crystal Growth and Characterization of Materials* 52 (2006) 247.
- [3]. M. Powalla & D. Bonnet, *Advances in OptoElectronics* 2007 (2007) 97545.
- [4]. <http://investor.firstsolar.com/releasedetail.cfm?ReleaseID=639463>
- [5]. D.J. Larson et al., *Ultramicroscopy*, 79 (1999) 287, M.K. Miller et al., *Micro. Microanal.*, 13 (2007) 428.
- [6]. P. P. Choi et al., *Microscopy Today*, 20 (2012) 18.
- [7]. D. J. Larson et al., *Microscopy and Microanalysis* (2012), in press.

AS-TuP19 Mapping of a Natural Lubricant Network on the Surface of Silicone Hydrogel Materials Using Surface and Bulk Chemistry Techniques, K.A. Wygladacz, D.J. Hook, M. Merchea, E.P. Maziarz, Bausch + Lomb

Commercial silicone hydrogel contact lenses (SiHy) are ophthalmic devices designed to correct vision as well as function as an ocular bandage for therapeutic purposes. Surface wettability, modulus, surface topography as well as bulk water content are some of the factors that influence lens comfort and performance. Contact lens surface wettability is believed to be an important factor in comfort as well as overall patient satisfaction. Tear confluence across a lens surface may be improved by the presence of well-chosen biomolecules, capable of retaining moisture. Very recently the application of a natural lubricant hyaluronate (HA), to a daily use multi purpose solution (MPS), Biotrue™ has been reported.

In these studies HA was used in conjunction with a surfactant system present in Biotrue™ MPS. The exclusive formulation of Biotrue™ was designed to improve hydration and wettability of various SiHy contact lens materials. Improvements in moisture retention are attributed to the use of high molecular weight HA present in Biotrue™ capable of high water retention. Presence of HA on a lens surface acts as a wetting agent and improves the properties of SiHy contact lens materials. To our knowledge there is no published literature reporting on a visualization method of HA on SiHy contact lenses surfaces.

The purpose of this research was to develop a direct method to demonstrate the presence of a HA network on the surface of SiHy contact lenses using surface chemistry techniques. Senofilcon A® and balafilcon A® were chosen to investigate the interaction of HA with SiHy materials. Atomic Force Microscopy (AFM) was applied to examine the topography of both materials in the hydrated and dehydrated state. The visualization of HA chains was done using Confocal Laser Scanning Microscopy (CLSM) and Differential Interference Contrast (DIC) microscopy using a dye selective for HA (Safranin).

Senofilcon A® and balafilcon A® were soaked in Biotrue™ for 4 hours. Lenses were then soaked in 3 mL of Safranin solution. After 3 min the samples were rinsed with DI water for 3 min to remove any unbound dye. Samples were imaged using an Olympus CLSM equipped with a DIC attachment. Individual confocal images were captured using an air objective sequentially across the sample. A large mosaic was generated using fiducial marks stitched together from the individual images. SiHy lenses incubated with Safranin solution but not exposed to Biotrue™ were characterized as control. Additionally applicability of X-ray Photoelectron Spectroscopy (XPS) for HA mapping on the lenses surface was examined. AFM was used in parallel to study modification of the lens surfaces with HA biopolymer.

AS-TuP20 Kinetics and Mechanism Studies of Copper Nano-Structures Formation on Functionalized Si Surfaces, J.M. Lin, University of Delaware, K.A. Perrine, University of California, Irvine, A.V. Teplyakov, University of Delaware

The manufacture of modern electronic devices has been longing for the higher control over chemical deposition processes and interface properties, as the electronic devices kept scaling down. As a result, a comprehensive understanding of surface reaction mechanisms between the precursor molecule and surface reactive sites is desired.

Numerous studies have addressed that chemically functionalized Si surfaces are promising solutions.

In this work, Copper (hexafluoroacetylacetonato) vinyltrimethylsilane, or Cu(hfac)VTMS, was used to deposit copper nanoparticles on several functionalized Si surfaces including H-Si(100), H-Si(111), NH₂-Si(100),

NH-Si(100), NH₂-Si(100), and OH-Si(100). With atomic force microscopy (AFM), infrared spectroscopy (MIR-FTIR), X-ray photoelectron spectroscopy (XPS) and temperature programmed desorption (TPD) supported with density functional theory calculations (DFT), we have investigated the reaction kinetics and mechanism of the surface reaction and the effects of Si surface functionalization on particle size control and elemental composition of the as-deposited film.

AS-TuP21 Dry Cleaning Methods for Single Reconstructions of (100) InGaAs Following Air Exposure and Post Annealing Conditions, W. Melitz, M. Edmonds, T.J. Kent, A.C. Kummel, University of California San Diego

In effort to further reduce the EOT scaling process while simultaneously maintaining low Ditand high mobility on III-V semiconductor surfaces, dry cleaning methods have been implemented to help create uniform and ordered semiconductor surfaces. The scaling of gate oxides on MOSFETs requires ALD oxide nucleation in every unit cell of the semiconductor channel surface, a process which depends having a highly ordered semiconductor with the minimization of surface defect sites which prevent ALD oxide deposition thereby inducing pihole formation. Through the use of in situ scanning tunneling microscopy (STM) and an atomic hydrogen cleaning technique, air exposed (001) InGaAs samples with an In/Ga rich 4x2 surface reconstruction and an As rich 2x4 surface have been restored to the order and cleanliness of MBE grown samples.

The InGaAs samples were exposed to air, containing NO_x, ozone, and hydrocarbons, and returned to UHV for STM atomic imaging. Imaging confirmed the surfaces became amorphous upon air exposure. The samples were exposed to 150L dose of atomic hydrogen at 380°C. After atomic hydrogen dosing, STM revealed the restoration of the ordered pure In/Ga rich 4x2 surface reconstruction with highly flat atomic terraces. Atomic H cleaning results in formation of deep etch features but a subsequent anneal at 460 °C for 30 min can reduce this effect. Etch pit density has been quantified for samples both after hydrogen dosing and after the post annealing process. Results showed a 98% reduction in etch pit density following the post annealing process [1]. For formation of the pure As-rich 2x4 reconstruction with no group III rich regions, a relatively small processing window was found introducing the air exposed sample to a 1800L dose of atomic hydrogen at 285°C to form the pure 2x4 reconstruction. Etch pit formation occurred following hydrogen dosing and the samples were subsequently annealed to 290°C for 30 minutes. Etch pit density was quantified for samples before and after post deposition annealing and results showed a decrease in etch pit density by 55% following the post annealing process.

[1] W. Melitz, J. Shen, T. Kent, A. C. Kummel, and R. Droopad, " InGaAs surface preparation for ALD by hydrogen cleaning and improvement with high temperature anneal," *J. Appl. Phys.*, vol. 110, p. 013713, 2011.

AS-TuP22 The Effect of Gas Environment on the Electronic and Optical Properties of Amorphous Indium Zinc Tin Oxide Thin Films, Y.R. Denny, S.Y. Lee, K.I. Lee, S.J. Seo, Chungbuk National University (CBNU), Republic of Korea, S. Heo, J.G. Chung, J.C. Lee, Samsung Advanced Institute of Technology, Republic of Korea, H.J. Kang, Chungbuk National University (CBNU), Republic of Korea

The electronic and optical properties of Indium Zinc Tin Oxide (IZTO) thin films were investigated by X-ray photoelectron spectroscopy (XPS) and reflection electron energy loss spectroscopy (REELS). IZTO thin films on a glass substrate have been prepared by RF magnetron sputtering. The composition ratios of In:Zn:Sn in IZTO thin films are 20:56.7:23.3. The films were deposited at the annealing temperature of 350 °C for 1 hour in air, oxygen mixed with water (annealed at 350°C), and 80% oxygen mixed with argon (without annealing). The XPS spectra shows that all IZTO thin films have the Sn-O, In-O, and Zn-O bonds. The REELS spectra revealed that the band gaps of IZTO thin films are 3.23 and 3.07 eV for water mixed oxygen and argon mixed oxygen, respectively. The value of band gap increased to 3.46 eV when the sample was annealed in air. All the measured band gaps by REEL are consistent with the optical band gaps determined by UV-Spectrometer. The average optical transmittance of all IZTO thin films in the visible light region was 86%. The sheet resistivity of IZTO thin films deposited in water and argon mixed oxygen was 5 times lower than that of air, which indicates that gas environment plays an important role in increasing the figure of merit (ϕ_{TC}) and thus improving the electrical and optical properties of IZTO thin films.

AS-TuP23 Modification of Metal – InGaAs Schottky Barrier Height by Atomic Layer Deposition of Ultrathin Al₂O₃ Interlayers. *L. Chauhan*, Dublin City University, Ireland, *S. Gupta, P. Jaiswal, N. Bhat, S.A. Shivashankar*, Indian Institute of Science Bangalore, India, *G.J. Hughes*, Dublin City University, Ireland

High indium content InGaAs is a leading candidate for n-channel devices in future generations of complementary metal-oxide-semiconductor (CMOS) technology due to its high electron mobility and high saturation velocity. In recent years significant progress has been made in improving the electrical quality of the high-k dielectric InGaAs interface by the atomic layer deposition (ALD) of high-k materials on passivated surfaces. An additional technological issue which needs to be addressed for metal oxide semiconductor field effect transistors (MOSFETs) fabrication is the relatively high source/drain (S/D) contact resistance which results from poor dopant activation in III-V semiconductors. One proposed solution to this issue is to fabricate metal S/D Schottky-barrier MOSFET devices which requires control over the barrier height at the metal-InGaAs interface. It has recently been reported that the insertion of an ultrathin layer dielectric layer at the contact interface between the metal and the semiconductor can help in releasing the Fermi level to obtain a rectifying contact.

In this study we investigate the effectiveness of the insertion of an ultrathin ALD deposited Al₂O₃ dielectric layer on the Schottky barrier formed at the interface between the metal and the InGaAs. Schottky contacts were fabricated on 1nm and 2nm Al₂O₃ layers deposited on native oxide and sulphur passivated In_{0.53}Ga_{0.47}As for both n and p doped substrates. To investigate the dependence of Schottky barrier height (SBH) on metal work function (WF), both low (Al~4.30 eV) and high (Pt~5.65 eV) WF metals were deposited on these surface.

Rectifying behaviour was observed for the p-type substrates for the Al-InGaAs and Al/Al₂O₃/InGaAs junctions and the SBH was measured to be ~0.60eV. Ohmic behaviour was observed on the Pt-InGaAs and Pt-Al₂O₃-InGaAs junctions regardless of the dielectric thickness. The Al₂O₃/InGaAs interfacial chemistry of these surfaces was investigated with x-ray photoelectron spectroscopy and no arsenic oxide was found on the Al₂O₃-native and sulphur treated InGaAs surfaces which suggests that on the native oxide InGaAs surface, Al₂O₃ deposition resulted in the consumption of the interfacial oxide.

Ohmic behaviour was observed on the all n-type metal/InGaAs and metal/Al₂O₃/InGaAs junctions regardless of the metal WF or thickness of the dielectric layer which suggests that the Fermi level is pinned near to the top of the conduction band for these InGaAs samples.

AS-TuP26 STM Imaging and Manipulation of a Three-Metal-Center Organometallic Molecule. *N.A. Wasio, R.C. Quardokus, Y. Lu, S.A. Kandel*, University of Notre Dame

The electronic properties of a trimetallic molecule, [$\{Cp^*(dppe)Fe(C\equiv C)\}_3(1,3,5-C_6H_3)\}$ (**Fe3**), are characterized to explore potential uses of these molecules in molecular-electronic devices. Scanning tunneling microscopy (STM) at 77 K under ultra-high vacuum is used to study the adsorption of **Fe3** on the Au(111) surface. Neutral **Fe3** and mixed-valence species (**Fe3⁺** and **Fe3²⁺**) are investigated, and STM images are shown to be sensitive to the intramolecular distribution of charge. Experimental data are compared to simulated theoretical results and tip-molecule manipulation is also explored.

AS-TuP27 Development of Advanced SIMS Single Stage Accelerator Mass Spectrometer Instrument at the Naval Research Laboratory. *K. Fazel, K. Grabowski, D. Knies, G. Hubler*, Naval Research Laboratory

The Naval Research Laboratory (NRL) will be constructing a SIMS Single Stage Accelerator Mass Spectrometer (SSAMS) instrument starting at the end of 2013 for use with nuclear forensics, cosmology, and other applications. The instrument will enable analysis of both positive and negative ions, and will have a molecular destruction capability. These features will address our goal to improve sensitivity and precision of select species, broaden the range of elements and isotopes to measure, and ease sample chemical pre-processing requirements.

To provide these features, the front portion of a Cameca IMS 6f will be combined with an NEC SSAMS system. The NEC SSAMS system will include a bipolar 300-kV air insulated single stage accelerator, custom multi-port 90° high mass resolution injection magnet (ME/Z² = 2.6 amu-MeV), 90° double focusing analysis magnet (ME/Z² = 75 amu-MeV), electrostatic spherical analyzer, and a molecular ion dissociator. High-speed electrostatic switching is also included in both magnets to allow high efficiency and precision of measurements of small sample particles. The multi-port injector magnet enables nearly continuous matrix normalization over a large mass range without having to change the magnetic field of the injector. The bipolar power supply for the accelerator allows measurement of both electropositive and electronegative elements, while the molecule destruction feature minimizes molecular interferences. Access to

electropositive elements should provide improved sensitivity for rare earth elements, Uranium, and Plutonium. Before NRL can apply the instrument, the fundamentals of the instrument must be established.

The fundamentals include establishing molecular destruction cross sections of anticipated molecular ions, charge state distributions, overall transmission, and molecule fragment patterns. Upon establishing the performance characteristics of the instrument, the NRL SIMS-SSAMS will be unique tool able to better understand the constituents of an unknown material in nuclear forensics, cosmology, and other applications.

AS-TuP28 Catalytic Effect of Ni in the Gasification of Flexicoke with Water Steam. *J.C. De Jesus, I.J. Gonzalez*, PDVSA Intevep, Venezuela (Bolivarian Republic of), *E.A. Rendon*, Universidad Central de Venezuela, (Bolivarian Republic of)

In Venezuela, the hydrocarbon refining industry produces approximately 400 TPD of flexicoke, a by-product of the Flexicoking™ process, a technology that thermally transforms heavy oils to lighter more valuable products. This solid material concentrates large amounts of vanadium and nickel, and it is usually traded for power generation or metal recovery. However, the indigenous metals in this carbonaceous solid present inherently an excellent dispersion and therefore some potential for complementary catalytic applications. For solid carbonaceous feedstocks, V has been reported to enhance combustion while Ni has shown a good activity to promote gasification with steam for the generation of valuable synthesis gas. However, most conclusions have been extracted from experiences at laboratory scale with synthetic samples, and not with real world ones collected from commercial plants. In this contribution, a real flexicoke sample obtained from a refinery is lixiviated with base and acid to allow the selective removal of each metal, and the assessment of the activity of the individual elements towards the promising gasification with steam is monitored in a thermogravimetric analyzer coupled to a quadrupole mass spectrometer for evolved gas analysis. Analysis by XPS permits the correlation of surface metal composition with catalytic activity monitored during the course of the test reaction. It is shown that Ni catalytically enhances the conversion of the flexicoke to CO and H₂ at a temperature much lower than the one observed thermally both in the original sample and in the fully demetalized carbon matrix. In addition, Ni activity is inhibited in the presence of V, presumably due to the formation of a deactivating layer on top of the Ni surface and, therefore, V must be selectively removed from the original material for the catalysis to take place.

Spectroscopic Ellipsometry Focus Topic

Room: Central Hall - Session EL+TF+AS+EM+SS-TuP

Spectroscopic Ellipsometry Poster Session

EL+TF+AS+EM+SS-TuP1 Ellipsometric Characterization of Iron Pyrite (FeS₂) and Samarium Sesquisulfide (Sm₂S₃) Thin Films. *A. Sarkar, N.J. Ianno*, University of Nebraska-Lincoln, *J.R. Brewer*, Rare Earth Solar

Iron pyrite (FeS₂) and samarium sesquisulfide (Sm₂S₃) are transition metal chalcogenides characterized as absorbing semiconductors with bandgaps of 0.95 eV and 1.8 eV respectively. Synthesis of both n-type and p-type samples have been reported in the form of single crystals and thin films for both materials. As a result of these properties they have received considerable interest as photovoltaic absorber materials. We present the characterization of FeS₂ and Sm₂S₃ thin films using spectroscopic ellipsometry. FeS₂ thin films were synthesized by sulfurizing DC magnetron sputtered iron films and reactive ion sputtered iron (III) oxide films in H₂S / Ar atmosphere. Sm₂S₃ thin films were synthesized by reactive ion sputtering of Sm in an H₂S / Ar atmosphere. This analysis gives the optical properties of chalcogenide films from near-UV (300 nm) to the mid-IR (20 μm). This can then be correlated to the structural and electronic properties as well. The analysis is corroborated with results obtained from Raman spectroscopy, scanning electron microscopy, profilometry, X-ray diffraction (XRD), and Van der Pauw measurements. The ellipsometric results can be used to access different processing methods for synthesizing FeS₂ and Sm₂S₃, to determine the presence of different phases and intermediate products. This work will lay the foundation for employing *in situ* ellipsometry as a process monitor and quality control tool during manufacture of earth abundant chalcogenide thin films.

EL+TF+AS+EM+SS-TuP2 Temperature Dependence of the Dielectric Function of Germanium by Spectroscopic Ellipsometry. *A.A. Medina, L.S. Abdallah, S. Zollner*, New Mexico State University

Germanium has important applications in photovoltaics as a substrate for III/V triple-junction solar cells, especially in space vehicles and for

terrestrial concentrator-based applications. Unfortunately, the optical properties of germanium (complex refractive index and absorption coefficient) and their temperature dependence (important to consider the effects of the space environment or the radiation-induced heating in concentrators) are not as well known as for silicon, which limits the accuracy of modeling for solar cells and Ge-based optical interconnects. In this work, we report precision measurements of the complex refractive index of germanium from 0.5 to 6.6 eV at room temperature using variable-angle spectroscopic ellipsometry. To improve accuracy, especially at photon energies below 2 eV, we used a Berek waveplate compensator. By cleaning a commercial Ge wafer in isopropanol followed by deionized water, we were able to reduce the native oxide thickness to 1.3 nm. Heating the wafer in UHV at 700 K did not reduce the oxide thickness further. (The oxide thickness can be determined with precision measurements of Δ below the band gap on a single-side polished wafer.) From the ellipsometric angles of the Ge wafer measured at three angles of incidence (65, 70, and 75°), we calculated the dielectric function from 0.5 to 6.6 eV, by correcting for the effects of a native oxide.

Mounting our wafer in a compact UHV cryostat allowed temperature-dependent measurements from 80 to 700 K at 70° angle of incidence. Using similar methods as described above, we determined the dielectric function at different temperatures. We also determined the critical-point parameters (amplitude, energy, phase angle, and broadening) of the E_0 , E_1 , $E_1+\Delta_1$, E_0' , and E_2 critical points as a function of temperature. To separate the non-resonant contributions from the critical-point line shapes, we calculated the second derivative of the dielectric function with respect to photon energy and fitted the result to analytical line shapes with two-dimensional critical points. In general, our results are in good agreement with those of Viña *et al.* However, our results cover a wider spectral range and are more accurate because of the use of a compensator. Work is in progress to form thermal oxides on Ge wafers by annealing in oxygen, which will allow a multi-wafer analysis for Ge similar to work on Si by Herzinger *et al.*

This work was supported by NSF (HRD-0803171 and DMR-11104934) and the New Mexico Louis Stokes Alliance for Minority Participation.

Reference: L. Viña, S. Logothetidis, M. Cardona Phys. Rev. B **30**, 1979 (1984).

Wednesday Morning, October 31, 2012

Applied Surface Science
Room: 20 - Session AS-WeM

Surface Analysis of Biological Materials Using Vibrational & Non Linear Optical Spectroscopy Techniques (8:00-10:00 am) / 3D Imaging & Nanochemical Analysis - Part 1 (10:40 am-12:00 pm)

Moderator: R.P. Richter, CIC biomaGUNE & MPI for
Intelligent Systems, Spain, D. Roy, National Physical
Laboratory, UK, V.S. Smentkowski, General Electric Global
Research Center

8:00am AS-WeM1 Fibril Formation within the Extracellular Matrix, from Preventing Bacterial Infections to Artificial Tissue Generation, P. Koelsch, University of Washington **INVITED**

The ability to probe an interface beneath a layer of living cells *in vitro* without the need for labeling and fixation has the potential to unlock key questions in cell biology and biointerfacial phenomena. In particular fibril formation within the first steps of cell adhesion has been identified to play a key role for cell-implant interactions, for microbial biofilm formation on industrial surfaces, or for understanding basic phenomena in the context bacterial infections mediated through fibrillar assemblies. In this contribution we show how the technique of second-harmonic-generation microscopy and sum-frequency-generation spectroscopy can be utilized to detect ordered structures within tissue and at interphases between substrates and living, adherent cells. These were detected within the first steps of cell adhesion in real-time and *in vitro* with no labeling and/or fixation required.

References:

- [1] Diesner, M.-O.; Welle, A.; Kazanci, M.; Kaiser, P.; Spatz, J.; Koelsch, P., *In vitro* observation of dynamic ordering processes in the extracellular matrix of living, adherent cells. *Biointerphases* **2011**, 6, (4), 171-179.
- [2] Diesner, M. O.; Howell, C.; Kurz, V.; Verreault, D.; Koelsch, P., *In Vitro* Characterization of Surface Properties Through Living Cells. *J. Phys. Chem. Lett.* **2010**, 1, (15), 2339-2342.
- [3] Howell, C.; Diesner, M. O.; Grunze, M.; Koelsch, P., Probing the Extracellular Matrix with Sum-Frequency-Generation Spectroscopy. *Langmuir* **2008**, 24, (24), 13819-13821.

8:40am AS-WeM3 *In Situ* Monitoring of SDS Adsorption on Positively Charged Surfaces, S.-H. Song, P. Koelsch, T. Weidner, University of Washington, M.S. Wagner, The Procter & Gamble Company, D.G. Castner, University of Washington

Surfactants are important compounds used in many industrial applications, with sodium dodecyl sulfate (SDS) being one of the most widely used surfactant. This study uses vibrational sum-frequency-generation (SFG) spectroscopy and surface plasmon resonance (SPR) analysis to investigate molecular ordering and orientation within SDS films formed on positively charged surfaces. Substrates with different charge density and polarity include CaF₂ at different pH values and chemically modified CaF₂ and Au surfaces prepared by RF glow discharge plasma deposition of allylamine (AAm) films and heptylamine (HApp), respectively. SFG spectra were recorded in various spectral regions for SDS concentrations ranging from μ M to mM. At 0.2 mM SDS concentration, the intensity of CH and OH peaks decreased to background levels independently of the substrate. Previous studies have suggested that the SFG intensity minimum at 0.2 mM is due to neutralization effects of the positively charged (CaF₂) surface by the anionic charged head group of SDS.¹ In our studies, we found out that (i) the loss of SFG signal occurring at 0.2 mM is independent of surface charge density and (ii) SFG spectral intensities of lower concentrations vary significantly, whereas above 0.2 mM signals become reproducible. Therefore, in analogy to the behavior observed for alkane thiols on gold,² we interpret the loss of signal to a loss in order induced by a transition from a striped phase to a stand-up phase. As the number density of adsorbed SDS molecules increases above 0.2 mM, a second minimum in SFG intensity can be observed for all substrates, but at concentrations that are substrate dependent. Here we propose a model in which a monolayer is built up, but with opposing head group orientations (towards the substrate and the solution phase). This is supported by (i) SPR data showing a saturating number density towards SDS monolayer coverage at concentrations around the critical micelle concentration and above, (ii) a minimum for methyl vibrations related to an equal number in downward and upward orientations in the monolayer, and (iii) SFG spectral analysis for the polar SO₃⁻ band

revealed a band structure with two contributions of positive and negative phases. This can be associated to spectral shifts in close proximity to the substrate and opposing headgroup orientations (towards the substrate and the solution).

1. Becraft, K. A.; Moore, F. G.; Richmond, G. L., *Journal of Physical Chemistry B* **2003**, 107, (16), 3675-3678.
2. Schreiber, F., *Progress in Surface Science* **2000**, 65, (5-8), 151-256.

9:00am AS-WeM4 Enhanced Infrared Spectroscopy and Near-Field Microscopy with Infrared Antennas, T. Taubner, RWTH Aachen University, Germany **INVITED**

Infrared (IR) spectroscopy allows for the investigation of chemical, structural or electronic properties of a sample material by directly probing molecular, crystal lattice or charge carrier oscillations. Combined with scattering-type near-field optical microscopy (s-SNOM), which relies on the scattering of light at a sharp metallic tip, it is possible to obtain such spectroscopic information in images with strongly subwavelength spatial resolution [1-4] of typically about 20-30 nm. Currently, the main limitation of this technique comprises of the low signals that demand tunable laser sources and restrict the spectral range of operation.

Recently, new broadband IR light sources enabled s-SNOM near-field spectroscopy on different polar crystals [5], semiconductor nanostructures [6] as well as biominerals [7]. The majority of these experiments has been performed on samples which provide a resonant optical interaction between the sample and the probing tip, thus resulting in comparably strong signals. For the detection of weak molecular vibrations like polymers and proteins however, the SNOM signals either have to be enhanced or stronger IR light sources have to be developed.

Here we present a way to enhance the near-field probing process by suitable substrates [8], increasing both signals and contrasts in infrared s-SNOM when probing thin sample layers. In a next step, we investigate the use of resonant nanostructures ("infrared antennas", [9,10]) to enhance s-SNOM sensitivity even further. Additionally, we compare enhanced near-field spectra with the corresponding far-field spectra obtained by diffraction-limited FTIR-Microscopy. We will also present our latest results obtained with a new powerful broadband IR laser source that is currently developed at the Fraunhofer ILT.

References

- [1] T. Taubner, R. Hillenbrand, F. Keilmann, *APL* **85**, 5064 (2004).
- [2] R. Hillenbrand, T. Taubner, F. Keilmann, *Nature* **418**, 159 (2002).
- [3] A. Huber et al., *Nano Letters* **7**, 774 (2006).
- [4] B. Knoll, F. Keilmann, *Applied Physics Letters* **77**, 3980 (2000).
- [5] S. Amarie, T. Ganz & F. Keilmann, *Optics Express* **17**, 21794 (2009).
- [6] F. Huth et al., *Nature Materials* **10**, 352 (2011).
- [7] S. Amarie et al., *Beilstein J. Nanotechnol.* **3**, 312 (2012).
- [8] J. Aizpurua et al., *Optics Express* **16**, 1529 (2008).
- [9] F. Neubrech et al., *Physical Review Letters* **101**, 157403 (2008).
- [10] R. Adato et al., *PNAS* **106**, 19227 (2009).

9:40am AS-WeM6 FT-IR Spectrochemical Imaging: Applications with Focal Plane Array and Multiple Beam Synchrotron Radiation Source, M. Unger, E. Mattson, J. Sedlmaier, Z. Alavi, R. Dsouza, B. Manandar, C. Hirschmugl, University of Wisconsin Milwaukee

FT-IR spectrochemical imaging, which combines the chemical specificity of mid-infrared spectroscopy with spatial specificity, is an important demonstration of label-free molecular imaging. Mid-infrared optical frequencies are resonant with the vibrational frequencies of functional groups, thus an absorption spectrum is a "molecular fingerprint" of the material at every pixel. Each spectrum can be correlated with known material properties to extract chemical information. Synchrotron based FT-IR spectrochemical imaging, as recently implemented at the Synchrotron Radiation Center in Stoughton, WI, demonstrates the new capability to achieve diffraction limited chemical imaging across the entire mid-infrared region, simultaneously, with high signal to noise ratio.

IRENI [1] (Infrared Environmental Imaging) extracts a large swath of radiation ($320 \text{ hor.} \times 25 \text{ vert. mrad}^2$) to homogeneously illuminate a commercial IR microscope equipped with an infrared Focal Plane Array (FPA) detector. Wide field images are collected. IRENI rapidly generates high quality, high spatial resolution data. The relevant advantages (spatial oversampling, speed, sensitivity and signal to noise ratio) will be presented and demonstrated using examples from a variety of disciplines, including

formalin fixed [1] and flash frozen tissue samples [2], live cells, fixed cells, paint cross sections and polymer fibers will be presented.

* This work has been done with support from NSF (MRI-DMR-0619759 and CHE-1112433) and the Synchrotron Radiation Center, which is also supported by NSF (DMR-0537588) and UW-Milwaukee and UW-Madison.

[1] M.J. Nasse, et al. "High resolution Fourier-transform infrared chemical imaging with multiple synchrotron beams", *Nature Methods*, 8, (2011) 413-416

[2] M.Z. Kastyak-Ibrahim, et al. "Biochemical label-free tissue imaging with subcellular resolution synchrotron FTIR with Focal Plane Array Detector," *NeuroImage* 60, (2012) 376-383.

10:40am **AS-WeM9 3D Analysis using X-ray Computed Tomography, S.R. Stock**, Northwestern University **INVITED**

X-ray Computed Tomography (CT) can be performed on meter-sized objects or micrometer wide samples, and introduction of commercial x-ray tube-based instruments and dedicated synchrotron systems has produced an explosion of studies spanning the sciences and engineering disciplines. Using one of several numerical reconstruction methods, CT combines x-ray projections (radiographs) into a cross-sectional map, generally in 3D, of the x-ray absorption of the specimen. Other modalities (x-ray phase contrast, scattering, etc.) can also be used for reconstruction. The noninvasive interrogation allows the specimen to be studied multiple times during its evolution or to be returned undamaged to the museum collection.

This talk briefly introduces the fundamentals of x-ray CT and the different approaches to data acquisition and reconstruction. Most of the examples will focus on microCT, that is, reconstructions with isotropic volume elements (voxels) from 1-50 micrometers on edge. The first example is quantification of crack opening in a metal sample as a function of 3D position and applied load. In the second example, microCT data forms the basis of finite elements (FE) modeling of response of a spine of the sea urchin *Diadema setosum* to different applied loads. The third example illustrates local tomography, where data for high resolution reconstruction is only collected over a portion of the sample cross-section. Differences in x-ray phase contrast instead of x-ray absorption can be used as the basis for reconstruction; and the examples show how differences in polymers and soft tissues can be imaged using this approach. Intensity diffracted from the different phases within a specimen provide the basis for reconstructing the distribution of crystallographic phases; one example is SiC fibers in an Al matrix.

11:20am **AS-WeM11 High Spatial Resolution 2D and 3D TOF-SIMS Analysis using Cluster Ion Beams, F. Kollmer, S. Kayser**, ION-TOF GmbH, Germany, *N. Havercroft*, ION-TOF USA, Inc., *D. Rading, R. Moellers, W. Paul, E. Niehuis*, ION-TOF GmbH, Germany

Time-of-flight secondary ion mass spectrometry (TOF-SIMS) is a very sensitive surface analytical technique. It provides detailed elemental and molecular information about surfaces, thin layers, interfaces and full three-dimensional analysis of a sample. A major improvement especially for the analysis of molecular surfaces on a small scale has been the introduction of cluster ion beams that increases the sensitivity by orders of magnitude [1].

In recent years Bi clusters have become a standard primary ion species for all TOF-SIMS imaging applications providing a lateral resolution of down to 80 nm. Recent developments allow pushing the performance further towards the physical limits of the technique. Under optimized conditions we will present a lateral resolution of less than 20 nm by applying Bi₃ clusters on a certified reference material [2] and real world samples.

Usually for TOF-SIMS depth profiling and 3D-analysis, a dual beam approach is accomplished with dedicated analysis and sputter beams. However, the analysis of structures at greater depth (> 10 μm) needs long sputter times and the build-up of surface roughness at the crater bottom limits the achievable spatial resolution. In order to overcome these limitations we used a combined SIMS/FIB setup for the analysis of inorganic samples. Hereby, the Bi cluster beam is used to FIB mill a crater into a sample and the vertical crater wall is subsequently analysed by TOF-SIMS. We will present 2D and 3D data of reference samples, as well as, real world samples analysed by this approach.

The challenge of three dimensional analysis of molecular surfaces is to maintain the molecular structure of the exposed surface while removing the covering material. In this respect the development of new sputter ion sources using massive Ar clusters allows the preservation of molecular information under high dose sputtering [3]. This has enabled TOF-SIMS to do depth profiling and 3D analysis of organic materials. In our contribution we will present 3D analysis of an OLED display device using an Ar gas cluster ion beam for sputtering in combination with a Bi cluster beam for analysis.

[1] F. Kollmer, *Appl. Surf. Sci.* 231-232, **2004**, 153-158

[2] M. Senoner, W. E. S. Unger, *Surf. Interface Anal.* 39, **2007**, 16-25

[3] S. Ninomiya, K. Ichiki, H. Yamada, Y. Nakata, T. Seki, T. Aoki, J. Matsuo, *Rapid Communications in Mass Spectrometry* **2009**, 23, 1601-1606

11:40am **AS-WeM12 An Evolution of TOF-SIMS for Biological Analysis: From 2D Imaging to 3D FIB-TOF Tomography, G.L. Fisher, J.S. Hammond, S.R. Bryan**, Physical Electronics

TOF-SIMS has become an important tool for 2D and 3D imaging mass spectrometry of biological and complex material specimens due to its unique capability to detect molecular and elemental ions at a spatial resolution of ≤ 300 nm, a mass resolution of ~ 15,000 m/Am, and without the sample treatments or labeling required by e.g. MALDI or fluorescence microscopy. Among the advantages of TOF-SIMS are ~ 2 nm sampling depth, parallel detection and collection of the entire mass spectrum at every image pixel, and sensitivities in the ppm to ppb range. The ability to image surfaces having a large degree of topography while maintaining artifact-free chemical imaging is also highly desired; the resulting elemental and molecular images provide important information regarding the composition of biointerfaces, tissues and cells, and of materials such as oxide fuel cells and OLEDs.

Characterization of specimens to a depth of several microns below the sample surface has become somewhat routine with the use of a sputter ion beam to remove multiple layers of atoms and molecules between analysis (chemical imaging) cycles. Nevertheless, there are practical limitations to the use of ion beam sputtering for probing both organic and inorganic specimens beyond the surface region. Among the difficulties and limitations is the fact that the various matrix components sputter at different rates, called preferential or differential sputtering, which results in a distortion or complete loss of the true 3D chemical distribution as a function of depth. Many specimens also contain void spaces that are impossible to preserve in 3D images obtained by sputter depth profiling.

An alternative approach to achieve 3D chemical imaging of chemically complex specimens is to utilize *in situ* FIB milling and sectioning in conjunction with TOF-SIMS chemical imaging... what we have called FIB-TOF tomography. With FIB milling, the interior of a specimen is revealed to depths of more than 100 μm. 3D chemical imaging with a z-dimension of greater than 10 μm in tomographic increments of ≤ 0.5 μm may be achieved within a reasonable analysis time. The advantage of the FIB-TOF approach is that artifacts caused by sputter depth profiling such as differential sputtering and accumulated ion beam damage are avoided. 3D imaging by FIB-TOF tomography will be illustrated first with organic / inorganic composite materials. Applications in biological and clinical cancer research will also be presented with an emphasis on the conditions required to achieve FIB-TOF tomography.

Graphene and Related Materials Focus Topic
Room: 13 - Session GR+AS+BI+PS+SS-WeM

Graphene Surface Chemistry, Functionalization, Biological and Sensor Applications

Moderator: D.K. Gaskill, U.S. Naval Research Laboratory

8:00am **GR+AS+BI+PS+SS-WeM1 Structural Analysis of Chemically Functionalized Epitaxial Graphene with High-Resolution X-ray Reflectivity, J.D. Emery, Q.H. Wang, M. Zarrouati**, Northwestern University, *P. Fenter*, Argonne National Laboratory, *M.C. Hersam, M.J. Bedzyk*, Northwestern University

For graphene to realize its potential in next-generation electronics it must be incorporated with a variety of materials to form devices. Recently, the use of self-assembled organic monolayers deposited on epitaxial graphene (prepared by graphitization of the 6H-SiC(0001) surface) has been effective in the functionalization of the bare graphene sheet, enabling the additional chemistry necessary for device fabrication. In this work, we present high-resolution X-ray Reflectivity (XRR) studies of perylene-3,4,9,10-tetracarboxylic dianhydride (PTCDA) on epitaxial graphene. Initially, a model-independent vertical electron density profile of the graphene/silicon carbide interface is retrieved with the use of Feinup-based error correction algorithms in order to minimize ambiguities that can arise from model-based methods. This retrieved structure is then used as the foundation for model-based analysis, from which the final structures are extracted. A series of structures comprising 0, 1, and 2MLs of PTCDA deposited on 1-2ML graphene are discussed. The interlayer spacing between the PTCDA and top graphene layer are revealed to be approximately 0.35 nm, which supports the view that the PTCDA molecules are interacting only weakly (van der Waals) with the graphene layer. In addition to the characterization of PTCDA-functionalized graphene, we will also demonstrate the efficacy of

these molecules to form a weakly-interacting seeding layer for subsequent growth of high-k dielectrics via atomic layer deposition.

8:20am **GR+AS+BI+PS+SS-WeM2 In Situ FT-IR Study of Graphene Fluorination using XeF₂**, *J.-F. Veyan, N. Shafiq*, University of Texas at Dallas, *K. Novoselov*, University of Manchester, UK, *Y.J. Chabal*, University of Texas at Dallas

Graphene fluorination to obtain fluorographene has been successfully realized by exposing graphene flakes to molecular Xenon-Difluoride¹⁻³. To gain a mechanistic understanding of XeF₂ reaction with the graphene flakes, an all-aluminum custom-made two-stage reaction cell has been designed to fit into the main sample compartment of an FTIR Nicolet 6700 interferometer, for *in situ* infrared absorption spectroscopy. The first stage is a clean expansion chamber to isolate the pure XeF₂ in its gas phase, from solid XeF₂ (powder) stored in a storage vessel. The XeF₂ vapor is extracted by opening the valve V1 to the storage chamber and its pressure (up to ~4 Torr) is controlled by the valve V2. The second stage is a reactor equipped with two KBr windows, allowing the IR beam to penetrate and exit the enclosure. A pneumatic valve allows the transfer of gaseous XeF₂ from stage 1 into stage 2. Pressures in both storage and reactor chambers are measured with Baratron gauges (Ga1, Ga2). To avoid any contamination of the reactor and sample holders during sample preparation and loading, a N₂-purged glove bag is placed over the reactor to maintain a controlled environment. The graphene flakes in suspension in a NMP (N-Methylpyrrolidone) solution, are transferred onto three mechanically polished Aluminum plates at a temperature of 70°C. The plates are then mounted on the specially designed 3-reflection sample holder flange designed to fit stage 2.

By varying the sample temperature from 20 to 200°C as well as the XeF₂ pressure in the reactor stage from 0.1 to 4 Torr, the chemical attachment of fluorine on graphene is identified from a comprehensive FT-IR study performed under industrial conditions. Fluorine attached out of plane can be easily differentiated from fluorine attached at edges (i.e. remaining within the basal plane) and terminating the edge atoms.

¹ R. R. Nair, et al., *Small* **6**, 2877 (2010).

² J. T. Robinson, et al., *Nano Letters* **10**, 3001 (2010).

³ K.-J. Jeon, et al., *Acs Nano* **5**, 1042 (2011).

8:40am **GR+AS+BI+PS+SS-WeM3 Molecularly Resolved Chemical Functionalization of Graphene**, *M.C. Hersam*, Northwestern University
INVITED

Graphene has emerged as one of the leading materials in condensed matter physics due to its superlative electrical and mechanical properties. With an eye towards expanding its functionality and applications, this talk will highlight our latest efforts to tailor the surface chemistry of graphene [1]. At the molecular scale, we employ ultra-high vacuum (UHV) scanning tunneling microscopy (STM) and conductive atomic force microscopy (cAFM) to characterize chemically modified epitaxial graphene on SiC(0001) [2,3]. For example, a suite of perylene-based molecules form highly ordered self-assembled monolayers (SAMs) on graphene via gas-phase deposition in UHV [4,5]. Due to their noncovalent bonding, these SAMs preserve the superlative electronic properties of the underlying graphene while providing uniform and tailorable chemical functionality [6]. In this manner, disparate materials (e.g., high-*k* gate dielectrics) can be seamlessly integrated with graphene, thus enabling the fabrication of capacitors, transistors, and related electronic/excitonic devices [7]. Alternatively, via aryl diazonium chemistry, functional polymers can be covalently grafted to graphene [8], while exposure to atomic oxygen in UHV enables chemically homogeneous and thermally reversible covalent epoxy functionalization [9]. Beyond UHV STM characterization, this talk will also delineate our most recent efforts to exploit chemically modified graphene in technologically significant applications including photovoltaics [10], transparent conductors [11-13], flexible GHz transistors [14], *in vivo* biomedical applications [15,16], and photocatalysts [17].

[1] Q. H. Wang and M. C. Hersam, *MRS Bull.*, **36**, 532 (2011).

[2] J. A. Kellar et al., *Appl. Phys. Lett.*, **96**, 143103 (2010).

[3] J. M. P. Alaboson et al., *Adv. Mater.*, **23**, 2181 (2011).

[4] Q. H. Wang and M. C. Hersam, *Nature Chemistry*, **1**, 206 (2009).

[5] Q. H. Wang and M. C. Hersam, *Nano Lett.*, **11**, 589 (2011).

[6] J. D. Emery et al., *Surf. Sci.*, **605**, 1685 (2011).

[7] J. M. P. Alaboson, et al., *ACS Nano*, **5**, 5223 (2011).

[8] Md. Z. Hossain et al., *J. Am. Chem. Soc.*, **132**, 15399 (2010).

[9] Md. Z. Hossain et al., *Nature Chemistry*, **4**, 305 (2012).

[10] I. P. Murray et al., *J. Phys. Chem. Lett.*, **2**, 3006 (2011).

[11] A. A. Green and M. C. Hersam, *J. Phys. Chem. Lett.*, **1**, 544 (2010).

[12] A. A. Green and M. C. Hersam, *Nano Lett.*, **9**, 4031 (2009).

[13] Y. T. Liang and M. C. Hersam, *J. Am. Chem. Soc.*, **132**, 17661 (2010).

[14] C. Sire et al., *Nano Lett.*, **12**, 1184 (2012).

[15] M. C. Duch et al., *Nano Lett.*, **11**, 5201 (2011).

[16] J.-W. T. Seo et al., *J. Phys. Chem. Lett.*, **2**, 1004 (2011).

[17] Y. T. Liang et al., *Nano Lett.*, **11**, 2865 (2011).

9:40am **GR+AS+BI+PS+SS-WeM6 Structure of a Peptide Adsorbed on Graphene and Graphite**, *J. Katoch*, University of Central Florida, *S.N. Kim, Z. Kuang, B.L. Farmer, R.R. Naik*, Air Force Research Laboratory, *S.A. Tatulian, M. Ishigami*, University of Central Florida

Non-covalent functionalization of graphene using peptides is a promising method for producing novel sensors with high sensitivity and selectivity. We have performed atomic force microscopy, Raman spectroscopy, infrared spectroscopy and molecular dynamics simulations to investigate peptide-binding behavior to graphene and graphite. We studied a dodecamer peptide, GAMHLPWHMGTL, identified by phage display to possess affinity for graphite.

Optical spectroscopy reveals that the peptide forms secondary structures both in powder form and in an aqueous medium. The dominant structure in the powder form is α -helix, which undergoes a transition to a distorted helical structure in aqueous solution. The peptide forms a complex reticular structure upon adsorption on graphene and graphite, having a helical conformation different from α -helix due to its interaction with the surface. Our observation is consistent with our molecular dynamics calculations and our study paves way for rational functionalization of graphene using biomolecules with defined structures and, therefore, functionalities. Our results have recently been published [1].

[1] J. Katoch, S.N. Kim, Z. Kuang, B. L. Farmer, R. R. Naik, S. A. Tatulian, and M. Ishigami, dx.doi.org/10.1021/nl300286k, *Nano Letters* (2012).

10:40am **GR+AS+BI+PS+SS-WeM9 Controlling the Spatial Distribution of Graphene Chemistry**, *S.C. Hernández, E.H. Lock, S.G. Walton, C.J. Bennett, R. Stine, P.E. Sheehan, F.J. Bezares, L.O. Nyakiti, R.L. Myers-Ward, J.T. Robinson, J.D. Caldwell, C.R. Eddy, Jr., D.K. Gaskill*, Naval Research Laboratory

Graphene has attracted a widespread of interest because of its unique structural and electronic properties however, manipulation of these properties is necessary before realizing its full potential as the next generation material in a broad range of applications. Precise control of the surface chemistry of graphene can allow for subsequent surface procedures both for device fabrication (i.e. atomic layer deposition) and sensor applications. Chemical composition strongly impacts the electronic properties as well as chemical reactivity, both globally and locally. Electron-beam generated plasmas are capable of imparting a variety of functional group types over a range of coverages with minimal damage to the carbon backbone because of their inherently low ion energies and as such offer a unique approach for large area uniform processing of graphene films with controlled surface chemistry. The ability to manipulate the surface chemistry of this atomically thin material coupled with the capability to regulate the spatial distribution of functional will be discussed. Plasma processing conditions and characteristics, as well as the resulting chemical, structural, and electrical properties of the functionalized graphene will be demonstrated. This work is supported by the Naval Research Laboratory base program.

11:00am **GR+AS+BI+PS+SS-WeM10 Coverage-dependent Ordering of Adsorbed Iron Phthalocyanine on Epitaxial Graphene Grown on SiC(0001)-Si**, *A.A. Sandin, D.B. Dougherty, J.E. Rowe*, North Carolina State University

The crystallographic and electronic structure of monolayer and sub-monolayer Iron-Phthalocyanine (FePc) films are experimentally studied on graphene grown on SiC(0001) using Scanning Tunneling Microscopy and Spectroscopy (STM and STS) as well as Low Energy Electron Diffraction (LEED). At full monolayer coverage of FePc the STM images show that a nearly square overlayer lattice forms with flat-lying molecules and a densely-packed structure oriented 10° relative to the graphene principle lattice directions. This close-packed structure appears to be the same as that previously reported for FePc on graphite surfaces. For sub-monolayer coverage at room temperature, our STM images suggest that FePc forms a unique 2D molecular gas with images that have the hexagonal symmetry of the graphene honeycomb lattice. This is interpreted as suggesting that only a small diffusion barrier exists for molecular motion between neighboring sites in the 3-fold symmetry of the sub-monolayer overlayer lattice. The sub-monolayer gas condenses into islands at liquid Nitrogen temperatures with bare graphene regions and this implies that a weak attractive interaction exists between FePc molecules causing the close-packed

ordering. Near defects in the graphene lattice we observe ring-like structures at room temperature that suggest an increased residence time of the mobile 2-D gas of FePc molecules. Our results using Scanning Tunneling Spectroscopy suggest the possibility of a hybrid molecule-graphene state in the unoccupied density of both states near the Fermi level which could possibly be useful in modifying the charge injection into graphene in future devices.

11:20am **GR+AS+BI+PS+SS-WeM11 A Molecular Route to Carbon Nanomembranes, Graphene and Their Hybrids with Tailored Physical and Chemical Properties**, A. Turchanin, University of Bielefeld, Germany **INVITED**

Bottom-up approaches via molecular self-assembly have high potential to facilitate the applications of two-dimensional (2D) carbon materials in nanotechnology. In this talk it will be demonstrated how self-assembled monolayers (SAMs) of aromatic molecules can be employed to this end. These monolayers are converted into *carbon nanomembranes* (CNMs) with a thickness of one molecule by electron or photon irradiation. CNMs can be separated from their original substrates and transferred onto various other substrates, fabricated as suspended nanomembranes or stacked into multilayer films with precise control over their thickness and composition. They possess two chemically distinct faces, which can be used for their selective functionalization, opening broad avenues for the engineering of novel materials with tailored on demand properties. High temperature annealing induces the transformation of CNMs into *graphene*, which allows large-area fabrication of the homogenous sheets with tunable electrical, optical and chemical properties. Integration of graphene sheets with CNMs into novel hybrids presents a promising route to flexibly functionalize graphene for applications as optical, electrical, chemical and biofunctional coating in nanoelectronics and sensors. Various physical and chemical properties of these novel materials, their nanopatterning and functional applications will be presented.

- 1) A. Turchanin and A. Götzhäuser, *Prog. Surf. Sci.* (2012) in press.
- 2) A. Turchanin, D. Weber, M. Büenfeld, C. Kieselowski, M. Fistul, K. Eftov, R. Stosch, T. Weimann, J. Mayer, A. Götzhäuser, *ACS Nano* 5 (2011) 3896-3904.
- 3) C.T. Nottbohm, A. Turchanin, A. Beyer, R. Stosch, A. Götzhäuser, *Small* 7 (2011) 874-883.
- 4) Z. Zheng, C.T. Nottbohm, A. Turchanin, H. Muzik, A. Beyer, M. Heilemann, M. Sauer, A. Götzhäuser, *Angew. Chem. Int. Ed.* 49 (2010) 8493-8497.
- 5) A. Turchanin, A. Beyer, C.T. Nottbohm, X. H. Zhang, R. Stosch, A. Sologubenko, J. Mayer, P. Hinze, T. Weimann, A. Götzhäuser, *Adv. Mater.* 21, 1233-1237 (2009).

In Situ Microscopy and Spectroscopy Focus Topic Room: 7 - Session IS+AS+OX+ET-WeM

In Situ Characterization of Solids: Film Growth, Defects, and Interfaces

Moderator: P.W. Sutter, Brookhaven National Laboratory

8:00am **IS+AS+OX+ET-WeM1 Revealing Gas-Surface Radical Reaction Mechanisms of Self-Assembled Monolayers by Scanning Tunneling Microscopy**, D.Y. Lee, M.M. Jobbins, S.A. Kandel, University of Notre Dame

Scanning Tunneling Microscopy (STM) in ultra-high-vacuum is used *in situ* to investigate the surface changes of the octanethiolate self-assembled monolayer (SAM) on Au(111) upon reaction with atomic hydrogen and with atomic chlorine. For both reactions, the surface structure heavily influences the rate of monolayer degradation, but the effect of surface defects on reactivity is completely opposite when comparing the two systems. Monolayer reactivity increases with increasing hydrogen-atom exposure while decreases with further reaction with atomic chlorine. The monolayer-versus-exposure data are examined by kinetic Monte Carlo simulations and reveal that, for H-atom exposure, molecules located near surface defect sites are potentially over 500 times more reactive than close-packed areas. For Cl-atom interactions, however, the opposite occurs: close-packed regions are at least 100 times more reactive than defect sites. These observations result directly from the alkyl hydrogen abstraction and sulfur-gold bond cleavage mechanisms of SAM upon gas-phase radical bombardment.

8:20am **IS+AS+OX+ET-WeM2 In Situ Imaging of the Nucleation and Growth of Epitaxial Anatase TiO₂(001) Films on SrTiO₃(001)**, Y.G. Du, D.J. Kim, T.C. Kaspar, Pacific Northwest National Laboratory, S.E. Chamberlin, University of Wisconsin Milwaukee, I. Lyubnitsky, S.A. Chambers, Pacific Northwest National Laboratory

TiO₂ has attracted much attention because of its potential utility in hydrogen production via water splitting, environmental remediation, and dye-sensitized solar cell fabrication. Heteroepitaxial growth of anatase is a powerful and unique way to fabricate model surfaces of the less stable anatase polymorph for fundamental surface science studies. In this work, the growth of TiO₂ anatase films on Nb doped SrTiO₃(001) by molecular beam epitaxy has been studied *in-situ* by scanning tunneling microscopy. We show that the initial growth follows the Stranski-Krastanov mode, where islands form on top of a wetting layer consisting of two monolayers (ML) of TiO₂. Well-defined (4x1) and (1x4) terraces are observed for film thicknesses in excess of 3 nm. At larger film thicknesses, large oriented crystallites form as a result of the coalescence of smaller islands. Within a given crystallite, either (4x1) or (1x4) reconstructed terraces account for majority of the surface. The anatase grows in units of bilayers, resulting in a step height of 2 ML. This result explains the fact that the measured period of the RHEED specular-beam intensity oscillations corresponds to the time required for deposition of 2 ML. Ar ion sputtering and UHV annealing results in a transformation to coexisting (4x1) and (1x4) reconstructed terraces on individual crystallites, as commonly observed by *ex-situ* STM studies. In addition, we show that the nucleation and growth of anatase films are influenced by Nb doping in the SrTiO₃ substrates by comparing with similar growth occurring on pure SrTiO₃ substrates.

8:40am **IS+AS+OX+ET-WeM3 In Situ Synchrotron X-Ray Studies of Epitaxial Oxide Thin Film Synthesis Behavior**, J.A. Eastman, M.J. Highland, P.H. Fuoss, Argonne National Laboratory, T.M. McCleskey, Los Alamos National Laboratory, D.D. Fong, C.M. Folkman, S.K. Keun, E. Perret, P.M. Baldo, Argonne National Laboratory, E. Bauer, Q. Jia, Los Alamos National Laboratory **INVITED**

Intense interest is focused on the growth science of epitaxial oxide thin films because of continuing discoveries of new interesting and important properties. The key to achieving desired maximum functionality of oxide heterostructures is the ability to synthesize high-quality films with full control of factors such as composition, crystallographic orientation, surface termination, and strain state. Many of the most promising thin film synthesis techniques involve non-vacuum, high-temperature environmental conditions that are difficult or impossible to probe using standard spectroscopic or structural probes. However, the use of high-energy x-rays available at synchrotron sources such as the Advanced Photon Source (APS) provides an opportunity to obtain real-time atomic-level structural and chemical information during synthesis. This talk will describe results from recent studies at APS Sector 12ID-D using an *in-situ* x-ray approach to understand and control the synthesis behavior of complex oxide epitaxial thin films prepared by two very different techniques: sputter deposition or polymer assisted deposition (PAD).

We recently built a new RF magnetron sputter deposition system at the APS, which brings to bear state-of-the-art real-time *in-situ* x-ray scattering and spectroscopy techniques to provide insight into the growth behavior of epitaxial oxide thin film heterostructures. Initial studies of the growth behavior of epitaxial films such as (001) LaGaO₃, SrZrO₄, and LaGaO₃/SrZrO₃ multilayer heterostructures during off-axis sputtering will be described, focusing on the effects of epitaxial strain and electrical compensation (e.g., surface polarity) on growth behavior.

PAD is a solution technique capable of synthesizing dense epitaxial thin films. Past work at Los Alamos has demonstrated that PAD can be used to prepare aligned epitaxial films of many different materials. We recently performed initial *in-situ* synchrotron x-ray experiments aimed at obtaining a fundamental understanding of the nucleation and growth processes associated with epitaxial film formation. Studies of the synthesis behavior of (001) BaTiO₃ epitaxial films will be described in this talk, focusing on the effects of thermal history and choice of substrate material on crystallization behavior and the development of epitaxy.

Argonne researchers were supported by the U. S. Department of Energy (DOE), Basic Energy Sciences (BES), Materials Sciences and Engineering Division. Los Alamos researchers were supported by the DOE through the LANL/LDRD Program. Use of the APS was supported by BES, under Contract DE-AC02-06CH11357 between UChicago Argonne LLC and the Department of Energy.

9:40am **IS+AS+OX+ET-WeM6 Understanding the Dynamic Electronic Properties of Electrode Materials by *In Situ* X-ray Absorption Spectroscopy**, *M. Bagge-Hansen, J.R.I. Lee, A. Wittstock, M.D. Merrill, M.A. Worsley, T. Ogitsu, B.C. Wood, T. Baumann, M. Stadermann, M. Biener, J. Biener, T. van Buuren*, Lawrence Livermore National Laboratory

In situ characterization of the evolution in electronic structure of electrode materials during repeated charge-discharge cycling is fundamentally important for more fully understanding the processes of charge storage and degradation, which, in turn, is essential for the development of new electrical energy storage (EES) materials with tailored properties and improved performance. X-ray spectroscopies provide ideal tools with which to obtain enhanced insight into the origins of electrode behavior in EES systems due to their capabilities for direct, element specific, characterization of the electronic densities of states. To date, in situ studies of EES materials have primarily focused on hard x-ray experiments due to the challenges associated with UHV compatibility and high photon attenuation of cells for soft x-ray measurements. Nonetheless, the use of soft x-ray spectroscopies to EES systems is vital since they provide complementary information that cannot be obtained via hard x-ray studies. We report the development of a cell for in situ soft x-ray emission spectroscopy and x-ray absorption spectroscopy studies of EES materials and will discuss experiments focused upon the x-ray spectroscopy characterization of a series of novel electrode materials. Prepared by LLNL under Contract DE-AC52-07NA27344.

10:40am **IS+AS+OX+ET-WeM9 *In Situ* Studies of Al₂O₃ ALD Growth and Self-cleaning on III-V Surfaces by STM and XPS**, *L.N.J. Rodriguez, A. De Clercq*, IMEC, Belgium, *M. Tallarida*, BTU Cottbus, Germany, *D. Cuyppers*, IMEC, Belgium, *J.P. Locquet*, KU Leuven, Belgium, *S. Van Elshocht*, *C. Adelman*, *M. Caymax*, IMEC, Belgium

A custom built ALD UHV-compatible reactor has been used to study the growth of TMA on InP and InAlAs by STM in conjunction with additional studies performed in a reactor attached to a synchrotron XPS. The effects of selected ex-situ cleans has been measured along with the subsequent cycles of ALD growth from TMA and water. The STM data shows morphological differences between the ex-situ cleans on InP, with sulphuric acid cleans yielding plateaus but ammonium sulphide cleans yielding rough surfaces. In-situ measurements of these surfaces after TMA dosing shows the growth of islands which converge to film closure after ten cycles of ALD growth. In-situ measurements of the I-V curves by STS allowed the creation of bandgap maps of the III-V interfaces after TMA dosing. These bandgap maps showed a non-uniform distribution with regions of either higher or lower bandgap. The mean bandgap was seen to decrease with increasing numbers of ALD cycles. In-situ XPS data on similar systems showed a reduction in surface oxides for InAlAs but not for InP. The reduction of arsenic oxides with a creation of metallic arsenic, along partial reduction of indium oxides and a conversion of aluminium sub-oxides to aluminium oxide was seen in the former case. In the latter case, a formal oxidation of the phosphorus was seen with increased TMA dosing instead of a self-cleaning effect.

11:00am **IS+AS+OX+ET-WeM10 *In Situ* Transport Measurement of Kinetically Controlled Bi Atomic Layers**, *Y. Fujikawa, E. Saitoh*, Tohoku University, Japan

Thin film growth of Bi and related compounds has been attracted much attention because of their exotic properties originating in the large spin-orbit interaction of Bi. Growth of its simple substance is known to result in the formation of a thin-film phase in the initial stage, which is taken over by the bulk growth when the coverage exceeds several monolayers (ML). [1] With typical growth conditions, this transition takes place before the completion of the thin-film layer, which tends to agglomerate to form 4-ML thick islands, making it difficult to measure the intrinsic property of the thin-film phase. In this work, Bi growth on Si(111)-7x7 has been performed in a multi-probe VT-STM system, which provides wide-ranging opportunity of kinetic control and *in-situ* transport measurement during the thin film growth. By tuning the kinetic condition of the growth, it becomes possible to grow the thin-film phase uniformly covering the substrate. Its conductivity, monotonically increasing with the increase of the temperature, would suggest the variable-range hopping conduction rather than the carrier excitation of semiconductors. *In-situ* transport measurement has been performed during the layer-by-layer growth of the Bi thin-film phase, distinguishing the conductivity of each growth unit. It fluctuates with periods of 2 and 4 ML, which may reflect the atomic structure of the thin-film phase.

[1] Nagao *et al.*, Phys. Rev. Lett. **93**, 105501 (2004).

11:20am **IS+AS+OX+ET-WeM11 CAMECA IMS Series Advanced Ion Microscopy: High Throughput, Repeatability & Automation**, *P. Peres, F. Desse, F. Hillion, M. Schuhmacher*, Cameca, S.a., France, *A.N. Davis*, CAMECA Instruments, Inc.

The advantage of CAMECA IMS Series high performance secondary ion mass spectrometers are well established: extreme sensitivity, high mass resolution, and high dynamic range, providing low detection limits while keeping high analysis throughput. This instrument delivers high analytical performance for a wide range of applications: Si based devices, III-V and II-VI devices, both bulk materials and thin-film technology, as well as for different material science applications.

In order to meet the growing demand in terms of reproducibility and throughput performance as well as ease of use, CAMECA has developed a new IMS series, 7f-Auto.

The primary column has been redesigned in order to provide an easier and faster primary beam tuning. For high efficiency operation, automated routines for tuning the instrument are added for both primary and secondary columns, nominally: aperture adjustment, secondary ion beam centering, detector adjustment, among others. These routines not only increase the ease of use, but also enhance the reproducibility of the instruments by minimizing operator-related biases.

A motorized storage chamber has also been developed allowing to keep, under UHV environment, up to six sample holders. The holder exchange between the storage chamber and analysis chamber is fully motorized and computer controlled, allowing a set of analyses to be performed in automated, unattended mode on multiple sample holders. This significantly improves the throughput of the tool, since up to 24 samples (assuming 4 samples per holder) can be analysed in chained mode, possibly overnight. These developments will be presented and discussed in detail.

Nanometer-scale Science and Technology Room: 12 - Session NS+AS+SS+SP-WeM

Nanoscale Catalysis and Surface Chemistry Moderator: U.D. Schwarz, Yale University

8:20am **NS+AS+SS+SP-WeM2 Preparation and Performance of Solid Rocket Propellant Containing *In Situ*-Synthesized Nanoparticle Catalysts and Fuels**, *D. Reid, R. Draper*, University of Central Florida, *M. Johnson, T. Allen, A. Demko, E. Petersen*, Texas A&M University, *S.S. Seal*, University of Central Florida

Energetic nanocomposites have the potential to substantially increase the performance of rocket propulsion systems, but adoption outside the laboratory has been slow, largely due to manufacturing difficulties, safety challenges, and performance that falls short of theoretical potentials. In this study, we explore some novel synthesis methods to significantly improve performance and alleviate the difficulties of incorporating nanoparticles into energetic materials. Solid rocket propellants containing in-situ synthesized catalytic TiO₂ and energetic aluminum nanoparticles were prepared. These propellants exhibited significant performance improvements over those containing conventionally prepared nanoparticles. The performance gains are attributed to the small particle sizes, high degree of dispersion, and surface property control afforded by the in-situ synthesis methods.

9:00am **NS+AS+SS+SP-WeM4 Synthesis and Catalytic Activity of WS₂ Nanotube Supported Cobalt and Nickel Catalysts Towards Thiophene Hydrodesulfurization**, *M. Komarneni, Z. Yu, A. Chakradhar, U. Burghaus*, North Dakota State University, *Y. Tsvetin, R. Popovitz-Biro, Y. Feldman, R. Tenne*, Weizmann Institute of Science, Israel

Inorganic nanotubes (INT) including WS₂ INT are promising materials for heterogeneous catalysis due to their intriguing properties like enhanced surface area, defects, and confinement effects. The promotion effects of Co and Ni combined with novel nanomaterials such as INT-WS₂ may create the next generation hydrodesulfurization (HDS) catalysts. To verify this, M/INT-WS₂ (M = Co or Ni) catalysts were synthesized and their catalytic activity towards HDS of thiophene was characterized by gas chromatography/ambient pressure catalytic tests and ultra-high vacuum (UHV) thermal desorption spectroscopy (TDS) experiments. Synthesis of M/INT-WS₂ involved two steps: Surface activation of INT-WS₂ by palladium seeding process and electroless plating method to coat nanoparticles of M. The deposited nanoparticles of M formed non-uniform layer on the INT surface. Nanoparticles of size 10-20 nm for Co (*hcp* structure) and 10-20 nm for Ni (*fcc* structure) were coated on INT-WS₂. Next, the catalytic activity of M/INT-WS₂ towards thiophene HDS was characterized using an atmospheric flow reactor. M/INT-WS₂ catalysts exhibited enhanced HDS activity when compared to pristine INT-WS₂

mainly due to the promotion effects of Co and Ni. Hydrogen sulfide and hydrocarbons such as 1,3-butadiene, butane, cis-2-butene, and trans-2-butene were formed as HDS products by both pristine and M/INT-WS₂. Commercial HDS catalysts, CoMo and NiMo from Haldor Topsoe were found to show ~ 4 times higher activity than M/INT-WS₂ synthesized in this study. These results are promising and show that further optimization of the nanofabrication process yields better HDS nanocatalysts. Furthermore, the adsorption kinetics of thiophene on M/INT-WS₂ was studied by TDS at UHV conditions. Thiophene adsorbed on internal, external, and groove sites of the M/INT-WS₂ bundles. Binding energies of thiophene on Ni/INT-WS₂ are ~ 10 kJ/mol smaller than that of pristine INT-WS₂. Thiophene also decomposed on M/WS₂ NT at UHV conditions. In addition, catalytic screening of nanocatalysts such as Au and Co-Ni coated INT-WS₂, pristine MoS₂ nanoparticles with fullerene-like structure (IF), and Re-doped IF-MoS₂ for HDS was also performed. Overall, M/INT-WS₂ catalysts were the best HDS catalysts among the new nanocatalysts studied. The results also reflected the promotion effects of Co and Ni on the M/INT-WS₂ catalysts for higher thiophene conversion rates.

11:20am **NS+AS+SS+SP-WeM11 Charge Exchange and Molecule/Metal Coupling in Fulvalene Surface Chemistry**, *G. Rojas, B.G. Sumpter*, Oak Ridge National Laboratory, *J.A. Schlueter*, Argonne National Laboratory, *P. Maksymovych*, Oak Ridge National Laboratory

Understanding the epitaxy of organic semiconductors on the surface, and the ensuing processes of charge transfer and band-alignment is vitally important for the deterministic design of energy harvesting and light-emitting devices based on molecular heterojunctions. While most of the attention so far has been directed to pi-conjugated aromatic compounds, little is known about the properties of the fulvalene family in contact with metal surface. Here we will present a spectroscopic study of bis(ethylenedithio)tetrathiafulvalene (ET) on Ag(111) in the sub-monolayer to monolayer coverage. Varying coverages of ET adsorption show the molecules dimerize in parallel, bonding to the Ag surface along the long-axis of the molecule. The dimers remain mobile after adsorption, resulting in the formation of a two-phase surface material: unidimensional loosely stacked nanoclusters and finely packed, two-dimensional domains of interlocked molecules. These structures are an intermediate kinetic state, as the molecules further chemically react with the underlying Ag surface following annealing to temperatures as low as 40 C. It is thought based on these data that the dimers form chemical bonds with a single, shared Ag adatom upon adsorption, as observed for other pi orbital dominated aromatic molecules such as PTCDA. Formation of a reactive layer has significant implications for the orbital alignment at the interface. We have therefore probed the properties of the 2D ordered layer and the reacted layers using a combination of current-distance and image-potential state spectroscopy. The interpretation of these results will be presented in conjunction with the first-principles calculations of the respective structures, and correlated with the induced density of interface states (IDIS) model for orbital alignment at metal-molecule interface.

This research was conducted at the Center for Nanophase Materials Sciences, sponsored at the Oak Ridge National Laboratory by the Division of User Facilities, U.S. Department of Energy.

11:40am **NS+AS+SS+SP-WeM12 Subpicosecond-pulse Photoinduced Chemistry on Nanoscale Palladium Model Catalyst Surfaces**, *A. Bhattacharya*, Brookhaven National Laboratory, *R. Palomino, J.C. Lofaro*, Stony Brook University, *H. Park, M.G. White, N. Camillone*, Brookhaven National Laboratory

To date, time-resolved investigations of surface chemical reaction dynamics have almost exclusively been conducted on metal single crystals. However, current and proposed catalysts and photocatalysts generally consist of nanometer-scale metal particles supported on metal oxides. To conduct time-resolved investigations of the surface chemical dynamics of such systems we have synthesized and characterized arrays of palladium nanoparticles (approximately 4 to 10 nm in diameter) supported on clean rutile TiO₂(110). We will present our synthetic approach and the results of chemical and morphological characterization and thermal chemistry experiments on these arrays. We will also discuss the results of subpicosecond-pulse photoinduced desorption of molecular oxygen and carbon monoxide, as well as the photoinduced bimolecular reaction between adsorbed atomic oxygen and carbon monoxide. Comparisons to the same reactions on single crystal Pd(111) surfaces will be made, and the unique features of the chemistry and dynamics at the nanoscale highlighted.

Scanning Probe Microscopy Focus Topic

Room: 16 - Session

SP+AS+BI+ET+MI+NM+NS+SS+TF-WeM

Probe-Sample Interactions, Nano-Manipulation and Fabrication

Moderator: S. Allen, The University of Nottingham, UK,
A.-P. Li, Oak Ridge National Laboratory

8:20am **SP+AS+BI+ET+MI+NM+NS+SS+TF-WeM2 Controlled Coupling of Silicon Atomic Quantum Dots at Room Temperature: A Basis for Atomic Electronics?**, *R.A. Wolkow*, University of Alberta and The National Institute for Nanotechnology, Canada, *J. Pitters*, The National Institute for Nanotechnology, Canada, *G. DiLabio, M. Taucer, P. Piva, L. Livadaru*, University of Alberta and The National Institute for Nanotechnology, Canada **INVITED**

Quantum dots are small entities, typically consisting of just a few thousands atoms, that in some ways act like a single atom. The constituent atoms in a dot coalesce their electronic properties to exhibit fairly simple and potentially very useful properties. It turns out that collectives of dots exhibit joint electronic properties of yet more interest. Unfortunately, though extremely small, the finite size of typical quantum dots puts a limit on how close multiple dots can be placed, and that in turn limits how strong the coupling between dots can be. Because inter-dot coupling is weak, properties of interest are only manifest at very low temperatures (milliKelvin). In this work the ultimate small quantum dot is described – we replace an “artificial atom” with a true atom - with great benefit.

It is demonstrated that the zero-dimensional character of the silicon atom dangling bond (DB) state allows controlled formation and occupation of a new form of quantum dot assemblies - at room temperature. Coulomb repulsion causes DBs separated by less than ~2 nm to experience reduced localized charge. The unoccupied states so created allow a previously unobserved electron tunnel-coupling of DBs, evidenced by a pronounced change in the time-averaged view recorded by scanning tunneling microscopy. It is shown that fabrication geometry determines net electron occupation and tunnel-coupling strength within multi-DB ensembles and moreover that electrostatic separation of degenerate states allows controlled electron occupation within an ensemble.

Some speculation on the viability of a new “atomic electronics” based upon these results will be offered.

9:00am **SP+AS+BI+ET+MI+NM+NS+SS+TF-WeM4 Atomic Forces and Energy Dissipation of a Bi-Stable Molecular Junction**, *C. Lotze*, Freie Universität Berlin, Germany, *M. Corso, K.J. Franke, F.V. Oppen, J.I. Pascual*, Freie Universität Berlin, Germany

Tuning Fork based dynamic STM/AFM is a well established method combining the advantages of scanning tunneling and dynamic force microscopy. Using tuning forks with high stiffness, stable measurements with small amplitudes, below 1 Å can be performed. In this way, conductance and frequency shift measurements of molecular junction can be obtained simultaneously [1] with intramolecular resolution [2].

One of the most intriguing aspects of molecular junctions relates to the effect of structural bi-stabilities to the properties of the junction. These lead, for example, to conductance fluctuations, telegraph noise and the possibility to switch the electrical transport through the junction.

In this presentation, we characterize a model bi-stable molecular system using dynamic force spectroscopy. The effect of current-induced stochastic fluctuations of conductance are correlated with fluctuations in force. In our experiment we identified the last from both, frequency shifts and energy dissipation measurements, picturing a regime in which electrical transport and mechanical motion are coupled.

[1] N. Fournier *et. al*, PhysRevB 84, 035435 (2011),

[2] L. Gross *et. al*, Science 324, 1428 (2009)

9:20am **SP+AS+BI+ET+MI+NM+NS+SS+TF-WeM5 Acetylene on Cu(111): Imaging a Molecular Pattern with a Constantly Rearranging Tip**, *Y. Zhu, J. Wyrick, K.D. Cohen, K. Magnone, C. Holzke, D. Salib, Q. Ma, D.Z. Sun, L. Bartels*, University of California Riverside

Abstract: Using variable temperature STM and DFT simulation, we identify the phases of acetylene adsorbed on the Cu(111) surface. Depending on the coverage, a diffraction-derived surface pattern of acetylene on Cu(111) is validated by STM. The modification of the STM image transfer function

through the adsorption of an acetylene molecule onto the tip apex is taken into account. In this case, the images of acetylene patterns on Cu(111) also include direct evidence of the **rotational orientation and dynamics of the acetylene species attached to the tip apex**. DFT modeling of acetylene/Cu(111) reveals that the molecular orientation and separation is governed by a balance of repulsive interactions associated with stress induced in the top surface layer and attractive interactions mediated by the electronic structure of the substrate. Computationally modeling of the substrate with 3 layers obtains the periodicity of the intermolecular interaction that provides a theoretical underpinning for the experimentally observed molecular arrangement.

9:40am **SP+AS+BI+ET+MI+NM+NS+SS+TF-WeM6 Atomic Scale Imaging and Electronic Structure of Trimethylaluminum Deposition on III-V Semiconductor (110) Surfaces**, *T.J. Kent**, *M. Edmonds*, *E. Chagarov*, *A.C. Kummel*, University of California San Diego

Silicon based metal oxide semiconductor field effect transistors (Si-MOSFETs) are quickly approaching their theoretical performance limits, as a result many semiconductors are being explored as an alternative channel material for use in MOSFETs. III-V semiconductors are an appealing alternative to Si because of their higher electron mobilities. The limiting factor in III-V based MOSFET performance is defect states which prevent effective modulation of the Fermi level. The InGaAs (001) As-rich (2x4) surface contains two types of unit cells: ideal unit cells with double As-dimers and defect unit cells with single As-Dimers. The missing As-dimer unit cells, which comprise ~50% of the surface, are believed to cause electronic defect states at the semiconductor-oxide interface, specifically at the conduction band edge of the semiconductor. *In-situ* scanning tunneling microscopy and spectroscopy (STM/STS) and density function theory (DFT) modeling show that TMA readily passivates the As-As dimers in the ideal unit cell but the missing InGaAs(001)-2x4 may not be fully passivated by TMA. To improve the electronic structure of the interface, the sidewalls of the finFETs on InGaAs(001) can be fabricated along the (110) direction. The (110) surface contains only buckled III-V heterodimers in which the lower group III atom is sp² hybridized with an empty dangling bond and the upper group V atom is sp³ hybridized with a full dangling bond. This results in an electrically unpinned surface.

To investigate the benefits of using a (110) surface as a channel material, the atomic and electronic structure of the ALD precursor trimethylaluminum (TMA) monolayer deposited on III-V (110) surfaces has been studied using *in-situ* STM and STS. Both GaAs and InGaAs samples were studied. GaAs wafers were obtained from Wafertech with a Si doping concentration of 4x10¹⁸/cm³. The (001) samples were cleaved *in-situ* to expose the (110) surface. Samples were transferred to the STM chamber (base pressure 1x10⁻¹¹ torr) where the atomic bonding structure of the precursor monolayer unit cell was determined. STS, which probes the local density of states (LDOS), was used to determine Fermi level pinning. A model of TMA chemisorption was developed in which TMA chemisorbs between adjacent As atoms on the surface, giving a highly ordered monolayer with a high nucleation density which could allow for aggressive effective oxide thickness (EOT) scaling.

10:40am **SP+AS+BI+ET+MI+NM+NS+SS+TF-WeM9 A New Experimental Method to Determine the Torsional Spring Constants of Microcantilevers**, *G. Haehner*, *J.D. Parkin*, University of St Andrews, UK
Cantilever based technologies have seen an ever increasing level of interest since the atomic force microscope (AFM) was introduced more than two decades ago. Recent developments employ microcantilevers as stand-alone sensors by exploiting the dependence of their oscillating properties on external parameters such as adsorbed mass [1], or the density and the viscosity of a liquid environment [2,3]. They are also a key part in many microelectromechanical systems (MEMS) [4]. In order to quantify measurements performed with microcantilevers their stiffness or spring constants have to be known. Following calibration of the spring constants a change in oscillation behavior can be quantitatively related to physical parameters that are probed. The torsional modes of oscillation have attracted significant attention due to their high sensitivity towards lateral and friction forces, and recent developments in torsional-tapping AFM technology [5]. However, the methods available to determine the torsional spring constants experimentally are in general not simple, not very reliable, or risk damage to the cantilever [6].

We demonstrate a new method to determine the spring constants of the torsional modes of microcantilevers experimentally with high accuracy and precision. The method is fast, non-destructive and non-invasive. It is based on measuring the change in the resonance frequencies of the torsional

modes as a function of the fluid flow escaping from a microchannel. Results for rectangular cantilevers will be presented and compared to results obtained with other methods [7].

- [1] J. D. Parkin and G. Hähner, *Rev. Sci. Instrum.* **82** (3), 035108 (2011).
- [2] N. McLoughlin, S. L. Lee, and G. Hähner, *Appl. Phys. Lett.* **89** (18), 184106 (2006).
- [3] N. McLoughlin, S. L. Lee, and G. Hähner, *Lab Chip*, 1057 (2007).
- [4] S. Beeby, G. Ensell, N. Kraft, and N. White, *MEMS Mechanical Sensors*. (Artech House London, 2004).
- [5] O. Sahin and N. Erina, *Nanotechnology* **19** (44), 445717 (2008).
- [6] M. Munz, *Journal of Physics D-Applied Physics* **43** (6), 063001 (2010).
- [7] C. P. Green, H. Lioe, J. P. Cleveland, R. Proksch, P. Mulvaney, and J. E. Sader, *Rev. Sci. Instrum.* **75** (6), 1988 (2004).

11:00am **SP+AS+BI+ET+MI+NM+NS+SS+TF-WeM10 A Torsional Device for Easy, Accurate and Traceable Force Calibration of AFM Cantilevers**, *J.F. Portoles*, *P.J. Cumpson*, Newcastle University, UK

Accurate measurement of biologically-relevant forces in the range of pN to µN is an important problem in nanoscience.

A number of force probe techniques have been applied in recent years. The most popular is the Atomic Force Microscope (AFM). Accuracy of force measurement relies on calibration of the probe stiffness which has led to the development of many calibration methods[1], particularly for AFM microcantilevers. However these methods typically exhibit uncertainties of at best 15% to 20% and are often very time consuming. Dependency on material properties and cantilever geometry further complicate their application and take extra operator time. In contrast, one rapid and straightforward method involves the use of reference cantilevers (the "cantilever-on-cantilever" method) or MEMS reference devices. This approach requires that a calibrated reference device is available, but it has been shown to be effective in providing measurement traceability[2].

The main remaining difficulty of this approach for typical users is the positional uncertainty of the tip on the reference device, which can introduce calibration uncertainties of up to around 6%. Here we present a new reference device based on a torsional spring of relatively large dimensions compared to the typical AFM cantilever and demonstrate how it is calibrated. This method has the potential to calibrate the reference device traceably[3] to the SI with a 1% accuracy by applying techniques typically used for the characterisation of micromechanical devices. The large dimensions of the device reduce the positional uncertainty below 1% and simultaneously allow the use of the device as an effective reference array with different reference stiffnesses at different positions ranging from 0.090 N/m to 4.5 N/m

- [1] P J Cumpson, C A Clifford, J F Portolés, J E Johnstone, M Munz *Cantilever Spring-Constant Calibration in Atomic Force Microscopy*, pp289-314 in Volume VIII of *Applied Scanning Probe Methods*, Ed. B Bhushan and H Fuchs (Springer, New York, 2009)
- [2] P J Cumpson PJ, J Hedley, *Nanotechnology* 14 (2003) pp. 1279-1288
- [3] J F Portolés, P J Cumpson, J Hedley, S Allen, P M Williams & S J B Tendler, *Journal of Experimental Nanoscience* 1 (2006) pp51-62.

11:20am **SP+AS+BI+ET+MI+NM+NS+SS+TF-WeM11 Nanoscale Surface Assembly by Single-Molecule Cut-and-Paste**, *H.E. Gaub*, Ludwig-Maximilians Universität, Germany **INVITED**

Bottom up assembly of functional molecular ensembles with novel properties emerging from composition and arrangement of its constituents is a prime goal of nanotechnology. With the development of Single-Molecule Cut-and-Paste (SMC&P) we provided a platform technology for the assembly of biomolecules at surfaces. It combines the Å-positioning precision of the AFM with the selectivity of DNA hybridization to pick individual molecules from a depot chip and allows to arrange them on a construction site one by one. An overview on different applications of this technology will be given in this talk. One recent example demonstrates the functional of receptors for small molecules. By SMC&P we assembled binding sites for malachite green in a molecule-by-molecule assembly process from the two halves of a split aptamer. We show that only a perfectly joined binding site immobilizes the fluorophore and enhances the fluorescence quantum yield by several orders of magnitude. To corroborate the robustness of this approach we produced a micron-sized structure consisting of more than 500 reconstituted binding sites. To the best of our knowledge this is the first demonstration of a one by one bottom up functional bio-molecular assembly. Figure included in supplemental document. S. Kufer, Puchner E. M., Gump H., Liedel T. & H. E. Gaub *Science* (2008), Vol 319, p 594-S. Kufer, Strackham, M., Stahl S.W., Gump H., Puchner E. M. & H. E. Gaub *Nature Nanotechnology* (2009), Vol 4, p 45-M. Erdmann, R. David. A.N. Forno, and H. E. Gaub, *Nature*

* ASSD Student Award Finalist

Vacuum Technology

Room: 14 - Session VT+AS+SS-WeM

Surface Analysis and Vacuum Manufacturing for Accelerators

Moderator: M.L. Stutzman, Thomas Jefferson National Accelerator Facility

8:00am **VT+AS+SS-WeM1 Manufacturing and Welding Processes for TPS Large Aluminum Bending-Chambers and 14 m Vacuum Cells.** *C.L. Chen, C.C. Chang, C.K. Chan, Y.C. Yang, T.Y. Lee, G.Y. Hsiung, J.R. Chen*, NSRRC, Taiwan, Republic of China

A unique manufacturing and welding technique has been developed for building the 3 GeV Taiwan Photon Source (TPS) large aluminum bending chambers and 14-meter vacuum cells. There are total 48 bending chambers, which are about 3.8 meters long each. Combined with an appropriate manufacturing processes, such as with a precise CNC machine, lubrication with pure alcohol and cleaning with ozonated water, the aluminum chambers have an oil-free interior surface finished for an ultra-high vacuum environment before aluminum welding. Ozonated water has a high oxidation potential and can remove most organic contaminations. It is used to effectively clean aluminum chambers' surfaces, and provides with the lowest outgassing yield. After the bending chambers are cleaned with ozonated water, the chambers are moved to a welding room for following welding processes. A novel automatic gas-tungsten arc-welding (GTAW) system has been established at NSRRC for welding the aluminum bending chambers. This welding system has a XY stage that is built and configured to provide high-performance positioning along multiple welding axes. The automatic welding system comprises six welding torches to implement simultaneously two longitudinal side welds of a bending chamber, and is innovative in using computer-based software to control the welding movements and the welding parameters of the six-torch output. In traditional manual welding, the key success factors focus on elimination as much as possible the distortions of structural assemblies. The six-torch welding and a clamp-free approach together address the issue of reducing distortion and minimizing residual stresses with a novel one-step welding process. In addition, on-site welding sequence is introduced for assembling two straight and two bending chambers into one 14-meter vacuum cell. From the beginning of CNC machining to the end of vacuum cell assembly, deformations through all process sequences are measured and controlled under 300 μm . In this paper, both the manufacturing sequences, vacuum data and statistical analysis of deformation control are presented in detail.

8:20am **VT+AS+SS-WeM2 A High Power Electron Beam Stop for Cornell ERL Prototype Injector.** *X. Liu, Y. Li, K.W. Smolenski, I. Bazarov, B.M. Dunham*, Cornell University

The electron beam stop for Cornell University's Energy Recovery Linac (ERL) prototype injector was designed and manufactured for 600 kW electron beam power at beam energies between 5 and 15 MeV. To minimize neutron production from high energy electrons, aluminum was chosen over copper for the construction material. It consists of a 20 mm thick main body with machined outer cooling channels and a tight fit jacket, with the thickness mainly determined by the stopping power of the material. The stop body also serves as the vacuum envelope. The stop body is made of three sections, which are electron-beam welded together. It has a cylindrical shape with a cone at the end, about 0.5 m in diameter and 3 m in overall length. Flexibility is allowed at the body-jacket joint to minimize the thermal stress. The naturally small ERL electron beam is enlarged and rastered in a circular pattern using magnets at the entrance. The enlarged electron beam strikes the stop surface at an average angle of about 8 degrees. The electron scattering inside the stop body was simulated using GEANT4, and the inside profile of the body was optimized so that the thermal load is the most evenly distributed over the whole body. A quadrant detector is equipped at the entrance of the stop to monitor the electron beam centering and rastering. An array of thermocouples is installed on the outside surface of the jacket, providing a rough map of the heat load distribution. Gases generated in the close-circuit cooling water by radiolysis are vented and the concentration of hydrogen is monitored. The stop has been in operation since October 2008, and has been tested up to 250 kW to date.

8:40am **VT+AS+SS-WeM3 Ion Pump Starting Behaviour at High Pressures - Influence of Pump Design Diode / Triode and Power Supply.** *M. Thierley, C. Paolini*, Agilent Technologies, Italy

Today ion pumps are broadly seen as pumps for good high vacuum and ultra-high vacuum environments. Operated at these low pressures, the power consumption of ion pumps is also very low, making ion pumps one of the most energy efficient vacuum pump technologies. Power supplies, however, with several hundred Watts of power continue to be used, as in the past decades, often based on the fear of not being able to start the ion pump; historic issues associated with higher pressures. In this presentation/paper, the differences in starting behaviour of Diode and Triode pump elements are discussed, based on experimental data. Questions addressed will include; how does the pumping speed of these elements change while starting with voltage and current? What impact does the power and design of the pump control unit have on the start and the pump down time of the vacuum system? What is the impact of the power supply unit's technology (ie. classic transformer based design vs. more modern switching power supplies)? In addition to controller experimental data and discussion of the operation theory of the pump elements, pictures of the actual plasma development inside the pump will be featured.

9:00am **VT+AS+SS-WeM4 Superconducting Niobium for Accelerator Cavities: Status and Prospects.** *M.J. Kelley*, Jefferson Lab and College of William & Mary **INVITED**

Radiofrequency accelerator cavities of superconducting niobium are the technology of choice for a number of recent and coming particle accelerators, largely because of their cost-for-performance. The principal aspects of performance are the amount accelerator needed to achieve a required final beam energy (accelerating gradient, E_{acc}) and energy consumption (cavity quality factor, Q_0). The former impacts chiefly initial cost; the latter both initial and operating costs. Research and development efforts are bearing fruit for both. Gaining the benefits need not await the construction of new accelerators or major upgrades, as accelerator modules are regularly cycled out of existing machines. A challenge that is under-appreciated by physics researchers, but is well familiar to the AVS community, is the manufacturing excellence needed to translate research progress into hardware on the ground.

Authored by Jefferson Science Associates LLC under US DOE Contract De-AC05-06OR23177

9:40am **VT+AS+SS-WeM6 Niobium Nitride Thin Films and Multilayers for Superconducting Radio Frequency Cavities.** *W.M. Roach*, D.B. Beringer, Z. Li*, The College of William and Mary, *J.R. Skuza*, National Institute of Aerospace, *C. Clavero, R.A. Lukaszew*, The College of William and Mary

Niobium nitride in thin film form has been considered for a number of applications including multilayered coatings onto superconducting radio frequency (SRF) cavities which have been proposed to overcome the fundamental accelerating gradient limit of 50 MV/m in niobium based accelerators [1]. In order to fulfill the latter application, the selected superconductor's lower critical field, H_{C1} , must be larger than that of niobium and separated from the niobium surface by an insulating layer in order to shield the niobium cavity from field penetration, therefore allowing higher field gradients. Thus, for the successful implementation of such a multilayered stack it is important to consider not just the material's inherent properties, but also how these properties may be affected in thin film geometry and also by the specific deposition techniques used. Here, we present the results of our correlated study of structure and superconducting properties in niobium nitride thin films. Additionally, we explore how growth parameters can affect the surface morphology, since the quality of the surface has major implications on the ultimate performance of SRF cavities. Combining our findings on the surface morphology, microstructure, and superconducting properties in niobium nitride thin films, we discuss their potential application in multilayered coatings for accelerator cavities.

[1] A. Gurevich, *Appl. Phys. Lett.* **88**, 012511 (2006).

This work was funded by the Defense Threat Reduction Agency (HDTRA-10-1-0072).

* ASSD Student Award Finalist

10:40am **VT+AS+SS-WeM9 Characterization of Anisotropic Surface Morphology in Epitaxial Superconducting Thin Films by Wavelet Analysis.** *D.B. Beringer, J.B. Hackett, W.M. Roach, R.A. Lukaszew*, The College of William and Mary

Surface morphology and interface roughness are critical factors impacting the ultimate performance of many thin film materials and nano-scale devices. Next generation superconducting radio frequency (SRF) materials for particle accelerator cavities depend upon the ability to tailor and finely control the microstructure and morphology of superconducting / insulating /superconducting (SIS) multilayer thin film structures. The evolving surface of grown epitaxial thin films, influenced by nucleation and growth kinetics, may exhibit dendritic or fractal patterning where the resulting anisotropic features dominate a coarsening morphology. As such, a quantitative understanding of superconducting thin film morphology and the thin film deposition parameters leading to optimal SRF surfaces is desirable. Quantitative characterization of surface morphology is typically achieved with Fourier transform (FT) analysis and fractal characterization; however, this approach suffers intrinsic limitations as the FT is localized in the frequency domain and therefore cannot differentiate between specific features with isolated spatial coordinates. Wavelet analysis transcends these limitations by effectively isolating and quantifying surface features belonging to a designated length scale, thus enabling independent analysis of local surface features with varied spatial resolutions. Here we present our work with surface characterization by wavelet analysis of epitaxial superconducting Nb thin films.

11:00am **VT+AS+SS-WeM10 NbN-AlN-Nb Multilayer Thin Films for Superconducting Radio Frequency Cavities.** *Z. Li, W.M. Roach, D.B. Beringer, C. Clavero, R.A. Lukaszew*, College of William and Mary

Linear accelerators that are used in high-energy or nuclear physics experiments use superconducting radio frequency (SRF) cavities made with bulk Nb. However, as technology is improved for bulk Nb cavities, the accelerating gradient for these cavities is reaching the fundamental limit of 50 MV/m. Since the critical surface of Nb in SRF cavities is less than one micron, it is possible to use thin films and multilayers to overcome the accelerating gradient limit. It has been proposed to apply a superconductor-insulator-superconductor (SIS) multi-layer structure onto Nb based cavities in order to provide an improved lower critical field (H_{c1}) that will shield the Nb and therefore allow for an increase in the accelerating gradient [1]. NbN is one of the superconductors that may be implemented in this SIS structure. However, the choice of insulator is crucial in determining the performance of NbN thin films. Here, we present our study of epitaxial thin films prepared on both MgO and AlN templates. The effect of substrate choice on microstructure and superconducting properties is explored in order to determine which insulator provides optimal performance of NbN thin films for SRF applications.

[1] A. Gurevich, Appl. Phys. Lett. **88**, 012511 (2006).

Wednesday Afternoon, October 31, 2012

Applied Surface Science

Room: 20 - Session AS+NS+SS+TF-WeA

3D Imaging & Nanochemical Analysis - Part 2 (2:00-3:20 pm)/ Advanced Data

Analysis and Instrument Control (4:00-6:00 pm)

Moderator: V.S. Smentkowski, General Electric Global Research Center, M.R. Linford, Brigham Young University, S.J. Pachuta, 3M Company

2:00pm AS+NS+SS+TF-WeA1 From Atomic Scale to Materials Behavior: Using Atom-Probe Tomography to Understand the Behavior of Alloys and Ceramics, E.A. Marquis, University of Michigan INVITED

The ability to improve the performance of functional materials is driven by how well microstructure can be understood and controlled. The three-dimensional distribution of solutes, dopants or impurities in particular, in relation to structural features determines such properties as fracture toughness, strength, ductility, as well as electrical and magnetic response. After a brief introduction to atom-probe tomography, I will illustrate how high resolution characterization approaches can be used systematically to understand the atomic scale processes controlling materials microstructures and their evolution, focusing on alloys and ceramic systems. Several topics will be presented: precipitation and coarsening behavior of Al-based alloys, grain boundary chemistry and role of impurities during irradiation in ferritic steels which may play an important role in fracture and corrosion resistance, the development of oxide-dispersion strengthened steels for structural applications in future nuclear reactors and the role of minor elements in controlling the oxidation behavior of Ni-base alloys for high temperature power generation applications.

2:40pm AS+NS+SS+TF-WeA3 Three Dimensional Atomic Scale Characterization of Binary and Complex Oxides using Atom Probe Tomography, A. Devaraj, R. Colby, D.E. Perea, S. Thevuthasan, EMSL, Pacific Northwest National Laboratory

The development of three dimensional, high spatial and mass resolution characterization techniques is important for several materials used in applications ranging from catalysis, sensors to optoelectronics. Laser assisted atom probe tomography (APT) technique offers such an opportunity to perform atomic scale three dimensional analysis of materials including metals, semiconductors and dielectrics, with subnanometer spatial resolution and sub-ppm level mass resolution. The Cameca LEAP 4000XHR Atom Probe equipped with 355nm UV pulsed laser is used to analyze technologically important binary bulk oxides like MgO, Al₂O₃, TiO₂ and CeO₂. A strong correlation between applied UV laser energy and measured stoichiometry was observed for all these binary oxides. Using those results the importance of laser energy optimization on obtaining accurate stoichiometric composition analysis for oxides will be highlighted. Extension of such laser parametric investigation to complex oxides including SrTiO₃, LaCrO₃ and LaSrMnO₃ will also be presented. In addition the impact of laser pulsing on atomic scale structure of the oxide APT sample surface was studied by a direct cross correlation with aberration corrected TEM. The information on the atomic scale structure of the field evaporated oxide APT samples will be utilized to postulate the laser-oxide material interaction occurring during APT analysis of such oxides leading to the dependency of applied laser energy on measured stoichiometry.

3:00pm AS+NS+SS+TF-WeA4 Atom Probe Tomography of Complex Heterogeneous Low Dimensional Materials, S. Thevuthasan, A. Devaraj, R. Colby, D.E. Perea, V. Subramanian, V. Shutthanandan, Pacific Northwest National Laboratory

EMSL, a national scientific user facility of the DOE, is developing a comprehensive chemical imaging capability combining atom probe tomography with high resolution (scanning) transmission electron microscopy(HR(S)TEM) and high resolution Rutherford back scattering spectrometry (HRRBS) to provide solutions to problems pertaining to energy and environmental applications. We will emphasize on a chemical imaging effort aimed at atomically-resolved composition and structural analysis of low dimensional materials such as nanowires and embedded metal nanoparticles highlighting the benefits and challenges for APT. A unique benefit of APT is the ability to characterize the ppm level concentration and distribution of dopants across semiconducting nanowire heterojunctions. The preferential incorporation of dopants at specific atomic facets at the heterojunction interface in Si-Ge nanowires can only be characterized by using APT. Another important class of low dimensional

materials includes embedded metal nanoparticles in oxides with applications in catalysis, sensors and optoelectronic applications. In order to extent APT analysis capability to such materials a cross correlative approach of combining APT with aberration corrected HRSTEM is employed. The results from the model system of ion beam synthesized Au and Ag nanoparticles embedded in MgO will be presented.

4:00pm AS+NS+SS+TF-WeA7 Upgrading a 25 Year Old ims-4f Magnetic Sector SIMS Instrument: Teaching an Old Dog New Tricks and Keeping Research in its Future, A.J. Fahey, B.E. Naes, G. Hager, Pacific Northwest National Laboratory

The CAMECA ims-4f at PNNL is nearly 25 years old. Although much of the vacuum system, electrostatic optics and associated apertures and slits have been maintained and remain operational the electronics that control the critical components of this machine has gone beyond the typical "mean-time-between failure" of nearly all components, which is typically 10 years.

The original electronics designs, many of which are no longer employed on the newer CAMECA models, incorporated multiple series of relays to control lens voltages that allowed isolation of low control and high voltage output. These relays, among other components, are failing.

Some components of the electrostatic optics and vacuum system are targeted to be replaced to upgrade the capabilities of the instrument and to use physical components from our "surplus" ims-4f system than would enhance the operation of the PNNL ims-4f giving in near-equivalence to the operation of an ims-7f.

The upgraded electronics and control systems are being designed in a modular way using as many commercial components as possible, such as modular high voltage power supplies and commercially available high-voltage operational amplifiers. The new system will allow for complete control of all subsystems on the instrument and will improve repeatability of settings and measurements. We will be able to perform measurements sets and sequences that are currently not possible on any existing SIMS instrument. In addition, the new computer controlled system should make operation of the SIMS instrument more accessible to other investigators as it should reduce the level of training needed to operate the instrument. Currently, the operator must adjust "knobs" to tune the instrument and reproduce prior operating conditions. With the upgraded system conditions will be recalled from saved files.

All modular components are being housed in ANSI-standard DIN modules and sub-racks. Control, monitoring and data acquisition will largely be performed via PXI subsystems. The Vacuum will be controlled and monitored via a commercial process control system. Also, several other individual instruments will be used in critical positions around the instrument.

Details of the upgrade will be discussed as well as improvements to the flexibility of measurements and the performance of the system. An outline of the types of measurements that should be available with all modern systems will be presented and discussed as well as the results of improvements implemented to the PNNL ims-4f SIMS instrument.

4:20pm AS+NS+SS+TF-WeA8 Automated Processing of X-ray Photo-Electron Spectra, K. Macak, E. Macak, S.J. Coultas, S.J. Hutton, A.J. Roberts, R. Raso, S.J. Page, C.J. Blomfield, Kratos Analytical Ltd, UK

Modern XPS instruments are capable of generating a large amount of data in a hands-off automated fashion. Many new material challenges are increasingly reliant upon XPS for sample screening and other high throughput, low operator intervention applications.

The interpretation of XPS data and reliable quantification from the acquired results presents an opportunity to improve the whole experimental automation still further. We present an algorithm for fully automated processing of X-ray photo-electron spectra. The analysis is split into three stages: background subtraction, peak identification and quantification of element composition.

Each step can be carried out separately and the user can provide prior knowledge of the sample by manually selecting regions, assigning their labels and/or explicitly include/exclude specific elements. This additional information then helps to improve the accuracy of the results.

The algorithm was tested on more than 1000 spectra, selected from a wide range of different materials; including steels, polymers, semiconductors and ceramics. These spectra were processed using the automated procedure and the outcomes were compared to those determined by expert users. The average element detection success rate was 87 %.

The influence of various experimental conditions (such as signal-to-noise ratio and operating conditions) on the identification procedure is also discussed.

4:40pm AS+NS+SS+TF-WeA9 Correlating Structure and Chemistry – A Multitechnique Study using Light Microscopy (LM), SEM and XPS, M.L. Pacholski, P.Y. Eastman, The Dow Chemical Company

Understanding the distribution of carbon-rich chemistries on organic substrates can be very difficult, particularly when the substrates are not uniform, such as cellulose fibers. Recently we have been challenged to measure the distribution of an olefin polymer on a fibrous cellulose sheet. In order to verify that measured chemical distributions were definitively from polymer, as well as to understand the morphology of the deposited polymer, it was highly desired to study identical areas using SEM and other imaging techniques. Although several chemical imaging methods were investigated, it became apparent that XPS imaging was the only chemical technique capable of obtaining distributions over the desired fields of view (1 mm-3 mm). Registry of the SEM images with XPS images proved to be difficult since many of the traditional registry methods, such as marking with ink or gluing markers to the surface are ill-suited to absorbent cellulose. The first step was to align relatively low magnification light microscope images from a stereoscope with optical images captured directly in the XPS instrument. These images were then used as a “bridge” to align the higher magnification SEM and XPS images. With this method, deposited polymer and chemical information were correlated with high spatial accuracy. Composite images showing the chemical information as colored overlays on the SEM images were generated to clearly display the correlation.

Biointerphases Focus Topic: Bioimaging

Room: 23 - Session BN+AS-WeA

Bioimaging

Moderator: M. Grunze, University of Heidelberg, Germany

2:00pm BN+AS-WeA1 Label-free Non-Invasive Imaging of Live Cells by Raman Micro-Spectroscopy, I. Nottingher, University of Nottingham, UK

INVITED

Stem cells have enormous potential for cell replacement therapies in curing age-related illnesses such as Alzheimer's and Parkinson's disease, as well as diabetes and cardiovascular disorders. In addition, they are a reliable cell source in tissue engineering and stem cell seeded scaffolds could provide an unlimited supply of grafts to replace and repair diseased tissues.

However, the current conditions to derive specific cell types remain suboptimal, generally producing only low yields of the desired differentiated lineages within highly heterogeneous populations that are not suitable for clinical use due to the presence of mainly unwanted cell types. This current limitation in the delivery of validated stem cells suitable for clinical applications, highlights the immediate need for non-invasive techniques capable of phenotypic identification of live cells within highly heterogeneous populations.

Raman micro-spectroscopy (RMS) is a label-free technique which can be used for imaging of live cells. This technique combines the high chemical specificity of Raman spectroscopy with the high spatial resolution of optical microscopy to provide detailed molecular information of complex biological samples. Since RMS has only a minimal background signal from water, it allows repeated observations of viable cells maintained under physiological conditions, which is difficult by other molecular vibrational techniques.

In the first part we will focus on using RMS to detect molecular markers for individual live cardiomyocytes (CMs) derived from human embryonic stem cells (hESCs). The ability to monitor and quantify these spectral markers during differentiation periods as long as 5 days is also demonstrated. The analysis of Raman spectra of hESC-derived CMs were characterised by increased signals associated to myofibrils and glycogen compared to the other differentiated cells present in the cultures. The prospects of label-free Raman activated cell sorting are also discussed.

The second part will present results on using RMS for imaging and quantifying spectral markers in neuronal stem cells (NSCs). Raman spectra of undifferentiated NSCs are compared to those of glial cells derived from NSCs, with the aim to identify molecular markers which can be used for assessing the differentiation status of the NSCs. High resolution spectral maps corresponding to nucleic acids show that NSCs are characterized by increased concentrations of cytoplasmic RNA.

These studies demonstrate that RMS represents a feasible approach for label-free non-invasive characterization of individual live cells and can be used to assess the differentiation status and the phenotypes of individual cells.

2:40pm BN+AS-WeA3 Perfluoropentane Gas and Liquid Filled Hollow Silica Micro/Nano Spheres for Ultrasound Guided Surgery and HIFU Therapy, A. Liberman, H.P. Martinez, Z. Wu, C.V. Barback, S.L. Blair, Y. Kono, R.F. Mattrey, W.C. Trogler, A.C. Kummel, University of California San Diego

The reported positive margin rate from wire localized excisions of breast cancers is approximately 20-50%; however, by preoperatively injecting a radio active seed into the tumor under CT guidance, the excision rate is halved because the surgeon can constantly reorient the dissection to place the seed in the center of the specimen. Unfortunately, radioactive seed localization has several safety challenges, only single foci can be localized, and incisions are required to implant the seeds, so it is rarely employed. As a safe alternative, gas-filled hollow Fe-doped silica particles have been developed, which can be used for ultrasound-guided surgery even for multiple foci. The function of the Fe doping is to render the silica shells biodegradable. The particles are synthesized through a sol-gel method on a polystyrene template, and subsequently calcined to create hollow, rigid microspheres. The Fe-doped silica shell is derived from tetramethoxy orthosilicate (TMOS) and iron (III) ethoxide, which forms a rigid, mesoporous shell upon calcination. The microspheres are filled with perfluoropentane (PFP) vapor or liquid. The flourous phase is contained within the porous shell due to its extremely low solubility in water. Considerable testing of particle functionality, signal persistence and acoustical properties have been performed in various phantoms including ultrasound gel, chicken breast, and excised human mastectomy tissue. *In vitro* studies have shown that continuous particle imaging time is up to approximately 45 minutes, and will persist for over five days. Furthermore, preliminary *in vivo* particle injection longevity studies have been performed in a rabbit model which are consistent with *in vitro* data showing signal presence even five days post injection. These silica spheres may be used as a sensitizing agent in high intensity focused ultrasound (HIFU). Traditional ultrasound agents pose several potential drawbacks such as poor *in vivo* persistence (minutes) and high risk (cardiac complications) during continuous perfusion. Preliminary *in vitro* results in HIFU ablation in an agar tissue phantom model suggest that very few particles are needed in order to develop a sensitizing effect to HIFU (approx. 1-10 µg/ml particles/agar varying by particle size). A novel technique has been developed to fill the particles with perfluorocarbon liquid which vaporizes upon exposure to HIFU thereby increasing the sensitivity compared to gas filled particles.

3:00pm BN+AS-WeA4 Differentiation of Breast Cancer Cell Lines with ToF-SIMS, L.J. Gamble, M. Robinson, University of Washington, F. Morrish, D. Hockenbery, Fred Hutchinson Cancer Research Center

Cancer is a heterogeneous malignancy that manifests itself in a variety of morphological types and clinical outcomes. Tumor metabolism plays a large role in cancer onset and progression, and its causes and effects are under intense scrutiny. Time-of-flight secondary ion mass spectrometry (ToF-SIMS) has been increasingly utilized for examining biological samples including biomaterials, cells, and tissues. The incorporation of cluster ion sources has allowed the detection of many high mass organic species that can be used to characterize biological surfaces. In combination with principal component analysis (PCA), we use ToF-SIMS to determine differences in the chemical makeup of eight different breast cancer cell lines. Four cell types are of the triple-negative (TN) phenotype, and four cell types are the luminal phenotype. Spectra have been acquired on an IONTOF TOF.SIMS V using Bi_3^+ before and after C_{60} etching. Using positively charged mass fragments, many of the cell lines can be separated from one another within a 95% confidence interval, with only two TN lines overlapping. Biological significance of the loadings peaks will be discussed with species such as diacylglycerols and cholesterol playing a role in the separation. This work is the foundation for future studies using human tumor biopsy samples that will help elucidate the link between fatty acid composition within a tumor and the potential drug resistance of that tumor.

4:00pm BN+AS-WeA7 Biological Applications of Lipid Imaging with Cluster-TOF-SIMS and MALDI-TOF, A. Brunelle, CNRS, Institut de Chimie des Substances Naturelles (ICSN), France

INVITED

Time-of-Flight Secondary Ion Mass Spectrometry (TOF-SIMS) using keV energy metal cluster beams as primary ions is now recognized as a powerful method for *in situ* chemical, biological and medical applications [1,2]. It opens a new field of surface imaging, particularly for biological tissue sections. Compared to the more established MALDI (Matrix Assisted Laser Desorption Ionisation) imaging approach, TOF-SIMS imaging provides the incomparable advantages of a routine micrometre scale resolution and of an

easy sample preparation which does not require matrix coating of the surface. However TOF-SIMS suffers from some limitations, such as the narrow mass range, the lack of structural analysis of the species by tandem mass spectrometry, and the fact that mainly lipids are preferentially released from the biological samples.

This lecture intends to show the wealth of powerful information that can be obtained from the chemical analysis of biological surfaces, with several examples chosen among various applications such as the localization of xenobiotics, natural substances, lipid markers from genetic diseases and non-alcoholic fatty liver disease. The strengths and weaknesses of lipid imaging using TOF-SIMS and MALDI-TOF will also be compared, showing the complementarity between the two methods.

Tissue imaging using TOF-SIMS can also be associated with histology for medical diagnosis in order to correlate structural features with ion images. The possibility to use the same tissue section for both histology and mass spectrometry imaging has been tested. It is a major advantage in terms of sample preparation and precision on the histological structure localization, provided that none of the two methods disturbs the performances of the other [3].

Massive cluster ion sources of argon have recently been used for SIMS experiments [4]. These ion beams interact with surfaces with incomparable physical properties, and thus hold the promise for new opportunities such as organic depth profiling or large increases of sensitivity. Recent results will be presented showing the possibility of depth profiling in organic samples, but also the enhancement of the sensitivity, using both massive clusters and bismuth for dual beam depth profiling.

[1] F. Benabdellah, A. Seyer, L. Quinton, D. Touboul, A. Brunelle, O. Lapr votte, *Anal Bioanal Chem* 396 (2010) 151-162

[2] D. Touboul, O. Lapr votte, A. Brunelle, *Curr Opin Chem Biol* 15 (2011) 725-732

[3] C. Bich, S. Vianello, V. Gu r neau, D. Touboul, S. De La Porte, A. Brunelle, *Surf Interface Anal* in press DOI:10.1002/sia.4846

[4] H. Gnaser, K. Ichiki, J. Matsuo, *Rapid Commun Mass Spectrom* 26 (2012) 1-8

4:40pm **BN+AS-WeA9 ToF-SIMS Image Analysis of Mouse Diaphragm Muscle Cross-Sections**, *D.J. Graham, N.P. Whitehead, S.C. Froehner, D.G. Castner*, University of Washington

Duchenne muscular dystrophy (DMD) is a common, X-linked, neuromuscular disease, caused by mutations in the dystrophin gene. The absence of dystrophin in DMD patients causes progressive muscle degeneration, characterized by inflammation, fibrosis and failure of muscle regeneration. Profound muscle weakness ensues, ultimately leading to respiratory or cardiac failure, and death around the age of 20 to 30. The *mdx* mouse is a dystrophin-deficient animal model of DMD. In addition to being a model for DMD, *mdx* mice have been found to be resistant to obesity when fed a high fat diet.

In this study we used ToF-SIMS imaging to study the differences in lipid composition of skeletal muscle cross-sections of *mdx* and wild type mice. Results show differences in both the morphology of the tissue and the distribution of lipids within the tissue. For example the *mdx* mouse tissue shows a more loosely organized muscle fiber structure with fibrotic tissue formation, whereas the fibers in the wild type mice show more tightly packed muscle fibers. Understanding differences in lipid composition between these mice can hopefully provide new insight into differences in muscle lipid metabolism and help understand the metabolic pathways that protect *mdx* mice from diet-induced obesity.

5:00pm **BN+AS-WeA10 ToF-SIMS Characterisation of the Distribution and Permeation of Topically Applied Pharmaceuticals**, *D.J. Scurr*, University of Nottingham, UK, *A. Judd*, Keele University, UK, *K. Wan*, University of Central Lancashire, UK, *J. Heylings*, Dermal Technology Laboratory Ltd., UK, *G. Moss*, Keele University, UK

Drug delivery through skin provides opportunities to reduce compliance challenges and is suited to use in environments in the developing world, e.g. micro needle patch delivery of vaccines. In this study, a widely applied chemical antiseptic, chlorhexidine is considered. This is utilised in low concentrations in topical skin treatments where permeation through the stratum corneum of the skin is of particular importance, as insufficient permeation leads to bacterial re-colonisation. Current standard practice for assessing the permeation of this, or any active pharmaceutical ingredient (API), through the upper skin layer is to firstly remove microscopic layers of pre-treated in vitro skin using adhesive tape ('tape stripping'). The removed material is then analysed using high performance liquid chromatography (HPLC) to evaluate the API penetration. The sensitivity of HPLC often requires several tape strips to quantify the API. [1] Using this protocol, the permeation of the API is difficult to confirm and no information regarding lateral distribution is gleaned. Here, we develop a

novel alternative method for assessing the permeation of this molecule within skin tissue and apply this protocol to assess the effectiveness of a permeation enhancing dendrimer pre-treatment.

In order to characterise permeation and lateral distribution of chlorhexidine through the skin, this study uses the high spatial resolution of time of flight mass secondary ion mass spectroscopy (ToF-SIMS) to analyse cross-sectioned skin. The samples are treated with chlorhexidine, cryomicrotomed and analysed by ToF-SIMS under cryo conditions. The results of these studies provide the specific localisation and real permeation depth of the chlorhexidine within the stratum corneum. Additionally, freeze dried tape stripped materials have also been analysed using ToF-SIMS as an independent cross-validation, the results from which support the observations made for the skin cross-sections. This ToF-SIMS methodology has also been applied to demonstrate the increased permeation of chlorhexidine following a dendrimer pre-treatment of the skin. In these samples the secondary ion fragments specific to the chlorhexidine structure are identified at higher intensities and are localised at increased depths within the skin tissue. This methodology which shows great promise in the development of transdermal delivery of pharmaceuticals. The high lateral resolution and molecular specificity complement label based approaches such as confocal microscopy and optical approaches that can function in vivo such as stimulated Raman scattering microscopy.

[1] Wagner et al, (2002) *J. Pharm. Sci.*, 91 (8)

5:20pm **BN+AS-WeA11 Coherent X-ray Microscopy of Vitrified Biological Samples**, *A. Rosenhahn*, Ruhr-University Bochum, Germany, *T. Gorniak, T. Senkbeil, A. Buck, M. Beckers, M.H. Grunze*, Karlsruhe Institute of Technology, Germany

Coherent X-ray microscopy of hydrated biological samples – especially in the 'water window' at photon energies of 284–540 eV – is of tremendous interest for life sciences due to the high contrast of organic matter with respect to the aqueous background. We present recent progress in imaging of biological samples with coherent X-ray microscopy (holography and ptychography) and scanning X-ray nano/microprobe imaging. The main goal is application of these emerging techniques to the in-situ analysis of vitrified biological specimen. Ptychography uses coherent diffraction patterns at different sample positions while maintaining a fixed spatial overlap between the fields of view. By introducing this spatial redundancy to the data an additional constraint for the iterative reconstruction algorithm is achieved. This enhances the convergence of phase retrieval drastically and allows imaging of extended samples. We supplement these results with resonant ptychographic imaging at the oxygen K-edge core level resonances of test particles where both, absorption and phase shifts, revealed information about the chemical composition of the samples. First results on imaging of frozen hydrated specimen and samples in the liquid environment will be shown and discussed.

5:40pm **BN+AS-WeA12 Characterization of Nanoparticles Implanted into Tissues for Enhancement of Ion-Mobility Mass Spectrometry Surface Imaging of Sagittal Brain Sections**, *E.K. Lewis*, Ionwerks, Inc., *J.F. Moore*, MassThink, *T.F. Egan*, Ionwerks, Inc., *B. Chen, B. Brinson*, Rice University, *V.M. Womack, D. Barbacci*, Ionwerks, Inc., *R. Hauge*, Rice University, *A.S. Woods*, National Institute on Drug Abuse / IRP, *J.A. Schultz*, Ionwerks, Inc.

Our research previously included the first demonstration of implanting nanoparticles nanometers below the surface of a biological tissue to provide a completely new method MALDI imaging. Now, we are working towards combining optical histology and molecular surface imaging. We are currently using x-ray photoelectron spectroscopy (XPS) to characterize the nanoparticle coverage, composition, and the depth nanoparticles are implanted into our biological tissue(s). Nanoparticles were implanted at energies from 2-6kV, initial XPS depth profiles demonstrated they are implanted into tissue at depths from 10-30nm. The use of nanoparticulate implantation provides a basis from which future surface imaging techniques can be developed and tested. This method is important in that not only are we preserving the optical histology, and location of lipids and peptides, but MALDI signals are increased on the order of 2-4 times over typical preparation with several orders of magnitude less matrix.

Graphene and Related Materials Focus Topic Room: 13 - Session GR+AS+EM+NS+SS-WeA

Dopants and Defects in Graphene; Graphene Interfaces with Other Materials

Moderator: D. Gunlycke, Naval Research Laboratory

2:00pm **GR+AS+EM+NS+SS-WeA1 Increasing Interface Bonding and Tuning Doping Behavior at Metal-Graphene-Metal Sandwich Contact**, C. Gong, R.M. Wallace, K.J. Cho, Y.J. Chabal, The University of Texas at Dallas

Two types of interfaces can be formed between metals and graphene depending on the strength of the metal-graphene interaction: weak (metal physisorption) and strong (metal chemisorption) interfaces. "Physisorption" interfaces (e.g., with Al, Ag, Cu, Ir, Pt and Au) are characterized by a larger metal-carbon distance ($>3 \text{ \AA}$) with some charge transfer between metal and graphene (i.e. doping of graphene) that maintains its overall π -band dispersion. "Chemisorption" interfaces (e.g. with Ni, Co, Pd, and Ti) are characterized by a smaller metal-carbon distance ($<2.5 \text{ \AA}$) and strong orbital hybridization between metal- d and carbon- p_z orbitals, resulting in the destruction of the graphene's π -band dispersion around the Dirac point. Till now, only a small fraction of all available metals has been used as electrode materials for carbon-based devices due to metal-graphene interface debonding problems. The issue therefore is to keep graphene's intrinsic π bandstructure by using weakly interacting metals while enhancing the interface stability.

We report an enhancement of the bonding energy of weakly interacting metals by using a metal-graphene-metal sandwich geometry, without sacrificing the intrinsic π -electron dispersions of graphene that is usually undermined by strong metal-graphene interface hybridization. This sandwich structure further makes it possible to effectively tune the doping of graphene with an appropriate selection of metals. Density functional theory calculations reveal that the strengthening of the interface interaction is ascribed to an enhancement of interface dipole-dipole interactions. Raman scattering studies of metal-graphene-copper sandwiches are used to validate the theoretically predicted tuning of graphene doping through sandwich structures.

2:20pm **GR+AS+EM+NS+SS-WeA2 Defects in Two-Dimensional Materials and their Heterostructures**, L. Adamska, I.I. Oleynik, University of South Florida

Recent developments in graphene electronics have stimulated an interest in other two dimensional materials such as hexagonal boron nitride (BN) and molybdenum disulfide (MoS_2). In contrast to graphene, BN and MoS_2 possess appreciable band gap and may form good interfaces with graphene, which opens up exciting opportunities for development of novel nanoelectronic devices. For practical applications, it is important to understand the effect of defects, which appear during growth and processing, on resulting electronic properties. The defects in graphene, BN, MoS_2 and their heterostructures have been investigated by first-principles density functional theory. Their effect on electronic properties including density of states and simulated STM images will be discussed.

4:00pm **GR+AS+EM+NS+SS-WeA7 Metal Oxide Growth and Characterization on CVD Graphene**, A. Matsubayashi, College of Nanoscale Science and Engineering, University at Albany

Thin metal oxide layers deposited on graphene can be utilized as dielectric barriers between metals and graphene to help isolate a metal contact from the graphene channel. This is important for graphene based spintronic devices as dielectric layers between the ferromagnetic electrode and graphene have been shown to increase the spin relaxation time measured utilizing non-local detection and spin precession measurements^[1]. However, simply depositing metal oxide layers such as aluminum oxide on graphene results in non-uniform film lowering the quality of the interface barrier^[2]. In addition it is important to understand the stoichiometry of the resulting film. We will present a systematic study of aluminum oxide layers grown on CVD (chemical vapor deposition) graphene under ultra-high vacuum conditions with and without titanium seed layers. The aluminum oxide layers with the titanium seed layers showed reduced surface roughness. The chemical and structural composition determined by XPS (X-ray photoelectron spectroscopy) will be also presented that shows full oxidation of the aluminum and partial oxidation of the titanium.

References:

- (1) E. I. Rashba, Phys. Rev. B, **62**, 16267 (2000)
- (2) W. Han *et al*, Phys. Rev. Lett., **105**, 167202 (2010)

4:20pm **GR+AS+EM+NS+SS-WeA8 Bi-layer Graphene Growth on Ni(111): The Role of Monolayer Graphene Rotation**, A. Dahal, A. Rafik, University of South Florida, P.W. Sutter, Brookhaven National Laboratory, M. Batzill, University of South Florida

Bi-layer graphene synthesis by chemical vapor deposition is of importance for field effect devices because the band gap can be tuned in bi-layer graphene by an applied electric field. Here, we demonstrate that bi-layer graphene can be synthesized above 650°C by chemical vapor deposition on thin Ni(111) films grown on YSZ(111) substrates in ultra high vacuum (UHV). We characterize the bi-layer graphene growth by low energy electron microscopy (LEEM), Auger electron spectroscopy (AES) and low energy electron diffraction (LEED). Below 600°C graphene grows in registry with the Ni(111) lattice and no second layer graphene is formed upon cooling. At 650°C rotationally misaligned graphene domains are formed on Ni(111) and we observe second layer graphene to grow by carbon-segregation under those rotated monolayer graphene domains. The difference in second layer graphene nucleation and growth is explained by the graphene-Ni interaction, which is much stronger for graphene in registry with the substrate than for rotated graphene. The segregated second layer graphene sheet is in registry with the Ni(111) substrate and this suppresses further carbon-segregation, effectively self limiting graphene formation to two layers.

4:40pm **GR+AS+EM+NS+SS-WeA9 Energetic and Kinetic Factors of Graphene Nucleation on Cu**, N. Safron, M.S. Arnold, University of Wisconsin-Madison

Chemical Vapor Deposition (CVD) of graphene on Cu substrates uniquely allows for growth of uniform monolayer graphene and is a promising route for its scalable production for many industrial applications due to low cost. The growth is a purely surface driven process, due to carbon's low solubility in the Cu substrate, and relies on the Cu surface catalytically decomposing a carbon precursor (methane). As the growth of graphene proceeds across the surface, the reactivity of the Cu is passivated by the graphene, making the growth self-limiting to monolayer coverage. Research interest on the control of nucleation is intensifying, as the polycrystalline character of the graphene films can limit mobility, thermal conduction, and mechanical strength via grain boundaries.

In this paper, we study the nucleation dependencies of graphene at ambient pressure CVD in the context of surface nucleation theory. At low methane partial pressures, the concentration of carbon on the surface on the copper is low and carbon clusters cannot grow to a critical size for nucleation. As the partial pressure is increased, the methane partial pressure reaches a critical value and nucleation occurs. Tracking the critical pressure as a function of temperature from 880 to 1075°C , we have determined the formation energy of the critical graphene nucleus to be $\sim 1.5 \text{ eV/carbon atom}$, via the relation $c_{\text{nuc}} \sim \exp(-E_{\text{form}}/k_B T)$. Additionally, we have found that the nucleation density of the graphene varies by 5 orders of magnitude over this temperature range at the critical methane concentration. The results are described under the desorption controlled regime of surface cluster nucleation.

Growths near the critical methane concentration yield hexagonal growing graphene domains characteristic of attachment limited kinetics, while at higher rates yield other growth shapes. Characterization by Raman Spectroscopy has been used to identify defects in the graphene layers. We find that the Raman defect band (D-Band) scales with the root of the nucleation density, indicating the majority of defects are located at the domain boundaries and the D-band intensity scales with the distance between them. Electrical mobility measurements show nearly constant values in samples across the range of temperatures indicating other limiting factors besides internal defects. Growths at 900°C yield $\mu > 1000 \text{ cm}^2/\text{Vs}$, ON/OFF ratio ~ 10 , and Raman D/G ratio < 1 , demonstrating high quality of growth even at relatively low temperatures.

5:00pm **GR+AS+EM+NS+SS-WeA10 Magnetic Spin Reorientation Transition in Graphene Covered Cobalt on Iridium(111)**, A.T. N'Diaye, Lawrence Berkeley National Laboratory, J. Coraux, N. Rougemaille, C. Vo-Van, O. Fruchart, Institut NÉEL, CNRS & Université Joseph Fourier, France, A.K. Schmid, Lawrence Berkeley National Laboratory

One of graphene's promises is to be material for spintronic applications. While the influence of a magnet on graphene is under intense investigation by many groups little attention is given to the influence of graphene on a magnet.

With spin polarized low energy electron microscopy (SPLEEM) we studied thickness dependent spin reorientation transition on this system and compare with Co/Ir(111) without graphene. Monitoring the spin orientation in three dimensions while increasing the film thickness by one ML at a time, we find that the presence of graphene on the film at least doubles the thickness at which the spin reorientation from out-of-plane to in-plane

occurs from 6ML Co to transition to 12ML-13ML at 300°C and to between 14ML and 20ML at room temperature.

We attribute the significant contribution of the graphene/Cobalt interface to the magnetic anisotropy energy to a strong hybridization of graphene with Cobalt in directional bonds.

This work was supported by the U.S. Department of Energy under Contract No. DE-AC02-05CH11231, by the French ANR contract ANR-2010-BLAN-1019-NMGEM and by the Alexander von Humboldt Foundation.

5:20pm **GR+AS+EM+NS+SS-WeA11 Nucleation and Growth of Rh and Au Clusters on Graphene Moiré/Ru(0001)**, *B. Habenicht*, Oak Ridge National Laboratory, *D. Teng*, Georgia Institute of Technology, *L. Semidey-Flecha*, Oak Ridge National Laboratory, *D. Sholl*, Georgia Institute of Technology, *Y. Xu*, Oak Ridge National Laboratory

Nanometer and sub-nanometer sized metal clusters may possess electronic and catalytic properties that differ greatly from those of the corresponding bulk metals. For potential applications, dense arrays of uniform metal clusters are desirable. However, the synthesis of such cluster materials remains a formidable challenge. Moiré superstructures that develop in graphene supported on certain metals have been shown to be viable templates for driving the formation of uniform metal clusters.[1] On graphene moiré (GM) on Ru(0001), dispersed clusters are obtained for Rh whereas Au coalesces into very large 2D islands.[2,3] We carry out a computational study to understand the disparate morphologies of Rh and Au clusters on GM/Ru(0001) via a multi-scale approach. DFT calculations are performed to study the adsorption and diffusion of the adatom and ad-clusters of Rh and Au on GM/Ru(0001) and the bonding mechanism between the metals, graphene, and Ru substrate. The potential energy landscape is then used to perform kinetic Monte Carlo simulations for the diffusion, nucleation, and growth of Rh and Au clusters. This approach allows us to predict the spatial and size distribution of the metal clusters and may be generally applicable to identifying the conditions necessary for obtaining desired cluster morphologies on GM.

(1) N'Diaye, A. T.; Bleikamp, S.; Feibelman, P. J.; Michely, T. *Phys. Rev. Lett.* **2006**, *97*, 215501.

(2) Zhou, Z.; Gao, F.; Goodman, D. W. *Surf. Sci.* **2010**, *604*, L31.

(3) Xu, Y.; Semidey-Flecha, L.; Liu, L.; Zhou, Z.; Goodman, D.W. *Faraday Discuss.*, **2011**, *152*, 267.

5:40pm **GR+AS+EM+NS+SS-WeA12 Graphitic and Pyridinic N Species on N-doped HOPG Studied by STM, STS, PES and DFT**, *M. Sakurai*, *T. Shikano*, *D. Ushigome*, *T. Suzuki*, University of Tsukuba, Japan, *Y. Harada*, *M. Oshima*, University of Tokyo, Japan, *S. Casolo*, University of Milan, Italy, *M.I. Trioni*, ISTM, Italy, *G.F. Tantardini*, University of Milan, Italy, *T. Kondo*, *J. Nakamura*, University of Tsukuba, Japan

Nitrogen doped graphene and carbon nanotube have been reported to show superior catalytic activity or superior support effect in the fuel cell. However, effects of the dopant nitrogen on the modification of the electronic structure of such graphite-related materials have not been clarified because a wide variety of defects with different types of C-N bonding configurations can coexist in nitrogen doped graphite.

Here, we report comprehensive atomic-resolution characterization of the defects in a nitrogen-doped graphite surface by scanning tunneling microscopy (STM), scanning tunneling spectroscopy (STS), Photoemission spectroscopy (PES) and first-principles calculations based on the density functional theory (DFT). Nitrogen-doped graphite was produced by nitrogen ion bombardment of the HOPG (highly oriented pyrolytic graphite) followed by thermal annealing at about 900 K.

Two types of nitrogen species were identified at the atomic resolution. One is pyridinic N (N having two C nearest neighbors) with single-atom vacancy. The other is graphitic N (N having three C nearest neighbors). In the case of pyridinic N with single vacancy, the local electronic states of the non-bonding pz orbital of carbon are found to appear at occupied region near the Fermi level at the carbon atoms around pyridinic N. On the other hand, the local electronic states of the non-bonding pz orbital of carbon are found to appear at unoccupied region near the Fermi level at the carbon atoms around graphitic N.

These results indicate that in both cases more than 300 carbon atoms are found to be modified by the dopant N to show the non-bonding pz orbitals. Moreover, these results suggest that the graphitic-N and pyridinic-N as well

as their surrounding carbon atoms may act as "acid" and "base", because their non-bonding pz orbitals appear at empty and occupied region, respectively.

Helium Ion Microscopy Focus Topic Room: 19 - Session HI+AS+NS-WeA

Basics of Helium Ion Microscopy

Moderator: A. Gölzhäuser, University of Bielefeld, Germany

2:00pm **HI+AS+NS-WeA1 Basics of Imaging with Ions**, *D. Joy*, University of Tennessee **INVITED**

Imaging with a helium ion microscope (HIM) offers numerous advantages, both fundamental and practical, as compared to a conventional scanning electron microscope (SEM). At the same time, however, many aspects of ion microscopy seem very different to those found in the SEM. In this presentation therefore we will examine ;

Why ions are a better choice for imaging than electrons and which ion (or ions) might be the best

In which areas of performance and operation the ion beam image is 'better'

The optimum beam energy for ion imaging for different materials; how typical imaging conditions compare to those for the SEM; and why they are different

The types of signals that are available for imaging in the ion microscope and how they compare with their electron beam counterparts

The problems of specimen charging and beam damage with the ion beams

The options available for microanalysis with the HIM

2:40pm **HI+AS+NS-WeA3 Surface Analysis using Channeling Contrast in NUHV Helium Ion Microscopy**, *B. Poelsema*, University of Twente, Netherlands **INVITED**

Helium Ion Microscopy, HIM, is a novel high-performance technique to image surfaces and with its high resolution, great surface sensitivity, enhanced material contrast, ability to investigate insulating material and large depth of field, it provides a viable alternative to classical scanning electron microscopy. A number of applications require improved vacuum conditions to achieve ultimate performance. The sharply focused He ion beam is, compared to an electron beam in SEM set-ups, very efficient in decomposing, e.g., hydrocarbons present in the chamber and thus on the sample surface, which may obscure a clear view of the sample. Where this phenomenon is beneficial for high resolution structuring, it may well negate the benefits of small spot size and reduce the acquisition time available for spectroscopy in material analysis. To substantially reduce this problem a Near UHV version of the HIM has been developed in close collaboration between the manufacturer, Carl Zeiss NTS, LLC and our group at the University of Twente [1].

We will report on a number of recent observations with special attention for a new contrast mechanism, i.e. dechanneling of ions that extends the high surface sensitivity – usually achieved in secondary electron images – to backscattered ions. We demonstrate [2-4] how monolayer "thick" organic and inorganic films, as well as self assembled monolayers can be visualized, even when adsorbed on heavier substrates, by changes in the backscatter yield. Normally thin layers of a light element on a heavy substrate are "invisible" in backscattered ion yields. The results can be explained semi-quantitatively in terms of changes of the channelling probability. These results highlight the relevance of proper vacuum conditions for achieving monolayer sensitivity.

[1] R. van Gastel, L. Barriss, C. Sanford, G. Hlawacek, L. Scipioni, A.P. Merkle, D. Voci, C. Fenner, H.J.W. Zandvliet and B. Poelsema: *Microscopy and Microanalysis* **17(S2)**, 928-929 (2011)

[2] A. George, M. Knez, G. Hlawacek, D. Hagedoorn, H.H.J. Verputten, R. van Gastel and J.E. ten Elshof: *Langmuir* **28(5)**, 3045-3052 (2012)

[3] G. Hlawacek, V. Veligura, S. Lorbeck, T.F. Mocking, A. George, R. van Gastel, H.J.W. Zandvliet, B. Poelsema: submitted

[4] V. Veligura, G. Hlawacek, R. van Gastel, H.J.W. Zandvliet, B. Poelsema: submitted

Acknowledgments: Gregor Hlawacek, Vasilisa Veligura, Raoul van Gastel, Harold J.W. Zandvliet.

4:00pm **HI+AS+NS-WeA7 Evaluation of W(111) Gas Field Ion Sources Based on Single Atom Tips**, R. Urban, University of Alberta and The National Institute for Nanotechnology, Canada, J.L. Pitters, National Institute for Nanotechnology, NRC Canada, R.A. Wolkow, University of Alberta and The National Institute for Nanotechnology, Canada

Atomically defined tips gained significant attention over the past decade because they serve as high brightness electron and ion sources. The success of the Scanning Helium Ion Microscope is dependent on the development of an appropriate Gas Field Ion Source (GFIS) to generate the helium ion beam. Single atom tips (SATs) represent a unique subgroup of atomically defined tips where emission only occurs from a single atom at the tip apex. Small virtual source size makes these tips attractive candidates for advanced scanning imaging applications such as SEM, TEM, and scanning ion microscopy (SIM) as well as for non-staining ion beam writing applications.

In this study SATs were fabricated from single crystal W(111) wire using a gas and field assisted etching process. By carefully controlling etching parameters SATs with extraction voltages between 5 and 17 kV were formed for various tips. During tip formation, we also used neon as an imaging gas to evaluate a W(111) tip shape during nitrogen-assisted etching. The neon image allows for the observation of atomic structure not available while imaging with helium and helps to elucidate the atomic structure of the tip during and after the etching to a single atom. The field ion microscopy (FIM) patterns (intensity maps) from SAT were fitted with 2D Gaussian curve to evaluate ion beam divergence and amplitude. The divergence of helium beam with respect to helium pressure and applied voltage will be discussed for various SATs.

Angular current density of various SATs was evaluated from their FIM patterns recorded by a microchannel plate and ion current measurements using a Faraday cup. The volume under the 2D Gaussian surface was found to be directly proportional to total ion current carried by an ion beam. The ion current was found to be linearly proportional to He pressure. However, comparing various tips it was found that the ion current increased faster than the extraction voltage. This suggests improved He capture by a broader tip base. The effect of the shape of the base of the tip was also evaluated and it was found that the beam opening angle varied with the size of the tip base leading to a forward focussing effect. The relative angular current densities from SATs supported on different tip curvatures were also evaluated and found to increase at a faster rate than current, also indicating that a forward focusing effect was in effect. This indicates that SATs on large bases would prove optimal for ion current generation in a scanning ion microscope.

4:20pm **HI+AS+NS-WeA8 Single-atom Tip as an Emitter of Gas Field Ion Sources**, I.-S. Hwang, H.-S. Kuo, Academia Sinica, Taiwan, Republic of China, T.-Y. Fu, National Taiwan Normal University, Taiwan, Republic of China, J.-L. Hou, C.-Y. Lin, Y.-H. Lu, W.-T. Chang, T.T. Tsong, Academia Sinica, Taiwan, Republic of China

Thermally and chemically stable single-atom tips (SAT) or nanotips are highly desirable for emission of high-brightness gas field ion beams. In 2001, Fu et al. demonstrated a Pd-covered W(111) SAT through vacuum deposition of an ultra-thin Pd film on a clean W tip surface followed by thermal annealing [1]. Later, Kuo et al. further simplified the preparation process by replacing the tip cleaning and the vacuum deposition with electrochemical processes and successfully prepared several different types of noble metal-covered W(111) SATs [2]. This type of SATs is thermally stable and chemically inert, and thus can be regenerated through a gentle annealing if the apex is contaminated.

We have successfully generated hydrogen, helium, argon, and oxygen ion beams using a Ir/W SAT and characterized these ion sources [3]. The first two lightest ions provide the lowest sputtering rates, which is beneficial for scanning ion microscopy. The argon ion has a large mass and can provide a high sputtering rate, suitable for ion milling. Due to the high secondary ion yields, an oxygen ion beam may be applied to secondary ion mass spectrometry. The ion beam profiles indicate that the half opening angle is $\sim 0.5^\circ$. This single spot indicates that emission occurs only from the topmost atom. This small source size and the small opening angle are particularly favorable for achieving high angular intensity, high brightness, and low spherical aberration, which are important characteristics for a focused ion beam system. The ion current of these gas ion beams are very stable and the tip does not show any degradation under fields above 5 V/Å after a total operation time of 80 hours. Since the SAT can be regenerated for more than 50 times, therefore its lifetime is long enough for most practical applications.

In addition, we have also prepared a pure iridium SAT based on oxygen-induced crystal faceting of the Ir(210) [4]. We have shown that the Ir-SAT can be a good field ion emitter, capable of emitting a variety of gas ion beams, including He^+ , H_2^+ , N_2^+ , and O_2^+ , with high brightness and stability. In particular, nitrogen is a very corrosive gas for metal tips under strong positive electric fields. If we can achieve a stable emission of nitrogen ion,

it also means many other gas field ion beams may also be emitted from this Ir-SAT. This may greatly broaden the application of focused ion beam technology.

[1] T.-Y. Fu et al., Phys. Rev.B **64** (2001), 113401.

[2] H.-S. Kuo et al., Nano Lett. **4** (2004), 2379.

[3] H.-S. Kuo et al., Appl. Phys. Lett. **92** (2008), 063106.

[4] H.-S. Kuo et al., Nanotechnology **20** (2009), 335701.

4:40pm **HI+AS+NS-WeA9 Helium Ions for Imaging and Nanofabrication on the nm Scale**, E. Van Veldhoven, H.H.P.Th. Bekman, F.T. Molkenboer, N.B. Koster, D.J. Maas, TNO Technical Sciences, The Netherlands

The Helium ion microscope (HIM, Zeiss Orion Plus™) has unique features. This microscope unravels a new application area for imaging sensitive and charging surfaces with (sub) nm resolution [1]. The beam-sample interaction generates secondary electrons with low energy and a low quantity of backscattering ions. These properties are very interesting for using the microscope not just for imaging only, but for nanofabrication too [2]. To explore all the capabilities for nanofabrication, the HIM is equipped with a pattern generator (Raith Elphy Multibeam™) and a gas injection system (Omniprobe Omnisig™) to explore direct write, lithography and gas induced applications.

In this contribution we would like to focus on imaging charging materials and our latest results for using the HIM for developing new applications for mainly the Semiconductor Industry. We consider a few HIM-based methods for TEM sample preparation. It is possible to use the HIM for making a thin wedge without significant artifacts like bubble formation and amorphization. With the gas injection system we develop new recipes for very local deposition and etching. These recipes are used for feasibility studies for mask repair and circuit editing. The helium ion microscope offers a novel way for nanofabrication and imaging on the nm scale.

5:00pm **HI+AS+NS-WeA10 Towards Secondary Ion Mass Spectrometry on the Helium Ion Microscope**, T. Wirtz, N. Vanhove, L. Pillatsch, D. Dowsett, Centre de Recherche Public – Gabriel Lippmann, Luxembourg, S. Sijbrandij, J. Notte, Carl Zeiss

The ORION Helium Ion Microscope (HIM) has become a well-established tool for high-resolution microscopy [1]. The high brightness ALIS gas field ion source can operate with helium and, after special prototype modifications, with neon [2]. However, the detection of backscattered atoms can provide only limited specimen composition information. By contrast, Secondary Ion Mass Spectrometry (SIMS) is an extremely powerful technique for analyzing surfaces due to its excellent sensitivity, high dynamic range, very high mass resolution and ability to differentiate between isotopes. In order to get chemical information with a higher sensitivity and a high lateral resolution, we have investigated the feasibility of performing SIMS on the HIM.

Therefore, the secondary ion formation process under He^+ and Ne^+ bombardment has to be investigated and optimized. To investigate secondary ion formation an experimental study was performed; to investigate sputtering effects on resolution and practical implementation aspects a simulation approach was taken.

First, secondary ion yields for different elements sputtered from different materials exposed to helium and neon ion beams were experimentally determined on a test set-up. The basic yields could be increased by several orders of magnitude by using reactive gas flooding (i.e. O_2 and Cs^0 [3,4]). Afterwards, detection limits have been calculated taking into account the experimentally obtained useful yields. Depending on the dwell time, ppm sensitivity can be obtained for Ne^+ bombardment on silicon with oxygen flooding. Second, a detailed study of the sputtering phenomena using TRIM simulations was carried out in order to determine the effect of the collision cascade on the lateral resolution. The diameter (FW_{50}) of the area from which sputtered atoms originate has been determined for 10 keV He^+ and Ne^+ bombardment on different materials. While the obtained results are very encouraging, the practical instrumentation aspects have to be investigated as well in order to obtain a high secondary ion transmission and maintain the excellent primary beam characteristics. Therefore, the practical limitations imposed by adding an extraction system to the HIM have been studied in detail with respect to the extraction geometry.

In general, the combination of high-resolution microscopy and high-sensitivity chemical mapping on a single instrument will lead to a new level of correlative microscopy.

[1] L. Scipioni et al., J. Vac. Sci. Technol. B **27**, 3250 (2009)

[2] F. Rahman et al., Scanning **33**, 1 (2011)

[3] K. Franzreb et al., Surf. Sci. **573**, 291 (2004)

[4] P. Philipp et al., Int. J. Mass Spectrom. **253**, 71 (2006)

Scanning Probe Microscopy Focus Topic

Room: 16 - Session SP+AS+BI+ET+MI+TF-WeA

Emerging Instrument Formats

Moderator: A. Belu, Medtronic, Inc.

2:00pm **SP+AS+BI+ET+MI+TF-WeA1 Electrochemical Strain Microscopy: Nanoscale Imaging of Solid State Ionics**, *S. Jesse*, Oak Ridge National Laboratory **INVITED**

Electrochemical reactions in solids underpin multiple applications ranging from electroresistive non-volatile memory and neuromorphic logic devices memories, to chemical sensors and electrochemical gas pumps, to energy storage and conversion systems including metal-air batteries and fuel cells. Understanding the functionality in these systems requires probing reversible (oxygen reduction/evolution reaction) and irreversible (cathode degradation and activation, formation of conductive filaments) electrochemical processes. Traditionally, these effects are studied only on the macroscopically averaged level. In this talk, I summarize recent advances in probing and controlling these transformations locally on nanometer level using scanning probe microscopy. The localized tip concentrates an electric field in a nanometer scale volume of material, inducing local ion transport. Measured simultaneously, the electromechanical response (piezo response) or current (conductive AFM) provides the information on bias-induced changes in a material. Here, I illustrate how these methods can be extended to study local electrochemical transformations, including vacancy dynamics in oxides such as titanates, $\text{LaSr}_{1-x}\text{CoO}_3$, BiFeO_3 , and $\text{YxZr}_{1-x}\text{O}_2$. The formation of electromechanical hysteresis loops indistinguishable from those in ferroelectric materials illustrate the role ionic dynamics can play in piezoresponse force microscopy and similar measurements. In materials such as lanthanum-strontium cobaltite, mapping both reversible vacancy motion and vacancy ordering and static deformation is possible, and can be corroborated by post mortem STEM/EELS studies. The possible strategies for elucidation ionic motion at the electroactive interfaces in oxides using high-resolution electron microscopy and combined ex-situ and in-situ STEM-SPM studies are discussed. Finally, the future possibilities for probing electrochemical phenomena on in-situ grown surfaces with atomic resolution are discussed. This research was conducted at the Center for Nanophase Materials Sciences, which is sponsored at Oak Ridge National Laboratory by the Scientific User Facilities Division, Office of Basic Energy Sciences, U.S. Department of Energy.

2:40pm **SP+AS+BI+ET+MI+TF-WeA3 Probing Electrochemical Phenomena in Reactive Environments at High Temperature: In Situ Characterization of Interfaces in Fuel Cells**, *S.S. Nonnenmann, R. Kungas, J.M. Vohs, D.A. Bonnell*, University of Pennsylvania

Many strategies for advances in energy related processes involve high temperatures and reactive environments. Fuel cell operation, chemical catalysis, and certain approaches to energy harvesting are examples. Scanning probe microscopy provides a large toolbox of local and often atomic resolution measurements of phenomena at a scale that enables understanding of complex processes involved in many systems. Inherent challenges exist, however, in applying these techniques to the realistic conditions under which these processes operate. To overcome some of these challenges, we have designed a system that allows SPM at temperatures to 850° C in reactive gas environments. This is demonstrated with the characterization of an operating fuel cell. Solid oxide fuel cells (SOFCs) offer the highest conversion efficiencies with operating temperatures ranging from 400° C - 1000° C; and operate under variable gaseous fuel environments – H₂-based environments (anode side) and O₂-based environments (cathode side). Topography and the temperature dependence of surface potential are compared to impedance. While not (yet) at atomic levels of spatial resolution, these probes are at the scale to examine local interface properties.

3:00pm **SP+AS+BI+ET+MI+TF-WeA4 High-Resolution Scanning Local Capacitance Measurements**, *M. Brukman*, University of Pennsylvania, *S. Nanayakkara*, National Renewable Energy Laboratory, *D.A. Bonnell*, University of Pennsylvania

Spatial variation of dielectric properties often dictates the behavior of devices ranging from field effect transistors to memory devices to organic electronics, yet dielectric properties are rarely characterized locally. We present methods of analyzing 2nd harmonic-based local capacitance measurements achieved through non-contact atomic force microscopy. Unlike contact-based methods, this technique preserves tip shape and allows the same probe to realize high-resolution topographic imaging and scanning surface potential imaging. We present an improved analysis of the electrical fields between tip and sample, yielding high sensitivity to the capacitance-induced frequency shift.

The techniques are applied to thin-film ceramics (SrTiO₂ and HfO₂), metals (Pt and Ti), and mixed-phase self-

assembled monolayers to illustrate application over all orders of dielectric constant. Conversion from frequency shift signal to dielectric constant κ is demonstrated, with sub-5 nm spatial resolution and dielectric constant resolution between 0.25 and 1.

4:00pm **SP+AS+BI+ET+MI+TF-WeA7 Experimental Calibration of the Higher Flexural Modes of Microcantilever Sensors**, *J.D. Parkin, G. Hähner*, University of St Andrews, UK

Microcantilevers are widely employed as probes not only in atomic force microscopy [1], but also as sensors for mass [2], surface stress [3], chemical identification [3], or in measuring viscoelastic properties of cells [4].

Use of the higher flexural modes of microcantilever sensors is an area of current interest due to their higher Q-factors and greater sensitivity to some of the properties probed [2]. A pre-requirement for their exploitation, however, is knowledge of their spring constants [5]. None of the existing cantilever calibration techniques can calibrate the higher flexural modes easily.

We present a method that allows for the determination of the spring constants of all flexural modes. A flow of gas from a microchannel interacts with the microcantilever causing a measurable shift in the resonance frequencies of all flexural modes [6]. The method is non-invasive and does not risk damage to the microcantilever. From the magnitude of the frequency shifts the spring constants can be determined with high accuracy and precision. Experimental data for the response of the first four flexural modes of microcantilever beams used in AFM with spring constants in the range of ~0.03-90 N/m will be presented.

The spring constants of the first mode determined using our method are compared to those obtained with the Sader method [7]. Finite element analysis computational fluid dynamics (CFD) simulations of the experimental setup are used to provide an insight into the interaction of the flow with the microcantilever.

References

- [1] F.J. Giessibl, Rev. Mod. Phys. **75**, 949 (2003).
- [2] J.D. Parkin and G. Hähner, Rev. Sci. Instrum. **82**, 035108 (2011).
- [3] A. Boisen *et al.* Rep. Prog. Phys. **74**, 036101 (2011).
- [4] M. Radmacher *et al.* Biophys. J. **70**, 556 (1996).
- [5] G. Hähner, Ultramicroscopy **110**, 801 (2010).
- [6] G.V. Lubarsky and G. Hähner, Rev. Sci. Instrum. **78**, 095102 (2007).
- [7] J.E. Sader, J.W.M. Chon, and P. Mulvaney, Rev. Sci. Instrum. **70**, 3967 (1999).

4:20pm **SP+AS+BI+ET+MI+TF-WeA8 Atomic Imaging with Peak Force Tapping**, *B. Pittenger, Y. Hu, C. Su, S.C. Minne*, Bruker AFM, *I. Armstrong*, Bruker Nano Surfaces Division

As its name implies, Atomic Force Microscopy (AFM) has long been used to acquire images at the atomic scale. However these images usually only show the lattice of atoms in the crystal and do not show individual atomic defects. In order to achieve atomic resolution, researchers have typically had to design their systems for the ultimate in noise performance, sacrificing ease of use, flexibility, and scan size. Recently we have demonstrated that, by using Peak Force Tapping, our large sample platforms (Dimension Icon, Dimension FastScan) are capable of obtaining atomic resolution imaging along with maps of the tip-sample interaction. Unlike standard TappingMode, or FM-AFM, Peak Force Tapping uses instantaneous force control, allowing the system to be insensitive to long range forces while maintaining piconewton level control of the force at the point in the tapping cycle that provides the highest resolution – the peak force. Since the modulation frequency is far from resonance, the technique is less sensitive to the cantilever thermal noise (Brownian motion). In addition to topography, this technique can provide maps of the interaction between the tip and the sample. This is possible since Peak Force Tapping has access to the instantaneous force between tip and sample at any point in the modulation cycle. To study the details of a tip-sample interaction, Atomic Peak Force Capture can acquire the entire force distance curve used to create the interaction maps. These curves can be exported for easy analysis with models of tip-sample interaction. In this talk we will discuss the latest atomic resolution results using Peak Force Tapping and the implications of this with regard to studies of dissolution, crystallization, ordered liquids, and corrosion.

4:40pm **SP+AS+BI+ET+MI+TF-WeA9 Nanoscale Chemical Composition Mapping with AFM-based Infrared Spectroscopy**, C.B. Prater, M. Lo, Q. Hu, Anasys Instruments, C. Marcott, Light Light Solutions, B. Chase, University of Delaware, R. Shetty, K. Kjoller, E. Dillon, Anasys Instruments **INVITED**

The ability to identify material under an AFM tip has been identified as one of the "Holy Grails" of probe microscopy. While AFM can measure mechanical, electrical, magnetic and thermal properties of materials, until recently it has lacked the robust ability to chemically characterize unknown materials. Infrared spectroscopy can characterize and identify materials via vibrational resonances of chemical bonds and is a very widely used analytical technique. We have successfully integrated AFM with IR spectroscopy (AFM-IR) to obtain high quality infrared absorption spectra at arbitrary points in an AFM image, thus providing nanoscale chemical characterization on the sub-100 nm length scale. Employing the AFM-IR technique, we have mapped nanoscale chemical, structural and mechanical variations in multilayer thin films, nanocomposites, polymer blends, organic photovoltaics, and biological materials including hair, skin, and bacterial and mammalian cells. Light from a pulsed infrared laser is directed at a sample, causing rapid thermal expansion of the sample surface at absorbing wavelengths. The rapid thermal expansion creates an impulse force at the tip, resulting in resonant oscillations of the AFM cantilever. The amplitude of the cantilever oscillation is directly related to the infrared absorption properties of the samples, enabling measurements of IR absorption spectra far below the conventional diffraction limit. AFM-IR can be used both to obtain point spectra at arbitrary points and to spatially map IR absorption at selected wavelengths. Simultaneous measurement of the cantilever's contact resonance frequency as excited by the IR absorption provides a complimentary measurement of relative mechanical properties. We have used these techniques to chemically identify individual chemical components in polymer nanocomposites and multilayer films and performed subcellular spectroscopy and chemical imaging on biological cells. Using self-heating probes we have been able to locally modify the state of a semicrystalline polymer and observe the resulting change in absorption spectra on the nanoscale. Using polarization sensitive AFM-IR, we have mapped spatial variations in molecular orientation in electrospun fibers.

5:20pm **SP+AS+BI+ET+MI+TF-WeA11 Quantifying Nanomechanical Properties with Simultaneous AM-FM and $\tan\delta$ Imaging**, T. Mehr, A. Moshar, R. Proksch, I. Revenko, N. Geisse, S. Hohlbauch, D. Walters, J. Cleveland, J. Bemis, C. Callahan, D. Beck, Asylum Research

Frequency-Modulated (FM) is a powerful, quantitative technique for mapping interaction forces between an oscillating tip and sample. Since FM-AFM typically requires the use of three feedback loops, one ongoing challenge has been stable and cross-talk free operation. Amplitude-modulated Atomic Force Microscopy (AM-AFM), also known as tapping mode, is a proven, reliable and gentle imaging method with wide spread applications. Recently, the phase signal of the first resonant mode has been recast in terms of the tip-sample loss tangent.[1] This allows quantitative imaging of a response term that includes both the dissipated and stored energy of the tip sample interaction. Combining AM and FM imaging allows reaping the benefits of both techniques.[2] Because the feedback loops are decoupled, operation is more robust and simple than conventional FM imaging. In this mode, the topographic feedback is based on the AM signal of the first cantilever resonance while the second resonance drive is frequency modulated. The FM image returns a quantitative value of the frequency shift that in turn depends on the sample stiffness and can be applied to a variety of physical models. We will present results on a wide variety of materials as well as discussing quantitative separation of the elastic and dissipative components of the tip-sample interactions.[3]

References

[1] R. Proksch and D. Yablou, Appl. Phys. Lett. 100, 073106 (2012) and R. Proksch, D. Yablou, and A. Tsou, ACS Rubber Division 180th Technical Meeting, 2011-24 (2011).

[2] G. Chawla and S. Solares, Appl. Phys. Lett., 99, 074103 (2011) and R. Proksch and R. C. Callahan, US Patents 8,024,963 and 7,603,891.

[3] R. Proksch and S. V. Kalinin, *Nanotechnology* 21, 455705/1 (2010).

5:40pm **SP+AS+BI+ET+MI+TF-WeA12 Simultaneous Scanning Tunneling and Atomic Force Microscopy with Subatomic Spatial Resolution**, F.J. Giessibl, University of Regensburg, Germany

Frequency-modulation AFM can be combined with scanning tunneling microscopy, yielding a simultaneous data set for current and average force gradient. Ternes et al. [1] have shown that for some metallic contacts, force and current are proportional. The interaction of a tungsten tip with a CO molecule adsorbed on Cu(111), however, yields a much different symmetry and distance dependence of tunneling current and force [2]. The tunneling current yields a gaussian dip over the CO molecule, while the forces show a

strong angular dependence with force fields that vary strongly by distance and angle within the extent of the single front atom, displaying subatomic variations. While the simultaneous acquisition of current and force can reveal new information about the atomic and electronic structure of matter, the tunneling current can modify the atomic forces. This "phantom force" [3,4], a modification of the electrostatic attraction between tip and sample, originates in an alteration of the effective potential difference between tip and sample caused by strongly localized voltage drop induced by the tunneling current. The talk discusses the potential of combined STM/AFM as well as the challenges, in particular with respect to tip preparation and characterization.

[1] M. Ternes et al., *Phys. Rev. Lett.* **106**, 016802 (2011).

[2] J. Welker, F. J. Giessibl, *Science* **326**, 444 (2012).

[3] A.J. Weymouth et al. *Phys. Rev. Lett.* **106**, 226801 (2011).

[4] T. Wutscher et al. *Phys. Rev. B* **85**, 195426 (2012).

Transparent Conductors and Printable Electronics Focus Topic

Room: 7 - Session TC+EM+AS-WeA

Printable and Flexible Electronics

Moderator: G.S. Herman, Oregon State University

2:00pm **TC+EM+AS-WeA1 Metal Oxides and Organic Materials for Printed Electronics**, A. Facchetti, Polyera Corp. and Northwestern U. **INVITED**

Printed electronics is a new technology envisioning the fabrication of electronic devices using printing methodologies instead of conventional photolithography employed in the silicon industry. Metal oxide- and organic-based materials will be key players for this technology. In this presentation I will discuss our latest results in developing new printable organic semiconductors. Furthermore, I will describe amorphous and polycrystalline metal oxide formulations in which the corresponding films can be annealed at temperatures < 250 °C. For instance, solution-processed amorphous tin-doped indium oxide (ITO) films for TFT fabrication at temperatures <250 °C can be achieved by controlling film precursor solution In³⁺ vs. Sn⁴⁺ molar ratio resulting in electron mobilities > 2 cm² V⁻¹s⁻¹ and ~ 20 cm² V⁻¹s⁻¹ for TFTs using SiO₂ and a self-assembled nanodielectric (SAND) as the gate dielectrics, respectively. Finally, a new general strategy for fabricating solution-processed metal oxide TFTs at dramatically lower temperatures (as low as 200 °C for all TFT electrical components) using self-energy generating combustion chemistry will be presented. Our results show that by tuning the gate dielectric-semiconductor interface dramatically enhances performance, yielding In₂O₃, IZO, IZTO, and IGZO /amorphous alumina gate dielectric TFTs having electron mobilities of 40 cm²/Vs and 13 cm²/Vs at T_{anneal} = 250 °C and 200 °C, respectively.

2:40pm **TC+EM+AS-WeA3 Ion Dependence of Gate Dielectric Behavior of Beta-Aluminas in Transparent Oxide Field-Effect Transistors**, Y. Liu, B. Zhang, H.E. Katz, Johns Hopkins University

Sodium beta-alumina (SBA) is an excellent gate dielectric material which can be used in low-voltage (2 V), solution-processed transparent oxide field-effect transistors (FETs). Sodium ions have been experimentally proved to be the origin of the high capacitance observed in SBA gate dielectric. With this discovery, the investigation of dielectric properties of alumina with the incorporation of other alkali metal ions (for example K⁺, Li⁺) becomes compelling.

High field-effect mobility (about 20 cm²·V⁻¹·s⁻¹), high saturation drain current (about 1 mA), and small subthreshold swing (about 200 mV/decade) were achieved in low-voltage (2 V), spin-coated zinc-tin-oxide (ZTO) FETs with potassium beta-alumina (PBA) and lithium beta-alumina (LBA) dielectrics. This proves that the incorporation of alkali metal ions in beta-aluminas is a general route to reduce operation voltage of transistors while achieve excellent electrical performance.

To investigate the effect of alkali metal ions on beta-alumina capacitance, beta-alumina Metal-Insulator-Metal (MIM) capacitors (PBA, LBA, and SBA) were analyzed in a frequency range from 100 Hz to 1 MHz. A tendency for beta-alumina capacitance to increase with increasing atomic number of alkali metal ions was observed. Besides, beta-alumina capacitance was found to decrease as temperature increases and LBA showed the strongest temperature dependence of capacitance. Moreover, capacitance of beta-aluminas with different thickness was measured and they were independent of thickness. With these results, electric double layer (EDL) structure was proposed as one way to explain the high capacitance of beta-alumina dielectrics. Ion exchange experiments showed significant

diffusion of both lithium ion and potassium ion between PBA and LiNO₃ solution; however, a high concentration difference did not seem to cause obvious diffusion of either lithium ion or potassium ion between LBA and KNO₃ solution. This selective ion exchange behavior in beta-aluminas showed that the Al₂O₃ matrix structure would be affected by the alkali metal ions incorporated, and/or that Li ions are much more strongly bound. Thus, varying intercalated ion types and concentrations can be a means of tuning frequency-dependent capacitance of alumina films.

3:00pm **TC+EM+AS-WeA4 Selection Rule of Preferred Doping Site for N-Type Transparent Conducting Oxides**, *S.-H. Wei*, National Renewable Energy Laboratory, *C. Li, J.B. Li*, Institute of Semiconductor Physics, CAS, China

Traditionally, it is believed that the conduction band edges of d^0 or d^{10} oxides are derived mostly from cation s states, thus doping on anion sites is expected to cause less perturbation and produce shallow donor levels in these materials. Using first-principles calculations, we show that although this paradigm is applicable for more covalent oxides such as SnO₂ where F_O is a better n-type dopant than Sb_{Sn}, for more ionic oxides such as ZnO, the conduction band edge actually contains a considerable amount of O s orbitals, thus F_O in ZnO causes larger perturbation and consequently produces deeper donor levels than cation site doping such as Al_{Zn}. The rule that anion site doping is preferred for more covalent oxides and cation site doping is preferred for more ionic oxides for n-type metal oxides should be general and can be used to guide future study of and search for functional oxide materials.

4:00pm **TC+EM+AS-WeA7 Single-Walled Carbon Nanotube Aerogel Based Elastic Conductors**, *K.H. Kim, Y. Oh, I. Lee, M.F. Islam*, Carnegie Mellon University **INVITED**

Flexible conductors of various shapes and sizes with high electrical stability under large elastic stretching and bending are of significant importance in diverse fields ranging from microelectronics to biological implants. A major roadblock in the development of flexible conductors is the disparity between elastomers and stiff conducting materials used in microelectronics. We have developed a novel scheme to create flexible conductors by completely backfilling a prefabricated conducting porous single wall carbon nanotube (SWCNT) three-dimensional network, called SWCNT aerogel, with an elastic polymer polydimethylsiloxane (PDMS). Our approach allowed us to control SWCNT dispersion quality, and tune shapes, sizes and thicknesses of the SWCNT-aerogel/PDMS composite films to make them transparent. The resistance of our stretchable conductors remains nearly unchanged under repeated stretch-release cycles up to a tensile strain of 100% and high bending strain. We believe that the simple but unique fabrication method can be combined with different types of elastic polymers for different electrical, mechanical or biological demands.

4:40pm **TC+EM+AS-WeA9 Networked Metal Nanowire-Polymer Composites for Flexible, Transparent and Conducting Devices**, *S. Narayanan, S. Fu, M.R. Bockstaller, L.M. Porter*, Carnegie Mellon University

Transparent conductive metal oxides (TCOs) exhibit inherent disadvantages such as limited supply, brittle mechanical properties, expensive processing that present major barriers for the more widespread economic use in applications such as flexible transparent conductors. A promising alternative route towards flexible, transparent conductive materials is based on silver nanowire network structures, which can be easily processed from solution. We report a systematic analysis of the effect of nanowire geometry and solution processing on the network characteristics of nanowire deposits, and the associated electronic and optical properties of silver nanowire-based transparent electrodes. Ag nanowire (of average diameter ~100 nm) films drop-cast from solution were shown to exhibit bulk-like electrical conductivity (~2-50 Ω/sq) and high transparency (~70-75%). The electrical properties of nanowire networks were found to be sensitive to geometric parameters of the wire assembly that can be interpreted by use of percolation theory. At concentrations below the percolation threshold the sheet resistance increases dramatically, effecting a marked deviation from bulk-like behavior [1]. The dispersion of Ag nanowires in a conducting medium, like that of a conducting polymer was found to significantly reduce nanowire aggregation and thus decrease the percolation threshold. Preliminary results of spun-cast films of composites of these nanowire networks with PEDOT:PSS show higher transmittances (~79-82%) with similar conductivities (~10-170 Ω/sq) combined with better film forming properties. The use of composites was found to bring about a consistent improvement in electrical conductivity with very little change in the transmittance. Samples prepared on flexible PET substrates showed no degradation in conductivity on flexing thereby showing ample promise for incorporating flexibility in such structures. Through analysis of microstructural characteristics of these films, a quantitative correlation of the density of nanowires with conductivity and transmittance will be

presented. The advantages of using such a composite structure in reducing the percolation threshold will be discussed.

[1] Sukanta De *et al.* ACS Nano 4 12 (2010) 7064-7072

Thin Film

Room: 11 - Session TF+AS-WeA

Thin Films: Growth and Characterization-I

Moderator: M.R. Davidson, University of Florida

2:00pm **TF+AS-WeA1 Studying the Microstructure of Cu₂ZnSn(S,Se)₄ Thin Film Solar Cells**, *L. Zhang, Y. Cao, D.H. Rosenfeld, M. Lu, J. Caspar, C. Chan*, DuPont Central Research and Development

To advance the next generation photovoltaic technology, the new ink-based Cu₂ZnSn(S,Se)₄ (CZTSSe) solar cells have attracted rapid growth attention in the thin film photovoltaic areas. As a potential alternative to CIGS, the CZTSSe technology offers a non-vacuum based and likely low manufacturing cost process with active area efficiency above 9%. In particular, the fact that CZTSSe utilizes only earth abundant elements enables the sustainability & renewability for future green energy demand.

The overall CZTSSe solar cell developed by DuPont scientists consists of multi-layer inorganic structures of ITO/ ZnO/ CdS / CZT(S,Se) / Mo on sodalime glass substrate. A novel synthetic method has been developed to produce the active CZTSSe layer. During the process, binary and ternary chalcogenide nanoparticles are first synthesized as starting materials, formulated into a precursor ink, applied onto a substrate, and then converted into CZTSSe upon a thermal annealing process. To aid product development for optimum efficiency, chemical and structural characterization of the active CZTSSe layer and interfaces between different layers are performed using multiple analytical techniques. For example, sputter depth profiling with XPS and Auger, and cross-section SEM/EDX helped us to visualize the structural chemistry at specific locations in the films which enabled the team to adjust ink formation as well as processing conditions for better and more efficient cell production. This presentation will cover the characterization of CZTSSe solar cells, including the study of film composition and morphology, inter-layer diffusion, and their correlation with device performance.

2:20pm **TF+AS-WeA2 Seed-Mediated Growth of 1D Pyrite (FeS₂) Structures**, *Y.J. Kwon, N. Berry, M. Law, J.C. Hemminger*, University of California Irvine

Iron pyrite is a promising semiconductor for use in solar cells due to its earth-abundance, suitable bandgap, and high absorption coefficient. Pyrite device efficiency is only about 3% due to a low open-circuit photovoltage and high dark current, possibly as a result of sulfur deficiency at the surface resulting in thermionic field emission. Although fabrication of pyrite thin films has been studied by various methods, specific details of the pyrite growth process in the presence of homogeneous nucleation sites has not been studied. In this project, the role of pyrite nucleation sites is investigated in the growth of pyrite thin films by atmospheric-pressure chemical vapor deposition (AP-CVD). The pyrite nanoparticle nucleation sites are fabricated by sulfurization of pre-deposited Fe₂O₃ grains on the step edges of highly oriented pyrolytic graphite (HOPG) using H₂S, elemental sulfur or a combination of the two annealing treatments and characterized by transmission electron microscopy (TEM), X-ray photoelectron spectroscopy (XPS), X-ray diffraction (XRD) and Raman spectroscopy. H₂S-sulfurized Fe₂O₃ nuclei coalesce to form FeS₂ nanowires containing both pyrite and marcasite phases. A subsequent elemental sulfur treatment on either H₂S-sulfurized samples or pre-deposited Fe₂O₃ samples yield pure pyrite; however, the nanowires convert to a less desirable morphology of randomly sized spherical grains as a result of this annealing treatment. Atmospheric Pressure-CVD of FeS₂ from iron-(III) acetylacetonate and *tert*-butyl disulfide was performed to grow pyrite on these seeded substrates. Initial deposition on the H₂S-annealed samples leads to only seed-mediated growth and the formation of linear arrays of polycrystalline FeS₂ nanowires. However, due to marcasite phase presence on pre-covered FeS₂ nanoparticle seeds, both marcasite and pyrite phases could be observed. Initial deposition on elemental sulfur treated samples with pure pyrite phase showed deposition occurring throughout the substrate. No preferential growth on seeded pyrite nucleation sites was observed. It is proposed that during elemental sulfur treatment, new nucleation sites form, leading to deposition covering the substrate. Further work is in process to clearly determine or identify the growth mechanism of

pyrite. In this work, we will gain a greater understanding of early stages of pyrite growth process in the presence of homogeneous nucleation sites.

2:40pm TF+AS-WeA3 Investigation of Recrystallization in Low-Temperature Grown CdTe Solar Cells in Substrate and Superstrate Configuration, L. Kranz, C. Gretener, J. Perrenoud, S. Buecheler, A.N. Tiwari, EMPA, Switzerland **INVITED**

CdTe solar cells and modules on glass substrates have already shown high performance and low cost. Production costs and energy payback time can be further reduced by minimizing the thermal budget of the production process, increasing the throughput and by the use of low-cost substrates. We developed a process for the conventional superstrate configuration which involves substrate temperatures below 450°C. The low temperatures enable the growth on flexible polyimide foil. Efficiencies up to 15.6% and 13.8% on glass and polyimide were achieved, respectively.

In the conventional superstrate configuration sputtered ZnO:Al/ZnO was used as transparent front electrical contact. CdS and CdTe were evaporated at low temperatures of 160 and 350°C followed by an annealing treatment in the presence of CdCl₂ at 420°C and the cells were finished with a metallic electrical back contact. The annealing treatment is essential for highly efficient CdTe solar cells as it leads to grain growth of CdTe, improves electronic properties of CdTe and leads to an intermixing between CdTe and CdS.

For the growth on opaque substrates like flexible metal foils, we developed a growth process of CdTe solar cells in substrate configuration, where light does not need to pass the substrate. It enabled efficiencies of 11.3% and 8.7% on glass and flexible steel foil, respectively.

A combination of Mo, MoO₃ and Te was deposited as back contact and in some cases Cu was added. Evaporated MoO₃ grew with low crystallinity and recrystallized during subsequent processing. CdTe was deposited by vacuum evaporation while CdS was grown by chemical bath deposition. In substrate configuration, the CdTe and CdS layers were annealed separately as a combined annealing step would lead to excessive CdS-CdTe intermixing. The annealing treatment of the CdTe layer leads to similar grain growth as in superstrate configuration. The CdCl₂ treatment after deposition of CdS was optimized, resulting in increased grain size and wurtzite structure. CdS-CdTe intermixing, which is commonly observed in superstrate configuration was less pronounced in substrate configuration. The effects of the recrystallization treatments in substrate configuration are compared to the conventional superstrate configuration.

4:00pm TF+AS-WeA7 High Quality ZnMgO Thin Films Grown on Sapphire and ZnO Substrates by Molecular Beam Epitaxy, M. Wei, R.C. Boutwell, W.V. Schoenfeld, University of Central Florida

Zinc oxide (ZnO) based material is attractive for high efficiency ultraviolet (UV) optoelectronics devices. We will report growth of high quality ZnMgO on both sapphire and ZnO substrate by plasma-assisted molecular beam epitaxy (MBE). With relatively low growth rate and optimized growth condition, we were able to achieve step flow growth of ZnO thin films. ZnO thin films grown on sapphire showed high crystalline quality, low carrier concentration, high mobility and sub-nanometer surface roughness with terrace steps, indicating suitability for UV application. Homoepitaxial ZnO films were grown on both c-plane and miscut ZnO substrates with atomically flat surface, no threading dislocation and same crystallinity as the substrate. Ga doping was demonstrated for ZnMgO films on sapphire and ZnO substrates. This work may lead to the realization of high efficient UV emitters such as Laser diodes.

4:20pm TF+AS-WeA8 Epitaxial Growth of Zirconium Diboride Thin Film on Ge(111) Wafer, C. Hubault, A. Baba, A. Fleurence, Y. Yamada-Takamura, Japan Advanced Institute of Science and Technology

GaN-based semiconductors are widely used in optoelectronic devices. To grow these films, substrates such as sapphire, SiC and Si are used. However, recently, Lieten *et al.* [1] have proposed to grow GaN on Ge(111) substrate to have a more closely matching thermal expansion coefficient and to decrease the lattice mismatch. Despite the good quality of the film, misoriented domain and voids can be found in it. While the domains can be suppressed, the voids cannot, as they come from a diffusion of Ge atoms in the film. This is a problem for the growth of p-type or semi-insulating GaN layers.

Using ZrB₂ as a buffer layer on Ge substrate could help by providing a diffusion barrier. Moreover, ZrB₂ substrate has already been used as a conductive growth template for GaN and has proven to be interesting thanks to the low lattice mismatch and close in-plane thermal expansion coefficient [2]. Therefore, ZrB₂ has been used as a buffer layer for the growth of GaN films on Si wafer [3] and those films were shown to be promising.

It was also demonstrated that on top of ZrB₂(0001) thin film on Si(111) substrate, silicene, which has a similar structure to graphene was present

[4]. In the periodic table, C, Si and Ge are in the same column. Therefore, we can envisage the possibility of the formation of germanene in the same manner as silicene on top of the ZrB₂ layer grown on germanium substrate.

Here, we report on the epitaxial growth of ZrB₂ thin films on Ge(111) by thermal decomposition of Zr(BH₄)₄ in a dedicated UHV-chemical vapour deposition system. The growth was monitored *in situ* by RHEED, and the samples were further analysed by XRD and TEM. The film grows with epitaxial relationship of ZrB₂(0001)/Ge(111). Under slow growth conditions (substrate temperature, T_s=750°C), two types of in-plane orientations, which are rotated by 30° can be observed, while under faster growth condition (T_s=650°C), the layer is monocrystalline. The single-crystalline film has in-plane orientation of ZrB₂[11-20]/Ge[-110], similar to the case of single-crystalline ZrB₂ film on Si(111) [4], but with a different surface reconstruction of (√3x√3) when cooled down under 450°C. There is a good epitaxy between the layer and the substrate with the presence of a second phase at the interface, which tends to disappear when the growth was carried out at 550°C.

[1] R.R. Lieten *et al.*, J. Cryst. Growth, 314, 71 (2011).

[2] H. Kinoshita *et al.*, Jpn. J. Appl. Phys., 42, 2260 (2003).

[3] Y. Yamada-Takamura *et al.*, Phys. Rev. Lett., 95, 266105 (2005).

[4] A. Fleurence *et al.*, Phys. Rev. Lett., accepted for publication.

4:40pm TF+AS-WeA9 Effect of Growth Conditions on Cubic ZnMgO films, C. Boutwell, M. Wei, W.V. Schoenfeld, University of Central Florida

ZnMgO films were grown on MgO substrates by Plasma-Enhanced Molecular Beam Epitaxy. Epilayer morphology, stoichiometry, and crystalline orientation were investigated. Films were produced by varying cation source temperature/flux, substrate temperature, and oxygen plasma power and flow rate. Crystalline immiscibility was determined in the phase mixed cubic/wurtzite range. Growth rate varied from 30nm/hr to 175nm/hr while roughness varied from 4nm to 110nm in cubic to mixed-phase samples. Wurtzite ZnO peaks at (002) and (101) were apparent from θ -2 θ X-Ray Diffraction on phase separated films, indicating multiplanar ZnO crystallite growth on the (001) MgO substrate. Growth condition information will be useful for optimization of optoelectronic devices functional in the deep ultraviolet/solar-blind range.

5:00pm TF+AS-WeA10 Properties of Ytterium Doped Zinc Oxide Thin Films Deposited by r.f. Magnetron Sputtering, K. VanSant, T. Barnes, J. Burst, J. Duenow, T.A. Gessert, National Renewable Energy Laboratory

Transparent conducting oxides (TCOs) based on zinc oxide (ZnO) and aluminum (Al) doped ZnO (AZO) are important for many large-scale commercial applications because they exhibit good optical and electrical properties. Further, their constituent elements are non-toxic and abundant, and high-quality thin-films can be deposited at room temperature using a variety of deposition processes. These characteristics make AZO appealing for use as part of the top contact in copper indium gallium diselenide (CIGS) PV modules. Although the present generation of ZnO-based TCOs meet many of the technical requirements of present-generation technologies, it is known that the material could be much more widely applied if some of its properties were more consistent with another important TCO, In₂O₃:Sn (i.e., ITO). In this comparison, the main properties requiring improvement include increasing the mobility from ~20 to ~50 cm² V⁻¹s⁻¹ while maintaining carrier concentrations > 5x10²⁰ cm⁻³ and improving the moisture-tolerance of the films. Earlier work has already shown that AZO with mobility approaching 50 cm² V⁻¹s⁻¹ can be achieved by careful control of the sputtering ambient and the dopant concentration. This study investigates the use of the Group IIIA material yttrium (Y) as a dopant, as well as the impact it has on the optical properties of ZnO. The Y-doped ZnO films are deposited on glass by r.f. magnetron sputtering using pressed powder targets, and the Y concentration is varied by simultaneous co-sputtering from a ZnO:Y target. The films will be analyzed using a combination of Hall measurements, UV-Vis-NIR spectrophotometry, spectroscopic ellipsometry, and Auger/X-ray photoelectron spectroscopy (XPS) and Secondary Ion Mass Spectrometry (SIMS). Based on prior research related to the addition of zirconium (Zr) to ITO, it is suspected that the addition of Y in ZnO may lead to similar changes in the optical properties of this material. Understanding the functionality of these changes could have significant implications for device applications requiring greater control of the dielectric properties of ZnO.

5:20pm TF+AS-WeA11 Effect of Process Parameters on Molybdenum Thin Films and Development of Single Layer Molybdenum Film for CIGS Thin Film Solar Cells, S. Pethe, A. Kaul, N. Dhere, Florida Solar Energy Center, University of Central Florida

Molybdenum back contact in CuIn_{1-x}Ga_xSe_{2-y}S_y (CIGSeS) solar cells is usually deposited using DC magnetron sputtering. Properties of thin films

are dependent on process parameters. Films deposited at high power and low pressure, tend to be more conductive. However, such films exhibit poor adhesional strength since the films are under compressive stress. Films deposited at low power and high pressure tend to be under tensile stress and exhibit higher roughness and resistivity, while the films adhere very well to the sodalime glass substrate. Therefore, it has been a practice to deposit multi-layered Mo back contact to achieve properties of good adhesion and higher conductivity. Deposition of multi-layered back contact results in either increase in deposition time if a single target is used or increase in footprint if multiple targets are used resulting in increase in the total cost of production. Experiments were carried out to understand effects of working pressure, sputtering power and working distance on molybdenum film properties with the final aim to develop a process recipe for deposition of a single molybdenum film with acceptable properties of both good adhesion and higher conductivity. Experiments were carried out at a fixed working distance by varying the working pressure and keeping the sputtering power constant and then varying the sputtering power keeping the working pressure constant. The same set of experiments were repeated with varying working distance. Moreover, the effect of the relative position of the substrate with respect to the sputtering target for a moving target was studied. Adhesive tape test was performed on each film to determine the adhesional strength of the films. Moreover, the sheet resistance and the average roughness for each film were measured using a four probe measurement setup and the Dektak Profilometer, respectively. All experiments were also carried out on narrow and long glass strips in order to estimate the residual stress in the film by using the bend test method. Based on the results obtained from the experiments carried out a process recipe was developed for depositing on a moving substrate, a single layer molybdenum film with acceptable properties of good adhesion and higher conductivity.

5:40pm **TF+AS-WeA12 Oxygen Reservoir Effect and its Impact on HfO₂**, C. Vallee, C. Mannequin, P. Gonon, L. Latu-Romain, LTM (CNRS / UJF-Grenoble1 / CEA), France, A. Salatin, H. Grampeix, V. Jousseau, CEA, LETI, MINATEC Campus, France

ReRAM device is a non-volatile memory based on resistive switching phenomena in a dielectric in a MIM (Metal Insulator Metal) structure. Depending on the nature of the oxide and the metallic electrode, the switching is based on a unipolar thermochemical mechanism (TCM), a bipolar valence change mechanism (VCM), as well as a bipolar electrochemical metallization mechanism (ECM). For all these devices, the choice of the oxide (nature, crystallization, density, doping, vacancies), the metal (inert electrode, its free energy formation of the oxide) as well as the interfacial layer (role of the electrode, role of the process) are impacting the operation sets and reliability of the device. For example, it has been shown that electrode reaction is one of the major factors determining the functionality of ECM cells [1].

This work is focused on HfO₂ based ReRAMs which are good candidates for embedded non-volatile memories [2-4]. For this material, forming/set and reset processes are correlated with the respective generation of oxygen vacancies and recombination of Vo²⁺ positive charges with oxygen ions (O²⁻). It has been recently proposed that during the negative reset the passivation occurs by the back-diffusion of oxygen ions stored in the oxide portion near the conductive filaments and at the electrode, which serve as oxygen reservoir [5].

With this work we propose to discuss on the reservoir effect by studying HfO₂ memories obtained with top electrodes of different chemical compositions and morphologies. The HfO₂ dielectric (10 nm) is deposited by Atomic Layer Deposition on Pt and TiN. X-ray Photoelectron Spectroscopy and Transmission Electron Microscopy characterization have been used to investigate the chemical composition, morphology and crystalline structure of the oxide and metallic layers. It is hence demonstrated that devices with gold deposited by a PVD process give better results than those obtained with gold deposited by evaporation. This can be related to a modification of oxygen diffusion through the top electrode via a difference in the electrode morphology (roughness, thickness...) induced by the process. Moreover, it is shown that alloying the gold target of the PVD process with a suitable metal considerably helps to improve the reliability of the memory. This is discussed in terms of catalytic effect and modification of the electrode morphology and reservoir effect.

[1] I. Valov *et al*, *Nanotech.* **22** (2011) 254003

[2] P. Gonon *et al*, *J. Appl. Phys.* **107** (2010) 074507

[3] J.J. Yang *et al*, *Appl. Phys.* **A102** (2011) 785

[4] Ch. Walczyk *et al*, *J. Vac. Sci. Technol.* **B29** (2011) 01AD02-1

[5] S. Yu *et al*, *IEDM* (2011) 17.3.1

Thursday Morning, November 1, 2012

Applied Surface Science
Room: 20 - Session AS-ThM

Applications of Large Cluster Ion Beams

Moderator: A.V. Walker, University of Texas at Dallas,
C.M. Mahoney, Pacific Northwest National Laboratory,
M.L. Pacholski, The Dow Chemical Company

8:00am AS-ThM1 Comparison of Primary Ion Beams for XPS Sputter Depth Profiling of Organic Samples, *S.J. Hutton, C.J. Blomfield, S.J. Page, W. Boxford*, Kratos Analytical Ltd., UK

Several types of cluster ion sources are available aimed at facilitating X-ray Photoelectron Spectroscopy (XPS) sputter depth profiling of organic materials. These ion sources may be categorised as either carbon based sources (e.g. Coronene) or Ar cluster ion sources. Both types of source may be fitted to modern XPS instruments. Experimental parameters such as primary ion voltage, primary ion incidence angle and cluster size may be optimised to improve profiling results. The sample environment may also be controlled to extend the range of polymers which are amenable to sputter profiling. Sample parameters which have been shown to be important include rotation with respect to the ion beam and sample temperature.

In this study we compare the performance of Carbon and Ar based cluster ion sources on a range of organic thin films, from fields as diverse as organic PV materials, OLED's, cross-linked plasma polymers and multilayers. Samples were analysed under a range of sample conditions with both sources. Direct comparison allows the efficacy of ion beams to be rated for a range of sample types.

8:20am AS-ThM2 Molecular SIMS - Revolutionized by Cluster Primary Ion Beams?, *J.C. Vickerman*, The University of Manchester, UK **INVITED**

The introduction of metal cluster and polyatomic primary ion beams had dramatically enhanced the capability of SIMS for the molecular analysis of complex, particularly organic materials. The metal cluster beams, based on gold and bismuth resulted in a very significant increase in ion yield of larger 'molecular' ions in the m/z range above 300. This has enabled significant advances in 2D imaging of bio-systems, although the analysis is still restricted to the static regime. Polyatomic ion beams such as SF₅⁺, C₆₀⁺ and Ar_n⁺ (n>50) have introduced a completely new analysis paradigm by enabling analysis and imaging far beyond the static limit such that molecular depth profiling and 3D imaging of organic and biological systems has become possible.

The paper will discuss some of the most recent advances and seek to assess the future opportunities for SIMS analysis using cluster ion beams.

9:00am AS-ThM4 New Organic Reference Materials for Cluster Ion Sputter Depth Profiling, *A.G. Shard, S. Spencer, S. Smith, I.S. Gilmore, R. Havelund*, National Physical Laboratory, UK

Over the past three years, the availability of multilayered organic reference materials has enabled rapid progress in cluster ion beam sputtering for organic depth profiling. These materials have provided manufacturers and practitioners with a common benchmark against which the performance of different experimental methods can be judged. Furthermore, such reference materials are invaluable in providing experimental evidence against which theory can be tested. Reference materials based on Irganox 1010 and Irganox 3114 [1] have been extensively used in this regard [2,3,4]. Results from a VAMAS interlaboratory study, completed in 2011, using argon cluster ion beams as the sputtering source are briefly presented to demonstrate the relevance and utility of these reference materials. These sources demonstrate a remarkable repeatability of better than 1% relative standard deviation in sputtering yield. Depth resolutions close to 5 nm at low impact energies can be achieved. The materials also demonstrate that electrons used for charge compensation can cause very significant molecular damage which affects profiles to a significant depth, often over many tens of nanometers. Whilst this reference material has been extremely valuable, it is not suitable for the full range of analytical methods used in conjunction with cluster ion beam sputtering and may not be representative of all molecular species of analytical interest. As examples, the Irganox 1010 and Irganox 3114 are difficult to distinguish using either XPS or positive SIMS analysis. Alternatives are being studied, such as those materials which are of great commercial importance to the organic electronic industry, e.g. aluminium tris(hydroxyquinolate). In this work, we describe the development of new reference materials including amino acids,

fluorinated compounds, specifically for XPS analysis, and compounds used in organic displays. The precision and accuracy of the layer thicknesses and the stability of the materials will be described along with their performance in cluster ion sputter depth profiling experiments. Additionally, research into a new class of reference material based upon binary mixtures of organic compounds with known compositions will be described.[1] A. G. Shard, F. M. Green, P. J. Brewer, M. P. Seah and I. S. Gilmore, *J. Phys. Chem. B* 2008; 112: 2596.[2] A. G. Shard, R. Foster, I. S. Gilmore, J. L. S. Lee, S. Ray and L. Yang, *Surf. Interface Anal.* 2011; 43: 510.[3] P. Sjovald, D. Rading, S. Ray, L. Yang, and A. G. Shard, *J. Phys. Chem. B* 2010; 114: 769.[4] D. Mao, A. Wucher, and N. Winograd, *Anal. Chem.* 2010; 82: 57.

9:20am AS-ThM5 Characterization of Nano-objects with Nanoprojectile-Secondary Ion Mass Spectrometry, *C.-K. Liang, J.D. DeBord, M. Eller, S. Verkhovurov, E. Schweikert*, Texas A&M University

The uniqueness of nano-objects due to functionalities not present in bulk size is well documented. Yet methods for molecular characterizations of isolated entities below micrometer dimensions are lacking. One reason is the minute amount of sample for analysis; another is that the characteristics of analytical signals from objects of nanoscale dimensions can be affected by their size, shape and environment. Our approach for the characterization of nano-objects is based on the method of event-by-event bombardment-detection. Bombardment is with a sequence of individual nanoprojectiles, specifically Au₄₀₀⁴⁺ accelerated to velocities of up to 30 km/s. The impacts cause abundant secondary ion emission. We will report on the modulation of the ejecta as a function of the nano-objects' size, shape and environment and describe the critical parameters for the accurate assay of their surface and core compositions.

9:40am AS-ThM6 Organic Solar Cell Composition Profiling by Large Clusters Ions: How can we Optimize the Information Retrieved?, *T. Conard, A. Franquet, E. Voroshazi, D. Cheyns, P. Favia, W. Vandervorst*, IMEC, Belgium

Organic material composition profiling has always been very challenging. Recently, it has been shown that using a Gas Clusters Ion Beam source (GCIB) with large Ar-clusters, organic information can be preserved while profiling. However, very little studies have been performed yet about the influence of beam parameters on the spectra/profiles obtained. We investigated systematically the influence of the sputter parameters in a dual beam TOFSIMS experiment (Bi_n⁺/Ar_m⁺) on organic solar cells composed of PCBM and P3HT. Environmental stability of organic solar cells prepared with oxide transport layers is considerably enhanced; hence the critical importance to be able to also investigate organic/inorganic interfaces with large ion clusters.

Qualitatively, it is known that the average energy per atom is an important parameter to keep organic information: For low eV/atom, no sputtering occurs and for high energy per atom, the molecular information is lost. We show for a layer of mixed P3HT:PCBM that the transition to the loss of molecular information occurs sharply at about 6eV/atom, independently of the primary cluster energy. However, we also observe a significant variation of the intensity of the molecular peaks within the energy-region where molecular information is kept. It occurs both towards the higher and the lower eV/atom limits. These are the consequence of the dual beam experiment. At the lower eV/atom limit, the molecular information is lost due to the damage induced by the analysis beam. Towards the higher eV/atom limit, we observed a decrease of the intensity of the molecular PCBM peak by a factor 2 between 2.8 and 4.0 eV/atom. This is interpreted as a partial degradation of the PCBM due to the sputtering.

Composition variations within the formed layers and/or polymer degradation are important for solar-cells devices performances. For a system like PCBM:P3HT mixed layer, one may follow the sulfur intensities throughout the layer as an indirect indication of segregation. This allows, for instance to use of energy-filtered TEM to analyze de-mixing of layers. By comparing TEM and molecular profiling, we show in this study that segregation within layers and degradation of solar cells can be analyzed by dual beam TOF-SIMS.

Finally, the interfaces between the organic and inorganic layers in a solar cell are also critical to the quality of the devices. However, the optimal analysis parameters of inorganic material using cluster ion source may significantly differ from the optimal parameters for organic layers (for instance sputtering rates). We will thus focus on the determination of the best trade-off parameters for heterogeneous systems.

10:40am **AS-ThM9 Molecular Imaging of Cells and Tissues with Ar Cluster Ion Beams**, J. Matsuo, S. Nakagawa, M. Py, T. Aoki, T. Seki, Kyoto University, Japan

Because molecular, structural and chemical state information is considered invaluable in life science, various mass spectroscopic techniques, such as secondary ion mass spectrometry (SIMS), matrix-assisted laser desorption ionization (MALDI) and desorption electrospray ionization (DESI), have been examined intensively during the last decade. The SIMS technique is considered to have the highest spatial resolution, but it is necessary to increase secondary ion yields of bio-molecules. It has been reported that cluster ion beams can enhance the secondary ion yields, because of the high-density energy deposition and multiple collisions near surfaces. Clusters such as SF₅, C₆₀, Au₃, and Bi₃ were found to be quite useful for SIMS of organic materials. Because these primary ion beams cause significant damage on organic surfaces, the primary ion dose is limited to a certain threshold value (known as "the static-limit", ~10¹² ions/cm²). Therefore, the intensity of bio-molecular ions (>500 Da) is too low to obtain high-resolution mass images.

Because Ar cluster ions provide much less damage on the surface than conventional ion beams, much attention is devoted to molecular depth profiling of organic multilayer and molecular imaging with Ar cluster-SIMS. We have developed a new SIMS imaging system with focused Ar cluster ion beam. An orthogonal acceleration time-of-flight (oa-TOF) mass spectrometer, which allows the use of a continuous beam, was employed in a new bio-imaging system. There was no need to use the ion-bunching technique in this system, and therefore there was no need for tradeoff between beam diameter and mass resolution, which is a problem in mass-imaging of biological samples with conventional SIMS. SIMS spectra of cells with Ar cluster ions are quite different from that with Bi₃ ions. Lipid molecular ions found in the mass range over 600 Da, are clearly observed with Ar cluster ions. Furthermore, background level of the spectra with Ar cluster ions is much lower than that with Bi₃ ions. This is attributed to the lower velocity of the primary ions.

The latest results of this system and its performance in molecular imaging of cells and tissues will be presented and discussed.

Acknowledgements

This work is supported by the Core Research of Evolutional Science and Technology (CREST) of Japan Science and Technology Agency (JST).

J. Matsuo, S. Ninomiya, H. Yamada, K. Ichiki, Y. Wakamatsu, M. Hada, T. Seki and T. Aoki, *Surf. Inter face Anal.* (2011) 42, 1612

11:00am **AS-ThM10 Observation of High Ionization Probability for Desorption/Ionization Induced by Neutral Cluster Impact and its Application in Bioanalytics**, B.-J. Lee, M. Baur, University of Applied Sciences Esslingen, Germany, C.R. Gebhardt, Bruker Daltonik GmbH, Germany, M. Dürr, University of Applied Sciences Esslingen, Germany

Desorption and ionization induced by neutral cluster impact is a very soft method for transferring surface-adsorbed biomolecules into the gas phase [1]. The neutral clusters with a mean size of 10³ to 10⁴ molecules are seeded in a He beam which results in a narrow velocity distribution and an energy density of 0.5 to 0.8 eV/molecule. Using SO₂ clusters, the method furthermore makes use of the dipole moment of the cluster's constituents which allows both for solvation and charge transfer processes in the cluster. Thus the cluster provides not only the energy for the desorption process but also serves as a transient matrix. As a consequence, desorption and ionization of oligopeptides and proteins is observed at comparably low energies of the impacting clusters and without any fragmentation of the biomolecules.

In order to quantify the ionization probability during cluster-induced desorption and ionization, samples with well defined amount of substance, especially oligopeptides such as angiotensin II and bradykinin, were prepared by means of drop casting the respective solution on a SiO₂ surface. A biased grid in front of the target was used to transfer ions of one polarity into the time-of-flight mass spectrometer; simultaneously, the correlated ion current from the target was measured. In case of oligopeptides, the positive ion signal is dominant and both positive ion mass spectra and extracted charge per pulse were measured as a function of the number of cluster pulses applied. Comparison of the total charge desorbed from the respective sample with the amount of substance applied then yields the ionization efficiency which was found to be 3 to 4 % in the case of the investigated oligopeptides. The result is discussed with respect to the desorption and ionization mechanism during cluster-surface impact, taking into account the influence of functional groups and preparation conditions.

We furthermore show that desorption and ionization induced by neutral cluster impact can be successfully combined with ion trap mass spectrometry for applications in bioanalytics. Especially when the cluster beam is produced by a pulsed nozzle with pulse duration in the sub-millisecond regime, all ions generated during one pulse can be collected in

the ion trap. In combination with the high ionization efficiency of the process, femtomol sensitivity was achieved in the case of various oligopeptides; multiple sample arrays and low sampling time then allows for batch-type analysis of biosamples.

[1] C. R. Gebhardt, A. Tomsic, H. Schröder, M. Dürr, and K.L. Kompa, *Angew. Chem. Int. Ed.* **48**, 4162 (2009).

11:20am **AS-ThM11 Analysis of Molecular Surfaces Using a Pulsed Beam of Large Argon Clusters**, N. Havercroft, ION-TOF USA, Inc., D. Rading, S. Kayser, R. Moellers, F. Kollmer, E. Niehuis, ION-TOF GmbH, Germany

In the last few years it has been demonstrated that massive argon cluster ions can successfully be applied as primary ion projectiles in SIMS [1-7]. They can not only be applied to sputter organic surfaces without damaging the molecular information, it also has been shown that they desorb larger molecular ions effectively [4] with little fragmentation [2][7]. Although the secondary ion yield decreases with increasing cluster size [4][6], the ability of these projectiles to produce cleaner spectra emphasizing molecular ion signals makes them interesting for analysis purposes as well [5-7]. However, the generation of short primary ion pulses has been difficult due to the large cluster size distribution which typically ranges from hundred to several thousand atoms/cluster. The resulting flight time dispersion of the different cluster sizes determines the primary ion pulse lengths and thus limits the mass resolution.

We equipped a standard TOF.SIMS 5 instrument with a newly developed Ar cluster ion source. The 90° pulsing system of this primary ion gun enables the generation of long as well as short primary ion pulses. The long pulses are suited for sputtering purposes in a dual beam experiment whereas the short pulses are used for high mass resolution TOF-SIMS spectrometry. The pulsing system also allows the selection of a specific cluster size range out of the large distribution with a mass resolution of about 2 for long and 80 for short pulses.

In this study we will apply large Ar clusters ranging from several hundred to several thousand atoms/cluster at different beam energies to a variety of molecular surfaces. We will present and compare data about the influence of the cluster size and beam energy on the sputtering as well as analysis capabilities emphasizing on the spectra appearance and the fragmentation behavior.

[1] N. Toyoda, J. Matsuo, T. Aoki, I. Yamada, D.B. Fenner, *Nucl. Instr. and Meth. in Phys. Res.*, **B 190**, (2002) 860-864

[2] S. Ninomiya, Y. Nakata, K. Ichiki, T. Aoki, J. Matsuo, *Nucl. Instrum. Methods*, **B 256** (2007), 493

[3] S. Ninomiya, K. Ichiki, H. Yamada, Y. Nakata, T. Seki, T. Aoki, J. Matsuo,

Rapid Communications in Mass Spectrometry, **23**, (2009), 1601-1606

[4] K. Mochiji, M. Hahinokuchi, K. Moritani, and N. Toyoda, *Rapid Commun. Mass Spectrom.* **23** (2009) 648

[5] S. Ninomiya, Y. Nakata, Y. Honda, K. Ichiki, T. Seki, T. Aoki, J. Matsuo, *App. Surf. Sci.*, **255** (2008), 1588-1590

[6] S. Rabbani, A.M. Barber, J.S. Fletcher, N.P. Lockyer, J.C. Vickerman, *Anal. Chem.*, **83**, (2011), 3793-3800

[7] S. Kayser, R. Moellers, D. Rading, F. Kollmer, E. Niehuis,

to be published in *Surf. Interface Anal.* SIMS XVIII Proceedings

11:40am **AS-ThM12 Electropray Droplet Impact/SIMS: Some Insights into the Collisional Events**, K. Hiraoka, Y. Sakai, S. Ninomiya, R. Takaishi, University of Yamanashi, Japan

Electropray droplet impact (EDI) uses the water droplets with charge number of 60-300 and masses of 6.2X10⁵-1.6X10⁷ u. The charged droplets impact the sample surface with the velocity of about 12 km/s. Because this value is higher than sound velocities of solids, the supersonic collision takes place at the moment of collision. The supersonic collision is followed by the enormous pressure build-up at the interface and electronic excitation for the species near the colliding interface will follow. The observation of the ionic products by mass spectrometry and the surface analysis by XPS are regarded as the study of the ionization/desorption processes induced by the supersonic collision. For the sample of self-assembled monolayers, only the molecular ions of organic layer but no adducts with gold atoms were observed. In addition, no gold cluster ions but only Au⁺ was observed after Au surface was exposed. This indicates no ablation but atomic- or molecular-level etching takes place in EDI. For all the organic and inorganic samples investigated, no modification of components on the surface was observed after EDI irradiation as far as XPS measurements are concerned. Non-selective etching means that all the elements of the samples are desorbed with the same probabilities. These results suggest that the collisional events taking place in EDI is highly non-thermal. The water

clusters do not penetrate into the sample but they are reflected backward in very short time, maybe in ps. The high ionization efficiency for EDI (useful yield: ~10%) may be explained by the curve crossing mechanism. The sample of AgF was only one example found so far that suffered from surface modification. Due to the very reactive nature of F atoms, the surface was enriched by Ag during EDI irradiation. The CF_3^- and CF_3COO^- ions observed at the start of irradiation decreased and were taken over by $[AgF_3OH]$ and $[CH_3COOAg + CH_3COO^-]$. The enrichment of silver on the AgF sample (i.e., reactive loss of fluorine) is evident. The ions CF_3^- and CF_3COO^- originated from CH_3COOH used for the electrospray of 1 M aqueous CH_3COOH solution. Supersonic collision and followed chemical reactions are complicated and the mechanism of desorption/ionization in EDI remains to be elucidated.

Electronic Materials and Processing

Room: 14 - Session EM+SS+AS+NS-ThM

Nanoelectronic Interfaces, Materials, and Devices

Moderator: M. Filler, Georgia Institute of Technology

8:00am **EM+SS+AS+NS-ThM1 Tensilely Strained Ge Nanomembranes for Applications in Group-IV Infrared Photonics, R. Paiella, Boston University** **INVITED**

Single-crystal semiconductor nanomembranes have emerged as a new materials platform offering unique opportunities for strain engineering, by virtue of their ultrasmall thicknesses that result in extremely high thresholds for plastic deformation under stress. This talk will review our recent work aimed at exploiting this property for the development of CMOS-compatible group-IV semiconductor light sources for the technologically important short-wave infrared spectral region. It is well known that Si, Ge, and related alloys are very inefficient light emitters and generally unsuitable for laser action, due to the indirect nature of their fundamental energy bandgap. A possible solution to this important drawback is provided by the ability of biaxial tensile strain in Ge to lower the conduction-band edge at the direct (G) point relative to the L-valley minima, until at a strain of about 1.9% the fundamental bandgap becomes direct. In our work, mechanically stressed Ge nanomembranes capable of accommodating the required strain levels have been developed, and used to demonstrate strong strain-enhanced photoluminescence. A maximum biaxial tensile strain of over 2% in a 24-nm-thick nanomembrane has been measured, above the accepted threshold for the formation of direct-bandgap Ge. A detailed theoretical model of the light-emission and optical gain properties of tensilely strained Ge has also been developed and applied to the measured luminescence spectra, providing evidence of population inversion at strain levels as low as about 1.4%. More recent work is focused on integrating optical cavities on these strained nanomembranes for the development of infrared photonic active devices.

8:40am **EM+SS+AS+NS-ThM3 Self-activating and Self-limiting Features of the Thermally Assisted Growth Mechanisms of Thin Oxide-, Nitride- and Carbide Films on Si Surfaces at Low Gas or Plasma Pressures, P. Morgen, J. Drews, R. Dhiman, University of Southern Denmark, Z.S. Li, Aarhus University, Denmark**

The thermally assisted growth of oxide-, nitride-, and carbide films on Si surfaces, in direct reactions, carried out with neutral gases or remote plasmas under ultrahigh vacuum background conditions, are self-limiting processes, reaching different thicknesses. The mechanisms have been studied using photoelectron spectroscopies with synchrotron radiation or conventional x-ray induced photoelectron spectroscopy (XS). For the oxidation with neutral oxygen molecules, or microwave-excited remote oxygen plasmas, and for the nitride formation reaction with microwave-excited remote nitrogen plasmas, the "kinetics" (uptake versus exposure plots) is well described with a Hill-function. For the nitrogen reaction, the variation of the temperature causes the Hill parameters to vary because this reaction has more latitude than the oxidation, in temperature range and final thickness, as well as in the resulting structure of the nitride, going from amorphous to crystalline at higher temperatures. One known instance of the "Hill reaction" is a self-activating enzymatic-like reaction, and such a mechanism is believed to be relevant also in our systems. The carbide reaction is different, due to defects in the growing film, which allow a relatively unhindered transport of Si to the surface, where it reacts with carbon species arriving at the surface, from remote microwave-excited plasmas of methane. Thus the limiting thickness of SiC/Si (111) is around 100 nm, while the thickness of oxide is 0.8 nm, and the nitrides between 1 and 3 nm.

9:00am **EM+SS+AS+NS-ThM4 Functional Conductive Polymer to Inexpensive and Portable Chemiresistive Biosensor, D. Bhattacharyya, K.K. Gleason, Massachusetts Institute of Technology**

Extensive research has focused on developing different types of biosensors for detecting bio-threat risks and the occurrence of toxins in the food supplies. However, these food screening processes involve many steps, have high labor costs, reagent costs and time delays of at least 2-3 days to obtain reliable data. Despite the current availability of various types of sensors, limitations of the current state-of-the-art biosensors for molecular recognition of biomolecules are well known. Among these limitations are the unacceptably long process times required for detection and user non-compliance as a result of the excessive weight of the sensor modules coupled with the inflexibility of the sensor platforms for routine uses. Chemiresistive biosensors detect changes in resistance when analyte molecules specifically bind to the sensor surface. Chemiresistive biosensing technique is attractive because it is label-free and can be developed for faster detection of analytes. In this work, oxidative chemical vapor deposition (oCVD) technique is employed for deposition of functional conductive copolymer thin films on the electro-spun fiber mats. The dry oCVD process allowed us to deposit uniform and conformal conducting -OH functional copolymeric film on the electro-spun fiber mat in a single step. For the proof-of-concept of the biosensor application, avidin molecules were covalently immobilized to the -OH functional groups. Various concentrations of biotin solutions were employed as the analytes. The responses and the response times of the devices were significantly improved when the high surface area electro-spun mat were used as a substrate in contrast to a flat substrate.

9:20am **EM+SS+AS+NS-ThM5 Semiconductor Nanomembranes for Biomedical Applications, J.A. Rogers, University of Illinois at Urbana Champaign** **INVITED**

Biology is curved, soft and elastic; silicon wafers are not. Semiconductor technologies that can bridge this gap in form and mechanics will create new opportunities in devices that adopt biologically inspired designs or require intimate integration with the human body. This talk describes the development of ideas for electronics that offer the performance of state-of-the-art, wafer-based systems but with the mechanical properties of a rubber band. We explain the underlying materials science and mechanics of these approaches, and illustrate their use in bio-integrated, "tissue-like" electronics with unique capabilities for mapping cardiac electrophysiology, in both endocardial and epicardial modes, and for performing electrocorticography. Demonstrations in live animal models illustrate the functionality offered by these technologies, and suggest several clinically relevant applications.

10:40am **EM+SS+AS+NS-ThM9 Structure, Dynamics and Mechanism of a Single-Molecule Electric Motor, C.J. Murphy, C.H. Sykes, Tufts University**

Future nano-electronic devices, such as fluid pumps, sensors and switches, will rely on rotating molecules bound to surfaces as key components. To operate these devices, it is important to understand and direct molecular rotation at this interface. We utilized a Low Temperature Scanning Tunneling Microscope (LT-STM) to both drive and measure the rotation of a single asymmetric thioether molecule bound to a copper (111) surface. Due to the hexagonal arrangement of the underlying Cu atoms the rotor molecule has six favorable orientations, with an asymmetrical barrier to rotation around the Cu-S bond. The symmetry of this barrier is dependent on the surface bound chirality. Rotation of the molecule can be driven by either thermal or electrical means. In thermally driven systems, there is no preferred direction of rotation. In order to measure the rate of anisotropic rotation, the system is cooled to 5 K, and a tunneling current is applied to periodically excite the molecule, resulting in a flashing ratchet like mechanism of molecular rotation. The progression of molecular orientations relative to the tip can be determined by the exponential dependence of tunneling current on distance. This allows evaluation of the rate, direction and magnitude of rotation between these orientations in real time. We aim to further interrogate this novel mechanism for electrically-driven motion by quantifying the lifetime of the rotor in each stable orientation and the transitions between these states as a function of tunneling current and voltage.

11:00am **EM+SS+AS+NS-ThM10 Semiconductor Nanostructures for Efficient Thermoelectric Energy Conversion, Z. Aksamija, University of Wisconsin Madison**

Thermoelectric (TE) refrigeration using semiconductor-based nanostructures, such as nanowires, nanoribbons, and superlattices, is an attractive approach for targeted cooling of local hotspots inside integrated circuits due to inherently no moving parts, ease of miniaturization and on-chip integration, and the nanostructures' enhanced TE conversion efficiency. In addition, thermoelectric power generation enables the reuse of

waste heat in a variety of applications, from low-power and energy-efficient designs to internal combustion engines and solar cells. Thermoelectric efficiency, measured by the figure-of-merit ZT , is dictated by the ratio of electronic power factor $S^2\sigma$ over the total thermal conductivity. Consequently, largest gains in TE conversion efficiency have come from the ability to reduce thermal conductivity. This is especially true in nanostructures, where small physical dimensions lead to reduced thermal transport due to the scattering of lattice waves, or phonons, with the boundaries of the nanostructure. The design of efficient semiconductor thermocouples requires a thorough understanding of both charge and heat transport; therefore, thermoelectricity in semiconductor-based nanostructures requires that both electronic and thermal transport are treated on equal footing. SOI nano-membranes and membrane-based nanowires and ribbons show promise for application as efficient thermoelectrics, which requires both high electronic power factor and low thermal conductivity. I will present numerical simulation and modeling of both carrier and phonon transport in ultrathin silicon nanomembranes and gated nanoribbons. We show that the thermoelectric response of Si-membrane-based nanostructures can be improved by employing the anisotropy of the lattice thermal conductivity, revealed in ultrathin SOI nanostructures due to boundary scattering, or by using a gate to provide additional carrier confinement and enhance the thermoelectric power factor. Furthermore, we explore the consequences of nanostructuring on silicon/germanium and SiGe alloy superlattices, and show that the drastic reduction of thermal conductivity in these structures comes from the increased interaction of lattice waves with rough interfaces and boundaries. Finally we demonstrate reduced thermal conductivity in both suspended and supported graphene nanoribbons (GNRs), which exhibit strong anisotropy due to interaction of lattice waves with line edge roughness (LER) and the competition between LER and substrate scattering. The talk will conclude with an outlook for future nanostructured thermoelectric based on nanocrystalline and nanocomposite semiconductors, and nanopatterned graphene.

11:20am **EM+SS+AS+NS-ThM11 UV Ozone Irradiation Induced Defect Formation in Graphene/PZT Devices**, *C.X. Zhang, D.M. Fleetwood, M.L. Alles, R.D. Schrimpf*, Vanderbilt University, *E.B. Song, S. Kim, K. Galatsis, K.L. Wang*, University of California at Los Angeles, *E.X. Zhang*, Vanderbilt University

Graphene based materials are promising candidates for integration into future integrated circuit technologies. Initial studies of the effects of electron-beam and proton irradiation have been performed on graphene materials, but there remain significant questions about the nature of the conductivity and the defects that influence its material and electronic properties. We have found that low-energy x-ray irradiation can lead to significant shifts in the charge neutral point and increases in resistance of suspended graphene layers and graphene layers on SiO_2 . For graphene-on- SiO_2 structures, the reaction oxygen atoms may be supplied either by ozone in the ambient air, or by the adjacent SiO_2 substrate. Similar reactions may be observed for hydrogen, for devices exposed to x-ray and/or UV ozone (UVO) irradiation. Moreover, we also have found that graphene/PZT ferroelectric field-effect transistors (FFETs) are sensitive to UVO irradiation. The conducting channel in these devices is a single graphene layer. The device functions as a nonvolatile memory with reverse hysteresis, where charge trapping and detrapping in the PZT layer leads to a large memory window that is robust to x-ray irradiation and/or memory state cycling. When these devices are exposed to UVO irradiation, the memory window of the device decreases slightly with exposure time. In addition, an increase is observed in the slope of the I-V curves, along with a small positive shift in current-voltage characteristics. These results are consistent with the formation of negatively charged surface states on the graphene layer during the UVO exposure, which are most likely associated with adsorbed oxygen. The degradation in the I-V characteristics recovers somewhat with room temperature annealing. At the AVS meeting, the detailed electrical response will be described, and a physical model will be presented for the UVO degradation and recovery mechanisms.

11:40am **EM+SS+AS+NS-ThM12 Switching Molecular Kondo Effect by Chemical Reactions**, *H. Kim*, ISSP, University of Tokyo, Japan, *Y.H. Chang*, KAIST, Korea, *M.H. Chang*, Korea University, *Y.-H. Kim*, KAIST, Korea, *S.-J. Kahng*, Korea University

Motivated by spintronics applications, the methods to control Kondo effect have been actively studied in magnetic adsorbates on metal surfaces using scanning tunneling microscopy, but they were limited to the processes that required external energy supply from scanning tunneling microscope tip. We report new methods to control molecular Kondo effect by using bimolecular chemical reactions. A chemical binding between diatomic molecules and Co-porphyrin was exploited to switch off, or reset the molecular Kondo effect. The Kondo effect was switched back on using scanning tunneling microscope manipulation as well as thermal desorption. These methods rely on the hybridized pairing of unpaired spins in d_{z^2} and

π^* orbitals of Co-porphyrin and diatomic molecules, respectively, as supported by our density functional theory calculation results. Our study opens up ways to control the molecular Kondo effect using an enormous variety of bimolecular chemical reactions.

12:00pm **EM+SS+AS+NS-ThM13 Quantifying the Local Seebeck Coefficient using Scanning Thermoelectric Microscopy (SThEM)**, *J.C. Walrath, Y.H. Lin, K.P. Pipe, R.S. Goldman*, University of Michigan

Thermoelectric (TE) devices allow reliable solid-state conversion of heat to electricity. The efficiency of a TE device is determined by the figure of merit, ZT , which is sensitive to the Seebeck coefficient, S . Traditional S measurements are used to quantify thermally-induced electron transport on a macroscopic scale. A promising alternative method for nanoscale measurements of S is scanning thermoelectric microscopy (SThEM). In SThEM, an unheated scanning tunneling microscopy (STM) tip acts as a high-resolution voltmeter to measure the thermally-induced voltage, V , induced by a temperature gradient in a heated sample. SThEM has been utilized to measure V across a GaAs p - n junction [1], with the spatial profile of S determined through a comparison of the measured V with a simulation of a network of resistors and voltage sources, based upon a theoretical S -value [2]. Although this approach is useful for predicting the measured V , it does not provide a method for direct conversion of the measured V to a local S . We have developed a Fourier heat conduction model to calculate a temperature profile matrix, thereby enabling direct conversion between the measured V and the local S . According to our model, SThEM can be optimized by fine-tuning several parameters, including the cone angle of the STM tip and the relative thermal conductivity of the tip and sample. We applied our model to SThEM data across a GaAs p - n junction [1] and improved the agreement between the measured and theoretical S by 40%. Our progress towards SThEM measurements of CoSb_3 and InAs quantum dots will also be discussed. This material is based upon work supported by the Department of Energy under Award Number DE-PI0000012. Y.H. Lin and R.S. Goldman are supported in part by DOE under contract No. DE-FG02-06ER46339.

[1] H.K. Lyeo, A.A. Khajetoorians, L. Shi, K.P. Pipe, R.J. Ram, A. Shakouri, and C. K. Shih, *Science* **303**, 816 (2004).

[2] Z. Bian, A. Shakouri, L. Shi, H.K. Lyeo and C.K. Shih, *Appl. Phys. Lett.* **87**, 053115 (2005)

Graphene and Related Materials Focus Topic Room: 13 - Session GR+AS+NS+SS-ThM

Graphene Nanostructures

Moderator: A. Kis, EPFL, Switzerland

8:00am **GR+AS+NS+SS-ThM1 Atomic and Electronic Structures of Graphene Nanoribbon made by MBE on Vicinal SiC Substrate**, *F. Komori, K. Nakatsuji, T. Yoshimura*, University of Tokyo, Japan, *T. Kajiwara, K. Takagi, S. Tanaka*, Kyushu University, Japan

Electronic states of graphene nanoribbon attract much interest because its intrinsic metallic band is modified to have a gap or a one-dimensional edge state at the Dirac energy E_D . Actually, microfabricated graphene [1] showed an energy gap at E_D , and the gap size increases with decreasing the width. Fabrication of well-controlled graphene nanoribbons on macroscopic area of a semiconductor substrate is, however, still one of the challenging issues in graphene research. Here, we report characterizations of graphene nanoribbon made by carbon molecular beam epitaxy (MBE) and a hydrogen treatment on a vicinal SiC(0001) substrate. Use of MBE is essential because graphene is made over the step edges of the SiC substrate in the case of graphene formation by widely-used thermal decomposition.

In the experiment, a $6\sqrt{3} \times 6\sqrt{3}$ structure was first made by MBE on the anisotropic terrace of the Si-terminated surface of a nitrogen-doped 6H-SiC(0001) substrate vicinal to the [1-100] direction. The tilting angle of the substrate was 4 degree, and a well-ordered step-and-terrace structure was made after cleaning the substrate by annealing in hydrogen as confirmed by atomic force microscopy. We optimized the substrate temperature and the carbon deposition rate to make a homogeneous $6\sqrt{3} \times 6\sqrt{3}$ structure on the terraces without thermal decomposition of the substrate. The surface structure was *in situ* monitored by reflection high energy electron diffraction, and the width of the $6\sqrt{3} \times 6\sqrt{3}$ area on the terrace was adjusted by monitoring the $6\sqrt{3} \times 6\sqrt{3}$ spots. After stopping the growth, the sample was exposed to hydrogen molecules at 600 °C to transform the surface $6\sqrt{3} \times 6\sqrt{3}$ layer to single-layer graphene by inserting hydrogen atoms at the interface. [2]

Graphene honeycomb lattice without the $6\sqrt{3} \times 6\sqrt{3}$ structure was confirmed by low energy electron diffraction and scanning tunneling microscopy

(STM). Few point defects are seen at the graphene on the terrace in the STM images of atomic resolution. The width of graphene nanoribbon on the substrate terrace is 10-15 nm, depending on the growth condition. The electronic states of the graphene nanoribbon were studied using angle-resolved photoemission spectroscopy (ARPES) at 130 K as in the previous report. [3] The top of the π band of the graphene nanoribbon was 0.05 ~ 0.25 eV below the Fermi energy. No signal from the π^* band was detected by ARPES above the top of the π band, indicating the gap formation at E_D .

References

1. M. Y. Han *et al.*, Phys. Rev. Lett. **98**, 206805 (2007).
2. C. Riedl *et al.*, Phys. Rev. Lett. **103**, 246804 (2009).
3. K. Nakatsuji *et al.*, Phys. Rev. **B82** 045428 (2010).

8:20am GR+AS+NS+SS-ThM2 Carrier Transport Behavior of Carbon Nanotube Transistors with Single Semiconducting and Metallic Tube, P. Sakalas, M. Schroter, Technische Universität Dresden, Germany

The high interest in using carbon nanotube FETs in advanced electronics is based on their unique 1D transport properties such as quasi-ballistic transport. The high carrier velocity together with the quasi 1D tube geometry yield a very low intrinsic capacitance per tube of approximately 80 aF/mm in multitube structures. Those properties makes CNTFETs very interesting for high frequency and power applications.

CNTFETs with a single semiconducting tube yield too low current (25 μ A) for useful applications and thus the transistors with thousands tubes in parallel are being fabricated [1][2]. Unfortunately, following theory 1/3rd of all tubes are metallic. Carrier scattering is better understood for metallic tubes and it is believed that for semiconducting tubes, despite more complexity, the same scattering mechanisms are applicable: CNTs defect scattering, physical bends and phonon scattering are present. Investigation of CNTFETs with a single semiconducting (ST), single metallic (MT) and metallic+semiconducting (MST) tubes at different lattice temperature environment was never done before and enables a deeper insight of CNT transport properties to further improve the application-oriented device behavior. It was shown that multifinger CNTFETs exhibited a weak temperature dependence of IV, RF and NF indicating a very weak electron-phonon interaction and the absence of charge-carrier freeze-out known for conventional doped semiconductors [3],[4].

In this work transistors with single ST, single MT and double MST were selected. Transistors have 800 nm channel length and features n-type behavior. IV characteristics were measured on wafer for manufacturable CNTFET process selected single CNTs at different lattice temperatures. The investigated structures have a fixed gate length of 0.35 μ m and gate width of 40 μ m. The source-drain spacing (channel length) is 800 nm. A 20 nm thick HfO₂ was used for the gate oxide. The devices were fabricated with the process technology described in [1][2]. The CNTFETs were embedded in DC pads for on-wafer measurements. Transfer characteristics of ST and MT transistor structures at ambient temperature $T_0 = 300$ K, are shown in Fig.1 and Fig.2, Fig.3, Fig.4. The drain current show saturation for ST device, typical for MOSFETs. Nevertheless the carrier transport is very different. The dependence of drain current over the temperature will enable the analysis of transport behavior of single ST and MT and coupled MST. As it is seen from Fig.3 and Fig.4 the MT transistor structure behaves as nonlinear resistor.

8:40am GR+AS+NS+SS-ThM3 Fabrication of Chemically-isolated Graphene Nanoribbons (GNRs) by Scanning Probe Nanolithography using a Heated Probe, W.K. Lee, J.T. Robinson, R. Stine, C.R. Tamana, D. Gunlycke, Naval Research Laboratory, M. Haydell, E. Cimpoiasu, U.S. Naval Academy, W. King, University of Illinois at Urbana Champaign, P.E. Sheehan, Naval Research Laboratory

One route to realizing graphene as a material for digital-type devices is through the lithographic patterning of graphene nanoribbons (GNRs). GNRs enable band gap engineering that is dependent on nanoribbon width and edge state. We employed two complementary AFM-based lithography techniques to pattern GNRs: (1) thermal dip-pen nanolithography (tDPN)¹ and (2) thermochemical nanolithography (TCNL)². Though inverse in approach, both techniques generate GNRs into a larger sheet of insulating chemically-modified graphene. Both lithographies were performed on CVD-grown single-layered graphene (SLG) on SiO₂/Si substrates using heated AFM probes. The first approach, tDPN, used the heated probe to deposit narrow polystyrene (PS) ribbons on pristine graphene. The areas of the graphene not protected by the polymer were then fluorinated, converting them to a highly insulating state, which leaves behind a chemically isolate GNR channel. We show that the PS protected ribbon was the only conductive pathway for active device. Secondly, we use the converse approach by using the heated AFM probe to locally reduce fluorographene back to graphene, leaving behind a conductive GNR channel. Both techniques can generate a wide range of nanoribbon widths while avoiding

electron beams which can damage graphene. We discuss the relative merits of each strategy, as well as their impact on electrical properties (e.g., doping).

1. WK Lee *et al.*, *Nano Letters*, **11**, 5461, 2011
2. Z Wei *et al.*, *Science*, **328**, 1371, 2010

9:20am GR+AS+NS+SS-ThM5 Growth of a Linear Topological Defect in Graphene as a Gate-tunable Valley Valve, A. Zettl, J.-H. Chen, N. Alem, Univ. of California at Berkeley, Lawrence Berkeley Lab, G. Autes, F. Gargiulo, Ecole Polytechnique Fédérale de Lausanne (EPFL), Switzerland, A. Gautam, M. Linck, Lawrence Berkeley National Lab, C. Kisielowski, Lawrence Livermore National Lab, O.V. Yazyev, Ecole Polytechnique Fédérale de Lausanne (EPFL), Switzerland, S.G. Louie, Univ. of California at Berkeley, Lawrence Berkeley Lab

INVITED

The valleytronics, a zero-magnetic-field equivalent of spintronics, could be realized in graphene if a simple scheme can be conceived to generate and to detect valley polarization in the material. Here we provide the first direct experimental observation of the self-sustained, atomically controlled growth of a peculiar linear defect structure in suspended graphene. The structure consists in units of octagon and pentagon pairs (termed 5-5-8 defect) and can be grown from a single pentagon seed in graphene under electrical bias. First-principle simulations show that the 5-5-8 defect can act as a gate-tunable valley valve. The result represents a critical step towards realizing valleytronics in graphene.

10:40am GR+AS+NS+SS-ThM9 Crystalline and Electrical Properties of Vertically-Laminated Carbon Nanowalls formed by Two-Step Growth Method, H. Kondo, T. Kanda, Nagoya University, Japan, M. Hiramatsu, Meijo University, Japan, K. Ishikawa, M. Sekine, M. Hori, Nagoya University, Japan

Carbon nanowall (CNW) is one of carbon nanomaterials consisting of stacked graphene sheets, which are vertically standing on the substrate. Due to the unique properties of graphene sheets, such as high carrier mobility, large current carrying capability, and so forth, it is expected that the CNW also have such the excellent electrical and physical properties. On the other hand, in the CNWs, the bending and branching graphene sheets take a maze-like form. Therefore, due to their unique morphology and properties, the CNWs are promising as channel and electrode materials in the various types of the future nanoelectrics devices. At the construction of the CNW devices, vertical lamination of different types of CNWs is one of the useful and important technique as basic elements of the devices.

In this study, we investigated sequential two-step growth of CNWs to form the vertically-laminated structures. In this experiment, two types of CNW growth processes with different conditions were sequentially performed on Si substrate by an electron beam excited plasma-enhanced chemical vapor deposition (EBEP-CVD) using CH₄/H₂ mixture gas. Firstly, the CNW was grown at 600°C and 2.67 Pa for 10 min. Then, the second-step growth process was performed at 480°C for 10 min. The CNW samples formed only by the single-step growth at 480°C or 600°C were also prepared for comparison. Morphology and crystalline structures of CNWs were analyzed by scanning electron microscopy and Raman spectroscopy.

In the case of the single-step growth, only after the growth at 600°C, about 600 nm-thick CNWs were formed, although CNWs hardly grew at 480°C. On the other hand, in the case of the step-growth, about 1200 nm-thick CNWs were formed after the second-step growth at 480°C, compared to the single-step growth at 600°C. No boundary was found between the lower and upper region. The stacks of graphene sheets formed seamless structures. According to the Raman spectra, the crystalline structures of the CNWs were hardly changed even after the first-step growth at 600°C and the second-step growth at 480°C. This result means that the nanographene can restart to grow easily and continuously at the edges of the previously-grown graphene even at 480°C without the nucleation. These results indicate the possibility to realize the vertical junction of different types of CNWs, such as a p-n junction. At the session, the interfacial structures and electrical properties of the vertically-laminated CNWs will also be discussed.

11:00am GR+AS+NS+SS-ThM10 Surface Modification of Vertically Oriented Graphene Electrochemical Double-Layer Capacitors, R.A. Quinlan, Naval Surface Warfare Center, Carderock Division, M. Cai, The College of William and Mary, A.N. Mansour, Naval Surface Warfare Center, Carderock Division, R.A. Outlaw, The College of William and Mary

Previously reported efforts have identified the potential of vertically oriented graphene nanosheets in electrochemical double-layer capacitors (Miller *et al.*, *Science* 2010) for efficient AC line-filtering performance. Continued investigations to improve performance suggest that the availability of a high edge and surface defect density could be the dominant mechanism. Furthermore, charge/discharge profiles over time show that

performance can actually increase as the device ages. In an effort to understand these findings, X-ray photoelectron spectroscopy, Auger electron spectroscopy and near edge absorption fine structure spectroscopy have been utilized to study the interaction of the electrolytes and solvents with the graphene-based electrode materials. The EDL capacitance of graphene nanosheets has been measured before and after Ar plasma bombardment for various times and after exposure to water, isopropanol, methanol, NaOH and KOH. Graphene nanosheet electrochemical capacitors have been disassembled and analyzed following short term and long term operation.

11:20am **GR+AS+NS+SS-ThM11 Electronic Properties and Device Applications of Wafer-Scale Graphene Nanoribbons**, *D. Jena*, University of Notre Dame **INVITED**

Graphene boasts unique physical, electronic, and optical properties. For conventional electronic device applications, the zero band gap of 2-dimensional graphene is an impediment. Opening of effective band gaps can be achieved by field-effect in bilayer graphene, or by using Klein-tunneling properties of graphene p-n junctions. However, these methods appear not to effectively scale to small dimensions. Another way to open band gaps in graphene is to make graphene nano ribbons (GNRs) and use size quantization. Though many of the properties of 2D graphene are lost in the process, GNRs become similar to semiconducting carbon nanotubes, but with planar structures and compatibility with conventional lithographic processes. In this talk, I will present our group's research progress in making such wafer-scale GNR transistors. Band gaps ~0.15 eV appear in ~10 nm wide single GNRs, and band gaps are preserved in parallel arrays of GNRs. Based on these GNRs, we measure current drives as high as 10mA/micron, which far exceeds all other semiconductor materials and seems attractive for both logic and interconnect applications. The effects of edge roughness on scattering and mobility, and the progress towards making GNR-based tunneling transistors will also be presented.

Helium Ion Microscopy Focus Topic

Room: 19 - Session HI+AS+BI+NS-ThM

Imaging and Lithography with the Helium Ion Microscope

Moderator: A. Götzhäuser, University of Bielefeld, Germany, V.S. Smentkowski, General Electric Global Research Center

8:40am **HI+AS+BI+NS-ThM3 Helium Ion Microscopy of Photonic Structures in Biological Systems**, *S.A. Boden, A. Asadollahbaik, H.N. Rutt, D.M. Bagnall*, University of Southampton, UK **INVITED**

The natural world is replete with examples of biological systems that have developed complex micro- and nano-scale structures to interact with light. Such structures, which include thin film multilayers, diffraction gratings, graded index layers and 2D and 3D photonic crystals, acting alone or in combination, allow the realization of a range of optical effects that would be impossible through the use of pigmentation alone. These effects range from the vivid iridescence observed on the skin of some species of bird, through the vibrant metallic sheen of some beetle species, to the dramatic interference patterns seen on the transparent wings of some species of fly. Lepidoptera (an order of insects that includes butterflies and moths) also provides a rich seam of examples of structural color ranging from the antireflective nipple arrays found on the eyes and wings of some species of moth to the photonic crystal structures producing vivid coloration on the wings of some butterfly species.

As these optical effects are a result of the scale of these structures being at or below that of visible light wavelengths, scanning electron microscopy (SEM) is often used to explore their form and to offer insights into their function. Recently, helium ion microscopy (HIM) has emerged as a surface imaging technique, similar to SEM but with the benefits of higher resolution and a larger depth of field. Here, HIM is used to probe the structures responsible for a number of optical effects observed in Lepidoptera. Images will be presented showing the fine details of the ribs and cross-ribs found on the highly-absorbing black ground wing scales of *Papilio ulysseus* (Blue Mountain Butterfly) and the complex gyroid 3D photonic crystal structure observed underneath the top lamina on vividly green wing scales from *Parides sesostris* (Emerald-patched Cattleheart). Other examples will include the antireflective close-packed nipple array on the wings of *Cephonodes hylas* (Pellucid Hawk Moth), and cross-sections of the multilayer structures that make up the various colored wing scales of *Chrysidia rhipheus* (Madagascan Sunset Moth).

The integrated electron flood gun on the helium ion microscope is employed to neutralize charge build-up, allowing samples to be imaged without the need of a conductive coating. This ensures that the natural surface itself is imaged at high resolution and details are not obscured by coating artefacts. In addition, by taking advantage of the large depth of field available with HIM, stereo pairs are generated to extract information on the three-dimensional nature of these structures.

9:20am **HI+AS+BI+NS-ThM5 Imaging of Carbon Nanomembranes (CNM) and Graphene with Helium Ion Microscopy**, *H. Vieker, A. Beyer, A. Polina, A. Willunat, N.-E. Weber, M. Bünenfeld, A. Winter, X. Zhang, M. Ai, A. Turchanin, A. Götzhäuser*, Bielefeld University, Germany

We present a Helium Ion Microscopy (HIM) study of carbon nanomembranes (CNMs). CNMs are extremely thin (~1 nm) nanolayers consisting only of surface. They are made via cross-linking of self-assembled monolayers (SAMs) with large-area exposures of electrons, photons or helium ions and a subsequent transfer to suitable substrates. Patterned radiation exposures allow the fabrication of perforated nanomembranes, e.g., nanosieves. After annealing at temperatures above 800K, CNMs become conductive and eventually transform into graphene. HIM images of CNMs with different precursor molecules are shown, and images of graphene from SAMs are compared with the CVD grown graphene. Capabilities of the HIM imaging of freestanding CNMs and graphene will be discussed.

10:40am **HI+AS+BI+NS-ThM9 Dopant Contrast in Helium Ion Microscopy**, *Y. Chen, H. Zhang, D. Fox, C.C. Faulkner, J. Wang, J. Boland, J. Donegan*, Trinity College, Ireland **INVITED**

Innovation in metrology is crucial to the future of semiconductor industry, since the miniaturization of transistors demands novel characterization technologies at and beyond the nanometre scale. Recent research has demonstrated that dopant contrast in the Helium-ion Microscope (HIM) is plausible and the HIM is a competitive platform for quantitative secondary-electron (SE) dopant mapping in terms of throughput, sensitivity, and resolution. However, the contrast mechanism of SE imaging is still debatable and it hinders further development of the technique. In this research, quantitative HIM dopant contrast of gallium-doped silicon samples has been investigated and compared with the contrast observed in a scanning electron microscope (SEM). Beam-sample interaction, signal general, as well as detection configuration have been considered via using a range of detectors in the two microscopes. It has been found that the Everhart-Thornley (E-T) secondary electron detector attached to HIM provides similar contrast to the images acquired from the InLens detector attached to SEM, while contrast reversal is observed with the SEM E-T detector. The contrast reversal also depends on the Dwell time. We have confirmed that the HIM is more sensitive to type-I SEs and a capacitance model based on charging effect has been proposed to explain the contrast reversal. Our results indicate that quantitative dopant contrast in the HIM is promising, while charging effect and imaging conditions must be carefully considered.

11:20am **HI+AS+BI+NS-ThM11 High Resolution Patterning of Carbon Nanomembranes and Graphene via Extreme UV Interference Lithography: A Helium Ion Microscopy Study**, *A. Winter, A. Willunat, A. Beyer*, University of Bielefeld, Germany, *Y. Ekinci*, Paul Scherrer Institute, Switzerland, *A. Götzhäuser, A. Turchanin*, University of Bielefeld, Germany

Two-dimensional (2D) carbon materials like graphene, graphene oxide, carbon nanomembranes (CNMs) or ultrathin polymeric films have recently attracted enormous interest due to their potential use in electronics, chemical and biological sensors, nanofilters, hybrid materials, etc. Most of these applications require lithographic patterning of these 2D carbon materials with the nanoscale resolution. In this respect, Extreme UV Interference Lithography (EUV-IL) provides both large-scale patterning and high resolution with an ultimate limit in the sub-10 nm range. We employ EUV-IL to generate nanopatterns in ~1 nm thick CNMs and graphene. We characterise these nanopatterns with a Helium Ion Microscope (HIM). Its high surface sensitivity and lateral resolution provide excellent conditions for imaging of the topographic and chemical features in CNMs and graphene. The possibility to routinely fabricate and characterize the nanopatterns via EUV-IL and HIM on various technologically relevant insulating substrates (e.g., oxidized silicon wafers, glass, and quartz) and with the resolution below 20 nm shows high potential of both techniques for applications in carbon-based nanotechnology.

11:40am **HI+AS+BI+NS-ThM12 Application of Helium Ion Microscope on Processing and Characterization of Nano Wires, H.X. Guo, S. Nagano, K. Onishi, D. Fujita**, National Institute for Materials Science (NIMS), Japan

Scanning helium ion microscope (SHIM) is advanced in high resolution and high focal depth of secondary electron imaging and Rutherford backscattered ion imaging.[1] It also employed in the nano pattern or fabrication on surface and other various structures, such as 2D materials, graphene.[2] It is an excellent candidate for the nano processing of 1D nano structures, such as nanowires and nanotubes.

Rhenium trioxide (ReO₃) is an unusual transition metal oxide with high electrical conductivity close to that of metals. It is well investigated for the applications of photovoltaics[3], catalyst[4], and tip for scanning tunneling microscope[5]. Various ReO₃ nano structures such as nano particles[3,6], nano wires[7], and core-shell structures have been synthesized and characterized by different methods.

In this research, ReO₃ nanowires were synthesized by a physical vapor deposition method. Etched by the helium ion beam, the diameter of part of the nanowire was decreased. During this processing, the structure and transport properties of the ReO₃ nanowire were modified with a controllable method. In this presentation, we will show the structure and properties characterization of the etched nanowires by using scanning probe microscope (SPM), transmission electron microscope (TEM) and other methods. An *in-situ* transport properties measurement system with SHIM will also be introduced in the presentation.

[1] J. Morgan, J. Notte, R. Hill, and B. Ward, *Microsc. Today*, **14**, 24(2006)

[2] D. C. Bell, M. C. Lemme, L. A. Stern, J. R. Williams, and C. M. Marcus, *Nanotech.*, **20**, 455301(2009).

[3] S. V. Bhat, S. B. Krupanidhi, and C. N. R. Rao, *Appl. Phys. Express*, **3**, 115001(2010)

[4] E. Cazzanelli, M. Castriota, S. Marino, N. Scaramuzza, J. Purans, A. Kuzmin, R. Kalendarev, G. Mariotto, and G. Das., *J. Appl. Phys.*, **105**, 114904 (2009)

[5] S. I. Ikebe, D. Shimada, T. Akahane, and N. Tsuda., *Jpn. J. Appl. Phys.*, **30**, L405(1991)

[6] K. Biswas and C. N. R. Rao, *J. Phys. Chem. B*, **110**, 842, (2006).

[7] D. Myung, Y. Lee, J. Lee, H. K. Yu, J. L. Lee, J. M. Baik, W. Kim, M. H. Kim, *phys. status solidi-R*, **4**, 365 (2010)

Magnetic Interfaces and Nanostructures

Room: 6 - Session MI+SP+AS-ThM

Emerging Probes in Magnetic Imaging, Reflectometry and Characterization

Moderator: Z. Gai, Oak Ridge National Laboratory, V. Lauter, Oak Ridge National Laboratory

8:00am **MI+SP+AS-ThM1 Toward Microscopy with Direct Chemical and Magnetic Contrast at the Atomic Level, V. Rose**, Argonne National Laboratory **INVITED**

In this talk we will discuss the development of a novel high-resolution microscopy technique for imaging of nanoscale materials with chemical, electronic, and magnetic contrast. It will combine the sub-nanometer spatial resolution of scanning tunneling microscopy (STM) with the chemical, electronic, and magnetic sensitivity of synchrotron radiation. [1] Drawing upon experience from a prototype that has been developed to demonstrate general feasibility, current work has the goal to drastically increase the spatial resolution of existing state-of-the-art x-ray microscopy from only tens of nanometers down to atomic resolution. The technique will enable fundamentally new methods of characterization, which will be applied to the study of energy materials and nanoscale magnetic systems. A better understanding of these phenomena at the nanoscale has great potential to improve the conversion efficiency of quantum energy devices and lead to advances in future data storage applications. The combination of the high spatial resolution of STM with the energy selectivity afforded by x-ray absorption spectroscopy provides a powerful analytical tool.

Work at the Advanced Photon Source, the Center for Nanoscale Materials, and the Electron Microscopy Center was supported by the U. S. Department of Energy, Office of Science, Office of Basic Energy Sciences, under contract DE-AC02-06CH11357.

[1] V. Rose, J.W. Freeland, S.K. Streiffer, "New Capabilities at the Interface of X-rays and Scanning Tunneling Microscopy", in Scanning

Probe Microscopy of Functional Materials: Nanoscale Imaging and Spectroscopy, S.V. Kalinin, A. Gruverman, (Eds.), Springer, New York (2011), pg 405-432.

8:40am **MI+SP+AS-ThM3 Effect of Sub-Micrometer Scale Magnetic Inhomogeneity on the Magnetoelectric Coupling in Manganites, A. Biswas**, University of Florida **INVITED**

The conventional magnetoelectric (ME) coupling in multiferroics is defined as the effect of a magnetic/electric field on the electric-polarization/magnetization. However, the strength of the ME coupling is usually small. Our recent results have revealed methods for significantly increasing the ME coupling in perovskite manganites and can be summarized in two broad categories: (1) in the phase separated manganite (La_{1-y}Pr_y)_{1-x}Ca_xMnO₃ (LPCMO), we have discovered that anisotropic strain leads to a fluid-like ferromagnetic material which can be manipulated using an electric field leading to an unconventional ME coupling [1,2] and (2) an ME coupling in BiMnO₃ (BMO) thin films which is about 30 times larger than previously observed in single phase multiferroics [3]. I will discuss the origin of the ME coupling in both multiferroic and phase-separated oxides and relate it to inhomogeneous magnetic properties of the thin films, measured using techniques such as low temperature scanning probe microscopy, spin-polarized neutron reflectometry, and strain dependent electric polarization. Acknowledgement: NSF DMR-0804452

1. Dhakal et. al., *Phys. Rev. B* **75**, 092404 (2007)

2. Jeon et. al., *Phys. Rev. B* **83**, 064408 (2011)

3. Jeon et. al., *J. Appl. Phys.* **109**, 074104 (2011)

9:20am **MI+SP+AS-ThM5 Impact of Interfacial Magnetism on Magnetocaloric Properties of Thin Film Heterostructures, C.W. Miller**, University of South Florida **INVITED**

In an effort to understand the impact of nanostructuring on the magnetocaloric effect, we have grown and studied gadolinium in W(5nm)/Gd(30nm)/W(5nm)₈ heterostructures. The entropy change associated with the second-order magnetic phase transition was determined from the isothermal magnetization for numerous temperatures and the appropriate Maxwell relation. The entropy change peaks at a temperature of 284 K with a value of approximately 3.4 J/kg K for 30 kOe field change; the full width at half max of the entropy change peak is about 70 K, significantly wider than that of bulk Gd under similar conditions. The relative cooling power of this nanoscale system is about 240 J/kg, somewhat lower than that of bulk Gd (410 J/kg). Polarized neutron reflectometry was used to determine the depth profile of the magnetic moment per Gd atom, m_{Gd} . Despite sharp interfaces observed by transmission electron microscopy, m_{Gd} is systematically suppressed near the Gd-W interfaces. Because the peak magnetic entropy change is proportional to $m^{2/3}$, the maximum achievable magnetocaloric effect in Gd-W heterostructures is reduced. By extension, our results suggest that creating materials with Gd-ferromagnet interfaces may increase the m_{Gd} relative to the bulk, leading to enhanced magnetocaloric properties. Together, these observations suggest that nanostructuring may be a promising route to tailoring the magnetocaloric response of materials.

Supported by AFOSR and NSF.

10:40am **MI+SP+AS-ThM9 Polarized Neutron Reflectometry on Exchange Biased Thin Films, K. Temst**, KU Leuven, Belgium **INVITED**

Polarized neutron reflectivity has established itself as an important tool in the study of magnetic thin film systems. It provides a high-resolution magnetic depth profile and it offers vectorial probing of the magnetization. In recent years polarized neutron reflectivity has played an influential role in elucidating the magnetic structure of exchange bias systems, i.e. structures in which a ferromagnetic layer is coupled to an antiferromagnetic layer. Exchange bias leads to a remarkable shift of the hysteresis loop, an increase in coercivity, and often a pronounced asymmetry of the hysteresis loop shape as well as a complex magnetic history. With this contribution we will take a closer look at two such exchange bias systems and highlight the role of polarized neutron reflectivity.

As a first model system, the archetypal exchange bias system Co/CoO will be highlighted. The antiferromagnetic CoO layer is prepared by oxidizing the surface of a Co thin film, by exposing it to a reduced oxygen atmosphere. We will review the properties of exchange bias in surface-oxidized Co thin films, with the emphasis on the asymmetry of the magnetization reversal mechanism and the training effect. We will also discuss how the training effect can be (partially) restored by applying a magnetic field perpendicular to the initial cooling field direction. Recently we explored an alternative way to establish exchange bias between Co and CoO: rather than creating the antiferromagnetic CoO layer by oxidizing a metallic Co layer, the antiferromagnetic CoO is produced by implantation of oxygen ions into a Co layer. Polarized neutron reflectivity (PNR) is used

to determine the magnetic depth profile and to probe the magnetization reversal mechanism. Simultaneously with the PNR measurements, in situ anisotropic magnetoresistance measurements were carried out.

The second example is a ferromagnet/antiferromagnet FePt/FePt₃ bilayer in which complementary use is made of polarized neutron reflectivity (for studying the magnetic depth profile in the ferromagnetic layer) and nuclear resonant scattering of synchrotron x-rays (making use of the Mössbauer effect) to probe the antiferromagnetic FePt₃ layer. Below the Néel temperature, antiferromagnetic order appears in the FePt₃ layer with a spin wavevector pointing along the [100] axis. A net magnetization of the FePt₃, which increases towards the FePt/FePt₃ interface is found.

This work was supported by the Fund for Scientific Research-Flanders (FWO), the KULeuven Concerted Research Action program (GOA/09/006), the Belgian Interuniversity Attraction Poles research programs (IAP P6/42), and the KULeuven BOF (CREA/07/005) program.

11:20am **MI+SP+AS-ThM11 Soft X-ray Microscopy to Study Complexity, Stochasticity and Functionality in Magnetic Nanostructures**, *P. Fischer, M.-Y. Im*, Lawrence Berkeley National Lab, *S.-K. Kim*, Seoul National University, Republic of Korea

Research in magnetism is motivated by the scientific curiosity to understand and control spins on a nanoscale and thus to meet future challenges in terms of speed, size and energy efficiency of spin driven technologies. Imaging magnetic structures and their fast dynamics down to fundamental magnetic length and time scales with elemental sensitivity in emerging multi-element and nanostructured materials is highly desirable. Magnetic soft X-ray microscopy is a unique analytical technique combining X-ray magnetic circular dichroism (X-MCD) as element specific magnetic contrast mechanism with high spatial and temporal resolution [1]. Our approach is to use Fresnel zone plates as X-ray optical elements providing a spatial resolution down to currently 10nm [2] thus reaching out into fundamental magnetic length scales such as magnetic exchange lengths. The large field of view allows to investigate both the complexity, but also the stochasticity of magnetic processes, such as nucleation or reversal. Utilizing the inherent time structure of current synchrotron sources fast magnetization dynamics such as current induced wall and vortex dynamics in ferromagnetic elements can be performed with a stroboscopic pump-probe scheme with 70ps time resolution, limited by the lengths of the electron bunches.

We will present studies of magnetic vortex structures, where we found a stochastic character in the nucleation process, which can be described within a symmetry breaking DM interaction [3]. We will also present time resolved studies of dipolar coupled magnetic vortices, where we find an efficient energy transfer mechanism, which can be used for novel magnetic logic elements [4].

This work was supported by the Director, Office of Science, Office of Basic Energy Sciences, Materials Sciences and Engineering Division, of the U.S. Department of Energy under Contract No. DE-AC02-05-CH11231.

[1] P. Fischer, *Exploring nanoscale magnetism in advanced materials with polarized X-rays*, Materials Science & Engineering R72 81-95 (2011)

[2] W. Chao, P. Fischer, T. Tyliczszak, S. Rekawa, E. Anderson, P. Naulleau, *Optics Express* **20(9)** 9777 (2012)

[3] M.-Y. Im, P. Fischer, Y. Keisuke, T. Sato, S. Kasai, Y. Nakatani, T. Ono, *Symmetry breaking in the formation of magnetic vortex states in a permalloy nanodisk*, (2012) submitted

[4] H. Jung, K.-S. Lee, D.-E. Jeong, Y.-S. Choi, Y.-S. Yu, D.-S. Han, A. Vogel, L. Bocklage, G. Meier, M.-Y. Im, P. Fischer, S.-K. Kim, *NPG - Scientific Reports* 1 59 (2011)

11:40am **MI+SP+AS-ThM12 Elemental and Magnetic Contrast using X-ray Excited Luminescence Microscopy**, *R.A. Rosenberg, S. Zohar, D. Keavney*, Argonne National Laboratory, *A. Mascarenhas, M. Steiner*, National Renewable Energy Laboratory, *D. Rosenmann, R.S. Divan*, Argonne National Laboratory

We have developed an imaging technique based on x-ray excited luminescence microscopy (XELM), that will enable elemental and magnetic specific imaging of a wide range of materials such as those used in solar cells, magnetic materials, spintronic devices, ferroelectrics, and solid-state lighting. This new scientific tool utilizes the benefits of pulsed, polarized, tunable synchrotron radiation excitation with microscopic detection of the resulting optical emission. A unique offshoot of the microscope is the ability to perform element specific magnetic microscopy of micron-sized features or domains in magnetic fields. X-rays transmitted through thin films are attenuated and the resultant absorption spectrum can be determined by changes in the substrate luminescence. Since many substrates, such as SrTiO₃ and GaAs, used in thin film growth have intense optical emission, this tool should impact many materials where photoelectron emission microscopy (PEEM) cannot be performed since it is not useable on insulating materials or if magnetic or electric fields are

required. This approach will be especially useful at low temperatures where luminescence yields are highest, and PEEM has difficulties. In this presentation we will present some initial results from the microscope on some prototype solar cell materials and lithographically patterned Permalloy/GaAs and Permalloy/Cu/Co/GaAs samples. The results demonstrate the potential of XELM for elemental and magnetic specific imaging.

This work was performed at the Center for Nanoscale Materials and the Advanced Photon Source. It was supported by the U.S. Department of Energy, Office of Science and Office of Basic Energy Sciences under the contract number DE-AC02-06CH11357 and by the Department of Energy, Energy Efficiency and Renewable Energy, Solid State Lighting Program.

Transparent Conductors and Printable Electronics Focus Topic

Room: 7 - Session TC+EM+AS+TF+EN-ThM

Transparent Conductors and Devices

Moderator: L.M. Porter, Carnegie Mellon University

8:20am **TC+EM+AS+TF+EN-ThM2 High Conductivity in Thin ZnO:Al Deposited by Means of the Expanding Thermal Plasma Chemical Vapor Deposition**, *K. Sharma, H.C.M. Knoops, M.V. Ponomarev*, Eindhoven University of Technology, The Netherlands, *R. Joy, M. Velden, D. Borsa, R. Bosch*, Roth and Rau BV, Germany, *W.M.M. Kessels, M. Creatore*, Eindhoven University of Technology, The Netherlands

Session: Transparent Conductors and Devices

The ever-increasing demand for transparent conducting oxides (TCO) for application in flat panel displays, light emitting diodes (LEDs), and thin film photovoltaics drives the present research in the field of TCOs. Aluminum-doped zinc oxide (ZnO:Al) is often referred to as a potential alternative to e.g. indium tin oxide. The ZnO:Al is considered appealing due to the relatively low cost, high abundance, non-toxicity, resistance to H₂ etching and, under specific conditions, surface texturing for light management/trapping. Thin ZnO:Al films (~ 100 nm) with low resistivity ($2.5 \cdot 10^{-4} \text{ ohm}\cdot\text{cm}$) along with high transmission (> 85 %) are desirable in many devices. Furthermore, large area processing/ high throughput are essential pre-requisites for industrial applications.

ZnO:Al thin films (< 150 nm) have been deposited by using an in-line industrial expanding thermal plasma chemical vapor deposition (ETP-CVD) technique,^{1,2,3} by means of O₂/diethylzinc/trimethylaluminium mixtures. High diethyl zinc flow rate conditions² were applied, which enable the development of a conductive ($5 \cdot 10^{-4} \text{ }\Omega\cdot\text{cm}$), 300 nm-thick ZnO:Al layer by promoting the development of a densely packed structure at early stages of growth, as very recently reported.²

In the present contribution, the effect of the dopant, i.e. trimethylaluminium, is investigated to further improve the electrical quality of even thinner ZnO:Al layers. ZnO:Al films were analyzed with spectroscopic ellipsometry, four point probe, hall measurements, X-ray photon spectroscopy (XPS), Rutherford backscattering (RBS), elastic recoil backscattering (ERD), and X-ray diffraction (XRD).

A remarkable low resistivity of $5 \cdot 10^{-4} \text{ }\Omega\cdot\text{cm}$ was measured for a ZnO:Al film with thickness of only 120 nm, characterized by a carrier concentration of $1 \cdot 10^{21} \text{ cm}^{-3}$, with an electron mobility in the range of $10\text{-}25 \text{ cm}^2/\text{V}\cdot\text{s}$.^{2,3} The obtained mobility values are higher than previously reported value of $13 \text{ cm}^2/\text{V}\cdot\text{s}$ for 300 nm thick ZnO:Al.² The improvement in terms of conductivity is attributed to the large hydrogen content ($2\text{-}4 \cdot 10^{21} \text{ at/cm}^3$) promoting the chemical passivation of the grain boundaries.

A broad characterization of highly conductive thin ZnO:Al films along with insights on charge transport process will be presented.

Reference List

1. B. Hoex *et al.*, *Progress in Photovoltaics* **13**, 705 (2005).
2. M. V. Ponomarev *et al.* *Journal of Applied Physics* **112**, 043708 (2012).
3. M. V. Ponomarev, *et al.*, *Journal of Applied Physics* **111**, 063715 (2012).

8:40am **TC+EM+AS+TF+EN-ThM3 Recent Progress in Oxide Semiconductors and Oxide TFTs**, *H. Hosono*, Tokyo Institute of Technology, Japan **INVITED**

Transparent conductive oxides (TCOs) and transparent oxide semiconductors (TOSs) have a long history since 1950s. The material design concept for TCOs looks almost established, i.e., ionic oxides p-block metals with an electronic configuration of $(n-1)d^{10}ns^0$ and a spatial spread of ns

orbitals which is enough to have large overlap with neighboring metal ns orbitals irrespective of intervening oxygen ion¹). Concretely, most of the TCOs have been realized in the material systems of $\text{In}_2\text{O}_3\text{-SnO}_2\text{-CdO-Ga}_2\text{O}_3\text{-ZnO}$. Materials based on light metal oxides such as Al_2O_3 and SiO_2 have not been regarded as the candidates of TCOs. In 2002, we²) reported high electronic conductivity in $12\text{CaO}\cdot 7\text{Al}_2\text{O}_3$ (C12A7) which had been a typical insulator and this discovery was followed by transparent conductivity in cubic SrGeO_3 in 2011.³) These two materials are TCOs realized by a new material design concept.

As for TOS, the striking advances are seen in transparent amorphous oxide semiconductors (TAOS) in science and technology due to strong demand for active layer materials in thin film transistors (TFTs). Amorphous In-Ga-Zn-O (IGZO) TFTs, which was first reported in late 2004,⁴) has adopted to drive high resolution displays of new iPad.⁵) This is a first mass production of TOS family. The major reasons for this adoption are high electron mobility (an order of larger than that of a-Si:H) and easy fabrication process. A major advance in TOS-TFTs is realization of p-channel TFTs and subsequent fabrication of C-MOS using ambipolar SnO.⁶)

In this talk, I review these progresses viewed from electronic state of these materials.

- 1) H. Kawazoe, H. Yanagi, K. Ueda, and H. Hosono. *MRS Bull.*, 25, 28 (2000)
- 2) K. Hayashi, S. M. Suishi, T. Kamiya, M. Hirano, H. Hosono. *Nature* 419, 462 (2002).
- 3) H. Mizoguchi, T. Kamiya, S. Matsuishi, H. Hosono. *Nat. Commun.*, 2, 470 (2011).
- 4) K. Nomura, H. Ohta, A. Takagi, T. Kamiya, M. Hirano, H. Hosono. *Nature* 432, 488 (2004).
- 5) Sharp Press Release April 6, 2012
- 6) K. Nomura, T. Kamiya, and H. Hosono. *Adv. Mater.*, 23, 3431 (2011)

9:20am **TC+EM+AS+TF+EN-ThM5 Surface Functionalization of Amorphous Zinc Tin Oxide Thin Film Transistors**, G.S. Herman, M.S. Rajachidambaram, Oregon State University, A. Pandey, S. Vilayrganapathy, P. Nachimuthu, S. Thevuthasan, Pacific Northwest National Laboratory

Amorphous zinc tin oxide semiconductor materials have been studied primarily as the active semiconducting material for thin film transistors (TFT) for applications including transparent and flexible electronics. Due to the amorphous nature of these materials excellent uniformity can be obtained over large areas while still having reasonably high electron mobilities ($>10\text{ cm}^2/\text{Vs}$). Considerable control over the electrical properties of ZTO can be maintained, where insulating, semiconducting, and conductive films can be obtained by varying the processing and post-annealing conditions. We have recently characterized sputter-deposited zinc tin oxide (ZTO) as the active material for TFTs and found that the switching properties of ZTO are closely related to deposition, post-annealing, and electrical test conditions. In this presentation we will discuss bias stress induced instabilities for ZTO TFTs. We have found that devices with a backchannel exposed to the atmosphere have a positive subthreshold shift under positive bias, which can be well explained by a stretched exponential model. Using this model the shifts may be related to either electron trapping at the dielectric semiconductor interface or due to metastabilities of the active material. We have found that the adsorption of a self-assembled monolayer (SAM) on the backchannel of the TFT effectively passivates the device and significantly reduces the bias stress induced instabilities. In this study we will present contact angle measurements and x-ray photoelectron spectroscopy to better understand the interaction of the SAM with the ZTO surface, and the improved stability of the ZTO TFTs will be discussed in regards to the interfacial chemistry of the backchannel.

9:40am **TC+EM+AS+TF+EN-ThM6 Work Function and Valence Band Structure of Oxide Semiconductors and Transparent Conducting Oxides Grown by Atomic Layer Deposition**, A. Yanguas-Gil, Argonne National Laboratory, R.T. Haasch, University of Illinois at Urbana Champaign, J.A. Libera, J.W. Elam, Argonne National Laboratory

Atomic Layer Deposition offers a low-temperature, scalable route to the synthesis of a wide range of oxide semiconductors and transparent conducting oxides both in flat and high aspect ratio surfaces. We have carried out studies on the influence of concentration and spatial distribution on the electrical properties within the $\text{ZnO-SnO}_2\text{-In}_2\text{O}_3$ compositional map, including standard TCO materials such as Al:ZnO and ITO. We will present results on the work function and valence band structure of transparent conducting oxides grown by ALD using ex-situ UPS measurements, including the influence of the surface termination on the interfacial properties of the materials. Finally, the ability of ALD to tailor the surface and interfacial properties of TCOs based on its layer-by-layer nature will be discussed.

10:40am **TC+EM+AS+TF+EN-ThM9 Low Temperature, High Performance Solution-Processed Metal Oxide Thin Film Transistors formed by a 'Sol-Gel on Chip' Process**, H. Siringhaus, University of Cambridge, UK **INVITED**

N-type amorphous mixed metal oxide semiconductors, such as ternary oxides, where M^1 and M^2 are metals such as In, Ga, Sn, Zn, have recently gained momentum because of high carrier mobility and stability and good optical transparency, but they are mostly deposited by sputtering. To date only limited routes are available for forming high-performance mixed oxide materials from solution at low process temperature $< 250^\circ\text{C}$. Ionic mixed metal oxides should in principle be ideal candidates for solution processible materials because the conduction band states derived from metal s-orbitals are relatively insensitive to the presence of structural disorder and high charge carrier mobilities are achievable in amorphous structures. Here we report the formation of amorphous metal oxide semiconducting thin films via a 'sol-gel on chip' hydrolysis approach from soluble metal alkoxide precursors, which affords unprecedented high field-effect mobilities of $10\text{ cm}^2/\text{Vs}$, reproducible and stable turn-on voltages $V_{\text{on}} \gg 0\text{V}$ and high operational stability at maximum process temperature as low as 230°C . We discuss the effect of film composition on device performance and stability.

11:20am **TC+EM+AS+TF+EN-ThM11 In Situ Measurements of Interface States and Junction Electrical Properties of Electrically Biased Metal / $\beta\text{-Ga}_2\text{O}_3$ Structures**, H. Pham, X. Zheng, B. Krueger, M.A. Olmstead, F.S. Ohuchi, University of Washington

A significant issue in application of wide-band-gap transparent conducting oxides is formation of reliable ohmic and rectifying metal contacts. The metal-oxide interface properties are dominated by chemical reactions during growth and the resultant interface state distribution once the interface is formed. We have investigated interface formation between the wide band gap TCO $\beta\text{-Ga}_2\text{O}_3$ ($E_g = 4.8\text{ eV}$) and the metals Pd, Ni, Ti and Al with in-situ x-ray photoemission spectroscopy (XPS) both during growth and during sputter profiling. The two techniques give very similar results, demonstrating that in this case sputter profiling does not significantly alter the interface chemistry. Consistent with the relative compound heats of formation, Ni and Pd show very little interface reaction with either Ga or O, while Ti interacts strongly with both Ga and O and Al interacts primarily with oxygen. Electrically, Ni and Pd have similar Schottky barriers on the intrinsically n-type oxide (about 0.9 eV), Ti forms a symmetric, nearly ohmic contact, while Al exhibits a smaller barrier (about 0.6 eV). To probe the nanoscopic origins of the Schottky contact behavior through the interface state energy distribution, we combined *in-situ* deposition of thin metal layers and application of forward/reverse biases to the metal-oxide junction with XPS measurements of the relative positions of the Ga_2O_3 bands (via the Ga 3d or O 1s core level) and the metal Fermi level. The density of interface states determines the rate at which the Fermi level can be moved through the oxide band gap, so variation of the oxide core-level shift with respect to the bias voltage yields the interface state density. We find the metal and oxide bands maintain their relative alignment under forward bias (back-plane negative with respect to metal), while they separate at a rate about half that of the applied bias under reverse bias (positive bias with respect to metal).

11:40am **TC+EM+AS+TF+EN-ThM12 Atmospheric Pressure Dielectric Barrier Discharge (DBD) Post Annealing of Aluminium Doped Zinc Oxide (AZO) Films**, Y.L. Wu, E. Ritz, J. Hong, T.S. Cho, D.N. Ruzic, University of Illinois at Urbana Champaign

Aluminum-doped Zinc Oxide (AZO) is a material that has high electrical conductivity while being highly transparent at the same time. It could find many useful applications in our daily lives such as displays, mobile devices, solar cells, etc. Currently AZO films are considered as attractive alternatives to materials such as Indium Tin Oxide (ITO) due to its much cheaper cost and comparable high electrical conductivity. A process of depositing AZO film by dual DC magnetron system has been developed. Film thicknesses were measured to be about 300nm by stylus contact profilometer and transparency of greater than 90% in the visible range were measured with spectrophotometry methods. Film conductivities were in the order of 10^{-3} Ohm-cm with the four-point probe method. By using a Dielectric Barrier Discharge operating at atmospheric pressure, conductivity of film can be further lowered. A 500mm x 30mm line source operating at a Nitrogen flow of 250L/min was used and $\sim 0.4\text{L/min}$ Hydrogen gas was also introduced into the discharge system to create Hydrogen radicals. A 10%-15% decrease in electrical resistance was observed with no changes in the optical properties of the AZO films. The elemental composition of the film was measured by X-ray photoelectron spectroscopy (XPS) and the change of crystal structure after DBD post annealing was measured by X-ray diffraction (XRD).

Thursday Afternoon, November 1, 2012

Applied Surface Science
Room: 20 - Session AS-ThA

Applications of Large Cluster Ion Beams - Part 2 (2:00-3:20 pm)/ Surface

Analysis using Synchrotron Techniques (3:40-5:40 pm)

Moderator: A.V. Walker, University of Texas at Dallas, C.M. Mahoney, Pacific Northwest National Laboratory, M.L. Pacholski, The Dow Chemical Company, A. Herrera-Gomez, UAM-Azcapotzalco and CINVESTAV-Queretaro, Mexico

2:00pm AS-ThA1 Applications of a C60 Ion Source for Surface Chemical Analysis: It's Not Just for Polymers, W.F. Stickle, M.D. Johnson, D. Bilich, HP

While C60⁺ ion sources are becoming one of the routinely used tools in the surface chemical analysis laboratory its primary value has been for the study of organic systems. Commonly used for ToF SIMS, the C60⁺ ion source is also a standard option for photoelectron spectroscopy tools. But many surface analysis laboratories study a wide variety of materials, not just organic thin films, which raises the question as to using this novel ion source for 'routine' analyses. Being able to use of this ion source in a 'routine' fashion requires characterization and understanding of the surface that is being created during the ion milling process. It is important to understand the sputter induced chemistry that may be created by the C60⁺ source as well as understanding the physical changes that occur to a sample surface during the ion milling. The effects of preferential sputtering, chemical changes or reactions and the nature of surface roughening than can occur will be presented. Several different material systems are examined and discussed with regard to using a C60⁺ ion gun for enhancing and clarifying 'routine' analyses. The different types of samples to be discussed will include inorganic oxides, multilayer structures as well as metal-metal oxide layered structures and polymers.

2:20pm AS-ThA2 Towards Ultimate Organic Depth Profiling using Argon Cluster Beams – Recommendations for Dual Beam Profiling and Sample Charge Compensation, R. Havelund, A.G. Shard, M.P. Seah, I.S. Gilmore, National Physical Laboratory, UK

The recent innovation of large argon cluster ion sources has revolutionised the ability of SIMS to give 3D chemical images of important classes of organic materials, such as organic electronic materials. Furthermore, sputtering with argon clusters gives the best depth resolution currently achievable of 5 nm [1], constant sputtering yields [2] and minimal chemical degradation [3]. It is clear that this important capability will have major impact in the innovation and manufacture of many advanced technologies. Consequently, there is an urgent need to develop the underpinning metrology. An essential first phase has been the VAMAS interlaboratory study [4] which has highlighted two key issues which we now study in detail. Firstly, the improved depth resolution using argon cluster sputtering and reduced chemical damage reveals effects of the primary beam in a dual beam depth profiling experiment become increasingly important. In this study, we use the Irganox organic multilayer reference material [5] and show that the apparent position of a delta-layer depends on which secondary ion signal is used. It is observed that the delta-layer profiles for small fragment ions appear before the molecular ion profile. The position shift increases with primary beam energy and can be more than 4 nm when a 50 keV Bi₃ ion beam is used. We understand this in terms of a simple sputtering model and provide recommended analytical conditions to reduce this effect. Secondly, it has been widely reported that an initial increase in intensity is observed when depth profiling some organic materials with argon clusters. This is observed for the Irganox reference material and we show this is due electron beam damage from the charge compensation system. Since, typically, lower sputtering yields are used for argon cluster sputtering (owing to the choice of low energy per atom to reduce the sputtering damage) the emitted flux of positive ions is reduced and more electron beam current is required than typically needed using C₆₀ sputtering. Previously, we have shown that a maximum limit of 6·10¹⁸ electrons per m² should be used to spectroscopy [6]. Here, we show that electron damage extends up to 100 nm into the profile. We conduct a systematic study of the electron beam damage as a function of electron dose and energy and give a recommend dose limit.

[1] A.G. Shard et al., This conference

[2] J.L.S. Lee et al., Anal. Chem. (2010), 82, 105

[3] S. Ninomiya et al., Rapid Commun. Mass Spectrom. (2009), 23, 1601

[4] A.G. Shard et al., Surf. Interface Anal. (2011), 43, 1240v

[5] A.G. Shard et al., J. Phys. Chem. B (2008), 112, 2596

[6] I.S. Gilmore and M.P. Seah, Appl. Surf. Sci. (2002), 187, 89

2:40pm AS-ThA3 Comparative Study of C₆₀ and Gas Cluster Ion Sputtering in XPS Depth Profiling for Thin Film Analysis, S.S. Alnabulsi, J.F. Moulder, S.N. Raman, S.R. Bryan, J.S. Hammond, Physical Electronics

The objective of successful XPS sputter depth profiling is to accurately identify the layer thicknesses and chemical composition of materials within thin film structures. Cluster ion beam sputtering has been widely used in recent years with the intent to address this essential analytical goal for a broader range of materials, including organic materials. C₆₀ cluster ion beam sputtering provided the first access to quantitative chemical state information below the surface for many polymers, organic and inorganic oxide materials [1].

The recent introduction of argon gas cluster ion beam sputtering to the XPS community has further expanded the capability of successful depth profiling with an emphasis on preserving the chemical structure of challenging polymer and organic materials that exhibit rapid radiation induced damage due to the mobility and reactivity of free radicals that are formed during the sputtering process when other ion sources are used [2].

The purpose of this study is to present a comparative evaluation to quantify the benefits of using either C₆₀ or argon gas cluster ion beam sputtering for XPS compositional depth profiling by characterizing several standard organic and inorganic thin film structures.

N. Sanada, A. Yamamoto, R. Oiwa, and Y. Ohashi, Surf. Interface Anal. 36, 280 (2004).

T. Miyayama, N. Sanada, M. Suzuki, J. S. Hammond, S.-Q. D. Si and A. Takahara, J. Vac. Sci. Technol. A, 28, No. 2, L1 (Mar/Apr 2010)

3:00pm AS-ThA4 Damage Profiles of Si (001) Surfaces Bombarded by Ar Gas Cluster Ion Beam, J.G. Chung, D.J. Yun, Y.K. Kyoung, H.I. Lee, J.C. Lee, Samsung Advanced Institute of Technology, Republic of Korea, H.J. Kang, Chungbuk National University (CBNU), Republic of Korea

The damage profiles of Si (001) surface bombarded by argon gas cluster ion beam (GCIB) and mono-atomic argon ion beam bombardment were investigated using X-ray photoelectron spectroscopy (XPS) and medium energy ion scattering (MEIS). The Ar-GCIB beam was 2 mm in diameter and scanned in an area of 3 mm × 4 mm and the beam current was about 60 nA. The incident angle of the GCIB was fixed at 55° from the surface normal and the mean cluster size was approximately 2500 argon atoms/cluster. The damage profiles of Si (001) bombarded by the Ar GCIB and the mono-atomic Ar ion beam sputtering were measured *ex-situ* MEIS system and *in-situ* MEIS system, respectively. The MEIS results showed that the thickness of the damaged layers on Si(100) is approximately 10 nm for 20 keV, 6.4 nm for 10 keV, and 4.2 nm for 5 keV after the Ar cluster ion dose of 2.3 × 10¹⁵ clusters/cm² and the maximum concentration of the implanted Ar atoms is 0.2 at% for 20 keV and 0.1 at% for both 10 keV and 5 keV. The MEIS spectra taken from the Si (001) surface before and after the Ar ion bombardment with the ion dose of 5 × 10¹⁶ ions/cm² showed that the maximum Ar atom concentration was 5.5, 5.8, and 7.8 at% and the damage depth was 5.3 nm, 8.5 nm and 12 nm at 1.0, 2.0, and 3.0 keV, respectively. The depth of the damaged layer is proportional to the in-depth distribution of the implanted primary ions which can be explained in terms of the collision cascade model. Our results showed that the damage did not result from the linear collision cascade for the sample bombarded by Ar GCIB sputtering since the primary cluster Ar atoms were not implanted into the subsurface. The mechanism for the damage generation via the Ar GCIB bombardment is not clear yet, but it should be understood to make it useful for practical applications in solid surface analysis such as SIMS, XPS and AES.

3:40pm AS-ThA6 Non-Destructive Depth Profiling using VKE-XPS and Maximum Entropy Regularization, C. Weiland, J.C. Woicik, National Institute of Standards and Technology

X-ray photoelectron spectroscopy (XPS) is an excellent tool for semi-quantitative analysis of the chemical structure of solid material systems. However, the in-depth distribution of elements in a solid is known to affect the intensity of the measured photoelectron peaks and can thus lead to errors in quantification. The depth distribution itself can be interesting for deposited thin-film systems and buried interfaces. Typically, depth

dependent measurements are made by sputtering layers of the material off the surface, but complications can arise due to knock-on effects, differential sputtering rates and implantation of the sputtering ions. Angle-resolved XPS (ARXPS) coupled with maximum entropy regularization can provide non-destructive depth sensitive information, but analysis is typically performed using a lab-based X-ray source, limiting the ultimate probe depth to tens of Angstroms. Here, we adapt the maximum entropy analysis method used for ARXPS to variable kinetic energy XPS (VKE-XPS) using hard X-rays. Using VKE-XPS with beam energies ranging between 2.1 and 6 keV, we can vary the photoelectron inelastic mean free path to adjust the effective analysis depth to technologically relevant thicknesses. Conversion from intensity vs. beam energy to depth profile can be accomplished using a regularization routine. Development of the routines will be discussed, followed by results of VKE-XPS analysis of plasma-enhanced chemical vapor deposited TiO₂ films on Si performed at NIST beamline X24A at the National Synchrotron Light Source.

4:00pm **AS-ThA7 The Early Stage of Corrosion of Cu₃Au Alloy, P. Rajput**, ESRF, France, *A. Gupta*, UGC-DAE Consortium for Scientific Research, India, *C. Meneghini*, Università di "Roma Tre", Italy, *G. Sharma*, UGC-DAE Consortium for Scientific Research, India, *J. Zegenhagen*, ESRF, France

Metallic alloys are important in our daily life and in industry, but unfortunately highly susceptible to corrosion in wet environment. De-alloying is a particular type of corrosion, attacking alloys which are composed of metals of different "nobility". When coming into contact with an electrolyte, the less noble metal may go into solution, typically causing crack formation and subsequent material failure upon stress. Potential controlled corrosion of a well ordered Cu₃Au crystal in sulfuric acid had been investigated *in situ* [1] showing that, far below the critical potential E_c , at which the alloy is massively dissolved, Cu goes into solution, leaving a \approx 1 nm thick film of small, Au-rich clusters. Just below E_c , the surface is eventually covered with about 10-20 nm large gold islands with a thickness of 2-3 nm. The Au-rich surface protects the bulk of the alloy against further corrosion (unless E_c is exceeded).

We used, hard x-ray photoelectron spectroscopy (HAXPES), x-ray standing waves (XSW) and depth-selective x-ray absorption fine structure (XAFS) to investigate the very early stages of the corrosion of a more 'realistic', disordered CuAu binary alloy. Ultra-thin Cu_xAu films (2.5 nm, $x \approx 3$) were deposited on a Ru/B₄C multilayer to produce the XSW field. The XSW study provides detailed information about the concentration profile of Cu and Au upon de-alloying. HAXPES provides the binding energies (oxidation states) of Au and Cu and XAFS reveals the local atomic structure around Cu and Au.

The pristine Cu_xAu film appeared partially oxidized (CuO and Cu₂O). After dealloying at 245 mV for 2 min in 0.1 M H₂SO₄, the partial Cu dissolution leads to the formation of a Au-rich film with CuAu₃-like composition. Quantitative XRF analysis showed that, surprisingly, even below E_c dealloying leads to the loss of some Au as well.

[1] F. U. Renner, A. Stierle, H. Dosch, T. L. Lee, D. M. Kolb, J. Zegenhagen, Nature 439, 707 (2006).

4:20pm **AS-ThA8 Hard X-ray Photoelectron Spectroscopy (HAXPES) Investigations of Electronic Materials and Interfaces, J.C. Woicik**, National Institute of Standards and Technology **INVITED**

Photoelectron spectroscopy can uniquely measure the chemical and electronic structure of solids and films; however, owing to the generally limiting electron inelastic mean-free path of lab based instruments, the technique is extremely surface sensitive, probing only the first several atomic layers of a given structure. For this reason, synchrotron based hard x-ray photoelectron spectroscopy (HAXPES) in which the photon energy can be varied between 2.1 and 6 keV has emerged as a technique that is ideally suited for studying the electronic and chemical structures of advanced materials systems. In this talk, we will discuss developments of the HAXPES technique at the NIST beamline X24A at the National Synchrotron Light Source for the study of electronic materials. Examples will include nitrogen treatment of HfO₂ gate stacks on Si, depth profiling of the HfO₂/SiO₂ interface, Ga and As "out-diffusion" at semiconductor/oxide interfaces, band offsets and Schottky barrier heights at semiconductor/oxide and diamond/metal interfaces, and oxygen vacancies in N doped TiO₂ and solid-oxide fuel cells. In all cases, the increased probing depth of HAXPES over traditional lab based XPS is crucial to study the electronic structure of entire overlayers and/or buried interfaces with thicknesses of industrial significance.

5:00pm **AS-ThA10 Hard X-ray Photoemission Spectroscopy used to Investigate the Resistive Switching Behavior of Manganite Heterostructures: The Case of Ti/PrCaTiO₃ Interface, F. Offi**, CNISM and Dipartimento di Fisica, Università Roma Tre, Italy, *F. Borgatti*, CNR-ISMN, Bologna, Italy, *Y. Yamashita*, *A. Yang*, *M. Kobata*, *K. Kobayashi*, Synchrotron X-ray Station at SPring-8, NIMS, Japan, *C. Park*, *A. Herpers*, *R. Dittmann*, Peter Grünberg Institut, Research Center Jülich, Germany, *G. Panaccione*, CNR-IOM, Basovizza-Trieste, Italy

Electrical pulse induced resistance change has been observed at several oxides interfaces but its microscopic origin is still an open issue. In order to shed light on this problem we investigated with hard x-ray photoemission spectroscopy (HAXPES) the interface electronic structure of Ti covered 40 nm PrCaMnO₃ (PCMO) film within SrRuO₃/PrCaMnO₃/Ti/Pt devices exhibiting resistive switching behaviour. In particular, we searched for differences arising among the spectra of the virgin (not formed) and the high-resistivity states (HRS). The electronic structure of the Ti top electrode has been probed by measuring the Ti 2*p* spectra. The identification of the Ti 2*p* chemical states on the basis of literature binding energy (BE) values, indicate that the dominant Ti peak at lower BE corresponds to metallic state. Evidence is also found for the presence of Ti(IV) chemical state, due to the formation of TiO₂, and of other intermediate oxide species. Interestingly, the peak corresponding to Ti(IV) is more intense for the HRS than for the virgin state of the samples, suggesting that formation of Ti oxide is induced in the HRS through redox reactions related to the migration of oxygen ions from the PCMO inside the Ti layer. Moreover, the core-level spectra of all the elements of the PCMO layer, when compared to the spectra of the reference (uncovered) thick films of these materials, show BE shift and a change of the spectral lineshape that strongly resembles the BE shift dependence of the photoemission spectra on the amount of hole doping, which is related to the change of the chemical potential. Therefore the HAXPES results show changes of the PCMO and Ti electronic structure for this manganite heterostructure, indicating the increment of Ti oxide in the high-resistivity state and pinning of the PCMO chemical potential.

Electronic Materials and Processing

Room: 14 - Session EM+TF+AS-ThA

Growth and Characterization of Group III-Nitride Materials

Moderator: N. Dietz, Georgia State University

2:00pm **EM+TF+AS-ThA1 AIN-based Technology for Deep UV and High-power Applications, Z. Sitar**, HexaTech, Inc. & North Carolina State University, *B. Moody*, *S. Craft*, *R. Schlessler*, *R. Dalmau*, *J. Xie*, *S. Mita*, HexaTech, Inc., *T. Rice*, *J. Tweedy*, *J. LeBeau*, *L. Hussey*, *R. Collazo*, *B. Gaddy*, *D. Irving*, North Carolina State University **INVITED**

For the first time in history of III-nitrides, the availability of low defect density ($<10^3$ cm⁻²) native AlN substrates offers an opportunity for growth of AlGaIn alloys and device layers that exhibit million-fold lower defect densities than the incumbent technologies and enable one to assess and control optical and electrical properties in absence of extended defects. Epitaxial AlN wafers are fabricated from AlN boules grown by physical vapor transport at temperatures between 2200 and 2300°C. Gradual crystal expansion is achieved through a scalable, iterative re-growth process in which the high crystal quality is maintained over many generations of boules. Despite the excellent crystal quality, below bandgap optical absorption bands in the blue/UV range affect the UV transparency of wafers. We use density functional theory (DFT) to develop a model to understand the interplay of point defects responsible for this absorption. We show a direct dependence of the mid-gap absorption band with the carbon concentration within the AlN. Low defect density AlN and AlGaIn epitaxial films are grown upon these wafers that exhibit superior optical properties in terms of emission efficiency and line width and can be doped with an efficiency that is several orders of magnitude higher than possible in technologies using non-native substrates. UV LED structures and Schottky diodes were fabricated on these materials that exhibit low turn-on voltages and breakdown fields greater than 10 MV/cm. This presentation will review state-of-the-art of AlN-based technology and give examples of potential applications in future devices and contrast these with other wide bandgap technologies.

2:40pm **EM+TF+AS-ThA3 Atomic Layer Deposition of AlN Thin Films as Gate Dielectrics for Wide Bandgap Semiconductors, Y.-C. Perng, J.P. Chang, D. Chien**, University of California at Los Angeles

Aluminum nitride (AlN) is a potential dielectric layer for wide bandgap semiconductor based power electronic devices, such as those demanded in radio frequency, high-speed and high-temperature communication, because

of its wide bandgap and high dielectric constant. In particular, for 4H-SiC, AlN is also a promising interfacial layer due to their similar atomic arrangement, small lattice mismatch (1.3%) and comparable thermal expansion coefficients. Although various deposition techniques have been investigated to synthesize AlN thin films with atomic controllability over a large substrate remains a challenge. Atomic layer deposition (ALD) was thus used in this work to grow AlN thin films.

AlN deposition was performed in an ultra-high vacuum chamber with base pressure of 10⁻⁷ Torr using trimethylaluminum (TMA) and ammonia (NH₃) as precursors. It was discovered that ALD of AlN is possible only when the minute amount of moisture in NH₃, which competed with and inhibited the nitride growth, was completely eliminated. The ALD window was found to be 500-570°C with a growth rate of 1.5 Å/cycle. The deposited film composition was evaluated via *in-situ* x-ray photoelectron spectroscopy (XPS) with Al/N determined to be 1.2. *In-situ* reflective high-energy electron diffraction (RHEED) measurements showed as-deposited AlN films were crystalline, which was confirmed by x-ray diffraction (XRD). AlN/4H-SiC MIS capacitors were fabricated to examine the electrical properties with the dielectric constant of AlN determined to be 8.3 and a leakage current density of 10⁻³ A/cm² at 4.3 MV/cm. The 150 Å ALD AlN passivated AlGaIn/GaN hetero-structure demonstrated 11% increase in the carrier density and 3% decrease in mobility compared to those of non-passivated hetero-structure as 8.3x10¹²cm⁻² and 1100 cm²/V-s. While with amorphous 150 Å Al₂O₃ surface passivation, the mobility decrease by 22% with carrier density increase by 12%, showing that the crystalline AlN providing a superior property on passivating the hetero-structure.

3:00pm EM+TF+AS-ThA4 Low-Temperature Behavior of the Surface Photovoltage in p-type GaN, J.D. McNamara, M. Foussekis, A.A. Baski, M.A. Reshchikov, Virginia Commonwealth University

The effect of low temperature on the surface photovoltage (SPV) in semiconductors is rarely studied and not well understood. We studied the SPV behavior for Mg-doped, p-type GaN using a Kelvin probe at temperatures from 80 to 300 K. Under band-to-band UV illumination at room temperature, the measured SPV signal in p-type GaN becomes negative as electrons are swept to the surface. However, we observed that at low temperatures, the SPV signal becomes positive under UV illumination, contrary to the SPV behavior of p-type GaN at room temperature. This positive SPV resembles the behavior of an n-type semiconductor. We assume that under UV illumination and at low temperatures, the conductivity of Mg-doped GaN does indeed convert from p- to n-type. This conversion was predicted from photoluminescence studies on Zn-doped GaN.^[1] At low temperatures, photo-generated electrons may accumulate in the conduction band which causes an upward shift in the bulk Fermi level towards the conduction band. This results in a positive SPV signal, since the Kelvin probe uses the bulk Fermi level as a reference for the measured SPV signal. Interestingly, the characteristic temperature at which we observe this transition from p- to n-type behavior depends on illumination intensity. As the excitation intensity increases from 10¹⁵ to 10¹⁷ cm⁻² s⁻¹, the characteristic temperature increases from 130 to 170 K. This result also agrees with previously reported photoluminescence data and further authenticates the above assumption.^[1]

[1] M. A. Reshchikov, A. Kvasov, T. McMullen, M. F. Bishop, A. Usikov, V. Soukhoveev, and V. A. Dmitriev, Phys. Rev. B **84**, 075212 (2011).

3:40pm EM+TF+AS-ThA6 Controlling GaN Polarity on GaN Substrates, J.K. Hite, M.E. Twigg, J.A. Freitas, Jr., M.A. Mastro, J.R. Meyer, I. Vurgaftman, S. O'Connor, N.J. Condon, F.J. Kub, S.R. Bowman, C.R. Eddy, Jr., U.S. Naval Research Laboratory

Gallium nitride is a high quality semiconductor widely used in both optical and electronic devices. The polarity of GaN (+/- c-direction) influences many properties of the resultant material, including chemical reactivity and electric field in these 'piezoelectric' materials. Control over the polarity of GaN grown on sapphire and SiC substrates has been previously demonstrated by controlling the growth conditions, doping levels, and buffer or nucleation layer properties. Further, in the case of heavily doped p-type layers, spontaneous polarity inversion has been demonstrated in GaN homoepitaxial layers, switching the doped layer from Ga-polar to N-polar. However, this approach leads to uncontrolled inversion domain boundaries and often results in dopant clustering within the film, impacting film quality and resultant device performance.

In this work we investigate the fabrication of Mg-free inversion layers (ILs) to control the polarity of MOCVD-grown GaN on GaN substrates. By changing the IL material, we demonstrate conversion of GaN polarity in both directions (N-polar to Ga-polar and Ga-polar to N-polar). By employing a patented selective growth method to deposit the IL, the lateral polarity of the GaN can also be alternated, allowing control of the polarity in both vertical and lateral directions. A one-dimensional grating of periodically oriented (PO) GaN stripes was achieved over square-centimeter

(or large) areas. The boundaries between polarities are found to be both sharp and vertical, and the growth conditions have been adjusted to result in equal growth rates of both polarities. Chemical etching of the material verifies the polarity of the material. Transmission electron microscopy (TEM) rules out the presence of alternating polar inclusions in the inverted material while showing a strong inversion domain boundary at the vertical interfaces. Dislocation density and grain size are determined through the use of electron channeling contrast imaging. The MOCVD-grown PO GaN structures have been extended in thickness by further HVPE growth. TEM and photoluminescence imaging confirms that the PO GaN structure is maintained throughout the extended growth (up to 80 μm in thickness). This method of GaN polarity inversion offers the promise of engineering both lateral and vertical polarity heterostructures and the potential of novel engineered polarity-based devices.

4:00pm EM+TF+AS-ThA7 Direct Green and Yellow Light Emitting Diodes – Polarization Control and Epitaxy, C. Wetzel, T. Detzprohm, Rensselaer Polytechnic Institute INVITED

Solid state lighting by means of GaInN/GaN light emitting diodes (LEDs) is rapidly progressing to a major factor in energy savings technology. By convergence of lighting and lighting control, however, smart lighting is an opportunity to elevate lighting to a holistic experience of human wellbeing beyond the obvious economic benefits. Full epitaxial control of the GaInN/GaN active region is prime to fulfill the promise of an optical bandgap tunable across the entire visible spectrum. As such it will serve both, as tunable absorption layer for multijunction solar cells and emitter for direct emitting LEDs. The later aspect is of particular promise to outperform the traditional phosphor conversion approach known from historic fluorescence lamps and current white light LEDs.

Rigorous defect reduction approaches have enabled us to continuously improve the emission efficiency in ever longer wavelength emission reaching beyond green, deep green to yellow and orange (590 nm). In contrast to conventional phosphor or AlGaInP-based LED, such emitters show a superior temperature stability of their light output performance. A further leap in defect reduction has been demonstrated by the implementation of heteroepitaxy on nanotextured templates. Unlike widely explored lateral epitaxial overgrowth, growth zones primarily coalesce through the generation of threading dislocations. Implemented at the sapphire substrate level in green LEDs, the texturing substantially boosts both, internal quantum efficiency and light extraction. Furthermore, by control of the crystallographic orientation of growth we achieve a modulation of the piezoelectric polarization within the active region. This for once results in the emission of highly linear polarized light but on the other hand holds the promise to move the actual sweet spot of LED performance from the blue into the green and yellow spectral region. We discuss our approaches in light of our latest achievements.

This work was supported by a DOE/NETL Solid-State Lighting Contract of Directed Research under DE-EE0000627. This work was supported in part by the Engineering Research Centers Program of the National Science Foundation under NSF Cooperative Agreement No. EEC-0812056.

4:40pm EM+TF+AS-ThA9 The Influence of Substrate and Gas Phase Temperatures on the Properties of InN Epilayers, M.K.I. Senevirathna, S.D. Gamage, R. Atalay, R.L. Samaraweera, A.G.U. Perera, Georgia State University, B. Kucukgok, A.G. Melton, I. Ferguson, University of North Carolina at Charlotte, N. Dietz, Georgia State University

The influence of the substrate growth temperature on the structural and optoelectronic properties of group III-nitride layers grown by various growth techniques has been extensively studied and reported on, due to the close relationship of substrate temperature with crystalline quality and the point defect chemistry of the alloy. Most thin film growth systems only control the substrate temperature and have limited control to adjust the gas phase decomposition dynamic independent to influence to growth surface chemistry.

In this contribution, we present results on the growth of InN epilayers grown the high-pressure chemical vapor deposition (HPCVD), studying in influence of and independent from the substrate temperature controlled gas phase temperature above the substrate reactor zone. The HPCVD reactor system has two heater elements: one that controls the substrate temperature and a second radiative heat source above, which allows the control of the gas phase temperature. While the substrate temperature dominantly controls the growth process and the crystalline layer properties, the heater above the substrate surface influences strongly the precursor decomposition processes and the diffusion and concentrations of the precursor fragments in the boundary layer and at the growth surface. InN epilayers grown with different gas phase heating settings were grown and analyzed with the respect to their short- and long-range crystalline ordering and their optoelectronic properties as function of the gas phase temperature. The long-range and the short-range crystalline order of the layers have been

analyzed by x-ray diffraction 2θ - ω scans FWHM and the Raman E_2 (high) FWHM, respectively. The optoelectronic properties have been studied by reflectance spectroscopy and are related to the structural properties and the additional gas phase heating.

The figure depicts the FWHM values of Raman- E_2 (high) peak of the InN epilayers as a function of reactor pressure for higher (red line) and lower (blue line) gas phase temperature. The results indicate that there is an improvement of the short-range crystalline order of the layers with lower gas phase temperature. However, the FWHM values of XRD 2θ - ω scans, which are not shown here, are indicating that there is an improvement of long-range crystalline order of the layers with increasing gas phase heating.

5:00pm EM+TF+AS-ThA10 Absence of Electron Accumulation at InN(11-20) Cleavage Surfaces, H. Eisele, Technische Universität Berlin, Germany, S. Schaffhausen, Forschungszentrum Jülich, Germany, A. Lenz, Technische Universität Berlin, Germany, A. Sabitova, Forschungszentrum Jülich, Germany, L. Ivanova, M. Dähne, Technische Universität Berlin, Germany, Y.-L. Hong, S. Gwo, National Tsing-Hua University, Taiwan, P. Ebert, Forschungszentrum Jülich, Germany

InN in principle opens up the possibility of using only one ternary III-V semiconductor alloy (InGaN) in optoelectronic devices to cover the whole visible spectral range. Despite this, key material properties of InN are still under debate. The intrinsic energetic position of the Fermi level is unclear, i.e., whether the Fermi level is located within the fundamental band gap or shifted slightly into the conduction band. The latter case induces electron accumulation at the surfaces of the crystal. Such an electron accumulation is typically observed at InN surfaces upon air contact, raising the question whether it is an intrinsic material property or not?

In order to probe intrinsic bulk properties by STM and not only contamination or surface effects, a clean and stoichiometric surface is necessary. This can be achieved by cleaving InN along non-polar planes. To analyze the origin of the different electronic states in detail, we investigated the clean non-polar (11-20) cleavage surface using cross-sectional scanning tunneling microscopy (XSTM) and spectroscopy (XSTS).

Using combined XSTM and XSTS we were able to locate an InN layer grown on an AlN buffer layer on top of a Si(111) substrate [1]. XSTS spectroscopy on the InN(11-20) cleavage surface yield normalized conductivity spectra, where three contributions to the tunneling current can be observed: (i) the contribution from the conduction band density of states for biases above the conduction band minimum at +0.3 V, (ii) a defect induced current, dominating the spectra between biases of 0 and -0.4 V, and (iii) a valence band related tunneling current rising at a bias of about -0.4 V and dominating the spectrum for biases below. The defect induced current arises from semi-filled defect states being present at the surface steps, and probably also from other (point) defects at the surface. Within the bulk band gap of $E_G = 0.7$ eV no intrinsic surface states could be observed. Furthermore, the Fermi level pinning at about 0.3 eV below the conduction band minimum indicates the absence of an electron accumulation layer.

The results illustrate that electron accumulation at InN surfaces is not a universal property on InN. For clean stoichiometric cleavage surfaces no electron accumulation is observed. Thus, electron accumulation results primarily from the details of the surface structure and is hence not an intrinsic property of the bulk InN material.

[1] Ph. Ebert, S. Schaffhausen, A. Lenz, A. Sabitova, L. Ivanova, M. Dähne, Y.-L. Hong, S. Gwo, and H. Eisele, Appl. Phys. Lett. **98**, in press (2011).

5:20pm EM+TF+AS-ThA11 Dependence of Gallium Incorporation and Structural Properties of Indium-rich $\text{In}_x\text{Ga}_{1-x}\text{N}$ Epilayers on Ammonia - MO Precursor Pulse Separation, S.D. Gamage, R. Atalay, M.K.I. Senevirathna, R.L. Samaraweera, Georgia State University, A.G. Melton, I. Ferguson, University of North Carolina at Charlotte, N. Dietz, Georgia State University

The large band gap tunability of ternary $\text{In}_x\text{Ga}_{1-x}\text{N}$ alloys has opened new avenues in the field of advanced optoelectronics devices fabrication. However, the growth process of the epilayers of these materials is yet to be well explored. In this contribution, the growth of $\text{In}_x\text{Ga}_{1-x}\text{N}$ epilayers under super atmospheric pressure is studied. In order to mitigate the gas phase reactions and the gap of dissociation temperatures between the binary alloys GaN and InN, and to improve the phase stability, high growth chamber pressure has been used together with a pulsed precursor injection system. This pulsed precursor injection scheme introduces two important process parameters; the precursor separation times between the metal organic (MO) sources (TMI and TMG) and ammonia (S_1), and ammonia and MO (S_2).

With the aim to find the optimum S_2 separation for high quality indium-rich InGaN epilayers, a set of $\text{In}_x\text{Ga}_{1-x}\text{N}$ samples with nominal $x=0.9$ has been grown with different S_2 timings. It will be shown that the S_2 separation is critical for the incorporation of gallium into the epilayers. In order to

maintain single-phase epilayers, the S_2 separation has to be increased from $S_2=400$ ms for InN to over 1200 ms for $\text{In}_x\text{Ga}_{1-x}\text{N}$. Raman spectroscopy and X-ray diffraction (XRD) spectroscopy are used to study the structural properties while the Fourier Transform Infra-red (FTIR) and transmission spectroscopy are utilized to investigate the electrical and optical properties of the epilayers.

5:40pm EM+TF+AS-ThA12 MBE-Growth of Coherent-Structure InN/GaN Short-Period Superlattices as Ordered InGaN Ternary Alloys for III-N Solar Cell Application, A. Yoshikawa, K. Kusakabe, N. Hashimoto, T. Okuda, T. Itoi, Chiba University, Japan

We have recently proposed "SMART" III-N tandem solar cells in which all sub-cells could be coherent-structure high-quality pn junctions with low leakage current, resulting in high performance solar cells. SMART means "Superstructure Magic Alloys fabricated at Raised Temperature". The most important feature in the proposed SMART solar cell is a novel idea for realizing ordered and/or quasi InGaN-ternary alloys with InN/GaN Short-Period Superlattices (SPS) enabling coherent-structure band engineering for the $(\text{InN})_n/(\text{GaN})_m$ SPSs with simple integer pairs of $(n, m) \leq 4$. In this symposium, detailed epitaxy processes, structural and physical properties of SPSs, and also the idea and features of proposed "SMART" III-N tandem solar cells are reported.

We have ever reported successful growth of fine and coherent-structure 1-ML InN/GaN matrix QWs, and they can be fabricated so under self-limiting and self-ordering growth processes at remarkably higher and/or "raised" temperatures (~ 650 °C) than the critical one (~ 500 °C) for growing thick InN layer under +c growth regime in MBE. We are now underway to extend this understanding and the corresponding epitaxy technology to realize the proposed $(\text{InN})_n/(\text{GaN})_m$ SPSs, and we have started to achieve $(\text{InN})_n/(\text{GaN})_m$ ($m=1-20$) SPSs. When fabricating high structural quality those SPSs, very careful surface stoichiometry control such as $(\text{In}+\text{Ga})/\text{N}$ and In/Ga composition in adlayers, and also periodical complete surface dry-up of In and Ga for each one-cycle growth of SPSs are necessary and quite important.

In brief, 50-100 periods of $(\text{InN})_1/(\text{GaN})_m$ SPSs were grown on MOCVD-grown +c-GaN template at 650 °C by a conventional plasma-assisted MBE. Surface stoichiometry and surface dry up were quite carefully monitored and controlled by in-situ Spectroscopic-Ellipsometry. First, structural properties of 50 periods of $(\text{InN})_1/(\text{GaN})_m$ SPSs were characterized with XRD diffraction patterns taking the m as a parameter. It was found that coherent structure SPSs could be fairly easily fabricated even when the m was decreased down to 4. Generally, much more careful surface stoichiometry control was necessary with decreasing the m , though it was confirmed coherent structure $(\text{InN})_1/(\text{GaN})_4$ SPSs could be grown finally after quite careful control, such as selective re-evaporation between In and Ga consuming a long time. This leads to complete In re-evaporation leaving only some Ga metals on the surface. Of course those Ga metals must be completely dried up with irradiating plasma-excited nitrogen just before the following deposition of 1ML InN on it. It is still difficult at present, however, to grow fine structure InN/GaN SPSs with the m below 3.

Energy Frontiers Focus Topic

Room: 15 - Session EN+AS-ThA

Characterization of Energy Materials and Systems

Moderator: L. Lohstreter, Medtronic, Inc.

2:00pm EN+AS-ThA1 Growth Temperature and Stoichiometry Effects on the Inherent Stability of CdS/CdTe Solar Cells, D.S. Albin, T.A. Gessert, R. Dhere, S.-H. Wei, J. Ma, D. Kuciauskas, A. Kanevce, R. Noufi, National Renewable Energy Laboratory

INVITED
Capacitance-voltage (CV) measurements are commonly used to characterize semiconductor junctions. A common observation when performing such measurements on polycrystalline CdTe solar cells is that the measured capacitance is a strong function of the voltage scan direction. These results in a noticeable hysteresis in the C-V profile when capacitance data is collected using both forward (fwd) and reverse (rev) voltage scan directions. Similarly, hysteresis curves for the usual derived quantities such as net carrier density, N_a , and depletion width, W , naturally follows. We have recently observed that in particular, the hysteresis in calculated carrier acceptor density, $N_{a,hys}$, arbitrarily defined as $N_{a,fwd} - N_{a,rev}$ decreases as the CdTe growth temperature is reduced. At higher CdTe growth temperatures, this value is positive and shifts to negative values at lower growth temperatures. This behavior is believed to reflect a transition of the CdTe stoichiometry in CdS/CdTe solar cells from Cd-poor at higher temperatures to Cd-rich at lower temperatures based upon recently published CdTe binary phase diagrams.

The impact of Cd/Te stoichiometry on cell performance is suspected. Cd-poor stoichiometry favors the formation of Cd-vacancies (V_{Cd}), a beneficial acceptor, but it also simultaneously increases the formation of the Te antisite (Te_{Cd}), an important recombination center in CdTe. Recent theoretical calculations using the hybrid Heyd-Scuseria-Ernzerhof (HSE) functional also suggests that Te interstitials (Te_i) may be an important recombination center under Cd-poor conditions. Increased Cd chemical potential will reduce the formation of these recombination centers, but also reduce hole carrier density. Thus, an optimal growth condition, which could include extrinsic p-type doping, may be needed for leading to higher performance CdTe solar cells.

Not discussed to date however is whether stoichiometry has an inherent impact on the stability of CdTe solar cells. In this talk, we contrast accelerated lifetime study results for CdTe cells grown at different growth temperatures. Open-circuit voltage (V_{oc}) stability in cells grown at lower temperatures was noticeably improved. $N_{a,hrs}$ in the latter cells was considerably smaller. Both V_{oc} and FF were well correlated with this capacitance-derived parameter. $N_{a,hrs}$ was observed to be relatively unchanged in devices where V_{oc} did not degrade. Finally, time-resolved photoluminescence lifetimes of nearly 10 ns were measured in these cells made at lower temperatures relative to values of around 2 ns measured in higher temperature devices.

3:00pm EN+AS-ThA4 XPS Characterization of Organic Gradients in Organic Photovoltaic and Organic Light Emitting Devices Using Ar GICB Depth Profiling. S.N. Raman, J.S. Hammond, J.F. Maulder, Physical Electronics

The use of organic materials for electronic applications such as Organic Photovoltaics (OPV's) and Organic Light Emitting Diodes (OLED's) is rapidly growing. The efficiencies of these devices are widely recognized to depend on the molecular gradients fabricated into the devices. Conversely, the degradation of these devices is suspected to depend on several factors including chemical degradation and chemical migration as a function of use. It is therefore very desirable to develop analytical techniques which can quantify chemical gradients as well as identify degradation products in these films.

Gas Cluster Ion Beam (GICB) sources with low energy per atom $Ar_{2,000}^+$ ions have recently been demonstrated to provide a depth profiling technique for molecular species (1,2). GICB depth profiling in an interleaved mode with the surface analysis spectroscopy of X-ray Photoelectron Spectroscopy (XPS) has been applied to model OPV and OLED devices. The 2 to 5 nm information depth of XPS, combined with the demonstrated "non-destructive" chemical information revealed after each GICB sputter interval, facilitates the chemical gradient analysis of a series of model samples up to several 100 nm in depth with molecular depth resolution < 10 nm.

Selected model OPV and OLED samples were exposed to annealing and environmental degradation testing. The XPS depth profiles measured the migration of organic components and dopants as a function of fabrication processes. This presentation will provide an overview of GICB depth profiling with XPS as well as discuss the insights into efficiencies and degradation processes elucidated by this chemical gradient analysis technique.

1. T. Miyayama, et al. *Surf. Interface. Anal.* 42 (2010) 1453-1457.
2. T. Miyayama, et al. *J. Vac. Sci. Technology A*, 28 (2) (2010) L1-L4.

3:40pm EN+AS-ThA6 Characterization of Degradation Mechanisms of Membrane Electrode Assemblies by XPS and SEM Imaging. A. Patel, K. Artyushkova, P. Atanassov, University of New Mexico, S. Wessel, V. Colbow, M. Dutta, Ballard Power Systems, Canada

Durability of catalyst layer (CL) is of key importance in the deployment of PEMFCs. Catalyst layer (CL) degradation is linked to several failure mechanisms including Pt dissolution and agglomeration and support corrosion. X-ray photoelectron spectroscopy (XPS), a powerful technique to study chemical changes, has been applied to quantitatively analyze catalyst layer degradation in PEM fuel cells. More specifically, ionomer degradation was characterized by a decrease of CF_3 and CF_2 species and an increase in oxidized forms of carbon (e.g. C-O and C=O). Chemical speciation as determined by XPS for catalysts powders was correlated with electrochemical performance losses. MEAs using catalyst coated membranes that are composed of Pt catalyst supported on differing carbon supports were subjected to aging protocols to accelerate the degradation mechanisms of the cathode CL. In-situ and ex-situ diagnostics were used to quantify performance losses and structural changes of the CL.

Large area XPS was used for analysis of fresh, conditioned and aged cathode catalyst layers. Spectroscopic analysis, which provides an integral spectrum from approximately $1mm^2$ area, may have a contribution from the GDL sublayer that was not fully removed from the catalyst layer side

during separation of the MEA components. The GDL sublayer exhibits a peak in the same BE range as fully fluorinated carbons that are detected in the catalyst layer. Changes that have been detected in CL may not be due to the changes within the ionomer, but rather due to physical intermixing of layers caused by the testing protocols. XPS imaging enabled separation of the differing component contributions. Using Pt 4f imaging, regions are clearly identified where no Pt is present, indicating that GDL pieces adhere to the CL. Fluorine images at two different binding energies (one for the ionomer, and another for the GDL) confirm this. High resolution C 1s spectrum extracted from the area where catalyst is present does not show a high BE component in the C 1s spectrum of the area where GDL is present, confirming that the high BE component detected by large area spectroscopy are contributions from the GDL. High-resolution spectra acquired from the area where only catalysts layer is present shows higher amounts of oxidized forms of carbons. In addition, morphological changes of aged cathode catalyst layers have been evaluated by Digital Image Processing of SEM images for roughness, porosity and texture parameters.

4:00pm EN+AS-ThA7 Selective Adsorption Behavior of CO₂ and C₂ Hydrocarbon Isomers over N₂ and Methane in a Flexible Metal Organic Frameworks. N. Nijem, P. Thissen, University of Texas at Dallas, P. Canepa, Wake Forest University, H. Wu, J. Li, Rutgers University, T. Thonhauser, Wake Forest University, Y.J. Chabal, University of Texas at Dallas

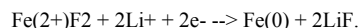
Post combustion carbon capture is a complementary approach to research in renewable energy to combat the exponential increase of CO₂ emission and global warming. An important outcome of enhancing gas separation in materials, for example, is the decrease in energy needed for separation of hydrocarbons. Metal-organic Frameworks (MOFs) have shown promise in this area because their high surface area, porosity and chemical/structural tailorability contribute to the preferential selective adsorption of gases. This work explores the incorporation of CO₂ and hydrocarbons into a flexible framework, $Zn_2(bpdc)_2(bpee)$, ($bpdc = 4,4'$ -biphenyl dicarboxylate, $bpee = 1,2$ -bis(4-pyridyl)ethylene) using infrared (IR), Raman spectroscopy and van der Waals density Functional (vdW-DF) calculations. We present evidence for "gate opening" phenomenon, where the structure of the framework changes only upon adsorption of CO₂ and C₂ hydrocarbon isomers but not for N₂ or methane. Understanding the specifics of CO₂ interaction with the framework was explored to identify parameters affecting its selectivity. We find that the high quadrupole moment of CO₂ and its interaction through its carbon with the $bpdc$ linker induces the transformations. The flexibility of the framework was found to be primarily due to the specific connectivity of the Zn metal center to the ligands, at one end in a monodentate mode and at the other in a bidentate mode. The unexpected gate opening behavior in this same framework upon the adsorption of C₂ hydrocarbon isomers was also studied. We find that the specific hydrogen bonding between the CH of the hydrocarbon and the C=O bond of the $bpdc$ linker is responsible for this interesting behavior. Furthermore, the strength of the hydrogen bond was found to affect the gate opening pressure point. This effect points towards the potential of this framework for uses such as pressure swing adsorption based separation. In conclusion, we have identified specific interactions of CO₂ and hydrocarbons in a flexible framework that lead to their selective adsorption properties. This knowledge allows the design of frameworks with optimized properties.

4:20pm EN+AS-ThA8 Fabrication and Characterization of a PCBM-Terminated Organic Monolayer on a Si(111) Surface. T.J. Miller, A.V. Tplyakov, University of Delaware

The energy sector is a large, growing field in research and technology. A growing subset of the solar field is organic photovoltaics (OPV). Two areas that have long challenged researchers are efficiency and stability of the OPV devices. An area that is in need of fundamental understanding that may increase efficiency of these devices is the charge transfer. However, a precise nature of the bulk-heterojunction OPV donor/acceptor interface is difficult to pinpoint. Thus, model systems can be used initially to mimic these interactions. In the system presented here, the donor/acceptor interface is well-defined. Phenyl-C₆₁-butyric acid methyl ester (PCBM) was reacted with an amino-terminated organic monolayer on a single crystalline Si(111) surface. Poly 3-hexylthiophene (P3HT) was then deposited onto this complex substrate, and the produced interface can be observed and investigated. Fourier transform infrared spectroscopy was used to identify the functional groups on the surface. The chemical and electronic states of the coating and the substrate were investigated by X-ray photoelectron spectroscopy, and the morphology was determined through atomic force microscopy. Preliminary charge carrier lifetime measurements will also be reported.

4:40pm **EN+AS-ThA9 Conversion Reaction of Thin Film Metal Fluorides and Metal Oxides Exposed to Atomic Lithium**, R. Thorpe, S. Rangan, R.A. Bartynski, Rutgers University

Modern Li-ion intercalation batteries use electrode materials that accommodate Li intercalation, enabling the exchange of Li ions during battery cycling without extensive alteration of the electrode's crystalline structure. Despite the stability of these materials to the intercalation process, the ability of such batteries to store energy is limited by the number of host sites in the electrodes to approximately one electron per formula unit. Conversion reaction materials could potentially store several times more energy than current generation batteries by utilizing the full range of charge states available to their constituent metal ions. For example, the following reaction occurs in a FeF₂ cathode:



Although conversion reaction materials have shown the promise of high energy storage density in electrochemical cells, their cycling stability is poor, and relatively little is known about the phase evolution and structural changes that occur during charge and discharge.

In order to study the fundamental properties of these materials, we have grown high purity thin films of conversion materials FeF₂, FeF₃, FeOF, FeOx, and CoO. By exposing these films to atomic Li in vacuum, can follow the evolution of these materials as they approach the reaction products reached in the discharge of a conversion battery. We have used UV and inverse photoemission to measure the electronic structure of the valence and conduction bands respectively. Using these techniques in tandem, we are able to measure the band gap of these materials, which can then be related to their electronic conductivity. Using x-ray photoemission, we have measured the stoichiometry and valence states of the compounds involved in these reactions. In addition, we have examined the structure of these nano-scale materials using TEM and LEED.

For FeF₂, our XPS results show immediate reaction upon exposure to Li, fully reducing the Fe to the metallic state and forming LiF, with no evidence of intermediary phases in the film due to the high mobility of lithium. TEM of the initial and final films indicates a drastic morphology alteration, leading to a local precipitation of Fe₀ and LiF formation, with an overall particle size reduction from 10nm to 2nm, consistent with what is found in electrochemical studies.

However, the Li-CoO and Li-FeOx reactions appear to diverge from the results of Li⁺ electrochemical reactions, leading to the simultaneous formation of both Li₂O and Li₂O₂, the latter of which hinders further reduction of the Fe and Co. These observations will be contrasted with results obtained from the related conversion reaction compounds FeOxF_y and FeF₃.

Thin Film

Room: 11 - Session TF+AS+SS-ThA

Thin Films: Growth and Characterization-III

Moderator: M.R. Davidson, University of Florida

2:00pm **TF+AS+SS-ThA1 Atomic Force Microscopy (AFM)-Based Nanografting for the Study of Self-Assembled Monolayer Formation of Organophosphonic Acids on Al₂O₃ Single Crystal Surfaces**, B. Torun, B. Oezkaya, G. Grundmeier, University of Paderborn, Germany

The surface chemistry of aluminum oxides plays a crucial role in the field of catalysis, corrosion and adhesion. Alumina (Al₂O₃) covered aluminum alloys are employed in the construction of lightweight automotive and aerospace parts. In order to protect these materials from environmental factors organic coatings are commonly used. In this context the adhesion between polymer and oxide surfaces is of utmost importance to improve the longevity of industrial parts. Using self-assembled adhesion promoting monolayers the complexity of surface pretreatment processes could be reduced tremendously. Long aliphatic phosphonic acids, such as octadecylphosphonic acid (ODPA), were found to be suitable for forming dense self-assembled monolayers on native oxide covered aluminum substrates. However in contrast to amorphous oxide films, single crystal surfaces provide a much more well-defined experimental and theoretical platform for studies on the adsorption mechanisms and the stability of organophosphonic acids.

In the presented study^[1], adsorption, stability, and organization kinetics of organophosphonic acids on single-crystalline alumina surfaces were investigated by means of atomic force microscopy (AFM)-based imaging, nanoshaving, and nanografting. The latter, nano-shaving and -grafting, are rather new techniques to study self-assembly processes. Since they were first reported^[2] in 1997, atomic force microscopy based nanografting has been used as a tool to investigate the adsorption of organic monolayers

mostly on noble metals, such as gold.^[3] Moreover recent studies focused on influences of the confinement between AFM-tip and background monolayer on the adsorption of molecules during the grafting process. [about:blank#_ENREF_1]

AFM friction and phase imaging have shown that chemical etching and subsequent annealing led to heterogeneities on single-crystalline surfaces with (0001) orientation indicating differences in the local surface termination. These findings were supported by angle resolved X-Ray photoelectron spectroscopy (AR-XPS) measurements suggesting a partially hydroxide terminated surface. Self-assembly and stability of ODPA were shown to be strictly dependent upon the observed heterogeneities of the surface termination, where it was locally shown that ODPA can loosely or strongly bind on different terminations of the crystal surface. Furthermore, organization kinetics of ODPA was monitored with nanografting on (0001) surfaces. Supported by measurements of surface wettability and diffuse reflectance infrared Fourier transform spectroscopy (DRIFTS), it was demonstrated that the lack of organization within the protective adsorbed hexylphosphonic acid (HPA) monolayer on alumina surfaces facilitated the reduced confinement effect during nanografting, such that kinetics information on the organization process of ODPA could be obtained.

[1] Torun, B. et al., *Langmuir* **2012**, 28, (17), 6919-6927.

[2] Xu, S. et al., *Langmuir* **1997**, 13, (2), 127-129.

[3] Yu, J. et al., *Langmuir* **2008**, 24, (20), 11661-11668.

[4] Xu, S. et al., *J. Amer. Chem. Society* **1998**, 120, (36), 9356-9361.

2:20pm **TF+AS+SS-ThA2 SIMS as a Method for Probing Stability of the Molecule-Substrate Interface in SAMs**, J. Ossowski, J. Rysz, Jagiellonian University, Poland, A. Terfort, Goethe University, Germany, P. Cyganik, Jagiellonian University, Poland

Despite the numerous structural studies of Self-Assembled Monolayers (SAMs) available nowadays, the structure and stability of the SAM-substrate interface is still poorly understood and controversial even for the most simple SAM system. As a consequence, the experimental and theoretical analysis of the bonding geometry and the stability of the molecule-substrate interface for technologically relevant, and therefore more complicated SAMs, is extremely difficult.

In this presentation we report extensive static secondary ion mass spectrometry (SIMS) studies¹ on homologous series of thiols (BPnS, CH₃-C₆H₄-C₆H₄-(CH₂)_n-S-Au(111), n = 2-6) and selenols (BPnSe, CH₃-C₆H₄-C₆H₄-(CH₂)_n-Se-Au(111), n = 2-6) where structure and stability of molecule-substrate interface was systematically modified as verified by our previous experiments²⁻⁵. Correlating SIMS data with previous microscopic², spectroscopic³ and very recent neutral mass spectrometry studies^{4,5} we show that SIMS can be successfully applied to monitor fine changes in the molecule-substrate interface stability of these model SAMs. Further, to demonstrate general applicability of SIMS for such analysis, we report use of this method for monitoring influence of S versus Se substitution in purely aliphatic (heksadecanethiol/selenol) and aromatic (anthracenethiol/selenol) SAMs on Au(111). In summary our experiments show that a new approach for probing the stability of molecule-substrate interface in SAMs can be proposed by using SIMS. Importantly, this technique is relatively fast and can be applied for virtually all complicated and technologically relevant SAMs.

References

(1) J. Ossowski, P. J. Rysz, A. Terfort and P. Cyganik *in preparation*.

(2) P. Cyganik, K. Szelagowska-Kunzman, et al. *J. Phys. Chem. C* **2008**, *112*, 15466.

(3) K. Szelagowska-Kunzman, P. Cyganik, et al. *Phys. Chem. Chem. Phys.* **2010**, *12*, 4400.

(4) S. Wyczawska, P. Cyganik, A. Terfort, P. Lievens, *ChemPhysChem* (communication) **2011**, *12*, 2554.

(5) F. Vervaecke, S. Wyczawska, P. Cyganik, et al. *ChemPhysChem* (communication) **2011**, *12*, 140.

2:40pm **TF+AS+SS-ThA3 Wet Chemical Surface Modification of Silicon Oxide and Oxide Free Silicon by Aluminum Oxide**, P. Thissen, A. Vega, T. Peixoto, Y.J. Chabal, University of Texas at Dallas

Wet chemical surface modification is a powerful method to change the chemical properties of surfaces. Although it has been used extensively, there are still many issues that limit the applicability of these reactions. Substrate dip coating in aqueous solutions is particularly useful to facilitate both organic and inorganic layer functionalization. For instance, the bonding of phosphonic acid to silicon oxide is weak in water because the Si-O-P bond is easily hydrolyzed. We demonstrate here that this problem is alleviated by the addition of an ultra-thin aluminum oxide layer to the silicon oxide surface via dip-coating a silicon substrate in an aqueous

solution of aluminum chloride. The growth kinetics of the aluminum oxide layer are characterized by several surface sensitive techniques and found to follow a Stranski-Krastanov mechanism. Once the aluminum oxide layer is in place, a self assembled monolayer (SAM) of octadecylphosphonic acid (ODPA) is attached by the "tethering by aggregation and growth" (T-BAG) method performed in a controlled environment. We demonstrate that this ODPA layer grafted on the aluminum oxide interlayer remains stable in water. We also show that, following the same wet chemical approach, we are able to attach aluminum hydroxyl directly on oxide-free silicon surfaces previously functionalized with 1/3 monolayer OH. [1] Finally, we show that our approach can easily be transferred to other metal oxides and discuss the most influencing parameters.

[1] Michalak, D. J.; Amy, S. R.; Aureau, D.; Dai, M.; Esteve, A.; Chabal, Y. J. *Nat. Mater.* **2010**, *9*, 266-271.

3:00pm TF+AS+SS-ThA4 Static and Dynamic Depth Profiling of Thin Films with Low Energy Ion Scattering (LEIS). *H.R.J. ter Veen, M. Fartmann*, Tascon GmbH, Germany, *T. Grehl*, ION-TOF GmbH, Germany, *B. Hagenhoff*, Tascon GmbH, Germany

With the ever increasing demand of thinner and better defined thin layer structures, good depth resolution becomes more and more critical in depth profiling techniques. Low Energy Ion Scattering (LEIS) is known as the most surface sensitive chemical analysis technique (see [1] for a review of LEIS technique). It is considerably less known that LEIS can also be applied for so called "static depth profiling" by interpreting the backgrounds on the low energy side of the LEIS peaks. The energy that the particles lose while travelling through the sample is a measure for the depth of the scattering atom, in a way similar to Rutherford Back Scattering (RBS) but for a much smaller depth range. New models have been developed to understand the process that gives rise to these backgrounds and that contains the information from layers below the surface up to depths of 10 nm. These models will be presented.

The models for this static depth profiling can be verified by dynamic (sputter) depth profiling. After each sputter step a full LEIS spectrum is recorded, which contains the surface information as well as the static depth profile at that point in the dynamic depth profile. In this way, the static depth profile can forecast the dynamic depth profile. This technique will be demonstrated for an Si/SiO₂/W/Al₂O₃ system.

LEIS is particularly suited for dynamic depth profiling. Since LEIS is so surface specific, the depth resolution is excellent, as long as the sputter conditions are chosen with care. Furthermore, LEIS can be quantified easily, in many cases - such as in depth profiles - without the use of references. However, any dynamic depth profile suffers from artifacts, such as preferential sputtering and ion beam mixing. By combining the dynamic depth profiling with static depth profiling there is an independent check on these artifacts. Furthermore, it will be shown how static depth profiling can give relevant information also at shallow depths where in a dynamic depth profile sputter equilibrium will not have been reached yet.

[1] H.H. Brongersma et al, *Surf. Sci. Rep.* **62** (2007)63

3:40pm TF+AS+SS-ThA6 Paul Holloway Award Talk: Surface Chemistry and Structure of Alloy Thin Films under Reaction Conditions and their Correlations to Catalytic Performances of CO₂ Conversion and Methane Partial Oxidation. *F. Tao**, University of Notre Dame

Formation of alloys is one of the important approaches to design of new catalysts with high activity and selectivity as a second metal could tune electronic structure of the first metal or/and create thermodynamically favorable sites for an ideal reaction channel. Co-Ru alloys are active catalysts for conversion of CO₂ into fuel molecules CH₄. Pd-based alloys are important catalysts for methanol partial oxidation to produce hydrogen. Thin films of model catalysts of alloys Co-Ru and Pd-Co were prepared through e-beam evaporation in UHV. In-house ambient pressure X-ray photoelectron spectroscopy using monochromatic Al K α were used to examine the evolution of surface compositions of alloy catalysts and the oxidation states of the constituting elements under reaction conditions and during catalysis in contrast to those before or after a reaction; Surface chemistry (composition and oxidation state) of active phases of Co-Ru and Pd-Co was revealed. High pressure STM provided visible information of surface structure at nano and atomic scale under reaction conditions. These studies clearly suggest a modification of Co electron state through coordinating Ru atoms and thus tuning the adsorption energy of intermediates on Co in CO₂ conversion, which enhances the selectivity to production of CH₄. The formed Co_{0.85}Ru_{0.15} alloy exhibits 100% selectivity to the production of CH₄ and a conversion of 40% which is higher than both pure Co and pure Ru. The promotion effect of the alloy film for CO₂

conversion was rationalized by electronic effects of Ru to Co in the alloy thin films under reaction conditions. In terms of Pd-Co alloy catalysts, segregation of Co to surface under reaction conditions was observed. Through the measurement of surface composition using AP-XPS and the coordination of Pd on surface visualized with STM, a correlation between surface chemistry and structure of Pd-Co alloy surface under reaction conditions and the corresponding catalytic performances were built. The modification of Co to the catalytic behaviors of Pd was identified.

4:20pm TF+AS+SS-ThA8 Time-resolved and Surface Plasmon Resonance Studies in Metal-Insulator Phase Transition in VO₂ Thin Films. *L. Wang, C. Clavero, K. Yang, E. Radue, M.T. Simons, I. Novikova, R.A. Lukaszew*, College of William and Mary

Vanadium dioxide (VO₂) is a prominent example for a material exhibiting a metal-insulator transition (MIT) as a function of temperature with a phase transformation around 340 K from a low-temperature insulator state to a high-temperature conducting state. During the MIT the lattice structure of VO₂ transforms from a monoclinic (insulator) to a tetragonal structure (conductor). Whether these structural changes are solely responsible for the nature of the transition or whether correlation effects also play a role, has been a subject of much debate. Two mechanisms have been generally considered to explain the origin of the MIT in VO₂. The Mott-Hubbard mechanism suggests that electron-electron correlation drives the first-order MIT whereas the Peierls mechanism proposes that a strong electron-lattice interaction leads to the MIT. In order to have a better understanding of the phase transition mechanism and the optical properties of this material across the MIT, we present our research studies on epitaxial VO₂ thin films. We have investigated the optical transmission of a VO₂ thin film during the thermally induced MIT in two different optical spectral regions, with cw THz light and low power (1 mW) IR light (1520 nm HeNe), to identify different mechanisms at play. We have found that the transmission of the THz light starts to decrease at higher temperature than that of the IR light thus probing different stages during the thermally induced MIT. We also investigated surface plasmon polariton excitation in VO₂ thin films in the IR region, and observed a clear trend from non-absorption in the insulator phase to a high absorption in the metallic phase while changing the VO₂ temperature. Our studies are aimed at helping to understand the evolution of the metallic phase in VO₂ thin films after the MIT and relaxation back to the insulator phase upon the MIT which is of paramount importance for ultra-fast switch applications. Finally, we note that Cavalleri *et al.* [1] reported that the light-induced phase transition happens in less than half a pico-second thus hinting at electronic processes, although they also found that it strongly depended on pump-laser power which is suggestive of lattice interactions. We will compare our time-resolved measurements also using pump-probe techniques but with the sample held at low-temperature vs. room-temperature to illustrate the role of the pump-power on the photo-induced MIT.

[1] A. Cavalleri, Cs. Tóth, C.W. Siders, J. A. Squier, F. Ráksi, P. Forget and J. C. Kieffer, *Phys. Rev. Lett.* **87** (23), 237401 (2001).

4:40pm TF+AS+SS-ThA9 Growth, Microstructure and Optical Properties of Sputter-Deposited Gallium Oxide Thin Films. *S.K. Samala, C.V. Ramana*, The University of Texas at El Paso

Gallium oxide (β -Ga₂O₃), which is a stable oxide of gallium, is a wide band gap material. The high melting point coupled with stable structure makes of β -Ga₂O₃ the best candidate for high temperature sensing. β -Ga₂O₃ thin films can be used for developing oxygen sensors operating at higher temperatures (≥ 900 °C). This feature opens the possibility of developing the integrated β -Ga₂O₃ based oxygen sensors for power generation systems. The present work was performed on the analysis of growth behavior, microstructure, and optical properties of β -Ga₂O₃ films grown by sputter deposition. Ga₂O₃ thin film were deposited on Si(100) and quartz substrate by varying the growth temperature from room temperature to 800 °C. The characteristic analysis of the samples was performed employing grazing incidence X-ray diffraction (GIXRD), scanning electron microscopy (SEM), and spectrophotometry measurements. GIXRD analyses indicate that the samples grown at lower temperatures were amorphous while those grown at ≥ 400 °C. SEM results indicate that the morphology evolution is dependent on the temperature. The characteristic shape of the grains changed from triangular to square and finally to spherical morphology with increasing temperature. Optical characterization indicates that the band gap varies from 4.1 to 5.1 eV as a function of increasing temperature. The correlation between growth conditions, microstructure and band gap is established.

* Paul Holloway Award Winner

5:00pm **TF+AS+SS-ThA10 Optical and Structural Properties of Hafnium Oxide Thin Films Prepared Using Different Deposition Techniques**, *L. Sun, N.R. Murphy, J.T. Grant, J.G. Jones, R. Jakubiak*, Air Force Research Laboratory

The high dielectric constant and optical transparency of hafnium oxide makes it a useful component in leading-edge integrated circuitry and optical coatings. The optical and structural properties of stoichiometric HfO₂ films vary significantly depending on the deposition mechanism. We prepared 200 nm thick films of HfO₂ on silicon (100) substrates derived from DC magnetron sputtering (DCMS), high power impulse magnetron sputtering (HIPIMS) and pulsed laser deposition (PLD). Analysis of x-ray diffraction data revealed that films deposited via PLD are amorphous, while those deposited using the magnetron sputtering methods had peaks at 2θ of 28.3°, 31.3°, 34.3° and 50.0° indicative of polycrystalline monoclinic HfO₂. This is further supported by the FT-IR data collected in the far-IR regime where absorption bands at 258, 341, 410 and 514 cm⁻¹ were present. AFM and SEM images indicate that the sputtered samples had rougher surface morphology and larger grain sizes than the PLD films where the surface was uniform and smooth (RMS surface roughness less than 0.1nm). The degree of surface roughness and grain size is inversely proportional to the refractive index. At 632 nm PLD films had an index of refraction of 2.10 while the index of the sputter coated films was 1.98, presumably due to presence of voids. The high refractive index and homogeneity of the PLD films indicate that they were highly packed without voids during growth. Additionally, the influence of the O₂/Ar ratio, working pressure, HIPIMS pulse profile and duty cycle on optical properties, surface roughness, particle size and structural properties of the HfO₂ thin films were characterized and evaluated.

5:20pm **TF+AS+SS-ThA11 Nitrogen Induced Changes in the Structure and Electronic Properties of WO₃ Thin Films**, *C.V. Ramana, R.S. Vemuri*, The University of Texas at El Paso, *M. Engelhard, S. Thevuthasan*, Pacific Northwest National Laboratory

Tungsten oxide (WO₃) is a wide band gap semiconductor (~ 3.2 eV), which exhibits excellent physical, chemical and electronic properties. WO₃ thin films have been widely used in electrochromics and chemical sensors. Recently, the band gap modification with anionic and cationic doping of WO₃ was gained importance to utilize these materials in photo-catalysis for energy production and utilization. The present work was performed on nitrogen incorporated WO₃ (N-WO₃) films to explore the options to engineer the microstructure and electronic properties. Specifically, the effect of nitrogen incorporation and processing parameters on the microstructure evolution and band gap of WO₃ thin films is investigated. The samples were grown using reactive RF magnetron sputtering where the nitrogen concentration in the films is varied by varying partial pressure of nitrogen during deposition while keeping all other process parameters constant. Quantitative measurements employing X-ray photoemission spectroscopy indicate the nitrogen content increases with increasing nitrogen partial pressure. Structural analysis employing grazing incidence X-ray diffraction demonstrated that the nitrogen atoms embedded in WO₃ crystal matrix changes the crystal-texturing and thus induce changes in the physical properties. Optical spectrophotometry analysis on the N-WO₃ films revealed a shift in the fundamental absorption edge which is in linear relation with the corresponding nitrogen concentration. The correlation between microstructure, dopant profile, dielectric constant and band gap in WO₃ films will be presented and discussed.

Friday Morning, November 2, 2012

Applied Surface Science

Room: 20 - Session AS+TF+VT-FrM

Surface Analysis using Synchrotron Techniques

Moderator: A. Herrera-Gomez, UAM-Azcapotzalco and CINVESTAV-Queretaro, Mexico, J.C. Woicik, National Institute of Standards and Technology

8:20am **AS+TF+VT-FrM1 Surface and Interface Analyses by X-ray Absorption and Hard X-ray Photoemission Spectroscopies**, *Q. Xiao, X. Cui*, Canadian Light Source, Canada, *H. Piao*, General Electric Global Research Center, *Y.F. Hu*, Canadian Light Source, Canada, *T.K. Sham*, The University of Western Ontario, Canada

Synchrotron-based techniques, such as X-ray absorption spectroscopy (XAS) and variable energy X-ray photoemission spectroscopy (XPS) are increasingly applied to the characterization of surfaces and interfaces of advanced materials. This presentation will introduce the XAS and variable energy XPS capabilities in the study of thin films and nanomaterials at the Canadian Light Source—the third generation synchrotron in Canada. Advantages of these techniques over the conventional techniques (such as lab-based XPS) will be demonstrated using examples in studies of two types of materials: (1) Gate oxide development on SiC and (2) heterogeneous nanocatalysts. In particular, examples using the recently commissioned high energy XPS at the SXRMB beamline (up to 10 KeV) will be highlighted.

8:40am **AS+TF+VT-FrM2 Differences in the Electronic Structure Highly-Oriented Films of H₂, Fe-, Co-, and Cu-Phthalocyanines Revealed by NEXAFS Spectroscopy**, *T.M. Willey, M. Bagge-Hansen, J.R.I. Lee, R. Call, L. Landt, T. van Buuren*, Lawrence Livermore National Laboratory, *C. Colesniuc, C.M. Monton, I. Schuller*, University of California, San Diego

Phthalocyanines are extensively studied as molecular semiconductor materials for chemical sensors, dye-sensitized solar cells, and other applications. Phthalocyanines offer high tunability through the choice of metal center atom; nearly all transition metals and many other heavier elements can reside at the relatively stable square planar center of the phthalocyanines. H₂, Fe-, Co-, and Cu-phthalocyanine molecules in films deposited on gold substrates show prostrate orientation, as opposed sapphire substrates, where phthalocyanines stand in a more upright conformation under deposition conditions used. Angular dependence in NEXAFS, commonly attributable to π^* and σ^* resonances, in both carbon and nitrogen K-edges, quantify the orientational order. H₂-phthalocyanine shows the cleanest angular dependence, with nearly no intensity in the π^* regime with normal beam incidence. Metal L-edges in prostrate films, on the other hand, have dramatic variation in angular dependence of resonances into empty states. Fe- and Co- resemble the K-edges; StoBe DFT shows that the lowest-energy allowed resonances are indeed molecular π^* states, with a high degree of mixing with the d_{xz} and d_{yz} orbitals of the metals. In contrast, the intense, in-plane resonance of the Cu-PC L-edge LUMO resembles a molecular σ^* state. Confirmed by StoBe, the $d_{x^2-y^2}$ character at the Cu center is responsible for this intense in-plane resonance. NEXAFS thus directly probes the electronic structure, illuminating the uniqueness of Cu-compared to H₂, Fe-, and Co- phthalocyanines.

9:00am **AS+TF+VT-FrM3 Hard X-ray Photoelectron Study of Graphene/h-BN Layer Structures Grown on Polycrystalline Cu Substrates**, *L. Kövér*, MTA ATOMKI, Hungary, *L. Tapasztó*, Inst. Tech. Physics and Materials Sci. & Korea-Hungary Joint Lab for Nanosciences, Hungary, *C. Hwang*, KRIS & Korea-Hungary Joint Lab for Nanosciences, Republic of Korea, *L.P. Biró*, Inst. Tech. Physics and Materials Sci. & Korea-Hungary Joint Lab for Nanosciences, Hungary, *I. Cserny, J. Tóth, A. Csik*, MTA ATOMKI, Hungary, *W. Drube, S. Thiess*, Deutsches Elektronen-Synchrotron DESY, Germany

INVITED

Graphene-hexagonal BN layer structures are recently in the focus of interest having a great potential importance as promising candidates to be utilized in many electronic and spintronic ultrathin device applications. Hard X-ray photoelectron spectroscopy (HAXPES) based on application of synchrotron radiation for excitation is a useful tool for revealing multilayer structures nondestructively providing information on the chemical state of the components at the surface and (even in the case of deeply embedded) interface layers. The aim of the present study is to test the applicability of the HAXPES method for characterizing graphene-hexagonal BN layer systems. h-BN and single layer graphene/multilayer h-BN structures were grown on polycrystalline Cu substrates using the Chemical Vapor Deposition technique [1]. HAXPES measurements were performed at the

BW2 beamline of the DORIS III synchrotron at DESY using the Tunable High Energy XPS facility [2] and monochromatic photons of 3000 eV energy. The surface layer structure of the same samples were also studied with conventional XPS in ATOMKI using non-monochromated Al K α radiation [3]. For obtaining information on the order and relative depth of the particular layers the dependence of the XPS and HAXPES spectra on the angle of emission of photoelectrons was also studied. Our results demonstrate the advantage of the combination of XPS and HAXPES measurements, the use of the Auger parameter for identifying the chemical state of the components at the interface between the layer structure and the substrate, the removal of the overlap between the Auger spectra from the substrate and the photoelectron spectra of the overlayer structure in the HAXPES spectra. In addition, HAXPES, due to the high energy resolution and sensitivity applied, makes possible the separation and identification of the contributions from atoms in different chemical states to photoelectron peaks of the components of the layer structure, and the quantitative estimation of their relative intensity, even at near grazing photon beam incidence (high surface sensitivity).

The research leading to these results has received funding from the European Community's Seventh Framework Programme (FP7/2007-2013) under grant agreement n° 312284, by OTKA grants PD 84244, K 101599 and in the framework of the Korea- Hungary Joint Laboratory for Nanosciences.

[1] C. Hwang, K. Yoo, S.J. Kim, E.K. Seo, H. Yu, L.P. Biro, J. Phys. Chem. C 115, 22369 (2011)

[2] W. Drube, T. M. Grehk, R. Treusch and G. Materlik, J. Electron Spectrosc. Relat. Phenom. **88-91**, 683 (1998).

[3] L. Kövér, D. Varga, I. Cserny, J. Tóth, K. Tökési, Surf. Interface Anal. **19**, 9 (1992).

9:40am **AS+TF+VT-FrM5 Beyond Hard X-ray Photoelectron Spectroscopy: Simultaneous Combination with X-ray Diffraction**, *G.R. Castro, J. Rubio-Zuazo*, SpLine at the European Synchrotron Radiation Facility, France

Nowadays, the great challenge in materials science is the incorporation of complex systems in the area of the nano-technologies. A fundamental aspect is the production of materials with specific and controlled properties. Many of these materials are aggregates of different components, frequently multilayer thin films where the interface and the surface play a key role. Therefore, it is very important to develop an experimental set-up capable to investigate different aspects under identical experimental conditions, in particular to differentiate between surface and bulk properties.

Hard X-ray photoelectron spectroscopy (HAXPES) is a powerful novel emerging technique for bulk compositional, chemical and electronic properties determination in a non-destructive way. It benefits from the exceptionally large escape depth of high kinetic energy photoelectrons enabling the study of bulk and buried interfaces up to several tens of nanometres depth. At SpLine, the Spanish CRG beamline at the European Synchrotron Radiation Facility (ESRF), we have developed a novel and exceptional set-up that combine HAXPES and X-ray diffraction (X-ray Reflectivity, Surface X-ray Diffraction, Grazing Incidence X-ray Diffraction and reciprocal space maps). Both techniques can be operated simultaneously on the same sample and using the same excitation source. The set-up includes a robust 2S+3D diffractometer with its main axis vertical hosting an UHV chamber equipped with a unique photoelectron spectrometer (few eV < E_{kin} < 15keV), X-ray tube (Mg/Ti), 15 keV electron gun and auxiliary standard surface facilities: MBE, ion gun, LEED, sample heating/cooling system, leak valves, load-lock port, etc.. The photon energy ranges between 7 and 45 keV. The HAXPES analyzer is an electrostatic cylinder-sector (FOCUS HV CSA), with a compact geometry and high transmission due to second order focusing. The analyzer is capable to handle kinetic energies both up to 15 keV and down to a few eV with the same analyzer setup and power supply. The SpLine station offers a unique opportunity to obtain, on a same sample and under identical experimental conditions, simultaneous information about the electronic properties, chemical composition and geometric/crystalline structure of bulk, buried interfaces and surfaces. This *novel tool* for non-destructive characterization of bulk and buried interfaces is available to the *scientific community*.

In this contribution, we will present a general view of HAXPES-XRD station available at SpLine. Three aspects will be specially addressed: physical background, experimental set-up and selected examples.

10:00am **AS+TF+VT-FrM6 Spectroscopic Imaging using Vector Potential Photoelectron Microscopy**, *R. Browning*, R. Browning Consultants

A new class of electron microscope, vector potential photoelectron microscopy (VPPEM) has been developed. This microscope will enable the chemical microanalysis of a wide range of samples using photoelectron spectroscopy (PES). The microscope is a full field spectroscopic imaging technique with a very large equivalent depth of focus. The unique imaging properties of this method opens up many experimental opportunities including the chemical microanalysis of a wide range of real world samples. Highly structured, three dimensional samples, such as fiber mats and fracture surfaces can be imaged, as well as insulators, and magnetic materials. The new microscope uses the vector potential field from a solenoid magnet as a spatial reference for imaging. A prototype instrument has demonstrated imaging of Au grids, uncoated silk, magnetic steel wool, and micron sized single strand tungsten wires.

10:20am **AS+TF+VT-FrM7 Trends in Synchrotron-based Photoemission; High Energy and High Pressure**, *H.J. Bergersen, J. Åhlund, R. Moberg*, VG Scienta, Sweden

The fields of Hard X-ray Photoelectron Spectroscopy (HAXPES) and High Pressure Photoemission (HiPP) are growing fast. In this contribution we present instrument development and results within HAXPES and HiPP as well as the merged field of HiPP-HAXPES.

Photoelectron spectroscopy (PES) is an excellent tool in surface science due to the possibility to probe electronic and geometric structure. During the past decade Angle Resolved Photoelectron Spectroscopy (ARPES) has had a remarkable upswing, due to the development of parallel angular detector analyzers, and is today used routinely for band mapping, depth profiling and X-ray diffraction (XPD) in the Ultra Violet (UV) and soft X-ray regime. With higher energies (hard X-rays), in combination with improvements in PES detection techniques, this tool can be extended to the HAXPES regime, enabling studies of bulk materials. Here we demonstrate new development of analysers capable of measuring angular resolved spectra in the High Energy regime as well as results obtained using such analyzers.

Experiments done under normal surface science conditions (Ultra High Vacuum) are of limited use in some applications, e.g catalysis, due to the pressure gap problem. This motivates the study of systems at ambient pressures. Here we present a HiPP instrument developed in collaboration with Advanced Light Source (ALS). This instrument allows standard PES measurements as well as spatial and angle resolved spectra at HiPP conditions. Some recent results include spatially resolved investigations of solid oxide electrochemical cells (SOC:s) and electrochemical properties of junctions.

Finally, we report on recent advances in constructing a new generation of instrumentation combining HiPP and HAXPES. A novel electron analyser, designed for optimal transmission in combination with very efficient differential pumping, will be presented together with preliminary results.

Authors Index

Bold page numbers indicate the presenter

— A —

Abdallah, L.S.: EL+TF+AS+EM+SS-TuP2, 32;
EL+TF+BI+AS+EM+SS-MoA9, 9
Abe, M.: SP+AS+BI+ET+MI+NS-TuA11, 24
Abel, J.: GR+AS+NS+SP+SS-TuA11, 21
Abel, M.-L.: AS-TuP4, 28
Adamska, L.: GR+AS+EM+NS+SS-WeA2, 46
Adelmann, C.: IS+AS+OX+ET-WeM9, 38
Adesanya, K.: MN+AS-MoM10, 5
Åhlund, J.: AS+TF+VT-FrM7, 72
Ai, M.: HI+AS+BI+NS-ThM5, 59
Akhmetov, A.: BI+AS-TuA8, 19
Aksamija, Z.: EM+SS+AS+NS-ThM10, **56**
Alaboson, J.M.P.: GR+AS+NS+SP+SS-TuA9, 20
Alavi, Z.: AS-WeM6, 34
Albert, M.: NM+AS+MS-MoM4, 6
Albin, D.S.: EN+AS-ThA1, **66**
Alcantara Ortigoza, M.: AS+BI-TuA1, **17**
Alcántara Ortigoza, M.: AS+BI-TuA3, 17
Alem, N.: GR+AS+NS+SS-ThM5, 58
Allen, S.: BI+SS+AS-TuM5, **12**;
SP+AS+BI+ET+MI+NS-TuA9, 24
Allen, T.: NS+AS+SS+SP-WeM2, 38
Alles, M.L.: EM+SS+AS+NS-ThM11, 57
Allred, D.D.: MN+AS-MoM4, 4
Al-Mahboob, A.: IS+AS+BI+ET+GR+NS-TuA8,
22
Alnabulsi, S.S.: AS-ThA3, **63**
Altman, E.I.: SP+AS+BI+ET+MI+NS-TuA10, 24
Alvarez, C.: IS+AS+BI+ET+GR+NS-TuA7, 22
Aminpour, M.: AS+BI-TuA1, 17; AS+BI-TuA3,
17
Ancona, M.G.: TF+AS-TuA3, 25
Andersen, J.N.: GR+AS+NS+SP+SS-TuA7, 20;
IS+AS+SS+EN-TuM12, 15
Aoki, T.: AS-ThM9, 55
Apkarian, V.A.: SP+AS+BI+ET+MI+NS-TuA3,
23
Arcot, A.R.: BI+AS-TuA3, 18
Areias, A.C.: AS-TuP11, 30; BI+AS-TuA7, 18
Arenholz, E.: GR+AS+EM+MI+MN-TuM9, 13
Arlinghaus, H.F.: AS-TuP1, **28**
Arman, M.A.: GR+AS+NS+SP+SS-TuA7, 20;
IS+AS+SS+EN-TuM12, 15
Armstrong, L.: SP+AS+BI+ET+MI+TF-WeA8, **49**
Arnebrant, T.: BI+SS+AS-TuM3, **12**
Arnold, M.S.: GR+AS+EM+NS+SS-WeA9, 46
Artyushkova, K.: EN+AS-ThA6, 67;
IS+AS+SS+EN-TuM6, **15**
Asadollahbaik, A.: HI+AS+BI+NS-ThM3, 59
Atalay, R.: EM+TF+AS-ThA11, 66; EM+TF+AS-
ThA9, 65
Atanassov, P.: EN+AS-ThA6, 67; IS+AS+SS+EN-
TuM6, 15
Attili, S.: BI+AS-TuA9, 19
Autes, G.: GR+AS+NS+SS-ThM5, 58
Axnanda, S.: IS+AS+SS+EN-TuM4, **14**

— B —

Baba, A.: TF+AS-WeA8, 52
Baer, D.R.: AS+BI-TuA12, **18**
Bagge-Hansen, M.: AS+TF+VT-FrM2, **71**;
IS+AS+OX+ET-WeM6, **38**
Bagnall, D.M.: HI+AS+BI+NS-ThM3, 59
Baldo, P.M.: IS+AS+OX+ET-WeM3, 37
Balog, J.: IS+AS+BI+ET+GR+NS-TuA3, 22
Barbacci, D.: BN+AS-WeA12, 45
Barback, C.V.: BN+AS-WeA3, 44
Barnes, T.: TF+AS-WeA10, 52
Barrett, L.: MN+AS-MoM4, 4
Barrett, N.: GR+AS+NS+SP+SS-TuA1, 19
Bartels, L.: SP+AS+BI+ET+MI+NM+NS+SS+TF-
WeM5, 39
Bartha, J.W.: NM+AS+MS-MoM4, 6
Bartynski, R.A.: AS-MoA10, 8; EN+AS-ThA9, 68
Baski, A.A.: EM+TF+AS-ThA4, 65

Batzill, M.: GR+AS+EM+NS+SS-WeA8, 46
Bauer, E.: IS+AS+OX+ET-WeM3, 37
Baumann, T.: IS+AS+OX+ET-WeM6, 38
Baur, M.: AS-ThM10, 55
Baykara, M.Z.: SP+AS+BI+ET+MI+NS-TuA10,
24
Bazarov, I.: VT+AS+SS-WeM2, 41
Beck, D.: SP+AS+BI+ET+MI+TF-WeA11, 50
Beckers, M.: BN+AS-WeA11, 45
Bedzyk, M.J.: GR+AS+BI+PS+SS-WeM1, **35**;
GR+AS+NS+SP+SS-TuA9, 20
Beechem, T.E.: GR+AS+NS+SP+SS-TuA8, 20
Bekman, H.H.P.Th.: HI+AS+NS-WeA9, 48
Belu, A.: AS+BI-TuM4, 10
Bemis, J.: SP+AS+BI+ET+MI+TF-WeA11, 50
Benavidez, T.: EL+TF+BI+AS+EM+SS-MoA3, 9
Bennett, C.J.: GR+AS+BI+PS+SS-WeM9, 36
Bera, K.: TF+AS-TuA11, **26**
Bergersen, H.J.: AS+TF+VT-FrM7, **72**
Beringer, D.B.: VT+AS+SS-WeM10, 42;
VT+AS+SS-WeM6, 41; VT+AS+SS-WeM9,
42
Berkh, O.: MN+AS-MoM10, 5
Berry, N.: TF+AS-WeA2, 51
Beyer, A.: HI+AS+BI+NS-ThM11, 59;
HI+AS+BI+NS-ThM5, 59
Bezares, F.J.: GR+AS+BI+PS+SS-WeM9, 36
Bhardwaj, C.: BI+AS-TuA8, 19
Bhat, N.: AS-TuP23, 32
Bhattacharya, A.: NS+AS+SS+SP-WeM12, 39
Bhattacharyya, D.: EM+SS+AS+NS-ThM4, **56**
Biegalski, M.D.: IS+AS+SS+EN-TuM5, 15
Biener, J.: IS+AS+OX+ET-WeM6, 38
Biener, M.: IS+AS+OX+ET-WeM6, 38
Bilich, D.: AS-ThA1, 63
Bíró, L.P.: AS+TF+VT-FrM3, 71
Biswas, A.: MI+SP+AS-ThM3, **60**
Blair, S.L.: BN+AS-WeA3, 44
Blaze, M.: BI+AS-TuA8, 19
Blomfield, C.J.: AS+BI-TuM10, 11; AS+BI-
TuM3, 10; AS+NS+SS+TF-WeA8, 43; AS-
ThM1, 54; AS-TuP13, 30; AS-TuP14, **30**
Bluhm, H.: IS+AS+SS+EN-TuM1, **14**;
IS+AS+SS+EN-TuM5, 15
Bockstaller, M.R.: TC+EM+AS-WeA9, 51
Boden, S.A.: HI+AS+BI+NS-ThM3, **59**
Boland, J.: HI+AS+BI+NS-ThM9, 59
Bonnell, D.A.: SP+AS+BI+ET+MI+TF-WeA3, 49;
SP+AS+BI+ET+MI+TF-WeA4, 49
Bora, D.: IS+AS+SS+EN-TuM3, 14
Borgatti, F.: AS-ThA10, 64
Borisov, V.: BI+AS-TuA9, 19
Borsa, D.: TC+EM+AS+TF+EN-ThM2, 61
Bosch, R.: TC+EM+AS+TF+EN-ThM2, 61
Bouchoule, S.: AS-MoM4, 2
Boufnichel, M.: MN+AS-MoM6, 4
Boutwell, C.: TF+AS-WeA9, **52**
Boutwell, R.C.: TF+AS-WeA7, 52
Bowman, S.R.: EM+TF+AS-ThA6, 65
Boxford, W.: AS-ThM1, 54; AS-TuP13, 30; AS-
TuP14, 30
Braun, A.: IS+AS+SS+EN-TuM3, 14
Bravo-Sanchez, M.: AS-TuP15, **30**
Brenner, D.W.: TF+AS-TuA12, 26; TF+AS-TuA7,
26
Brewer, J.R.: EL+TF+AS+EM+SS-TuP1, 32
Brinson, B.: BN+AS-WeA12, 45
Browning, R.: AS+TF+VT-FrM6, **72**
Brukman, M.: SP+AS+BI+ET+MI+TF-WeA4, **49**
Brunelle, A.: BN+AS-WeA7, **44**
Bryan, S.R.: AS-ThA3, 63; AS-WeM12, 35
Buck, A.: BN+AS-WeA11, 45
Buecheler, S.: TF+AS-WeA3, 52
Büenfeld, M.: HI+AS+BI+NS-ThM5, 59
Burden, D.: BI+AS-TuA4, 18
Burghaus, U.: NS+AS+SS+SP-WeM4, 38

Burkett, S.L.: MN+AS-MoM5, 4
Burst, J.: TF+AS-WeA10, 52
Bushell, A.: AS-MoM10, 3; AS-TuP10, 29
Busse, C.: GR+AS+NS+SP+SS-TuA7, 20
Butz, T.: GR+AS+EM+MI+MN-TuM9, 13

— C —

Cai, M.: GR+AS+NS+SS-ThM10, 58
Caillard, L.: EL+TF+BI+AS+EM+SS-MoA2, 8
Caldwell, J.D.: GR+AS+BI+PS+SS-WeM9, 36
Call, R.: AS+TF+VT-FrM2, 71
Callahan, C.: SP+AS+BI+ET+MI+TF-WeA11, 50
Calzolari, L.: BI+SS+AS-TuM12, 13
Camillone, N.: NS+AS+SS+SP-WeM12, **39**
Canepa, P.: EN+AS-ThA7, 67
Cao, Y.: TF+AS-WeA1, 51
Cardinaud, C.: AS-MoM4, **2**
Casolo, S.: GR+AS+EM+NS+SS-WeA12, 47
Caspar, J.: TF+AS-WeA1, 51
Castner, D.G.: SP+AS+BI-TuA11, 17; AS-WeM3, 34;
BI+SS+AS-TuM6, **12**; BN+AS-WeA9, 45;
IS+AS+BI+ET+GR+NS-TuA1, 21
Castro, G.R.: AS+TF+VT-FrM5, **71**
Caymax, M.: IS+AS+OX+ET-WeM9, 38
Ceccone, G.: BI+SS+AS-TuM12, **13**
Chabal, Y.J.: EL+TF+BI+AS+EM+SS-MoA2, 8;
EN+AS-ThA7, 67; GR+AS+BI+PS+SS-
WeM2, 36; GR+AS+EM+NS+SS-WeA1, 46;
TF+AS+SS-ThA3, 68
Chagarov, E.:
SP+AS+BI+ET+MI+NM+NS+SS+TF-WeM6,
40
Chakradhar, A.: NS+AS+SS+SP-WeM4, 38
Chamberlin, S.E.: IS+AS+OX+ET-WeM2, 37
Chambers, S.A.: IS+AS+OX+ET-WeM2, 37
Chan, C.: TF+AS-WeA1, 51
Chan, C.K.: VT+AS+SS-WeM1, 41
Chang, C.C.: VT+AS+SS-WeM1, 41
Chang, J.P.: EM+TF+AS-ThA3, 64
Chang, M.H.: EM+SS+AS+NS-ThM12, 57
Chang, W.-T.: HI+AS+NS-WeA8, 48
Chang, Y.H.: EM+SS+AS+NS-ThM12, 57
Chanson, R.: AS-MoM4, 2
Chase, B.: SP+AS+BI+ET+MI+TF-WeA9, 50
Chauhan, L.: AS-TuP23, **32**
Chen, B.: BN+AS-WeA12, 45
Chen, C.L.: VT+AS+SS-WeM1, **41**
Chen, J.: GR+AS+NS+SP+SS-TuA2, 20
Chen, J.-H.: GR+AS+NS+SS-ThM5, 58
Chen, J.R.: VT+AS+SS-WeM1, 41
Chen, S.: GR+AS+NS+SP+SS-TuA11, 21
Chen, Y.: HI+AS+BI+NS-ThM9, 59
Cheng, S.-F.: GR+AS+EM+MI+MN-TuM1, 13
Cheyns, D.: AS-ThM6, 54
Chien, D.: EM+TF+AS-ThA3, **64**
Chirita, V.: TF+AS-TuA4, **25**; TF+AS-TuA9, 26
Cho, K.J.: GR+AS+EM+NS+SS-WeA1, 46
Cho, T.S.: TC+EM+AS+TF+EN-ThM12, 62
Christen, H.M.: IS+AS+SS+EN-TuM5, 15
Christiani, G.: TF+AS-TuA10, 26
Chumbuni-Torres, K.: EL+TF+BI+AS+EM+SS-
MoA3, 9
Chung, J.G.: AS-ThA4, **63**; AS-TuP22, 31
Chupas, P.: IS+AS+SS+EN-TuM9, 15
Cimpoiasu, E.: GR+AS+NS+SS-ThM3, 58
Clark, T.: BI+AS-TuA4, 18
Clavero, C.: TF+AS+SS-ThA8, 69; VT+AS+SS-
WeM10, 42; VT+AS+SS-WeM6, 41
Cleveland, J.: SP+AS+BI+ET+MI+TF-WeA11, 50
Clifton, P.H.: AS-TuP18, 30
Cohen, K.D.:
SP+AS+BI+ET+MI+NM+NS+SS+TF-WeM5,
39
Colbow, V.: EN+AS-ThA6, 67
Colby, R.: AS+NS+SS+TF-WeA3, 43;
AS+NS+SS+TF-WeA4, 43

Colesniuc, C.: AS+TF+VT-FrM2, 71
 Collazo, R.: EM+TF+AS-ThA1, 64
 Conard, T.: AS-ThM6, 54
 Condon, N.J.: EM+TF+AS-ThA6, 65
 Conrad, E.: GR+AS+NS+SP+SS-TuA1, 19
 Constable, E.C.: IS+AS+SS+EN-TuM3, 14
 Cook, K.: EL+TF+BI+AS+EM+SS-MoA10, 9
 Coraux, J.: GR+AS+EM+NS+SS-WeA10, 46
 Corso, M.: SP+AS+BI+ET+MI+NM+NS+SS+TF-WeM4, 39
 Coultas, S.J.: AS+BI-TuM10, 11; AS+BI-TuM3, 10; AS+NS+SS+TF-WeA8, 43
 Counsell, J.D.P.: AS+BI-TuM10, 11; AS+BI-TuM3, 10
 Cowin, J.: IS+AS+BI+ET+GR+NS-TuA12, 23
 Craft, S.: EM+TF+AS-ThA1, 64
 Creatore, M.: TC+EM+AS+TF+EN-ThM2, 61
 Croad, O.: BI+SS+AS-TuM5, 12
 Crumlin, E.: IS+AS+SS+EN-TuM5, 15
 Csery, I.: AS+TF+VT-FrM3, 71
 Csik, A.: AS+TF+VT-FrM3, 71
 Cui, S.: GR+AS+NS+SP+SS-TuA2, 20
 Cui, X.: AS+TF+VT-FrM1, 71
 Cummings, P.T.: TF+AS-TuA1, 25
 Cumpson, P.J.: AS-MoA1, 7;
 SP+AS+BI+ET+MI+NM+NS+SS+TF-WeM10, 40
 Cuypers, D.: IS+AS+OX+ET-WeM9, 38
 Cyganik, P.: TF+AS+SS-ThA2, 68
 Czaplewski, D.A.: MN+AS-MoM3, 4

— D —

Dahal, A.: GR+AS+EM+NS+SS-WeA8, 46
 Dähne, M.: EM+TF+AS-ThA10, 66
 Dalmau, R.: EM+TF+AS-ThA1, 64
 Davis, A.N.: IS+AS+OX+ET-WeM11, 38
 Davis, R.C.: MN+AS-MoM4, 4
 Day, D.: BI+AS-TuA4, 18
 De Clercq, A.: IS+AS+OX+ET-WeM9, 38
 De Jesus, J.C.: AS-TuP28, 32
 DeBord, J.D.: AS-ThM5, 54
 Demko, A.: NS+AS+SS+SP-WeM2, 38
 Denny, Y.R.: AS-TuP22, 31
 Desai, T.V.: IS+AS+BI+ET+GR+NS-TuA2, 22
 Desse, F.: IS+AS+OX+ET-WeM11, 38
 Detchprohm, T.: EM+TF+AS-ThA7, 65
 Detslefs, B.: GR+AS+NS+SP+SS-TuA9, 20
 Devaraj, A.: AS+NS+SS+TF-WeA3, 43;
 AS+NS+SS+TF-WeA4, 43
 Dhere, N.: TF+AS-WeA11, 52
 Dhere, R.: EN+AS-ThA1, 66
 Dhiman, R.: EM+SS+AS+NS-ThM3, 56
 Diao, Z.: MN+AS-MoM9, 5
 Diebold, A.C.: GR+AS+NS+SP+SS-TuA11, 21;
 NM+AS+MS-MoM3, 5
 Dietz, N.: EM+TF+AS-ThA11, 66; EM+TF+AS-ThA9, 65
 DiLabio, G.:
 SP+AS+BI+ET+MI+NM+NS+SS+TF-WeM2, 39
 Dillon, E.: SP+AS+BI+ET+MI+TF-WeA9, 50
 Dimitrakopoulos, C.: GR+AS+NS+SP+SS-TuA11, 21
 Dittmann, R.: AS-ThA10, 64
 Divan, R.S.: MI+SP+AS-ThM12, 61; MN+AS-MoM5, 4
 Donegan, J.: HI+AS+BI+NS-ThM9, 59
 Dongare, A.D.: TF+AS-TuA7, 26
 Dougherty, D.B.: GR+AS+BI+PS+SS-WeM10, 36; GR+AS+NS+SP+SS-TuA11, 21
 Dowsett, D.: HI+AS+NS-WeA10, 48
 Draper, R.: NS+AS+SS+SP-WeM2, 38
 Draude, F.: AS-TuP1, 28
 Drews, J.: EM+SS+AS+NS-ThM3, 56
 Drube, W.: AS+TF+VT-FrM3, 71
 Dsouza, R.: AS-WeM6, 34
 Du, Y.G.: IS+AS+OX+ET-WeM2, 37
 Dubruel, P.: MN+AS-MoM10, 5
 Duenow, J.: TF+AS-WeA10, 52
 Dunham, B.M.: VT+AS+SS-WeM2, 41

Dürr, M.: AS-ThM10, 55
 Dussart, R.: MN+AS-MoM6, 4
 Dutta, M.: EN+AS-ThA6, 67

— E —

Eastman, J.A.: IS+AS+OX+ET-WeM3, 37
 Eastman, P.Y.: AS+NS+SS+TF-WeA9, 44
 Ebert, P.: EM+TF+AS-ThA10, 66
 Eddy, Jr., C.R.: EM+TF+AS-ThA6, 65;
 GR+AS+BI+PS+SS-WeM9, 36;
 GR+AS+EM+MI+MN-TuM1, 13;
 GR+AS+NS+SP+SS-TuA9, 20
 Edmonds, M.: AS-TuP21, 31;
 SP+AS+BI+ET+MI+NM+NS+SS+TF-WeM6, 40
 Egan, T.F.: BN+AS-WeA12, 45
 Eisele, H.: EM+TF+AS-ThA10, 66
 Ekinci, Y.: HI+AS+BI+NS-ThM11, 59
 Elam, J.W.: IS+AS+SS+EN-TuM9, 15;
 TC+EM+AS+TF+EN-ThM6, 62
 El-Khoury, P.Z.: SP+AS+BI+ET+MI+NS-TuA3, 23
 Eller, M.: AS-ThM5, 54
 Emery, J.D.: GR+AS+BI+PS+SS-WeM1, 35;
 GR+AS+NS+SP+SS-TuA9, 20
 Engel, L.: MN+AS-MoM10, 5
 Engelhard, M.: TF+AS+SS-ThA11, 70
 Engstrom, J.R.: IS+AS+BI+ET+GR+NS-TuA2, 22
 Espinosa-Magaña, F.: AS-TuP15, 30
 Esquinazi, P.: GR+AS+EM+MI+MN-TuM9, 13
 Exarhos, A.L.: GR+AS+EM+MI+MN-TuM2, 13

— F —

Facchetti, A.: TC+EM+AS-WeA1, 50
 Fahey, A.J.: AS+NS+SS+TF-WeA7, 43
 Fairley, N.: AS+BI-TuM12, 11
 Farmer, B.L.: GR+AS+BI+PS+SS-WeM6, 36
 Fartmann, M.: TF+AS+SS-ThA4, 69
 Faulkner, C.C.: HI+AS+BI+NS-ThM9, 59
 Favia, P.: AS-ThM6, 54
 Fazel, K.: AS-TuP27, 32
 Fears, K.: BI+AS-TuA4, 18
 Feenstra, R.: GR+AS+NS+SP+SS-TuA10, 21
 Feigelson, B.: GR+AS+EM+MI+MN-TuM1, 13
 Feldman, Y.: NS+AS+SS+SP-WeM4, 38
 Felhofer, J.L.: EL+TF+BI+AS+EM+SS-MoA3, 9
 Feng, G.: TF+AS-TuA1, 25
 Feng, X.-L.: MN+AS-MoM1, 3
 Fenter, P.: GR+AS+BI+PS+SS-WeM1, 35
 Ferguson, G.S.: EL+TF+BI+AS+EM+SS-MoA10, 9
 Ferguson, I.: EM+TF+AS-ThA11, 66;
 EM+TF+AS-ThA9, 65
 Fernandez, M.-C.: AS-MoM4, 2
 Fernandez-Torre, D.: SP+AS+BI+ET+MI+NS-TuA11, 24
 First, P.N.: GR+AS+NS+SP+SS-TuA3, 20
 Fischer, P.: MI+SP+AS-ThM11, 61
 Fisher, G.L.: AS-WeM12, 35
 Fleetwood, D.M.: EM+SS+AS+NS-ThM11, 57
 Fleurence, A.: TF+AS-WeA8, 52
 Folkman, C.M.: IS+AS+OX+ET-WeM3, 37
 Fong, D.D.: IS+AS+OX+ET-WeM3, 37
 Foussekis, M.: EM+TF+AS-ThA4, 65
 Fox, D.: HI+AS+BI+NS-ThM9, 59
 Franke, K.J.:
 SP+AS+BI+ET+MI+NM+NS+SS+TF-WeM4, 39
 Franquet, A.: AS-ThM6, 54
 Freeman, M.R.: MN+AS-MoM9, 5
 Freitas, Jr., J.A.: EM+TF+AS-ThA6, 65
 Froehner, S.C.: BN+AS-WeA9, 45
 Fruchart, O.: GR+AS+EM+NS+SS-WeA10, 46
 Fu, S.: TC+EM+AS-WeA9, 51
 Fu, T.-Y.: HI+AS+NS-WeA8, 48
 Fujikawa, Y.: IS+AS+OX+ET-WeM10, 38
 Fujita, D.: HI+AS+BI+NS-ThM12, 60
 Fuoss, P.H.: IS+AS+OX+ET-WeM3, 37

— G —

Gaddy, B.: EM+TF+AS-ThA1, 64

Gajdardziska-Josifovska, M.:
 GR+AS+NS+SP+SS-TuA2, 20
 Galatsis, K.: EM+SS+AS+NS-ThM11, 57
 Galla, S.: AS-TuP1, 28
 Gamage, S.D.: EM+TF+AS-ThA11, 66;
 EM+TF+AS-ThA9, 65
 Gamble, L.J.: BN+AS-WeA4, 44
 Garces, N.Y.: GR+AS+EM+MI+MN-TuM1, 13
 Garcia, C.D.: EL+TF+BI+AS+EM+SS-MoA3, 9
 Gargiulo, F.: GR+AS+NS+SS-ThM5, 58
 Garino, T.J.: AS-TuP5, 28
 Gartstein, Yu.N.: EL+TF+BI+AS+EM+SS-MoA2, 8
 Gaskill, D.K.: GR+AS+BI+PS+SS-WeM9, 36;
 GR+AS+NS+SP+SS-TuA9, 20
 Gaub, H.E.:
 SP+AS+BI+ET+MI+NM+NS+SS+TF-WeM11, 40
 Gautam, A.: GR+AS+NS+SS-ThM5, 58
 Gebhardt, C.R.: AS-ThM10, 55
 Geidel, M.: NM+AS+MS-MoM4, 6
 Geidobler, R.: AS+BI-TuM3, 10
 Geisse, N.: SP+AS+BI+ET+MI+TF-WeA11, 50
 Gerber, T.: GR+AS+NS+SP+SS-TuA7, 20
 Gessert, T.A.: EN+AS-ThA1, 66; TF+AS-WeA10, 52
 Ghorai, S.: IS+AS+BI+ET+GR+NS-TuA9, 23
 Giannuzzi, L.A.: AS+BI-TuA10, 17
 Giessibl, F.J.: SP+AS+BI+ET+MI+TF-WeA12, 50
 Gilles, M.K.: IS+AS+BI+ET+GR+NS-TuA9, 23
 Gilliland, D.: BI+SS+AS-TuM12, 13
 Gilmore, I.S.: AS-MoA9, 8; AS-ThA2, 63; AS-ThM4, 54
 Girard-Laurialt, P.-L.: AS+BI-TuM5, 10
 Gleason, K.K.: EM+SS+AS+NS-ThM4, 56
 Goldman, R.S.: EM+SS+AS+NS-ThM13, 57
 Goldstein, C.: TF+AS-TuA12, 26
 Gölzhäuser, A.: HI+AS+BI+NS-ThM11, 59;
 HI+AS+BI+NS-ThM5, 59
 Gong, C.: GR+AS+EM+NS+SS-WeA1, 46
 Gonon, P.: TF+AS-WeA12, 53
 Gonzalez, I.J.: AS-TuP28, 32
 Gorman, B.P.: AS+BI-TuA10, 17
 Gormiak, T.: BN+AS-WeA11, 45
 Götzén, J.: SP+AS+BI+ET+MI+NS-TuA10, 24
 Gowda, M.H.: GR+AS+EM+MI+MN-TuM1, 13
 Grabowski, K.: AS-TuP27, 32
 Graham, D.J.: BN+AS-WeA9, 45
 Grampeix, H.: TF+AS-WeA12, 53
 Grånäs, E.: GR+AS+NS+SP+SS-TuA7, 20;
 IS+AS+SS+EN-TuM12, 15
 Grant, J.T.: TF+AS+SS-ThA10, 70
 Grassian, V.: NM+AS+MS-MoM10, 6
 Grätzel, M.: IS+AS+SS+EN-TuM3, 14
 Greeley, J.: IS+AS+SS+EN-TuM9, 15
 Greene, J.E.: TF+AS-TuA4, 25
 Grehl, T.: TF+AS+SS-ThA4, 69
 Gretener, C.: TF+AS-WeA3, 52
 Grill, A.: GR+AS+NS+SP+SS-TuA11, 21
 Gross, L.: SP+AS+BI+ET+MI+NS-TuA1, 23
 Grundmeier, G.: TF+AS+SS-ThA1, 68
 Grunze, M.H.: BI+SS+AS-TuM2, 11; BN+AS-WeA11, 45
 Guallar-Hoyas, C.: IS+AS+BI+ET+GR+NS-TuA3, 22
 Gunlycke, D.: GR+AS+NS+SS-ThM3, 58
 Guo, H.X.: HI+AS+BI+NS-ThM12, 60
 Guo, J.H.: IS+AS+SS+EN-TuM3, 14
 Gupta, A.: AS-ThA7, 64
 Gupta, S.: AS-TuP23, 32
 Guttmann, P.: BP+AS-SuA3, 1
 Gwo, S.: EM+TF+AS-ThA10, 66

— H —

Haasch, R.T.: TC+EM+AS+TF+EN-ThM6, 62
 Haase, A.: AS-TuP1, 28
 Habenicht, B.: GR+AS+EM+NS+SS-WeA11, 47
 Hackett, J.B.: VT+AS+SS-WeM9, 42

- Haehner, G.: SP+AS+BI+ET+MI+NM+NS+SS+TF-WeM9, 40
- Hagenhoff, B.: TF+AS+SS-ThA4, 69
- Hager, G.: AS+NS+SS+TF-WeA7, 43
- Hähner, G.: SP+AS+BI+ET+MI+TF-WeA7, 49
- Halevi, B.: IS+AS+SS+EN-TuM6, 15
- Hammond, J.S.: AS-ThA3, 63; AS-WeM12, 35; EN+AS-ThA4, 67
- Hanley, L.: BI+AS-TuA8, 19
- Hansen, R.: MN+AS-MoM4, 4
- Hao, Y.: GR+AS+NS+SP+SS-TuA11, 21
- Harada, Y.: GR+AS+EM+NS+SS-WeA12, 47
- Harari, I.: MN+AS-MoM10, 5
- Hashimoto, N.: EM+TF+AS-ThA12, 66
- Hauge, R.: BN+AS-WeA12, 45
- Havelund, R.: AS-ThA2, 63; AS-ThM4, 54
- Havercroft, N.: AS-MoA4, 7; AS-ThM11, 55; AS-WeM11, 35
- Haydell, M.: GR+AS+NS+SS-ThM3, 58
- He, G.: GR+AS+NS+SP+SS-TuA10, 21
- Hell, S.W.: BP+AS-SuA5, 1
- Hemminger, J.C.: TF+AS-WeA2, 51
- Henderson, C.: EL+TF+BI+AS+EM+SS-MoA6, 9
- Henzler, K.: BP+AS-SuA3, 1
- Heo, S.: AS-TuP22, 31
- Herman, G.S.: TC+EM+AS+TF+EN-ThM5, 62
- Hernández, S.C.: GR+AS+BI+PS+SS-WeM9, 36
- Herpers, A.: AS-ThA10, 64
- Herrera-Gomez, A.: AS-MoM5, 2; AS-TuP15, 30; AS-TuP16, 30
- Hersam, M.C.: GR+AS+BI+PS+SS-WeM1, 35; GR+AS+BI+PS+SS-WeM3, 36; GR+AS+NS+SP+SS-TuA9, 20
- Herzing, A.: AS+BI-TuA9, 17
- Heylings, J.: BN+AS-WeA10, 45
- Hiebert, W.K.: MN+AS-MoM9, 5
- Highland, M.J.: IS+AS+OX+ET-WeM3, 37
- Hillion, F.: IS+AS+OX+ET-WeM11, 38
- Hinkov, V.: TF+AS-TuA10, 26
- Hiramatsu, M.: GR+AS+NS+SS-ThM9, 58
- Hiraoka, K.: AS-ThM12, 55; AS-TuP3, 28; AS-TuP6, 29
- Hirschmugl, C.: AS-WeM6, 34; GR+AS+NS+SP+SS-TuA2, 20
- Hite, J.K.: EM+TF+AS-ThA6, 65
- Hobbs, J.K.: SP+AS+BI+ET+MI+NS-TuA7, 24
- Hockenbery, D.: BN+AS-WeA4, 44
- Hoehne, R.: GR+AS+EM+MI+MN-TuM9, 13
- Hohlbauch, S.: SP+AS+BI+ET+MI+TF-WeA11, 50
- Holbrook, R.D.: AS+BI-TuA9, 17
- Holzke, C.: SP+AS+BI+ET+MI+NM+NS+SS+TF-WeM5, 39
- Hong, J.: TC+EM+AS+TF+EN-ThM12, 62
- Hong, W.T.: IS+AS+SS+EN-TuM5, 15
- Hong, Y.-L.: EM+TF+AS-ThA10, 66
- Hook, D.J.: AS-TuP19, 31
- Hori, M.: GR+AS+NS+SS-ThM9, 58
- Hosono, H.: TC+EM+AS+TF+EN-ThM3, 61
- Hou, J.-L.: HI+AS+NS-WeA8, 48
- Houssiau, L.: AS-MoA2, 7
- Hsieh, C.J.: MN+AS-MoM11, 5
- Hsiung, G.Y.: VT+AS+SS-WeM1, 41
- Hu, Q.: SP+AS+BI+ET+MI+TF-WeA9, 50
- Hu, Y.: SP+AS+BI+ET+MI+TF-WeA8, 49
- Hu, Y.F.: AS+TF+VT-FrM1, 71
- Hubault, C.: TF+AS-WeA8, 52
- Hubler, G.: AS-TuP27, 32
- Hughes, G.J.: AS-TuP23, 32; AS-TuP7, 29
- Hultman, L.: TF+AS-TuA4, 25; TF+AS-TuA9, 26
- Huo, Y.J.: BI+AS-TuA10, 19
- Hurley, P.K.: AS-TuP7, 29
- Hussein, R.: BI+SS+AS-TuM12, 13
- Hussey, L.: EM+TF+AS-ThA1, 64
- Hutton, S.J.: AS+BI-TuM10, 11; AS+BI-TuM3, 10; AS+NS+SS+TF-WeA8, 43; AS-ThM1, 54; AS-TuP13, 30; AS-TuP14, 30
- Hwang, C.: AS+TF+VT-FrM3, 71
- Hwang, H.H.: AS-TuP2, 28
- Hwang, I.-S.: HI+AS+NS-WeA8, 48
- I —
- Ianno, N.J.: EL+TF+AS+EM+SS-TuP1, 32
- Iida, S.: AS+BI-TuM9, 11
- Im, M.-Y.: MI+SP+AS-ThM11, 61
- Irving, D.: EM+TF+AS-ThA1, 64; TF+AS-TuA12, 26
- Ishigami, M.: GR+AS+BI+PS+SS-WeM6, 36
- Ishikawa, K.: GR+AS+NS+SS-ThM9, 58
- Islam, M.F.: TC+EM+AS-WeA7, 51
- Itoi, T.: EM+TF+AS-ThA12, 66
- Ivanova, L.: EM+TF+AS-ThA10, 66
- J —
- Jaiswal, P.: AS-TuP23, 32
- Jakubiak, R.: TF+AS+SS-ThA10, 70
- Jang, J.S.: AS-TuP2, 28
- Jelinek, P.: SP+AS+BI+ET+MI+NS-TuA4, 23
- Jena, D.: GR+AS+NS+SS-ThM11, 59
- Jennings, W.D.: AS-MoA6, 7
- Jensen, B.D.: MN+AS-MoM4, 4
- Jernigan, G.G.: TF+AS-TuA3, 25
- Jesse, S.: SP+AS+BI+ET+MI+NS-TuA12, 25; SP+AS+BI+ET+MI+TF-WeA1, 49
- Jia, Q.: IS+AS+OX+ET-WeM3, 37
- Jobbins, M.M.: IS+AS+OX+ET-WeM1, 37
- Johnson, C.E.: IS+AS+BI+ET+GR+NS-TuA7, 22
- Johnson, J.A.: IS+AS+BI+ET+GR+NS-TuA7, 22
- Johnson, M.: NS+AS+SS+SP-WeM2, 38
- Johnson, M.D.: AS-ThA1, 63
- Johnson, S.D.: GR+AS+EM+MI+MN-TuM1, 13
- Jones, J.G.: TF+AS+SS-ThA10, 70
- Jordan, M.B.: MN+AS-MoM5, 4
- Jousseume, V.: TF+AS-WeA12, 53
- Joy, D.: HI+AS+NS-WeA1, 47
- Joy, R.: TC+EM+AS+TF+EN-ThM2, 61
- Judd, A.: BN+AS-WeA10, 45
- Jungnickel, H.: AS-TuP1, 28
- Junige, M.: NM+AS+MS-MoM4, 6
- K —
- Kahng, S.-J.: EM+SS+AS+NS-ThM12, 57
- Kajiwaru, T.: GR+AS+NS+SS-ThM1, 57
- Kalinin, S.V.: SP+AS+BI+ET+MI+NS-TuA12, 25
- Kan, M.R.: MN+AS-MoM9, 5
- Kanda, T.: GR+AS+NS+SS-ThM9, 58
- Kandel, S.A.: AS-TuP26, 32; IS+AS+OX+ET-WeM1, 37
- Kanevce, A.: EN+AS-ThA1, 66
- Kang, H.J.: AS-ThA4, 63; AS-TuP2, 28; AS-TuP22, 31
- Karakoti, A.S.: AS+BI-TuA12, 18
- Karim, A.M.: IS+AS+SS+EN-TuM10, 15
- Karmel, H.J.: GR+AS+NS+SP+SS-TuA9, 20
- Kaspar, T.C.: IS+AS+OX+ET-WeM2, 37
- Katoch, J.: GR+AS+BI+PS+SS-WeM6, 36
- Katz, H.E.: TC+EM+AS-WeA3, 50
- Kaul, A.: TF+AS-WeA11, 52
- Kawakami, R.: GR+AS+EM+MI+MN-TuM3, 13
- Kayser, S.: AS-MoA4, 7; AS-ThM11, 55; AS-WeM11, 35
- Keavney, D.: MI+SP+AS-ThM12, 61
- Keimer, B.: TF+AS-TuA10, 26
- Kelkar, U.: TF+AS-TuA11, 26
- Kelley, M.J.: VT+AS+SS-WeM4, 41
- Kellogg, G.L.: GR+AS+NS+SP+SS-TuA8, 20
- Kelly, S.T.: IS+AS+BI+ET+GR+NS-TuA9, 23
- Kelly, T.F.: AS-TuP18, 30
- Kent, T.J.: AS-TuP21, 31; SP+AS+BI+ET+MI+NM+NS+SS+TF-WeM6, 40
- Kessels, W.M.M.: TC+EM+AS+TF+EN-ThM2, 61
- Keun, S.K.: IS+AS+OX+ET-WeM3, 37
- Kiefer, B.: IS+AS+SS+EN-TuM6, 15
- Kikkawa, J.M.: GR+AS+EM+MI+MN-TuM2, 13
- Kim, D.J.: IS+AS+OX+ET-WeM2, 37
- Kim, H.: EM+SS+AS+NS-ThM12, 57
- Kim, K.H.: TC+EM+AS-WeA7, 51
- Kim, K.J.: AS-TuP2, 28
- Kim, S.: EM+SS+AS+NS-ThM11, 57
- Kim, S.-K.: MI+SP+AS-ThM11, 61
- Kim, S.N.: GR+AS+BI+PS+SS-WeM6, 36
- Kim, Y.-H.: EM+SS+AS+NS-ThM12, 57
- King, W.: GR+AS+NS+SS-ThM3, 58
- Kingshott, P.: BI+AS-TuA3, 18
- Kinross, J.: IS+AS+BI+ET+GR+NS-TuA3, 22
- Kisielowski, C.: GR+AS+NS+SS-ThM5, 58
- Kjoller, K.: SP+AS+BI+ET+MI+TF-WeA9, 50
- Knaut, M.: NM+AS+MS-MoM4, 6
- Knies, D.: AS-TuP27, 32
- Knoops, H.C.M.: TC+EM+AS+TF+EN-ThM2, 61
- Knuudsen, J.: GR+AS+NS+SP+SS-TuA7, 20; IS+AS+SS+EN-TuM12, 15
- Kobata, M.: AS-ThA10, 64
- Kobayashi, K.: AS-ThA10, 64
- Koelsch, P.: AS-WeM1, 34; AS-WeM3, 34
- Kollmer, F.: AS-MoA4, 7; AS-ThM11, 55; AS-WeM11, 35
- Komarneni, M.: NS+AS+SS+SP-WeM4, 38
- Komori, F.: GR+AS+NS+SS-ThM1, 57
- Kondo, H.: GR+AS+NS+SS-ThM9, 58
- Kondo, T.: GR+AS+EM+NS+SS-WeA12, 47
- Kondoh, H.: IS+AS+SS+EN-TuM12, 15
- Konicek, A.R.: AS+BI-TuA9, 17
- Konneker, A.: MN+AS-MoM4, 4
- Kono, Y.: BN+AS-WeA3, 44
- Korolkov, V.: SP+AS+BI+ET+MI+NS-TuA9, 24
- Körsgen, M.: AS-TuP1, 28
- Koster, N.B.: HI+AS+NS-WeA9, 48
- Kotula, P.G.: AS-TuP5, 28
- Kövér, L.: AS+TF+VT-FrM3, 71
- Kranz, L.: TF+AS-WeA3, 52
- Kroemker, B.: GR+AS+NS+SP+SS-TuA1, 19
- Krueger, B.: TC+EM+AS+TF+EN-ThM11, 62
- Krylov, S.: MN+AS-MoM10, 5
- Kuang, Z.: GR+AS+BI+PS+SS-WeM6, 36
- Kub, F.J.: EM+TF+AS-ThA6, 65; GR+AS+EM+MI+MN-TuM1, 13
- Kuchibhatla, S.V.N.T.: AS+BI-TuA12, 18
- Kuciauskas, D.: EN+AS-ThA1, 66
- Kucukgok, B.: EM+TF+AS-ThA9, 65
- Kumar, A.: EL+TF+BI+AS+EM+SS-MoA8, 9
- Kumar, S.: EL+TF+BI+AS+EM+SS-MoA8, 9
- Kummel, A.C.: AS-TuP21, 31; BN+AS-WeA3, 44; SP+AS+BI+ET+MI+NM+NS+SS+TF-WeM6, 40
- Kungas, R.: SP+AS+BI+ET+MI+TF-WeA3, 49
- Kuo, H.-S.: HI+AS+NS-WeA8, 48
- Kusakabe, K.: EM+TF+AS-ThA12, 66
- Kwon, Y.J.: TF+AS-WeA2, 51
- Kyoung, Y.K.: AS+BI-TuM9, 11; AS-ThA4, 63
- L —
- LaBella, V.P.: GR+AS+NS+SP+SS-TuA11, 21
- Ladroue, J.: MN+AS-MoM6, 4
- Laera, S.: BI+SS+AS-TuM12, 13
- LaGoo, L.: AS+BI-TuM4, 10
- Lanceros-Méndez, S.: BI+AS-TuA7, 18
- Landt, L.: AS+TF+VT-FrM2, 71
- Larson, D.J.: AS-TuP18, 30
- Laskin, A.: IS+AS+BI+ET+GR+NS-TuA9, 23
- Latu-Romain, L.: TF+AS-WeA12, 53
- Law, M.: TF+AS-WeA2, 51
- Lawrence, D.: AS-TuP18, 30
- LeBeau, J.: EM+TF+AS-ThA1, 64
- Lee, B.-J.: AS-ThM10, 55
- Lee, D.Y.: IS+AS+OX+ET-WeM1, 37
- Lee, H.I.: AS-ThA4, 63
- Lee, I.: TC+EM+AS-WeA7, 51
- Lee, J.: SP+AS+BI+ET+MI+NS-TuA3, 23
- Lee, J.C.: AS+BI-TuM9, 11; AS-ThA4, 63; AS-TuP22, 31
- Lee, J.R.I.: AS+TF+VT-FrM2, 71; IS+AS+OX+ET-WeM6, 38
- Lee, K.I.: AS-TuP22, 31
- Lee, S.Y.: AS-TuP22, 31
- Lee, T.Y.: VT+AS+SS-WeM1, 41
- Lee, W.K.: GR+AS+NS+SS-ThM3, 58

- Lefaucheux, P.: MN+AS-MoM6, 4
 Lei, Y.: IS+AS+SS+EN-TuM9, 15
 Lenz, A.: EM+TF+AS-ThA10, 66
 Lewis, E.K.: BN+AS-WeA12, 45
 Li, C.: TC+EM+AS-WeA4, 51
 Li, J.: EN+AS-ThA7, 67
 Li, J.B.: TC+EM+AS-WeA4, 51
 Li, Q.: SP+AS+BI+ET+MI+NS-TuA12, 25
 Li, S.: TF+AS-TuA1, 25
 Li, Y.: VT+AS+SS-WeM2, 41
 Li, Z.: VT+AS+SS-WeM10, 42; VT+AS+SS-WeM6, 41
 Li, Z.S.: EM+SS+AS+NS-ThM3, 56
 Liang, C.-K.: AS-ThM5, 54
 Libera, J.A.: TC+EM+AS+TF+EN-ThM6, 62
 Liberman, A.: BN+AS-WeA3, 44
 Liddle, J.A.: NM+AS+MS-MoM1, 5
 Lin, C.-Y.: HI+AS+NS-WeA8, 48
 Lin, J.H.: AS-TuP7, 29
 Lin, J.M.: AS-TuP20, 31
 Lin, W.Z.: SP+AS+BI+ET+MI+NS-TuA12, 25
 Lin, Y.C.: MN+AS-MoM11, 5
 Lin, Y.H.: EM+SS+AS+NS-ThM13, 57
 Linck, M.: GR+AS+NS+SS-ThM5, 58
 Lindh, L.: BI+SS+AS-TuM3, 12
 Liou, J.C.: MN+AS-MoM11, 5
 Lippitz, A.: AS+BI-TuM5, 10
 Liu, B.: IS+AS+SS+EN-TuM9, 15
 Liu, X.: VT+AS+SS-WeM2, 41
 Liu, Y.: TC+EM+AS-WeA3, 50
 Liu, Z.: IS+AS+SS+EN-TuM4, 14; IS+AS+SS+EN-TuM5, 15
 Livadaru, L.: SP+AS+BI+ET+MI+NM+NS+SS+TF-WeM2, 39
 Lo, E.: IS+AS+BI+ET+GR+NS-TuA1, 21
 Lo, M.: SP+AS+BI+ET+MI+TF-WeA9, 50
 Lock, E.H.: GR+AS+BI+PS+SS-WeM9, 36
 Locquet, J.P.: IS+AS+OX+ET-WeM9, 38
 Lofaro, J.C.: NS+AS+SS+SP-WeM12, 39
 Logvenov, G.: TF+AS-TuA10, 26
 Lohstreter, L.: AS+BI-TuM4, 10; AS-MoA8, 8
 Lotze, C.: SP+AS+BI+ET+MI+NM+NS+SS+TF-WeM4, 39
 Louette, P.: AS-MoA2, 7
 Louie, S.G.: GR+AS+NS+SS-ThM5, 58
 Love, C.: BI+AS-TuA4, 18
 Lu, G.: GR+AS+NS+SP+SS-TuA2, 20
 Lu, J.: IS+AS+SS+EN-TuM9, 15
 Lu, M.: TF+AS-WeA1, 51
 Lu, Y.: AS-TuP26, 32
 Lu, Y.-H.: HI+AS+NS-WeA8, 48
 Luch, A.: AS-TuP1, 28
 Lui, Y.: IS+AS+BI+ET+GR+NS-TuA7, 22
 Lukaszew, R.A.: TF+AS+SS-ThA8, 69; VT+AS+SS-WeM10, 42; VT+AS+SS-WeM6, 41; VT+AS+SS-WeM9, 42
 Luo, H.: EL+TF+BI+AS+EM+SS-MoA9, 9
 Lyubinsky, I.: IS+AS+OX+ET-WeM2, 37
- **M** —
 Ma, J.: EN+AS-ThA1, 66
 Ma, Q.: SP+AS+BI+ET+MI+NM+NS+SS+TF-WeM5, 39
 Maas, D.J.: HI+AS+NS-WeA9, 48
 Macak, E.: AS+NS+SS+TF-WeA8, 43
 Macak, K.: AS+NS+SS+TF-WeA8, 43
 Mack, P.: AS+BI-TuM11, 11; AS-MoA2, 7; AS-MoM10, 3; BI+AS-TuA7, 18
 Macke, S.: TF+AS-TuA10, 26
 Maerkl, S.: BI+AS-TuA11, 19
 Magnone, K.: SP+AS+BI+ET+MI+NM+NS+SS+TF-WeM5, 39
 Magnuson, C.W.: GR+AS+NS+SP+SS-TuA11, 21
 Mahoney, C.M.: AS+BI-TuM6, 10
 Maidecchi, G.: EL+TF+BI+AS+EM+SS-MoA8, 9
 Majzik, Z.: SP+AS+BI+ET+MI+NS-TuA4, 23
 Maksymovych, P.: NS+AS+SS+SP-WeM11, 39
 Malko, A.V.: EL+TF+BI+AS+EM+SS-MoA2, 8
- Manandar, B.: AS-WeM6, 34
 Mannequin, C.: TF+AS-WeA12, 53
 Mansour, A.N.: GR+AS+NS+SS-ThM10, 58
 Mao, B.: IS+AS+SS+EN-TuM4, 14
 Marcott, C.: SP+AS+BI+ET+MI+TF-WeA9, 50
 Maria, J.-P.: TF+AS-TuA12, 26
 Marquis, E.A.: AS+NS+SS+TF-WeA1, 43
 Martinez, H.P.: BN+AS-WeA3, 44
 Mascarenhas, A.: MI+SP+AS-ThM12, 61
 Mastro, M.A.: EM+TF+AS-ThA6, 65
 Matsubayashi, A.: GR+AS+EM+NS+SS-WeA7, 46
 Matsuo, J.: AS-ThM9, 55
 Mattrey, R.F.: BN+AS-WeA3, 44
 Mattson, E.: AS-WeM6, 34; GR+AS+NS+SP+SS-TuA2, 20
 Maziarz, E.P.: AS-TuP19, 31
 McCleskey, T.M.: IS+AS+OX+ET-WeM3, 37
 McNamara, J.D.: EM+TF+AS-ThA4, 65
 McNeilan, J.D.: GR+AS+NS+SP+SS-TuA11, 21
 Medina, A.A.: EL+TF+AS+EM+SS-TuP2, 32
 Mehr, T.: SP+AS+BI+ET+MI+TF-WeA11, 50
 Melitz, W.: AS-TuP21, 31
 Melton, A.G.: EM+TF+AS-ThA11, 66; EM+TF+AS-ThA9, 65
 Mendes, G.P.: AS-TuP11, 30; BI+AS-TuA7, 18
 Meneghini, C.: AS-ThA7, 64
 Merchea, M.: AS-TuP19, 31
 Merrill, M.D.: IS+AS+OX+ET-WeM6, 38
 Meyer III, H.M.: AS-TuP12, 30
 Meyer, G.: SP+AS+BI+ET+MI+NS-TuA1, 23
 Meyer, J.R.: EM+TF+AS-ThA6, 65
 Meyer, R.L.: BI+AS-TuA3, 18
 Michael, J.R.: AS-TuP5, 28
 Michely, T.W.: GR+AS+NS+SP+SS-TuA7, 20
 Miller, C.W.: MI+SP+AS-ThM5, 60
 Miller, J.: IS+AS+SS+EN-TuM9, 15
 Miller, T.J.: EN+AS-ThA8, 67
 Mily, E.: TF+AS-TuA12, 26
 Min, H.: AS+BI-TuM5, 10
 Minne, S.C.: SP+AS+BI+ET+MI+TF-WeA8, 49
 Mita, S.: EM+TF+AS-ThA1, 64
 Moberg, R.: AS+TF+VT-FrM7, 72
 Moellers, R.: AS-MoA4, 7; AS-ThM11, 55; AS-WeM11, 35
 Mohn, F.: SP+AS+BI+ET+MI+NS-TuA1, 23
 Molkenboer, F.T.: HI+AS+NS-WeA9, 48
 Moll, N.: SP+AS+BI+ET+MI+NS-TuA1, 23
 Mönig, H.: SP+AS+BI+ET+MI+NS-TuA10, 24
 Monton, C.M.: AS+TF+VT-FrM2, 71
 Monya, Y.: IS+AS+SS+EN-TuM12, 15
 Moody, B.: EM+TF+AS-ThA1, 64
 Moon, D.W.: BP+AS-SuA1, 1
 Moore, J.F.: BN+AS-WeA12, 45
 Moore, R.: GR+AS+NS+SP+SS-TuA11, 21
 Morgen, P.: EM+SS+AS+NS-ThM3, 56
 Morita, S.: SP+AS+BI+ET+MI+NS-TuA11, 24
 Morrish, F.: BN+AS-WeA4, 44
 Moshar, A.: SP+AS+BI+ET+MI+TF-WeA11, 50
 Moss, G.: BN+AS-WeA10, 45
 Moulder, J.F.: AS-ThA3, 63; EN+AS-ThA4, 67
 Muirhead, L.: IS+AS+BI+ET+GR+NS-TuA3, 22
 Muñoz-Flores, J.: AS-TuP16, 30
 Munson, A.: GR+AS+NS+SP+SS-TuA11, 21
 Munusamy, P.: AS+BI-TuA12, 18
 Murphy, C.J.: EM+SS+AS+NS-ThM9, 56
 Murphy, N.R.: TF+AS+SS-ThA10, 70
 Mürthing, J.: AS-TuP1, 28
 Muthinti, G.R.: NM+AS+MS-MoM3, 5
 Mutombo, P.: SP+AS+BI+ET+MI+NS-TuA4, 23
 Mutoro, E.: IS+AS+SS+EN-TuM5, 15
 Myers-Ward, R.L.: GR+AS+BI+PS+SS-WeM9, 36; GR+AS+NS+SP+SS-TuA9, 20
- **N** —
 Nachimuthu, P.: TC+EM+AS+TF+EN-ThM5, 62
 Naes, B.E.: AS+NS+SS+TF-WeA7, 43
 Nagano, S.: HI+AS+BI+NS-ThM12, 60
 Naik, R.R.: GR+AS+BI+PS+SS-WeM6, 36
 Nakagawa, S.: AS-ThM9, 55
- Nakamura, J.: GR+AS+EM+NS+SS-WeA12, 47
 Nakatsuji, K.: GR+AS+NS+SS-ThM1, 57
 Nanayakkara, S.: SP+AS+BI+ET+MI+TF-WeA4, 49
 Narayanan, S.: TC+EM+AS-WeA9, 51
 Nasse, M.: GR+AS+NS+SP+SS-TuA2, 20
 N'Diaye, A.T.: GR+AS+EM+NS+SS-WeA10, 46
 Nelson, C.M.: EL+TF+BI+AS+EM+SS-MoA9, 9
 Nelson, F.J.: GR+AS+NS+SP+SS-TuA11, 21
 Nguyen, H.M.: EL+TF+BI+AS+EM+SS-MoA2, 8
 Niehuis, E.: AS-MoA4, 7; AS-ThM11, 55; AS-WeM11, 35
 Nigge, P.: IS+AS+BI+ET+GR+NS-TuA9, 23
 Nijem, N.: EN+AS-ThA7, 67
 Ninomiya, S.: AS-ThM12, 55; AS-TuP6, 29
 Nonnenmann, S.S.: SP+AS+BI+ET+MI+TF-WeA3, 49
 Notingher, I.: BN+AS-WeA1, 44
 Notte, J.: HI+AS+NS-WeA10, 48
 Noufi, R.: EN+AS-ThA1, 66
 Novikova, I.: TF+AS+SS-ThA8, 69
 Novoselov, K.: GR+AS+BI+PS+SS-WeM2, 36
 Nunney, T.S.: AS+BI-TuM11, 11; AS-MoA2, 7
 Nyakiti, L.O.: GR+AS+BI+PS+SS-WeM9, 36; GR+AS+NS+SP+SS-TuA9, 20
- **O** —
 Obare, S.: NM+AS+MS-MoM8, 6
 O'Brien, C.J.: TF+AS-TuA7, 26
 O'Connor, S.: EM+TF+AS-ThA6, 65
 Oezkaya, B.: TF+AS+SS-ThA1, 68
 Offi, F.: AS-ThA10, 64
 Ogaki, R.: BI+AS-TuA3, 18
 Ogitsu, T.: IS+AS+OX+ET-WeM6, 38
 Oh, Y.: TC+EM+AS-WeA7, 51
 Ohldag, H.: GR+AS+EM+MI+MN-TuM9, 13
 Ohlhausen, J.A.: AS-TuP5, 28
 Ohta, T.: GR+AS+NS+SP+SS-TuA8, 20
 Ohuchi, F.S.: TC+EM+AS+TF+EN-ThM11, 62
 Okuda, T.: EM+TF+AS-ThA12, 66
 Oleynik, I.I.: GR+AS+EM+MI+MN-TuM10, 14; GR+AS+EM+NS+SS-WeA2, 46
 Olmstead, M.A.: TC+EM+AS+TF+EN-ThM11, 62
 Olson, D.: AS-TuP18, 30
 Ondracek, M.: SP+AS+BI+ET+MI+NS-TuA4, 23
 Onishi, K.: HI+AS+BI+NS-ThM12, 60
 Oppen, F.V.: SP+AS+BI+ET+MI+NM+NS+SS+TF-WeM4, 39
 Oshima, M.: GR+AS+EM+NS+SS-WeA12, 47
 Ossowski, J.: TF+AS+SS-ThA2, 68
 Outlaw, R.A.: GR+AS+NS+SS-ThM10, 58
- **P** —
 Pacholski, M.L.: AS+NS+SS+TF-WeA9, 44
 Page, S.J.: AS+NS+SS+TF-WeA8, 43; AS-ThM1, 54
 Paiella, R.: EM+SS+AS+NS-ThM1, 56
 Palomino, R.: NS+AS+SS+SP-WeM12, 39
 Pan, M.H.: SP+AS+BI+ET+MI+NS-TuA12, 25
 Panaccione, G.: AS-ThA10, 64
 Pandey, A.: TC+EM+AS+TF+EN-ThM5, 62
 Paolini, C.: VT+AS+SS-WeM3, 41
 Park, C.: AS-ThA10, 64
 Park, H.: NS+AS+SS+SP-WeM12, 39
 Parkin, J.D.: SP+AS+BI+ET+MI+NM+NS+SS+TF-WeM9, 40; SP+AS+BI+ET+MI+TF-WeA7, 49
 Pascual, J.I.: SP+AS+BI+ET+MI+NM+NS+SS+TF-WeM4, 39
 Patel, A.: EN+AS-ThA6, 67
 Paul, W.: AS-WeM11, 35
 Peixoto, T.: TF+AS+SS-ThA3, 68
 Pelster, A.: AS-TuP1, 28
 Perdue, S.M.: SP+AS+BI+ET+MI+NS-TuA3, 23
 Perea, D.E.: AS+NS+SS+TF-WeA3, 43; AS+NS+SS+TF-WeA4, 43
 Perera, A.G.U.: EM+TF+AS-ThA9, 65
 Peres, P.: IS+AS+OX+ET-WeM11, 38

- Pérez Quintero, K.J.: MN+AS-MoM3, 4
Perez, R.: SP+AS+BI+ET+MI+NS-TuA10, 24;
SP+AS+BI+ET+MI+NS-TuA11, 24
Perkins, F.K.: TF+AS-TuA3, 25
Perng, Y.-C.: EM+TF+AS-ThA3, 64
Perrenoud, J.: TF+AS-WeA3, 52
Perret, E.: IS+AS+OX+ET-WeM3, 37
Perrine, K.A.: AS-TuP20, 31
Perriot, R.: GR+AS+EM+MI+MN-TuM10, 14
Perry, S.S.: BI+AS-TuA10, 19
Pertsin, A.J.: BI+SS+AS-TuM2, 11
Petersen, E.: NS+AS+SS+SP-WeM2, 38
Peterson, B.: NM+AS+MS-MoM3, 5
Petford-Long, A.: IS+AS+BI+ET+GR+NS-TuA7,
22
Pethe, S.: TF+AS-WeA11, 52
Petrov, I.: TF+AS-TuA4, 25
Petrovykh, D.Y.: AS-TuP11, 30; BI+AS-TuA7, 18
Pham, H.: TC+EM+AS+TF+EN-ThM11, 62
Piao, H.: AS+BI-TuM12, 11; AS+TF+VT-FrM1,
71
Pillatsch, L.: HI+AS+NS-WeA10, 48
Pipe, K.P.: EM+SS+AS+NS-ThM13, 57
Pireaux, J.J.: AS-MoA2, 7
Pittenger, B.: SP+AS+BI+ET+MI+TF-WeA8, 49
Pitters, J.: SP+AS+BI+ET+MI+NM+NS+SS+TF-
WeM2, 39
Pitters, J.L.: HI+AS+NS-WeA7, 48
Piva, P.: SP+AS+BI+ET+MI+NM+NS+SS+TF-
WeM2, 39
Poelsema, B.: HI+AS+NS-WeA3, 47
Polina, A.: HI+AS+BI+NS-ThM5, 59
Ponomarev, M.V.: TC+EM+AS+TF+EN-ThM2,
61
Popovitz-Biro, R.: NS+AS+SS+SP-WeM4, 38
Porter, L.M.: TC+EM+AS-WeA9, 51
Portoles, J.F.:
SP+AS+BI+ET+MI+NM+NS+SS+TF-
WeM10, 40
Pou, P.: SP+AS+BI+ET+MI+NS-TuA11, 24
Powell, C.J.: AS-MoM3, 2; AS-MoM6, 3
Prater, C.B.: SP+AS+BI+ET+MI+TF-WeA9, 50
Prochs, R.: SP+AS+BI+ET+MI+TF-WeA11, 50
Prosa, T.J.: AS-TuP18, 30
Pu, H.: GR+AS+NS+SP+SS-TuA2, 20
Py, M.: AS-ThM9, 55
- Q —
Quardokus, R.C.: AS-TuP26, 32
Quinlan, R.A.: GR+AS+NS+SS-ThM10, 58
- R —
Radi, A.: TF+AS-TuA10, 26
Rading, D.: AS-ThM11, 55; AS-WeM11, 35
Radja, A.: EL+TF+BI+AS+EM+SS-MoA2, 8
Radue, E.: TF+AS+SS-ThA8, 69
Rafati, A.: AS+BI-TuA11, 17
Rafik, A.: GR+AS+EM+NS+SS-WeA8, 46
Rahman, T.S.: AS+BI-TuA1, 17; AS+BI-TuA3, 17
Rajachidambaram, M.S.: TC+EM+AS+TF+EN-
ThM5, 62
Rajput, P.: AS-ThA7, 64
Raman, S.N.: AS-ThA3, 63; EN+AS-ThA4, 67
Ramana, C.V.: TF+AS+SS-ThA11, 70;
TF+AS+SS-ThA9, 69
Rangan, S.: EN+AS-ThA9, 68
Ranish, J.: TF+AS-TuA11, 26
Ranson, P.: MN+AS-MoM6, 4
Rao, M.: MN+AS-MoM5, 4
Raso, R.: AS+NS+SS+TF-WeA8, 43
Ratner, B.D.: BI+AS-TuA1, 18;
IS+AS+BI+ET+GR+NS-TuA1, 21
Rehbein, S.: BP+AS-SuA3, 1
Reid, D.: NS+AS+SS+SP-WeM2, 38
Reinhard, D.A.: AS-TuP18, 30
Rendon, E.A.: AS-TuP28, 32
Reshchikov, M.A.: EM+TF+AS-ThA4, 65
Revenko, I.: SP+AS+BI+ET+MI+TF-WeA11, 50
Rhallabi, A.: AS-MoM4, 2
Rhim, S.: GR+AS+NS+SP+SS-TuA2, 20
- Rice, T.: EM+TF+AS-ThA1, 64
Richter, R.P.: BI+AS-TuA9, 19
Rigby-Singleton, S.: BI+SS+AS-TuM5, 12
Ritz, E.: TC+EM+AS+TF+EN-ThM12, 62
Roach, W.M.: VT+AS+SS-WeM10, 42;
VT+AS+SS-WeM6, 41; VT+AS+SS-WeM9,
42
Roberts, A.J.: AS+BI-TuM10, 11; AS+BI-TuM3,
10; AS+NS+SS+TF-WeA8, 43; AS-TuP13, 30
Roberts, C.J.: BI+SS+AS-TuM5, 12;
SP+AS+BI+ET+MI+NS-TuA9, 24
Robinson, J.T.: GR+AS+BI+PS+SS-WeM9, 36;
GR+AS+NS+SP+SS-TuA8, 20;
GR+AS+NS+SS-ThM3, 58
Robinson, M.: BN+AS-WeA4, 44
Robinson, Z.R.: GR+AS+NS+SP+SS-TuA11, 21
Rodenhausen, K.B.: EL+TF+BI+AS+EM+SS-
MoA1, 8
Rodriguez Perez, A.: SP+AS+BI+ET+MI+NS-
TuA3, 23
Rodriguez, L.N.J.: IS+AS+OX+ET-WeM9, 38
Rogers, J.A.: EM+SS+AS+NS-ThM5, 56
Rojas, G.: NS+AS+SS+SP-WeM11, 39
Roodenko, K.: EL+TF+BI+AS+EM+SS-MoA2, 8
Rose, V.: MI+SP+AS-ThM1, 60
Rosenberg, R.A.: MI+SP+AS-ThM12, 61
Rosenfeld, D.H.: TF+AS-WeA1, 51
Rosenhahn, A.: BN+AS-WeA11, 45
Rosenmann, D.: MI+SP+AS-ThM12, 61
Rossi, F.: BI+SS+AS-TuM12, 13
Rougemmaile, N.: GR+AS+EM+NS+SS-WeA10,
46
Rowe, J.E.: GR+AS+BI+PS+SS-WeM10, 36;
GR+AS+NS+SP+SS-TuA11, 21
Rubio-Zuazo, J.: AS+TF+VT-FrM5, 71
Ruoff, R.S.: GR+AS+NS+SP+SS-TuA11, 21;
GR+AS+NS+SP+SS-TuA2, 20
Rutt, H.N.: HI+AS+BI+NS-ThM3, 59
Ruzic, D.N.: TC+EM+AS+TF+EN-ThM12, 62
Ryadnov, M.G.: BI+SS+AS-TuM11, 12
Rye, M.J.: AS-TuP5, 28
Rysz, J.: TF+AS+SS-ThA2, 68
- S —
Sabitova, A.: EM+TF+AS-ThA10, 66
Sadowski, J.T.: IS+AS+BI+ET+GR+NS-TuA8, 22
Saffron, N.: GR+AS+EM+NS+SS-WeA9, 46
Saitoh, E.: IS+AS+OX+ET-WeM10, 38
Sakai, Y.: AS-ThM12, 55; AS-TuP6, 29
Sakalas, P.: GR+AS+NS+SS-ThM2, 58
Sakurai, M.: GR+AS+EM+NS+SS-WeA12, 47
Salaün, A.: TF+AS-WeA12, 53
Sales, B.C.: SP+AS+BI+ET+MI+NS-TuA12, 25
Salib, D.: SP+AS+BI+ET+MI+NM+NS+SS+TF-
WeM5, 39
Salter, T.L.: AS-MoA9, 8
Samala, S.K.: TF+AS+SS-ThA9, 69
Samaraweera, R.L.: EM+TF+AS-ThA11, 66;
EM+TF+AS-ThA9, 65
Sandin, A.A.: GR+AS+BI+PS+SS-WeM10, 36;
GR+AS+NS+SP+SS-TuA11, 21
Sangiovanni, D.G.: TF+AS-TuA4, 25; TF+AS-
TuA9, 26
Sano, N.: AS-MoA1, 7; AS-TuP4, 28
Santeufemio, C.: AS+BI-TuA10, 17
Sarkar, A.: EL+TF+AS+EM+SS-TuP1, 32
Sasi-Zzabo, L.A.: IS+AS+BI+ET+GR+NS-TuA3,
22
Sauer, V.T.K.: MN+AS-MoM9, 5
Sawatzky, G.: TF+AS-TuA10, 26
Schaafhausen, S.: EM+TF+AS-ThA10, 66
Schafer, K.C.: IS+AS+BI+ET+GR+NS-TuA3, 22
Schlessler, R.: EM+TF+AS-ThA1, 64
Schlueter, J.A.: NS+AS+SS+SP-WeM11, 39
Schmid, A.K.: GR+AS+EM+NS+SS-WeA10, 46
Schmidt, D.: EL+TF+BI+AS+EM+SS-MoA1, 8
Schnadt, J.: IS+AS+SS+EN-TuM12, 15
Schneider, G.: BP+AS-SuA3, 1
Schnekenburger, J.: AS+BI-TuM1, 10
- Schoenfeld, W.V.: TF+AS-WeA7, 52; TF+AS-
WeA9, 52
Schofield, M.: GR+AS+NS+SP+SS-TuA2, 20
Schrumpf, R.D.: EM+SS+AS+NS-ThM11, 57
Schröder, U.: GR+AS+NS+SP+SS-TuA7, 20
Schroter, M.: GR+AS+NS+SS-ThM2, 58
Schubert, E.: EL+TF+BI+AS+EM+SS-MoA1, 8
Schubert, M.: EL+TF+BI+AS+EM+SS-MoA1, 8
Schuhmacher, M.: IS+AS+OX+ET-WeM11, 38
Schuller, I.: AS+TF+VT-FrM2, 71
Schulte, K.: GR+AS+NS+SP+SS-TuA7, 20
Schultz, J.A.: BN+AS-WeA12, 45
Schwarz, U.D.: SP+AS+BI+ET+MI+NS-TuA10,
24
Schweikert, E.: AS-ThM5, 54
Schwendemann, T.C.: SP+AS+BI+ET+MI+NS-
TuA10, 24
Schwerdtle, T.: AS-TuP1, 28
Scott, D.J.: BI+SS+AS-TuM5, 12
Scurr, D.J.: BN+AS-WeA10, 45
Seah, M.P.: AS-ThA2, 63
Seal, S.S.: AS+BI-TuA12, 18; NS+AS+SS+SP-
WeM2, 38
Sedlmaier, J.: AS-WeM6, 34
Sefat, A.S.: SP+AS+BI+ET+MI+NS-TuA12, 25
Seitz, O.: EL+TF+BI+AS+EM+SS-MoA2, 8
Seki, T.: AS-ThM9, 55
Sekine, M.: GR+AS+NS+SS-ThM9, 58
Semidey-Flecha, L.: GR+AS+EM+NS+SS-
WeA11, 47
Senevirathna, M.K.I.: EM+TF+AS-ThA11, 66;
EM+TF+AS-ThA9, 65
Senkbeil, T.: BN+AS-WeA11, 45
Seo, S.J.: AS-TuP22, 31
Serov, A.: IS+AS+SS+EN-TuM6, 15
Setvin, M.: SP+AS+BI+ET+MI+NS-TuA4, 23
Sgammato, B.: AS-TuP10, 29
Shacham-Diamand, Y.: MN+AS-MoM10, 5
Shafiq, N.: GR+AS+BI+PS+SS-WeM2, 36
Sham, T.K.: AS+TF+VT-FrM1, 71
Shao-Horn, Y.: IS+AS+SS+EN-TuM5, 15
Shard, A.G.: AS-ThA2, 63; AS-ThM4, 54
Sharma, G.: AS-ThA7, 64
Sharma, K.: TC+EM+AS+TF+EN-ThM2, 61
Sheehan, P.E.: GR+AS+BI+PS+SS-WeM9, 36;
GR+AS+NS+SS-ThM3, 58
Sherwood, P.M.A.: AS-MoM8, 3
Shetty, R.: SP+AS+BI+ET+MI+TF-WeA9, 50
Shikano, T.: GR+AS+EM+NS+SS-WeA12, 47
Shivashankar, S.A.: AS-TuP23, 32
Shklovsky, J.: MN+AS-MoM10, 5
Sholl, D.: GR+AS+EM+NS+SS-WeA11, 47
Shutthanandan, V.: AS+NS+SS+TF-WeA4, 43
Sijbrandij, S.: HI+AS+NS-WeA10, 48
Siligardi, G.: BI+SS+AS-TuM12, 13
Simons, D.S.: AS+BI-TuA9, 17
Simons, M.T.: TF+AS+SS-ThA8, 69
Sirringhaus, H.: TC+EM+AS+TF+EN-ThM9, 62
Sitar, Z.: EM+TF+AS-ThA1, 64
Sivula, K.: IS+AS+SS+EN-TuM3, 14
Skuzza, J.R.: VT+AS+SS-WeM6, 41
Smekal, W.: AS-MoM3, 2; AS-MoM6, 3
Smentkowski, V.S.: AS-TuP18, 30
Smith, S.: AS-ThM4, 54
Smolenski, K.W.: VT+AS+SS-WeM2, 41
Snow, A.W.: TF+AS-TuA3, 25
Sokolov, I.: MN+AS-MoM10, 5
Song, E.B.: EM+SS+AS+NS-ThM11, 57
Song, I.Y.: AS+BI-TuM9, 11
Song, S.-H.: AS-WeM3, 34
Sotres, J.: BI+SS+AS-TuM3, 12
Sousa, C.: AS-TuP11, 30; BI+AS-TuA7, 18
Spemann, D.: GR+AS+EM+MI+MN-TuM9, 13
Spencer, S.: AS-ThM4, 54
Spies, M.: EL+TF+BI+AS+EM+SS-MoA9, 9
Srivastava, N.: GR+AS+NS+SP+SS-TuA10, 21
Stadermann, M.: IS+AS+OX+ET-WeM6, 38
Steele, B.: GR+AS+EM+MI+MN-TuM10, 14
Stein, M.J.: IS+AS+BI+ET+GR+NS-TuA1, 21

- Steiner, M.: MI+SP+AS-ThM12, 61
Stevie, F.A.: AS+BI-TuA10, 17
Stickle, W.F.: AS-ThA1, 63
Stine, R.: GR+AS+BI+PS+SS-WeM9, 36;
GR+AS+NS+SS-ThM3, 58
Stock, S.R.: AS-WeM9, 35
Strohmeier, B.: AS+BI-TuM11, 11
Su, C.: SP+AS+BI+ET+MI+TF-WeA8, 49
Subramanian, V.: AS+NS+SS+TF-WeA4, 43
Sugimoto, Y.: SP+AS+BI+ET+MI+NS-TuA11, 24
Sumant, A.V.: AS-TuP12, 30; MN+AS-MoM3, 4;
MN+AS-MoM5, 4
Sumpter, B.G.: NS+AS+SS+SP-WeM11, 39
Sun, D.Z.: SP+AS+BI+ET+MI+NM+NS+SS+TF-
WeM5, 39
Sun, L.: TF+AS+SS-ThA10, 70
Sung, C.Y.: GR+AS+NS+SP+SS-TuA11, 21
Sutarto, R.: TF+AS-TuA10, 26
Sutter, P.W.: GR+AS+EM+NS+SS-WeA8, 46
Suzer, S.: AS-MoM11, 3
Suzuki, T.: GR+AS+EM+NS+SS-WeA12, 47
Swaraj, S.: AS+BI-TuM5, 10
Sykes, C.H.: EM+SS+AS+NS-ThM9, 56
Szakal, C.: AS+BI-TuA9, 17
- T —
Takagi, K.: GR+AS+NS+SS-ThM1, 57
Takaishi, R.: AS-ThM12, 55; AS-TuP3, 28; AS-
TuP6, 29
Takats, Z.: IS+AS+BI+ET+GR+NS-TuA3, 22
Tallarida, M.: IS+AS+OX+ET-WeM9, 38
Tamanaha, C.R.: GR+AS+NS+SS-ThM3, 58
Tanaka, S.: GR+AS+NS+SS-ThM1, 57
Tantardini, G.F.: GR+AS+EM+NS+SS-WeA12,
47
Tao, F.: TF+AS+SS-ThA6, 69
Tapasztó, L.: AS+TF+VT-FrM3, 71
Tasneem, G.: AS-MoM6, 3
Tatulian, S.A.: GR+AS+BI+PS+SS-WeM6, 36
Taubner, T.: AS-WeM4, 34
Taucer, M.:
SP+AS+BI+ET+MI+NM+NS+SS+TF-WeM2,
39
Temst, K.: MI+SP+AS-ThM9, 60
ten Elshof, A.: EL+TF+BI+AS+EM+SS-MoA8, 9
Tendler, S.J.B.: SP+AS+BI+ET+MI+NS-TuA9, 24
Teng, D.: GR+AS+EM+NS+SS-WeA11, 47
Tenne, R.: NS+AS+SS+SP-WeM4, 38
Tentschert, J.: AS-TuP1, 28
Teplyakov, A.V.: AS-TuP20, 31; EN+AS-ThA8,
67
ter Veen, H.R.J.: TF+AS+SS-ThA4, 69
Terfort, A.: TF+AS+SS-ThA2, 68
Theilacker, W.: AS+BI-TuM4, 10
Thevuthasan, S.: AS+BI-TuA12, 18;
AS+NS+SS+TF-WeA3, 43; AS+NS+SS+TF-
WeA4, 43; IS+AS+BI+ET+GR+NS-TuA12,
23; TC+EM+AS+TF+EN-ThM5, 62;
TF+AS+SS-ThA11, 70
Thierley, M.: VT+AS+SS-WeM3, 41
Thiess, S.: AS+TF+VT-FrM3, 71
Thissen, P.: EN+AS-ThA7, 67; TF+AS+SS-ThA3,
68
Thomas, W.: BI+SS+AS-TuM6, 12
Thonhauser, T.: EN+AS-ThA7, 67
Thorpe, R.: EN+AS-ThA9, 68
Tian, W.-C.: MN+AS-MoM11, 5
Tillocher, T.: MN+AS-MoM6, 4
Tivanski, A.: IS+AS+BI+ET+GR+NS-TuA9, 23
Tiwald, T.E.: EL+TF+BI+AS+EM+SS-MoA1, 8
Tiwari, A.N.: TF+AS-WeA3, 52
Todorovic, M.: SP+AS+BI+ET+MI+NS-TuA10,
24
Torun, B.: TF+AS+SS-ThA1, 68
Tóth, J.: AS+TF+VT-FrM3, 71
Tougaard, S.: AS-MoM1, 2
Trioni, M.L.: GR+AS+EM+NS+SS-WeA12, 47
Trogler, W.C.: BN+AS-WeA3, 44
Tronic, E.: BI+SS+AS-TuM6, 12
Tsong, T.T.: HI+AS+NS-WeA8, 48
- Tsverin, Y.: NS+AS+SS+SP-WeM4, 38
Turchanin, A.: GR+AS+BI+PS+SS-WeM11, 37;
HI+AS+BI+NS-ThM11, 59; HI+AS+BI+NS-
ThM5, 59
Turk, M.E.: GR+AS+EM+MI+MN-TuM2, 13
Tweedy, J.: EM+TF+AS-ThA1, 64
Twiggy, M.E.: EM+TF+AS-ThA6, 65
Tyagi, P.: GR+AS+NS+SP+SS-TuA11, 21
Tyliszczak, T.: GR+AS+EM+MI+MN-TuM9, 13;
IS+AS+BI+ET+GR+NS-TuA9, 23
- U —
Ugelow, M.: AS+BI-TuA9, 17
Ulfig, R.M.: AS-TuP18, 30
Ulijn, R.: BI+SS+AS-TuM9, 12
Unger, M.: AS-WeM6, 34
Unger, W.E.S.: AS+BI-TuM5, 10
Ungureneau, M.: GR+AS+EM+MI+MN-TuM9, 13
Ünverdi, Ö.: SP+AS+BI+ET+MI+NS-TuA10, 24
Urban, R.: HI+AS+NS-WeA7, 48
Ushigome, D.: GR+AS+EM+NS+SS-WeA12, 47
- V —
Vallee, C.: TF+AS-WeA12, 53
van Buuren, T.: AS+TF+VT-FrM2, 71;
IS+AS+OX+ET-WeM6, 38
Van Elshocht, S.: IS+AS+OX+ET-WeM9, 38
Van Veldhoven, E.: HI+AS+NS-WeA9, 48
Vanderleyden, E.: MN+AS-MoM10, 5
VanDerslice, J.: EL+TF+BI+AS+EM+SS-MoA1,
8
Vandervorst, W.: AS-ThM6, 54
VanFleet, R.: MN+AS-MoM4, 4
Vanhove, N.: HI+AS+NS-WeA10, 48
VanSant, K.: TF+AS-WeA10, 52
Vega, A.: TF+AS+SS-ThA3, 68
Velden, M.: TC+EM+AS+TF+EN-ThM2, 61
Vemuri, R.S.: TF+AS+SS-ThA11, 70
Ventrice, Jr., C.A.: GR+AS+NS+SP+SS-TuA11,
21
Verkhoturov, S.: AS-ThM5, 54
Veyan, J.-F.: GR+AS+BI+PS+SS-WeM2, 36
Vickerman, J.C.: AS-ThM2, 54
Vieker, H.: HI+AS+BI+NS-ThM5, 59
Vilayurganapathy, S.: TC+EM+AS+TF+EN-
ThM5, 62
Vlassioun, I.: AS-TuP12, 30
Vohs, J.M.: SP+AS+BI+ET+MI+TF-WeA3, 49
Vora, P.M.: GR+AS+EM+MI+MN-TuM2, 13
Voroshazi, E.: AS-ThM6, 54
Vo-Van, C.: GR+AS+EM+NS+SS-WeA10, 46
Vurgaftman, I.: EM+TF+AS-ThA6, 65
- W —
Wagner, M.S.: AS-WeM3, 34
Walker, R.: AS-TuP9, 29
Wallace, R.M.: GR+AS+EM+NS+SS-WeA1, 46
Walrath, J.C.: EM+SS+AS+NS-ThM13, 57
Walsh, L.A.: AS-TuP7, 29
Walters, D.: SP+AS+BI+ET+MI+TF-WeA11, 50
Walton, J.: AS+BI-TuM12, 11
Walton, S.G.: GR+AS+BI+PS+SS-WeM9, 36
Wan, K.: BN+AS-WeA10, 45
Wang, B.: IS+AS+BI+ET+GR+NS-TuA9, 23
Wang, J.: HI+AS+BI+NS-ThM9, 59
Wang, K.L.: EM+SS+AS+NS-ThM11, 57
Wang, L.: TF+AS+SS-ThA8, 69
Wang, L.B.: MN+AS-MoM11, 5
Wang, Q.H.: GR+AS+BI+PS+SS-WeM1, 35
Wang, Z.: AS-MoA3, 7
Wasio, N.A.: AS-TuP26, 32
Waterton, C.: IS+AS+BI+ET+GR+NS-TuA1, 21
Watts, J.F.: AS-TuP4, 28
Weber, N.-E.: HI+AS+BI+NS-ThM5, 59
Wehbe, N.: AS-MoA2, 7
Wei, M.: TF+AS-WeA7, 52; TF+AS-WeA9, 52
Wei, S.-H.: EN+AS-ThA1, 66; TC+EM+AS-
WeA4, 51
Weidner, T.: AS-WeM3, 34
Weiland, C.: AS-ThA6, 63
Weinert, M.: GR+AS+NS+SP+SS-TuA2, 20
- Werner, S.: BP+AS-SuA3, 1
Werner, W.S.M.: AS-MoM3, 2; AS-MoM6, 3
Wessel, S.: EN+AS-ThA6, 67
Wetzel, C.: EM+TF+AS-ThA7, 65
Wheeler, V.D.: GR+AS+NS+SP+SS-TuA9, 20
White, M.G.: NS+AS+SS+SP-WeM12, 39
White, R.G.: AS-MoA2, 7; AS-MoM10, 3; AS-
TuP11, 30
Whitehead, N.P.: BN+AS-WeA9, 45
Wielunski, L.S.: AS-MoA10, 8
Willey, T.M.: AS+TF+VT-FrM2, 71
Williams, P.M.: BI+SS+AS-TuM5, 12
Willunat, A.: HI+AS+BI+NS-ThM11, 59;
HI+AS+BI+NS-ThM5, 59
Windisch, Jr., C.F.: AS+BI-TuA12, 18
Winkler, K.: GR+AS+NS+SP+SS-TuA1, 19
Winter, A.: HI+AS+BI+NS-ThM11, 59;
HI+AS+BI+NS-ThM5, 59
Winter, G.: AS+BI-TuM3, 10
Wirtz, T.: HI+AS+NS-WeA10, 48
Wittstock, A.: IS+AS+OX+ET-WeM6, 38
Woicik, J.C.: AS-ThA6, 63; AS-ThA8, 64; AS-
TuP7, 29
Wolkow, R.A.: HI+AS+NS-WeA7, 48;
SP+AS+BI+ET+MI+NM+NS+SS+TF-WeM2,
39
Woll, A.R.: IS+AS+BI+ET+GR+NS-TuA2, 22
Wolstenholme, J.: AS+BI-TuM11, 11
Womack, V.M.: BN+AS-WeA12, 45
Wood, B.C.: IS+AS+OX+ET-WeM6, 38
Woods, A.S.: BN+AS-WeA12, 45
Wormeester, H.: EL+TF+BI+AS+EM+SS-MoA8,
9
Worsley, M.A.: IS+AS+OX+ET-WeM6, 38
Wright, A.E.: AS-MoM10, 3; AS-TuP10, 29
Wu, H.: EN+AS-ThA7, 67
Wu, S.: GR+AS+NS+SP+SS-TuA12, 21
Wu, Y.L.: TC+EM+AS+TF+EN-ThM12, 62
Wu, Z.: BN+AS-WeA3, 44
Wygladacz, K.A.: AS-TuP19, 31
Wyrick, J.: SP+AS+BI+ET+MI+NM+NS+SS+TF-
WeM5, 39
- X —
Xiao, Q.: AS+TF+VT-FrM1, 71
Xie, J.: EM+TF+AS-ThA1, 64
Xu, Y.: EL+TF+BI+AS+EM+SS-MoA9, 9;
GR+AS+EM+NS+SS-WeA11, 47
- Y —
Yamada-Takamura, Y.: TF+AS-WeA8, 52
Yamashita, Y.: AS-ThA10, 64
Yang, A.: AS-ThA10, 64
Yang, K.: TF+AS+SS-ThA8, 69
Yang, L.: IS+AS+BI+ET+GR+NS-TuA12, 23
Yang, Y.C.: VT+AS+SS-WeM1, 41
Yanguas-Gil, A.: TC+EM+AS+TF+EN-ThM6, 62
Yazyev, O.V.: GR+AS+NS+SS-ThM5, 58
Yoshikawa, A.: EM+TF+AS-ThA12, 66
Yoshimura, T.: GR+AS+NS+SS-ThM1, 57
Yu, J.: GR+AS+NS+SP+SS-TuA12, 21
Yu, X.-Y.: IS+AS+BI+ET+GR+NS-TuA12, 23
Yu, Z.: NS+AS+SS+SP-WeM4, 38
Yun, D.J.: AS-ThA4, 63
Yurtsever, A.: SP+AS+BI+ET+MI+NS-TuA11, 24
- Z —
Zandvliet, H.J.W.: EL+TF+BI+AS+EM+SS-
MoA8, 9
Zarrouati, M.: GR+AS+BI+PS+SS-WeM1, 35
Zegenhagen, J.: AS-ThA7, 64;
GR+AS+NS+SP+SS-TuA9, 20
Zettl, A.: GR+AS+NS+SS-ThM5, 58
Zhakhovskiy, V.: GR+AS+EM+MI+MN-TuM10,
14
Zhang, B.: TC+EM+AS-WeA3, 50
Zhang, C.X.: EM+SS+AS+NS-ThM11, 57
Zhang, E.X.: EM+SS+AS+NS-ThM11, 57
Zhang, H.: HI+AS+BI+NS-ThM9, 59
Zhang, L.: IS+AS+SS+EN-TuM3, 14; TF+AS-
WeA1, 51

Zhang, S.: BI+AS-TuA3, 18
Zhang, X.: HI+AS+BI+NS-ThM5, 59
Zhao, H.: IS+AS+SS+EN-TuM9, 15
Zheng, X.: TC+EM+AS+TF+EN-ThM11, 62
Zhou, C.: AS+BI-TuA10, 17

Zhu, J.F.: IS+AS+SS+EN-TuM3, 14
Zhu, Y.: SP+AS+BI+ET+MI+NM+NS+SS+TF-
WeM5, **39**
Zhu, Z.: AS-MoA3, **7**; IS+AS+BI+ET+GR+NS-
TuA12, 23

Zohar, S.: MI+SP+AS-ThM12, 61
Zollner, S.: EL+TF+AS+EM+SS-TuP2, 32;
EL+TF+BI+AS+EM+SS-MoA9, **9**